การจำลองเชิงสโตแคสติกของการเกาะแบบกลุ่มก้อนของ
แอโรซอลบนเส้นใยชนิดอิเล็กเทรต

นาย เกรียงไกร มณีอินทร์

STOCHASTIC SIMULATION OF AGGLOMERATIVE
DEPOSITION OF AEROSOL ON AN ELECTRET FIBER

Mr. Kreangkrai   Maneeintr

Thesis Title   Stochastic Simulation of Agglomerative

                       Deposition of Aerosol on an Electret Fiber

By   Kreangkrai Maneeintr

Field of study   Chemical Engineering

Thesis Advisor   Professor Wiwut Tanthapanichakoon, Ph.D.

 Co-advisor   Associate Professor Tawatchai Charinpanitkul, Dr.Eng.

_____

       Accepted by the Faculty of Engineering, Chulalongkorn University in Partial Fulfillment of the Requirements for the Master's Degree

                      ....…....................... Dean of Faculty of Engineering

                      (Professor Somsak Panyakeow, Dr.Eng.)

THESIS COMMITTEE

                   ....Chairman

                   (Associate Professor Chirakarn Muangnapoh, Dr.Ing.)

                   ....Thesis Advisor

                   (Professor Wiwut Tanthapanichakoon, Ph.D.)

                   ....Thesis Co-Advisor

                   (Associate Professor Tawatchai Charinpanitkul, Dr.Eng.)

                   ....Member

                   (Somprasong Srichai, Ph.D.)

เกรียงไกร มณีอินทร์ : การจำลองเชิงสโตแคสติกของการเกาะแบบกลุ่มก้อนของแอโรซอลบนเส้นใยชนิดอิเล็กเทรต (STOCHASTIC SIMULATION OF AGGLOMERATIVE   DEPOSITION OF AEROSOL ON AN ELECTRET FIBER) อาจารย์ที่ปรึกษาวิทยานิพนธ์ : ศ. ดร. วิวัฒน์ ตัณฑะพานิชกุล, อาจารย์ที่ปรึกษาวิทยานิพนธ์ร่วม : รศ. ดร. ธวัชชัย ชรินพาณิชกุล, 175 หน้า. ISBN 974-13-0513-3

การศึกษาลักษณะการเกาะของอนุภาคบนเส้นใย   และการเปลี่ยนแปลงประสิทธิภาพของเครื่องกรองอากาศ เมื่ออนุภาคจับตัวเป็นกลุ่มก้อนบนเส้นใย เป็นสิ่งจำเป็นในการพัฒนาออกแบบและยืดอายุการใช้งานของไส้กรองอากาศ ซึ่งรวมถึงเส้นใยกรองชนิดอิเล็กเทรต   โดยเส้นใยชนิดนี้จะประกอบไปด้วยประจุบวกและลบกระจายอยู่บนผิวของเส้นใย ประจุดังกล่าวจะอยู่กันอย่างหนาแน่นและถาวร และช่วยเพิ่มประสิทธิภาพการเก็บอนุภาคขนาดเล็กๆ ในการศึกษานี้ได้พัฒนาดัดแปลงแบบจำลองเชิงสโตแคสติก เพื่อจำลองลักษณะการเกาะตัวแบบกลุ่มก้อนของแอโรซอลบนเส้นใยอิเล็กเทรตโดยพิจารณาแรงทางไฟฟ้า 2 ชนิด คือ แรงเหนี่ยวนำ (กรณีที่อนุภาคไม่มีประจุ) และแรงคูลอมป์ (กรณีที่มีประจุไฟฟ้าสถิต) โดยคำนึงถึงการเคลื่อนที่แบบการแพร่ของอนุภาคขนาดไมโครเมตรเข้าไว้ด้วย ผลการจำลองรูปร่างการเกาะตัวของอนุภาคบนเส้นใยสอดคล้องอย่างดีกับผลการทดลองของคานาโอกะและคณะ ทั้งในกรณีอนุภาคที่ไม่มีและมีประจุ ลักษณะการกระจายตัวของกลุ่มก้อนอนุภาคที่ถูกจับบนเส้นใย   และการเปลี่ยนแปลงประสิทธิภาพการจับอนุภาคบนเส้นใยซึ่งได้มาจากการจำลองนี้ สามารถนำมาทำนายผลที่การแพร่ของอนุภาค(ตัวเลขเพคเลต), ค่าพารามิเตอร์ของการสกัดกั้น, ค่าพารามิเตอร์ของแรงทางไฟฟ้า และมุมบิดของการวางเส้นใยอิเล็กเทรต มีต่อรูปร่างของกลุ่มก้อนอนุภาคที่เกาะบนเส้นใย, การกระจายตำแหน่งเกาะของอนุภาคบนเส้นใย, การเปลี่ยนแปลงของจำนวนเดนไดรต์ขนาดต่างๆตามเวลากรอง,   อัตราเฉลี่ยของการเติบโตของเดนไดรต์ตามอายุ   และค่าสัมประสิทธิ์การเพิ่มประสิทธิภาพในการจับอนุภาคบนเส้นใย

อนึ่ง ความสัมพันธ์ระหว่างอัตราการส่วนของประสิทธิภาพการจับอนุภาคระหว่างเส้นใยที่กำลังใช้งานและเส้นใยที่สะอาด จะสามารถหาได้จากสมการเชิงเส้นในกรณีที่พารามิเตอร์ทางไฟฟ้ามีค่าน้อย แต่ในกรณีที่ค่าพารามิเตอร์ทางไฟฟ้ามีค่าสูงขึ้น ความสัมพันธ์ดังกล่าวจะแบ่งได้เป็นสองช่วง คือ ช่วงที่เส้นใยยังมีค่าภาระฝุ่นต่ำๆและช่วงที่ภาระฝุ่นสูงขึ้น นอกจากนี้ แบบจำลองเชิงสโตแคสติกที่เสนอขึ้นนี้ ยังให้ผลการทำนายที่สอดคล้องกับผลการทดลองมากกว่าแบบจำลองที่คานาโอกะและคณะได้พัฒนาขึ้น

ภาควิชา	วิศวกรรมเคมี	ลายมือชื่อนิสิต	
สาขาวิชา	วิศวกรรมเคมี	ลายมือชื่ออาจารย์ที่ปรึกษา	
ปีการศึกษา	2543	ลายมือชื่ออาจารย์ที่ปรึกษาร่วม	

To design a high-performance air filter with longer service life, it is important to study how the morphology of particles accumulating on an electret fiber changes and affects the collection efficiency of the filter at dust-loaded condition. An electret filter is composed of permanently charged electret fibers and is capable of collecting fine particles at a high efficiency. In this study, a three-dimensional stochastic model is utilized to simulate collection and agglomeration of particles on the cylindrical electret fiber by two different electrical deposition mechanisms, namely, induced forces (for uncharged particles) and coulombic forces (for charged particles) mechanisms. Moreover, the effect of diffusional mechanism is included. The morphology of particle agglomerates obtained in the simulated results is found to agree very well with experimental observations obtained by Kanaoka et al. for both uncharged and charged particles. The distribution of agglomerates on the fiber surface and the change in the fiber collection efficiency can be used to explain the effects of Peclet number, interception parameter, electrical parameters and twist angle of the fiber on the morphology of captured particles, the angular distribution of particles on the fiber, number distribution of dendrites as a function of time, average dendrite size by age and the collection efficiency raising factor.

In addition, the ratio of collection efficiency at any time instant, η, to the initial collection efficiency, η_0, can be represented as linear function in the case of low electrical parameters. However, when the electrical parameters are large, the normalized collection efficiency has to be represented by two linear correlations, i.e., at low dust load and high dust load. Furthermore, the results of this stochastic model agreed well with the experimental results better than that of Kanaoka's model.

Department   Chemical Engineering   Student's signature

Filed of study Chemical Engineering   Advisor's signature

Academic year   2000   Co-advisor's signature

ACKNOWLEDGEMENT

CONTENTS

LIST OF FIGURES

LIST OF TABLES

NOMENCLATURE

$A_{(t)}$ = fluctuating term (cm/s)

B = mobility of particle ($= C_m/3\pi\mu d_p$) (s/kg)

C_m = Cunnigham's correction factor (-)

d_f = fiber diameter (m)

d_p = particle diameter (m)

D_{BM} = diffusion coefficient ($= \dfrac{C_m kT}{3\pi\mu D_p}$) (m^2/s)

e = elementary electric charge ($= 1.6*10^{-19}$) (C)

E = particle collection efficiency of filter (-)

f_C = dimensionless coulombic force (-)

f_G = dimensionless gradient force (-)

f_R = dimension high-gradient force (-)

F = external force vector (N)

Gr = gravitation settling parameter ($= \dfrac{U_\infty}{V_g}$) (-)

h = thickness of filter (m)

H = half height of generation plane (-)

Ii = unit vector (-)

K = hydrodynamic factor (-)

K_C = dimensionless electrical parameter for coulombic force (-)

K_{In} = dimensionless electrical parameter for induced force (-)

L = Sample size (-)

m = dust load in a unit filter volume (kg/m^3)

M = maximum dendrite size of interest (-)

n = number of fibers (-)

n = number concentration of aerosol particles (-/m^3)

n = standard normal random vector = (n_x, n_y, n_z)

n_E = number of electron on particle (-)

N = total number of sampling points (-)

N_{gen} = number of incoming particles per unit dimensionless fiber length up to time t (-)

p = position vector (m)

P = dimensionless position vector (-)

Pe = Peclet number ($=\dfrac{D_f U_\infty}{D_{BM}}$) (-)

P_N = number of dendrites of size N per unit dimensionless fiber length (-)

r_E = radius of hemisphere of influence of high-gradient force (-)

Ri = interception parameter (d_p/d_f) (-)

R_c = dimensionless radius of Kuwabara's cell (-)

R_f = radius of fiber (m)

R_p = radius of particle (m)

St = Stoke number ($=\dfrac{C_m U_\infty \rho_p d_p^2}{9\mu d_f}$) (-)

t = time (s)

Δt = time step (s)

u = fluid velocity (-)

U_X = fluid velocity in x-direction (-)

U_Y = fluid velocity in y-direction (-)

U_Z = fluid velocity in z-direction (-)

U_∞ = approach velocity of air (m/s)

v = particle velocity (-)

V_g = settling velocity (m/s)

x = x-coordinate (m)

X = dimensionless x-coordinate (-)

y = y-coordinate (m)

Y = dimensionless y-coordinate (-)

z = z-coordinate (m)

Z = dimensionless z-coordinate (-)

Greek symbols

α = packing density of filter (-)

γ = twist angle of fiber or polarization direction (deg)

β = mobility of particle (-)

η = particle collection efficiency (-)

η_0 = single fiber collection efficiency (clean surface) (-)

λ = overall collection efficiency raising factor (m^3/kg)

λ_I = initial collection efficiency raising factor (m^3/kg)

ω = weighting factor in equation (7) (-)

μ = viscosity of air (Pa.s)

$\Delta\tau$ = step size (-)

ρ_p = particle density (kg/m^3)

ε_f = dielectric constant of fiber (-)

ε_p = dielectric constant of particle (-)

ε_0 = space permittivity ($=8.85*10^{-12}$) (F/m)

σ = average surface charge density on fiber (C/m^2)

σ_{max} = maximum average surface charge density on fiber (C/m^2)

ψ = stream function (-)

Subscripts

R = interception

D = diffusion

f = fiber

G = gravitaion

i = i^{th} step

I = inertia

o = initial

p   = particle

sto   = stochastic simulation

i   = size of dendrites

x   = x-direction

y   = y-direction

z   = z-direction

CHAPTER 1

INTRODUCTION

1.1 The Importance of Air Filtration

Particulate pollutants of micron-order size have been identified as the most hazardous pollutants from a public health point of view. Therefore, there is acute need for complete removal of contaminating particles from the inhaled air. Air cleaning may be achieved with the cyclone, scrubber, electrostatic precipitator, fibrous filter, etc. Most of air filters can remove fine particles smaller than 10 μm diameters. When there is need for efficiency, for instance, higher than 95%, removal of particles smaller than 1 μm diameter from the flow of air, a good fibrous air filter can be used. Aerosol filtration by a fibrous air filter is a widely adopted and highly efficient method for removing submicron particles from gas stream with the additional advantage of low energy consumption. But one disadvantage of using the fibrous air filter is the failure in developing convenient and effective methods for cleaning the filter. Hence, most industrial applications are still confined to some specific cases where high efficiency is demanded and use of disposable filter elements is practical for environmental protection such as clean rooms, emergency filtration system for radioactive aerosols, respiratory mask, etc.

   The deposition mechanism of aerosol particles in the fibrous air filter is of interest to many researchers because the filter is used in various industries for dust collection and environmental protection. It is well known that the deposition of aerosol particles on a fiber depends on the combined effects of inertial impaction, Brownian diffusion, gravitational settling, direct interception, static electricity, etc. When the filter is used for a long period of time, the morphology of aerosols collected on the fiber is different from that of a clean fiber. It was found that aerosol particles deposited not only on the fiber surface but also on formerly deposited particles forming tree-like agglomerates called dendrites (Davies 1973). Each dendrite is rooted at the fiber surface and hinders in the main flow. So, it acts as a collector and keeps growing as additional particles deposit on it.

Many experimental studies have found that these phenomena lead to an increase of both aerosol collection efficiency and pressure drop of the fibrous air filter with filtration time (Kimura et. al., 1964; Billing, 1966). The experimental aerosol collection efficiency

of the dust loaded fiber normalized by the corresponding collection efficiency of the clean fiber was found to be expressible by the following linear function of the mass of particles accumulated in a unit filter volume, i.e. $\frac{\eta}{\eta_0} = 1 + \lambda\, m$,where λ is the collection efficiency raising factor (Yoshioka et al., 1969). Over a long period of time, filtration results in the formation and growth of particle dendrites on fibers, which increase the filtration efficiency and pressure drop with dust load, the accumulation of collected particles in the filter. Initially, this is beneficial; that is, the filtration quality improves. However, eventually, the pressure becomes excessive and the filter is said to be clogged.

1.2 Introduction to Electret Filter

Electrically charged filter material has a history of several decades; in fact the first such material was used for a period of years before its mechanism of action was properly understood. The advantage of materials of this type is that the charge on the fibers considerably augments the filtration efficiency without making any contribution to the air flow resistance. Several materials carrying permanent electric charge now exist, finding wide use in situations where a high efficiency is required along with a long resistance, such as in respirator filters.

Although it is difficult to explain at the microscopic level, charged fibers can greatly enhance filter collection. This characteristic is used for filters that require high efficiency and low pressure drop, such as respirator filters (Hinds, 1999). The oldest type of charged-fiber filter is the resin-wool or Hansen filter, made of wool fiber impregnated with insulating resin particles about 1 μm in diameter. The mechanical action of carding the felt causes the resin particles to become highly charged, and they retain their charge for years under favorable conditions. The presence of this highly charged particles in the filter greatly enhances its collection efficiency without increasing its resistance. Unfortunately, charged fiber filers lose their charge and their effectiveness when exposed to ionizing radiation, high temperature, high humidity or organic liquid aerosols. Also accumulated dust can mask the charge the charge and reduce its effectiveness.

Another type of charged fiber is the electret fiber. This fiber is made from thin sheets of insulating plastic, such as polypropylene, that are corona charged so that one side is positive and the other negative in a more or less permanent configuration. The sheets are

split into fibers and incorporated into fibrous filters. Electret fiber filters have advantages and limitations similar to those of resin-wool filters.

An electret filter is composed of permanently charged electret fibers and is capable of collecting fine particles at a high efficiency in the beginning of the filtration because of strong electrostatic effects, but its collection performance is reported to decrease with time. However, the time dependency of the collection performance and the reason of the decrease in collection efficiency are not well understood yet (Kanaoka, 1984).

An electret filter carries permanent positive and negative charges inside each fiber. The aerosol collection efficiency of the electret fiber can be significantly higher, even if the aerosol particles are uncharged. Thus electret fibers have been used to enhance the collection efficiency of HEPA and ULPA filters. In some instances the collection efficiency of an electret fiber may drop substantially as deposition of particles progresses. Typically air filters are not equipped with any dust-cleaning systems and are discarded when captured particles clog the air passage. Kanaoka(1998) showed how to double the service life by designing a filter with larger dust-holding capacity at the same final pressure drop. This is achievable because filter performance depends not only on filtration conditions and particle properties but also on filter properties, such as fiber diameter, packing density and packing structure.

As more and more particles deposit on a fiber inside a filter and/or on previously captured particles, they form complicated accumulates, which lead to a marked increase in collection efficiency and pressure drop. To design a filter with improved service life, we need to predict filter performance under dust load, which requires good understanding of how the morphology of particle accumulates on a fiber affects the collection efficiency and pressure drop of a dust-loaded filter.

The collection performance of an electret fiber was investigated theoretically and experimentally. As a result, the collection efficiency of a single electret fiber was well correlated by a function of coulombic force and induced force parameters, when electrostatic effects are prevailing.

Electret filters can be used in particular for respirators, clean rooms and probably for the highly-efficient cleaning of waste laboratory air (e.g. in the case of toxic or radioactive pollution). The advantages of the electret filters are, in all cases, high initial collection efficiencies combined with a low flow resistance.

The process of filtration is complicated, and although the general principles are well known. There is a gap between theory and experiment. Nevertheless, filtration is an active

area for theoretical and experimental research, and there is an extensive scientific literature on the subject.

1.3 Objectives of the Present Study

1. To develop and apply the model to predict the dendritic growth of aerosol particles and the corresponding aerosol collection efficiency for convective diffusional deposition on a dust-loaded electret fiber for the case of uncharged particles or induction mechanisms.

2. To extend the above model for predicting the dendritic growth of aerosol particles and aerosol collection efficiency for convective diffusional deposition on the dust-loaded electret fiber for the case of charged particles or coulombic forces.

3. To estimate the optimal values of the collection efficiency raising factors of the model for both the induced force and coulombic force mechanisms.

1.4 Scope of Study

1. The model derived from studying the dendritic growing on a single electret fiber was applied to the convective diffusion and electrostatic deposition mechanism.

2. The Fortran programming language was chosen to code the model program. The resulting computer code will be tested on a personal computer.

3. The stochastic model was simulated under various filtration conditions such as Peclet number, electrical parameters, twist angle of electret fiber and particle size to obtain additional stochastic simulation results for the collection efficiency raising factors.

4. The results will be compared to both the experimental results and the previously simulated results of other researchers.

CHAPTER 2
LITERATURE REVIEW

The aerosol particles deposition in fibrous air filter is of interest by many researchers because fibrous air filter is used in various industries for dust collection and environmental protection. The highly complex phenomenon of aerosol particle deposition may be classified by four steps: 1) deposition on a clean fiber, 2) deposition on previously deposited particles to form dendrites and promote dendritic growth, 3) further growth resulting in intermeshing of neighboring dendrites and , finally, 4) internal cake formation. The re-entrainment of deposited particles may occur at any of the steps, depending on the relative magnitudes of particle-particle and particle-fiber adhesion forces.

In investigations, both experiment and theory, on aerosol filtration have been carried out extensively, and are too numerous to cite individually. Generally, most of the theoretical studies utilized the single fiber concept and were confined to the initial filtration period, i.e. when a filter is relatively clean; in other words, they did not cover the equally important period when deposition was at an advanced stage. An excellent review of the topic was given by Davies (1973). Other study on the theory of aerosol filtration with fibrous air filters were published by Fuchs (1964) and Kirsch et al. (1978). Then, the fiber with dust load was developed to be more practical in real life.

2.1 Experimental Study

2.1.1 Air filtration by non-electret fiber

The first systematic experimental study, Billing (1966) studied deposition of electrically neutral polystyrene monosized latex particles on a single glass fiber and took numerous photographs of the dendritic growth process. But a detailed analysis of his data was impeded at the time by the lack of an adequate theoretical model.

Barot (1977) used an apparatus similar to that of Billings to obtain dendritic growth data for monosized latex aerosols with nine different particle diameters ranging from 1.09 to 2.02 μm. His data were also in agreement with simulation studies (Tien et al., 1977).

Bhutra and Payatakes (1979) studied on deposition of monodisperse aerosol particles on a single metal fiber under condition of dominant inertial impaction and

interception. They fed a neutralized solid methylene blue aerosol through an aluminium tube of 31 mm. diameter at the center on which a stainless steel fiber of 25 μm. diameter is located. During each run, the deposition process was interrupted at regular intervals and deposits on the same area of the fiber surface were examined; the angular positions of all individual dendrites, and their sizes and configurations were recorded and photographed. Their data were in accordance with the predictions of deterministic models developed and modified by Payatakes (1977) and Payatakes and Gradon (1980).

Kanaoka et al., (1980) proposed simulation results along with experimental ones from their study on the growth processes of particle dendrites on a dust loaded fiber. Sodium chloride and methylene blue particles were used as test aerosols. They were generated by an ultrasonic nebulizer and a vibrating orifice monodisperse aerosol generator. Their theoretical predictions agreed qualitatively well with experimental results, but the values of the collection efficiency raising factor λ were about half of the predicted ones. The discrepancy between the experiment and the simulation can be understood by considering the following facts: 1) the microstructures of filter are different, one by one, even if the packing densities of the filters are the same, 2) the structure of a real filter is more complicated than that of a filter assumed in the simulation, and 3) re-entrainment of captured particles from fibers in the filter have not occured in the simulation.

2.1.2 Air filtration by electret fiber

Emi et al.(1984) studied the collection efficiency of a single electret fiber measured by using monodisperse sodium chloride particles ranging from 0.01-0.4 μm in diameter for filtration velocity from 5 to 200cm/s, under different charging state of particles, i.e., uncharged, singly and doubly charged. It was found that experimental efficiency was markedly influenced by the small change in the charging state of particles.

Baumgartner et al.(1986) studied the determination of single fiber charge and collection efficiency. They found that fractional separation functions of different types of electret filters are presented for the particle size range from 10 nm to 10 μm at the filtration velocity of 10 cm/s. The initial efficiencies are compared to that of a conventional (glass fiber) filter and also to those of electret filters in discharged state. The results of long-term filtration experiments show that a complex time-dependent behavior exists for different filter materials. Furthermore, two experimental methods are presented and discussed which determine the charge characteristics of single electret fibers.

Hiragi (1995) studied how the agglomerates of uncharged and charged particles, respectively, change with filtration time and location on an electret fiber. When uncharged particles are collected, they attach all around the fiber and form chainlike agglomerates, which subsequently become irregular and complicated as the electrostatic effect gradually weakens. In the case of charged particles, the shape is similar to the former but agglomertes concentrate in a limited area of opposite polarity to the particles.

2.2 Modelling Study

In formulating a theoretical model of the phenomenon, two different approaches can be discerned: first is deterministic approach and, second is stochastic approach. The deterministic approach is formulating a mathematical model which there is no uncertainty in the values of the variables and parameters. Other, the stochastic approach is using the variables and parameters to describe the input-output relationship, that is, not known precisely but governed by certain probability laws. The stochastic approach is, in general, more difficult to work with than the deterministic approach, but in many cases stochastic approachs provide more insight into the characteristics and behavior of a real process. The deterministic approach has been pursued mostly by Payatakes (1976a, 1976b, 1076c, 1977, 1980a, 1980b) for interception, and/or convective diffusional, and/or inertial impaction, and, corresponding the stochastic approach for the same case have been carried out by Tien et al. (1977); Wang et al. (1977); Kanaoka et al. (1980, 1981, 1983).

2.2.1 Deterministic approach

Radushkevich (1964) was the first to model the growth of particle clusters on collectors. He assumed that a given dendrite can be completely characterized by the number of member particles. This implied that no distinction existed between member particle at different positions in a dendrite, so no prediction regarding the dendrite configuration is possible, even though configuration was a factor of primary importance in the determination of the effect of the dendrites on both filtration efficiency and resistance to flow. Furthermore, the facts that a new dendrite is generally of a slimmer structure protruding from the collector surface in to the bulk flow and that the probability of a new particle additions depends on the site of deposition along the dendrite suggest that the configuration of the dendrite should significantly affect its rate of growth.

Payatakes and Tien (1976) proposed a preliminary model of the formation of chain-like agglomerates on fiber during filtration of aerosols in fibrous media. Their work was intended for the description of filtration performance, both filtration efficiency and pressure drop, over the entire loading period. The model was limited to two assumptions; first, the dendrite layer adjacent to the collector could contain only one particles at most; second, the particles colliding with the upper half of a dendrite particle became members of the immediately higher layer. Then, they found that the idealized dendrite configurations predicted theoretically were in agreement with those observed experimentally for comparison a photograph of particles dendrites on a single fiber (Billing 1966).

Payatakes (1977) extended previous work, which consider only contribution of particle deposition from the tangential flow component by pure interception. He developed a revised and generalized version of the model. The major revisions were made: allowance is mad for collisions with a particle in a give dendrite layer that lead to retension in the same layer, radial as well as angular contribution to depositions are considered, and the dendrite layer adjacent to the collector is allowed to contain more than one particle. These revisions led to a substantially more realistic theoretical model. The behavior of this model was demonstrated in the simple case of deposition by pure interception. The present treatment of deposition by pure interception is more rigorous than and superseded that adopted in previous work.

Payatakes and Gradon (1980) extended the model to include the case of deposition by inertial impaction and interception mechanism. Also the shadow effect was incorporated in the analysis. Furthermore, the model can be readily extended to deal with the case of deposition by convective Brownian diffusion. They showed the calculated profiles of the expected dendrite configuration as a function of age and angular position and the transient behavior of a fibrous filter of different thickness. These observations were in agreement with experimental data.

Payatakes and Gradon (1980a) extended the model to include the case of submicron particles, where the main transport of the model is convective Brownian diffusion. They presented solutions for the cases of non-slip flow around the fiber; and nonslip, slip and free molecular flow around particles. They found that dendrites form over the entire fiber surface. Moreover, the profiles of the expected dendrite configuration depend strongly on the angular position. In addition, a larger interception parameter values lead to more pronounced dendrite deposition.

Tanthapanichakoon et al. (1993) has developed a simple population balance model for predicting dendritic growth of aerosol particles and the accompanying increase in the collection efficiency on a single fiber via convective diffusional deposition by using only a fast personal computer without requiring much computational time. The simulation results of the new simplified model agreed fairly with those obtained previous by Monte-Carlo simulation of the stochastic model. Although a new simplified model has required the optimal values of the parameters.

2.2.2 Stochastic approach for non-electret fiber

Tien et al. (1977) were the first to use stochastic approach to represent the random location of incoming particles in their simulation. They proposed model for the formation and growth of dendrites on a two dimensional collector in an aerosol stream. Their simulations were carried out on a cross section of the collector by taking into account the randomness of individual particles together with the corresponding trajectories determined from the equation of motion. The formation and growth of particle dendrites were simulated and found to resemble those obtained from experiments.

Wang et al. (1977) proposed two concepts; first, characteristic of particle in suspension in terms of their interaction with a collector surface, namely, the shadow effect created by deposited particles and the singular and, second, random behavior of approaching particles. The random distribution of approaching particles in their upstream positions were stochastic nature to the process, but the deterministic equations of particle motion were used. They have simulated the dendritic growth process on a sphere and a two dimensional cylinder. They found that their simulation resulted in insufficient depiction of true phenomenon.

Kanaoka et al. (1980, 1980a) have also simulated the growing process of particles dendrites on dust load fiber via Monte-Carlo simulation of stochastic model for inertial interception collection mechanism. Moreover, they found that the shapes of dendrites thus obtained agreed fairly well with experimental investigations and the ratio of a single fiber collection efficiency with dust load to a clean fiber was expressed as a linear function of the mass of deposited particles in a unit filter volume. In addition, the values of a collection efficiency raising factor λ were in qualitative agreement with previous experimental study.

Kanaoka et al. (1983) proposed a three-dimensional stochastic model to the case of deposition of aerosol particle by convective Brownian diffusion. This model was developed starting from Langevin's equation and used to simulate collection and

agglomeration processes of particles on a cylindrical fiber. The equation of motion of particles including the Brownian effect is considered. The effect of Peclet number, interception parameter and the accumulated mass of particles on a fiber were also discussed to obtain the distribution of captured particles on a fiber and the evolution of the collection efficiency of a dust-loaded fiber through the simulation. Furthermore, they found that the ratio of collection efficiency of dust-loaded single fiber to clean fiber was expressed as a linear function of the mass of particles in a unit filter volume. In addition, the coefficient in the linear function and collection efficiency raising factor depended on Peclet number and interception parameter.

Wongsri et al.(1991) also proposed a three-dimensional method for the stochastic simulation of dendritic growth of polydispersed particles for the case of convective Brownian diffusion. They found that this study were almost the same as those obtained for monodispersed aerosols and the range of standard deviation of polydispersity of aerosol particles did not affect the average performances of the dust-loaded fiber.

Areephant (1996) Studied the growth of dendrite on a fiber in an air filter by using the deterministic dendritic growth model which Tanthapanichakoon et al.(1993) developed on the basis of population balance. This model was modified for particle deposition via convective diffusion and via inertial impaction. The optimal parameter values of the model could be estimated by comparison with the stochastic simulation results.

2.2.3 Stochastic approach for electret fiber

Emi et al.(1984) studied collection efficiency of an electret filter, both theoretically and experimentally by means of monodisperse particles in different changing states, namely, uncharged, singly or doubly charged and charged in Boltzmann equilibrium. Moreover, the theoretical collection efficiencies of a single electret fiber were calculated by considering the effects of both induced and coulombic forces, and approximate expressions of the efficiencies were obtained for the induced force effect, coulombic force effect and the combined effect of both. Experimentally, the collection efficiency of the filter is markedly influenced by the small change in the charging state of particles, and both coulombic and induced forces affect the collection of particles simultaneously. Finally, a semi-empirical expression for the collection efficiency of a single electret fiber was obtained.

Emi et al.(1987) experimentally studied the collection performance of an electret filter by means of very fine particles in different charging states, that is, uncharged, singly or multiply charged and charged in equilibrium at filtration velocity ranging from 5 to 200 cm/sec. They found that a general expression of a single electret fiber efficiency for fine particles was obtained by considering Brownian diffusion together with coulombic and induced forces. The expression successfully explained the complex behavior of penetration curve of particles charging in equilibrium.

Hiragi (1995) studied experimentally and a practical three-dimensional simulation method for predicting the agglomerative deposition process of submicron aerosol particles on an electret fiber. The simulated results were shown to agree quite well with the experimental observations for both uncharged and charged particles dealing with gradient force and coulombic force respectively. This study leaded to prediction of how the morphology of particle accumulates on a constituent fiber changed and effected the collection efficiency and pressure drop of the filter under the dust-loaded condition. Furthermore, he applied fractal to explain directly the characteristic of dendrite.

Kanaoka (1998) reviewed the performance of a dust-loaded air filter on which particles deposit and form complicated accumulates, thus increasing in collection efficiency and pressure drop. Therefore, the following topics will be reviewed: 1.) The collection process of particles and morphology of particle accumulates on a single fiber plus experimental observation and computer simulation by various collection mechanism, 2.) collection efficiency and pressure drop of a dust-loaded filter, 3.) prediction of filter performance with dust load and 4.) improvement of filter service life.

Kanaoka et al.(2001) proposed a practical three-dimensional simulation method for predicting the agglomerative deposition process of submicron aerosol particles on an eletret fiber. The simulated results are shown to agree quite well with the experimental observations for both uncharged and charged particles. For the former only the gradient force, and for the latter the coulombic force needs to be considered as long as an oncoming particle has not come in close proximity to any previously deposited particles. In contrast, once the oncoming particle enters a region of close proximity to a deposited particle at the tip of a dendrite or chain-like agglomerate, it suffices to consider only the high-gradient or particle-string formative force in the present stochastic model.

CHAPTER 3
THEORY

The success of any simulation study depends on the appropriateness of its mathematical model. This chapter presents a brief discussion of the basic theory of aerosol filtration, and the basic principle of the stochastic model.

3.1 Fundamental Theory of Aerosol Deposition on a Filter Fiber

3.1.1 Kuwabara flow field

Kuwabara (1959) solved the Navier-Stokes equations for viscous flow. Figure 3.1 shows the flow cells in a fibrous filter consisting of parallel fibers, spaced randomly and transverse to the flow. The mean flow is directed from left to right with a velocity equal to U. The vorticity would be negative on the upper side of a cylinder and positive on the lower side of a cylinder. An ideal cell for the mathematical model is shown in Figure 3.2. Kuwabara considered that each cylinder of radius R_f is enclosed by an imaginary cylindrical cell of radius R_c. If there are n parallel fibers per unit volume of filter, the volume fraction or packing density α is

$$\alpha = n \pi R_f^2 \tag{3.1}$$

and Rc is adjusted so that

$$n \pi R_c^2 = 1 \tag{3.2}$$

Thus
$$R_c = \frac{R_f}{\sqrt{\alpha}} \tag{3.3}$$

The boundary conditions used by Kuwabara were that air velocity is zero on the surface of fiber. The stream function, ψ, and the velocity component, U_x, U_y and U_z, obtained by Kuwabara and expressed in dimensionless form are

$$\psi = \frac{Y}{2K}\left[(1-\frac{\alpha}{2})\frac{1}{X^2+Y^2} - (1-\alpha) + \ln(X^2+Y^2) - \frac{\alpha}{2}(X^2+Y^2)\right] \tag{3.4}$$

$$U_x = \frac{\partial \psi}{\partial Y}, \ U_y = \frac{\partial \psi}{\partial X}, \ U_z = 0 \tag{3.5}$$
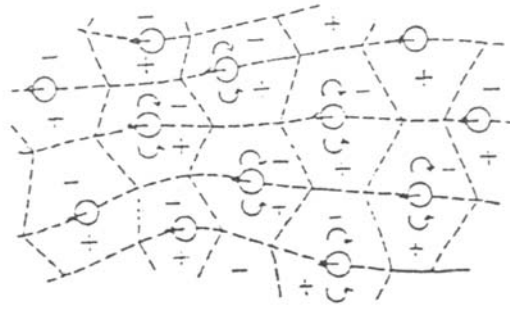
Figure 3.1a Vorticity around cylinder (the broken lines are zero vorticity)

Figure 3.1b Mean flow velocity around cylinder
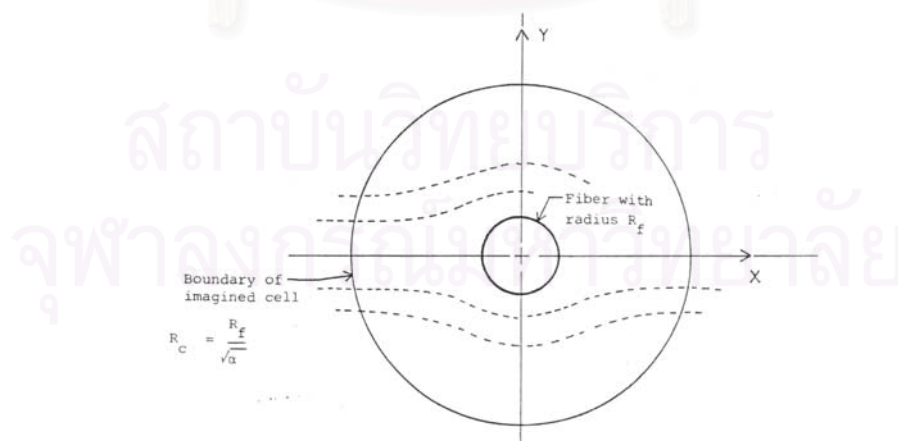
Figure 3.2 Cross section of Kuwabara's cell

where $K = -\dfrac{1}{2}\ln\alpha + \alpha - \dfrac{\alpha^2}{4} - \dfrac{3}{4}$ and $X = \dfrac{x}{R_f}$, $Y = \dfrac{y}{R_f}$, $Z = \dfrac{z}{R_f}$

3.1.2 Single fiber representation of a fibrous filter

A fibrous filter consists of a mass of fibers which are placed perpendicular to the direction of flow and oriented randomly. The single fiber may be used to explain the performance of a fibrous filter. The filter is thought of as a pad of thickness h at right angles to the airflow. Suppose the total length of every fiber in unit thickness of unit cross flow area is L. The packing density, α or volume fraction of the fibers is the ratio of the total volume of all the fibers to the volume of the filter. If R_f is the radius of the fiber, then

$$\alpha = \pi R_f^2 L \qquad (3.6)$$

If the filter consists of fibers of length L_i and radius R_{fi}, and so on

$$\alpha = \pi R_{fi}^2 L_i \qquad (3.7)$$

The definition of the dust collection efficiency of a single fibers, η, is the ratio of the distance between two the limiting streamline of the flow approaching the fiber to the fiber radius (cf. Figure 3.3).

$$\eta = \frac{Y}{R_f} \qquad (3.8)$$

The change in aerosol number concentration across a fibrous mat of thickness dx is given by

$$-\frac{dn}{dx} = \frac{2n\eta L R_f}{(1-\alpha)} \qquad (3.9)$$

where n is the number concentration of aerosol particles

From equation (3.6) and (3.9);

$$-\frac{dn}{n} = \frac{2\eta\alpha}{\pi(1-\alpha)R_f} dx \qquad (3.10)$$

Integrating across the thickness, h, of the filter gives

$$\frac{n}{n_0} = \exp[-\frac{2h\eta\alpha}{\pi(1-\alpha)R_f}] \qquad (3.11)$$

So, the total efficiency E of the filter composed of many fibers in the mat can be related to the single fiber efficiency η as follows

$$E = 1 - \frac{n}{n_0} = 1 - \exp[-\frac{2h\eta\alpha}{\pi(1-\alpha)R_f}] \qquad (3.12)$$
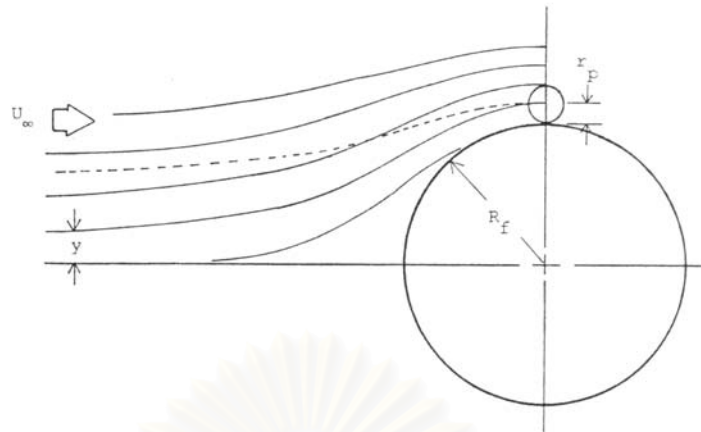
Figure 3.3 Streamlines near a cylinder cylinder fiber lying transverse to flow,
and the definition of single fiber efficiency

The values of the single fiber efficiency which are calculated from an accurate theory of deposition of aerosol particles on a single fiber, are higher than their experimental results because the dispersion of fibers in a real filter is non-uniform, some fibers might clump together, some screen one another and not all of them lie transverse to airflow.

3.1.3 Deposition mechanism.

The filtration by a fibrous air filter depends on several mechanisms. The important mechanism causing particle deposition, are interception, diffusion, inertial impaction, gravitational settling and electrostatic attraction. The single fiber efficiency η can be estimated as the sum of the individual efficiency caused by diffusion, η_D, interception, η_R, inertial impaction, η_I, gravitational settling, η_G and electrostatic attraction, η_E, mechanisms.

These five deposition mechanisms form the basis set of mechanisms for all types of aerosol particle deposition, including deposition in a lung, in a sampling tube, or in an air cleaner. The method of analysis and prediction is different for each situation, but the deposition mechanisms are the same. The first four mechanisms are called mechanical collection mechanisms. Each of five deposition mechanisms is described below, along with equations that predict the single fiber efficiency due to that mechanism. The theoretical analysis is complex, and only simplified equations are presented. Still, these equations are

accurate enough to show the trend of collection efficiency with filter parameters. Wherever possible, the equations are based on experimentally verified theory and except where noted, are valid for standard conditions and $0.005 < \alpha < 0.2$, $0.001 < U_0 < 2$ m/s (0.1-200 cm/s) and $0.01 < d_f < 50$ μm.

Interception

Even if a particle does not deviate from its streamline, if the distance between the particle to a capturing surface is less than one particle radius, the particle may be collected on the surface by the interception mechanism. The particle would adhere to it due to Van der Waal's force. The deposition by interception is shown in Figure 3.4c. This mechanism is directly related to the relative size of the particle. The dimensionless parameter describing the interception effect is the interception parameter R defined as the ratio of the particle diameter to the fiber diameter.

$$R = \frac{d_p}{d_f} \tag{3.13}$$

where d_p is the particle diameter and d_f is the fiber diameter.

If the Kuwabara flow field is used, the single fiber efficiency caused by interception can be expressed by

$$\eta_R = \frac{1+R}{2K}[2\ln(1+R) - 1 + \alpha + (\frac{1}{1+R})^2(1-\frac{\alpha}{2}) - \frac{\alpha}{2}(1+R)^2] \tag{3.14}$$

Diffusion

When a particle is very small, in the submicron order size, the main deposition mechanism is Brownian diffusion. Generally, the particle does not follow its streamline but continuously diffuse away from it. Thus the particle may be captured even on the rear surface. The deposition by diffusion is shown in Figure 3.4b. The diffusional deposition of particles increases when the particle size and air velocity decrease. From the convective diffusion equation describing this process, a dimensionless parameter called the Peclet number, Pe, can be expressed by

$$Pe = \frac{d_f U_\infty}{D_{BM}} \tag{3.15}$$

where U_∞ is the average air velocity and D_{BM} is the diffusion coefficient of the particle. The physical meaning of Peclet number is that Peclet number describes the relationship between diffusion and convection in a manner similar to the role played by the Reynolds

number in fluid flow. When the Peclet number is small, molecular diffusion predominates. When it is large, convective transport predominates and diffusion can be neglected (Reist, 1993). Moreover, the single fiber efficiency, based on Kuwabara flow field, can be expressed by (Stechkina and Fuchs, 1966)

$$\eta_D = 2.9K^{-\frac{1}{3}}Pe^{-\frac{2}{3}} + 0.624Pe^{-1} \tag{3.16}$$

$$\eta_{DR} = 1.24K^{-\frac{1}{2}}Pe^{-\frac{1}{2}}R^{\frac{2}{3}} \tag{3.17}$$

Inertial Impaction

A particle with a finite mass may not follow the streamlines exactly due to their inertia. If the streamlines are highly curved and the particle mass is high, the particle will deviate from the streamlines to collide with the capturing surface. The depostion by inertial impaction is shown in Figure 3.4a. Unlike the diffusion mechanism, the inertial impaction mechanism increases with an increase in particle size and/or air velocity. The effect of inertia on particle can be described by the dimensionless number Stokes number, St, defined as

$$St = \frac{C_m d_p^2 \rho_p U_\infty}{18\mu d_f} \tag{3.18}$$

The single fiber efficiency is calculated by Stechkina et al. (1969), using the Kuwabara flow field. Their expression gave

$$\eta_I = \frac{1}{(2K)^2}I.St \tag{3.19}$$

where $\qquad I = [(29.6 - 28\alpha^{0.62})R^2 - 27.5R^{2.8}]$

Gravitational settling

When a particle is in a gravitational force field, they will settle with a finite velocity. If the settling velocity is large, the particle may deviate from the streamlines and deposit on the capturing surface. The deposition by gravitational settling is shown in Figure 3.4d. The gravitational settling mechanism is important only for large particles and at low flow velocity. The dimensionless parameter governing the gravitational settling mechanism is

$$Gr = \frac{U_\infty}{V_g} \tag{3.20}$$

where V_g is the settling velocity of the particle.

The single fiber efficiency due to gravity, η_G, can be approximated (Davies 1973) as

$$\eta_G = \frac{Gr}{1 + Gr} \qquad (3.21)$$

Electrostatic deposition

Electrostatic deposition can be extremely important, but is difficult to quantify because it requires knowing the charge on the particles and on the fibers. Electrostatic collection is often neglected, unless the particles or fibers have been charged in some quantifiable way. Increasing the charge on either the particles or the fibers, or reducing the velocity, increases the collection efficiency. The theory of particle collection by charged fibers, charged particles or both is reviewed by Brown (1993). Charge particles are attracted to oppositely charged fibers by coulombic attraction. A neutral particle can also be attracted to a charged fiber: The electric field created by the charged fiber induces a dipole, or charge separation, in the particles. In the non-uniform field around the fiber, the near side of the particle experiences an attractive force that is greater than the repulsive force on the far side; hence, a net force exists in the direction of the fiber, and the particle migrates in that direction. Finally, a charged particle can be attracted to a neutral fiber at close range by image forces. The charged particle induces an equal and opposite charge in the fiber surface and thus creates its own field for attraction. Image forces are weaker than coulombic forces.

A single fiber collection efficiency is expressed by a function of dimensionless induced force and coulombic force parameter (K_{In}, K_C), neglecting mechanical collection mechanisms. The deposition by electrical force is shown in Figure 3.4e. The single collection efficiency is obtained as (Emi et al, 1987)

for uncharged particle or induced force

$$\eta_{In} = 0.18 K_{In}^{2/5} \qquad (3.22)$$

for charged particle or coulombic force

$$\eta_C = 0.2 K_C^{3/4} \qquad (3.23)$$

The following semi-empirical expression for the estimation of a single fiber collection efficiency was obtained taking account of two electrical force effects simultaneously.

$$\eta_E = 0.18 K_{In}^{2/5} + 0.2 K_C^{3/4} - 0.05 (K_{In} K_C)^{1/2} \qquad (3.24)$$

In actual filtration, Brownian diffusion is also effective to the collection of fine particle. Then taking account of Brownian diffusion and induced or coulombic force effect simultaneously, the following approximate expressions for uncharged and charged particle are obtained

for uncharged particle or induced force

$$\eta_{In} = 0.18K_{In}^{2/5} + 3.2Pe^{-2/3} \tag{3.25}$$

for charged particle or coulombic force

$$\eta_C = 0.2K_C^{3/4} + 3.2Pe^{-2/3} \tag{3.26}$$

a. Inertia, Inertia-Interception

d. Settling-Interception

(vertically downwards flow)

b. Diffusion, Diffusion-Interception

d. Settling-Interception (Horizontal flow)

c. Interception

e. Electrostatic, Electrostatic-Interception
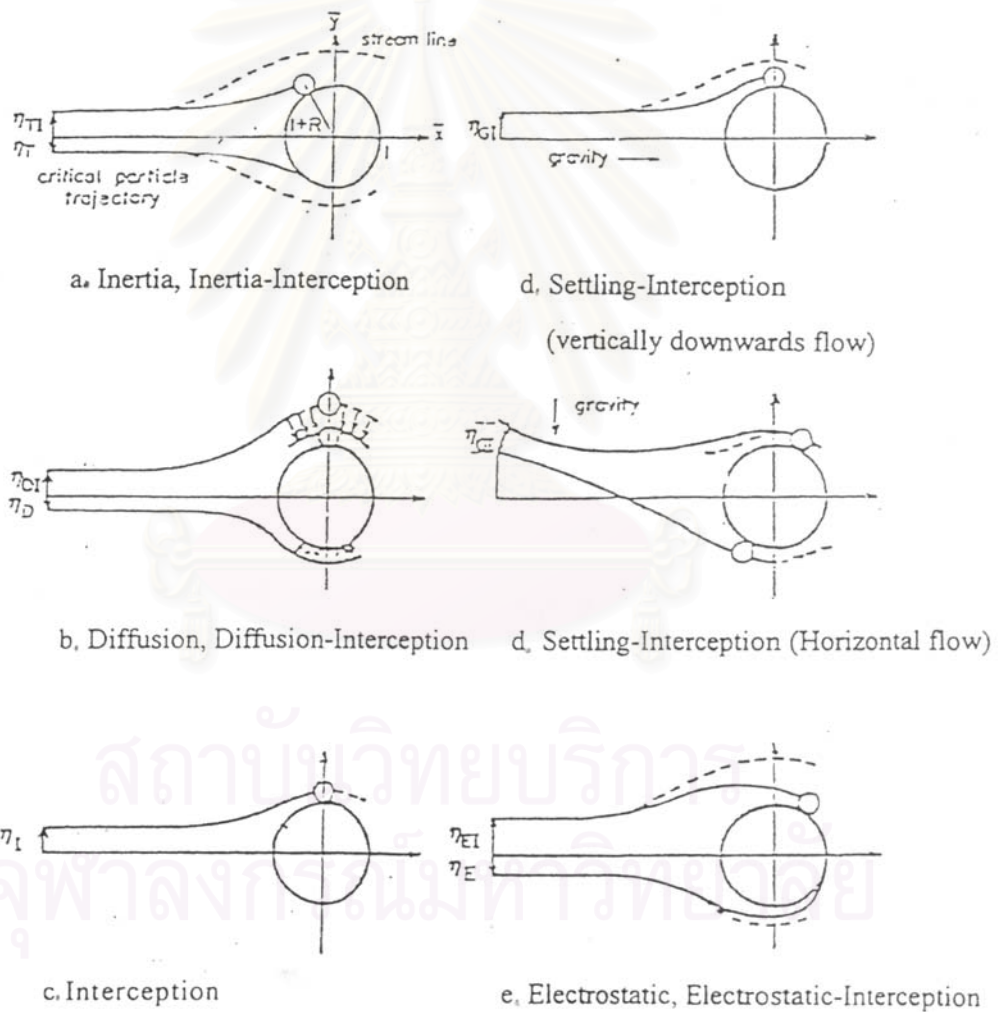
Figure 3.4 Deposition mechanisms of aerosol particle

3.2 The Stochastic Dendritic Growth Model for an Electret Fiber

Stochastic or random processes abound in nature such as the path of a particle in Brownian diffusional motion, the growth of population of bacteria ,and the mixing of pigment in plastics. If investigators would like to study these phenomena, they can easily make use of the theory of stochastic process.

This study extends the previous stochastic model (Kanaoka et al.,2001 and Hiragi, 1995) which was originally a stochastic model to simulate the induced force and coulombic force deposition of the aerosols via Monte Carlo method.

To calculate the collection performance of a single fiber, the motion of the aerosol particle can be described by Kuwabara stream function, which was shown in equation (3.4). Figure 4.1 is a schematic diagram of a representative fiber surrounded by Kuwabara's cell. Due to its stochastic nature, the uniform random number is used to represent the random location of each incoming particle at the generation plane of Kuwabara's cell. Furthermore, the standard normal random vector, n_{i-1}, in Equation 3.28 and 3.29 is acted as a direction vector of Brownian motion of each particle in the direction of x,y and z. The motion of each particle is governed by the Langevin's equation plus the effect of electrical force on particle, as follows

$$\frac{dv}{dt} = -\beta(v-u) + A(t) + \frac{FB}{\Delta t} \qquad (3.27)$$

where v is the velocity of the particle

u is the velocity of fluid stream

A(t) is a fluctuation force

F is external force

B is mobility of particle

3.2.1 Deposition via convective Brownian diffusion

In the case of convective diffusional deposition, the position p, P of a particle at time $t_i = t_{i-1} + \Delta t$ can be approximated by the following equation (3.28) and (3.29), respectively which was developed by Kanaoka et al. (1983)

$$p_i = p_{i-1} + u_{i-1}\Delta t + \sigma n_{i-1} + FB\,\Delta t \qquad (3.28)$$

where
$$\sigma = \sqrt{2 D_{bm} \Delta t}$$

σ is standard deviation

$n = (n_x, n_y, n_z)$ is a standard normal random vector with zero mean

Transform these variables to dimensionless form then equation 3.28 becomes

$$P_i = P_{i-1} + U_{i-1}\Delta\tau + 2\sqrt{\frac{\Delta\tau}{P_e}}\, n_{i-1} + F'B'\Delta\tau \qquad (3.29)$$

Here, the fluid velocity U of viscous flow across a random array of parallel fibers having packing density α is given by using equation (3.5), Pe is Peclet number. On the right of equation, the second term represents the convective movement of particle, the third term represents the diffusion movement of particle and the last term represents electrical force.

F'B' is electrical dimensionless term is meant to use for both uncharged and charge particle and defined as

for uncharged particle: $\qquad\qquad F'B' = K_{In}F_g \qquad\qquad (3.30a)$

for charged particle: $\qquad\qquad\quad F'B' = K_C F_c \qquad\qquad (3.30b)$

In addition, the equations to find these electrical parameters are shown below. Dimensionless electrical parameters

$$K_C = \frac{C_m n_p e \overline{\sigma}}{6\varepsilon_0 (1 + \varepsilon_f)\mu d_p u} \qquad (3.31a)$$

$$K_{In} = \frac{C_m \pi^2 \overline{\sigma}^2 d_p^2 (\varepsilon_p - 1)}{6\varepsilon_0 (\varepsilon_p + 2)(1 + \varepsilon_f)^2 \mu d_f u} \qquad (3.31b)$$

In the case of non-electret fiber, electrical term is omitted and equation (3.29) becomes equation (3.32)

$$P_i = P_{i-1} + U_{i-1}\Delta\tau + 2\sqrt{\frac{\Delta\tau}{P_e}}\, n_{i-1} \qquad (3.32)$$

3.2.2 Deposition via inertial impaction

In the case of the inertial impactional deposition, the position of a particle at time $t_i = t_{i-1} + \Delta t$ can be approximated by the following equations (3.33) and (3.34)

$$St\frac{d^2X}{dt^2} + \frac{dX}{dt} - U_x = BF_x \tag{3.33}$$

$$St\frac{d^2Y}{dt^2} + \frac{dY}{dt} - U_y = BF_y \tag{3.34}$$

For the case of non-electret fiber, this equation is reduced to equation (3.35) and (3.36)

$$St\frac{d^2X}{dt^2} + \frac{dX}{dt} - U_x = 0 \tag{3.35}$$

$$St\frac{d^2Y}{dt^2} + \frac{dY}{dt} - U_y = 0 \tag{3.36}$$

In short, Equations (3.29),(3.33) and (3.34) can be used to simulate the movement of a particle in Kuwabara's cell for electret fiber. To complete the stochastic simulation of the dendritic growth on an electret fiber, the following assumptions have been made.

1) Existence of dendrites on the fiber has little effect on the flow field around the fiber.

2) Spatial and time distribution of the incoming particles are random microscopically.

3) The next particle will not enter the Kuwabara's cell until the present one in it either deposits or passes through the cell.

4) A particle is always retained once it is captured on a dendrite or fiber surface.

5) There is no re-entrainment or detachment of captured particles or dendrites from the fiber.

6) The inlet particle size is uniform.

7) Both positive and negative charges on fiber surface are permanent.

8) Charge on each particle is equal to –1.

CHAPTER 4
SIMULATION PROCEDURE

Simulation is a powerful technique for solving a wide variety of problems and imitates the behavior of a system or phenomena under study. The basic idea behind simulation is simple, namely, to model the given system by means of mathematical equations, and then determine its time-dependent behavior. The simplicity of the approach, when combined with the computational power of a high speed personal computer, makes simulation a powerful and efficient apparatus. Fundamentally, simulation is used when either an exact analytical expression for the behavior of the system under investigation is not available, or the analytical solution takes too much time or cost.

In modeling natural phenomena, two different approaches are available : deterministic and stochastic. Deterministic models are those in which each variable and parameter can be assigned a definite number, or a series of definite numbers, for any given set of conditions. In contrast, for stochastic or random models, uncertainty is introduced. The variables or parameters used to describe the structure of the elements (and the constraints) may not be precisely known. The former approach is less demanding computationally than the latter and could frequently be solved analytically.

To represent random variables, a source of randomness is required. A random number generator and its appropriate use play significant roles of any simulation experiments involving a stochastic system. Methods of generating random numbers are obtained by Tanthapanichakoon (1978).

This chapter presents the simulation procedure of the stochastic model for non-electret and electret fiber, as well as the trajectory of particles at various electrical conditions including twist angle of fiber and flow chart of stochastic simulation procedure.

Algorithm for the Simulation of Non-electret and Electret Stochastic Model

The stochastic variable may be composed of deterministic and random components. The deterministic velocity component is described by the equation of motion of a particle. The random position at the aerosol generation plane of Kuwabara's cell is represented by a uniform random number. Furthermore, the dimensionless radius of the Kuwabara's cell (R_c) is related to the packing density α by

$$R_c = \frac{1}{\sqrt{\alpha}}$$

(4.1)

The total length of the fiber is subdivided into 5 sections with length Z_1, Z_2, Z_3, Z_4, Z_5, respectively (Figure 4.1). However, the effective length of the fiber was Z_3, which was expected to resemble those obtained from using a very long fiber. Here the length of the generation plane Zgen=$Z_1 + Z_2 + Z_3 + Z_4 + Z_5$ with Z_1=Z_5, and Z_2=Z_4.

For the case of electret fiber, there are so many kinds of forces acting on both particles and fiber. Coulombic forces F_C (between the particle and fiber), F_{CP} (between the particle and another nearby particle) and image force F_I come into play only when a particle has electric charge. For both charged and uncharged dielectric particles, the long-range non-uniform electric field around the electret fiber and the agglomerates lead respectively to the long-range gradient force F_G and particle-string formative or high-gradient force F_R. Under typical filtration conditions, Hiragi (1995) has calculated that F_R becomes dominant when an oncoming particle comes in close proximity to a deposited particle and that, until this proximity region is reached, only either F_C in the case of charged particles or F_G in the case of uncharged particles need to be considered. His conclusions agree with Zebel (1963) and are adopted here.

The ideal distribution of charges on the electret fiber surface is applied here. It is assumed that the surface charges will not decay as particles deposit on the fiber. The flow of fluid around the fiber is Kuwabara flow. For uncharged particles, the trajectory of an oncoming uncharged particle is essentially determined by the gradient force F_G except in a region of close proximity to a deposited particle. Since F_G depends only on the radial coordinate r and not on the polarization direction γ, the simulation region shown in Figure 4.2 is general and convenient to use. For charged particles, the coulombic force F_C essentially determines the trajectory, except in the region of close proximity to some deposited particle. Since F_C depends on the polarization direction γ as well as the
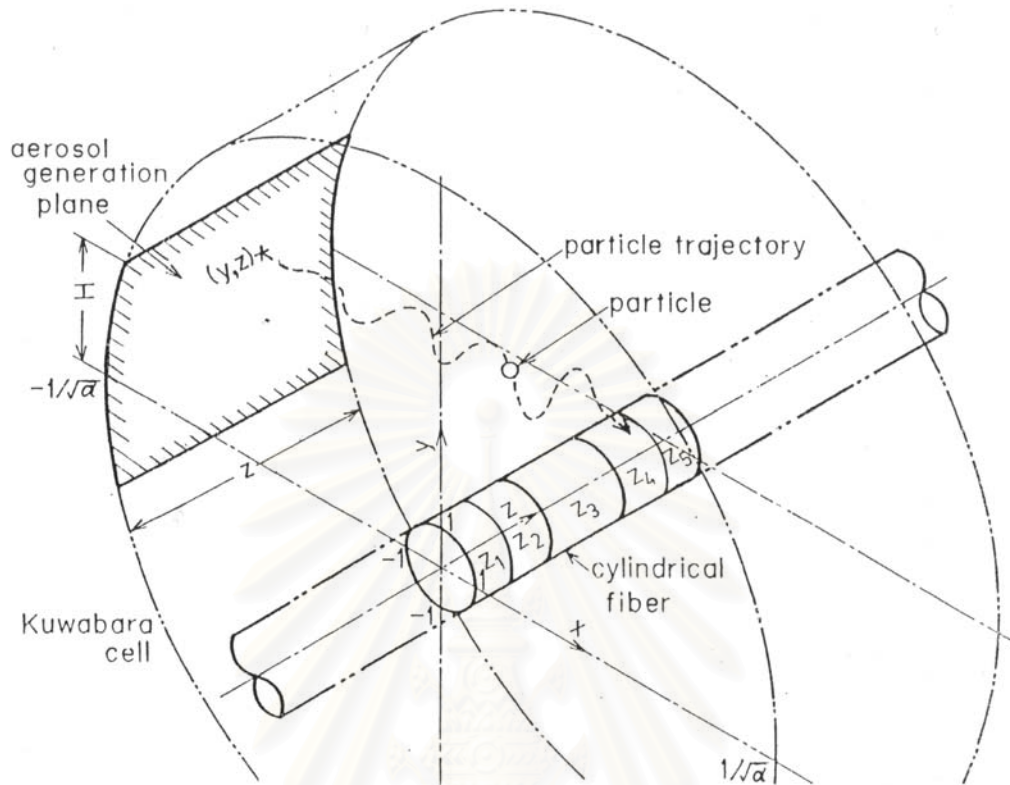
Figure 4.1 Schematic diagram of Kuwabara's cell

coordinates r and θ, the resulting trajectory changes drastically with γ. Figure 4.2 illustrates the effect of γ on the trajectories.

Using the stochastic model described in Equation (3.4), (3.5), (3.29), (3.33) and (3.34), the simulation is carried out according to the following procedure.

1. The starting point P_0 of an incoming particle was chosen randomly on the generation plane, which overlaps the cell surface and has height 2H and width Z. Two mutually independent uniform random number, Y_0 and Z_0, (-H ≤ y_0 ≤ H, 0≤ z_0 ≤ Z), were generated by using subroutine RANDOM (Tanthapanichakoon, 1978) to give $K_0 = (-\sqrt{R_c^2 - y_0^2}, y_0, z_0)$.

2. For convective Brownian diffusional deposition, the movement of the particle at each successive time interval, Δt, is simulated by using the equation (3.29), and the next position vector P_i was calculated. The random component in equation (3.29) uses three mutually uncorrelated standard normal random numbers, nx, ny, and nz, which are
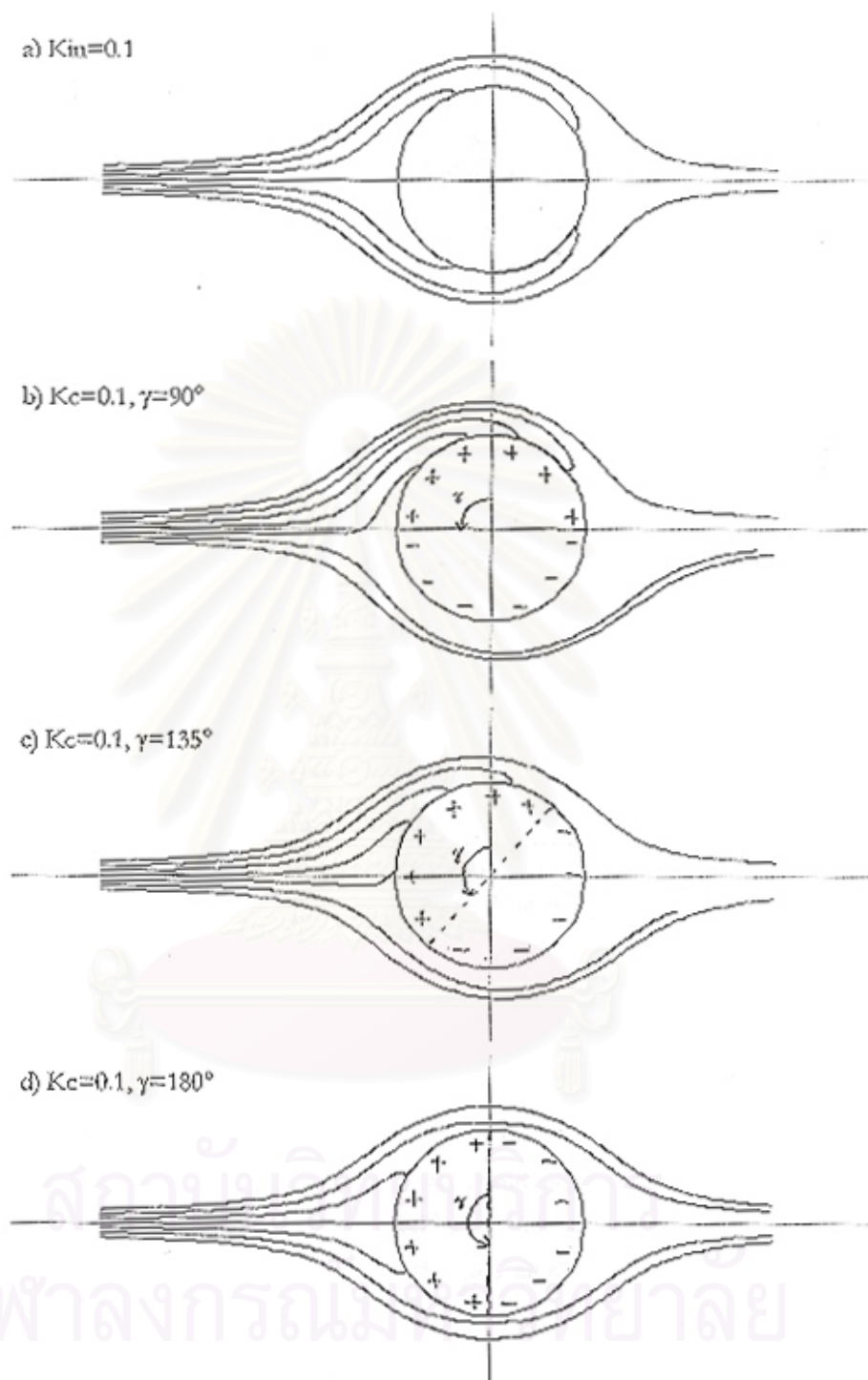
Figure 4.2 Particle trajectories of uncharged and charged particles for a
                    cylindrical fiber

generated by using subroutine RND (Tanthapanichakoon, 1978). In contrast, in the case of inertial impaction deposition, the next position vector P_i of the particle at each time step, was calculated by using the equation (3.33) and (3.34).

3. The new position vector P_i at the end of the each time step is checked to see whether the particle has come in close proximity to the end of deposited particle or dendrite tip. If it does so, its movement is controlled by the high-gradient force F_R which is prominent only at the tip of the particle string (dendrite). Thus only the electrostatic field around the dendrite tip needs to be considered. Once an oncoming particle enters this projected hemisphere of influence of the high-gradient field at the dendrite tip, it is assumed to deposit at the center of the hemisphere. And the location of captured particle is stored as you see in Figure 4.3.
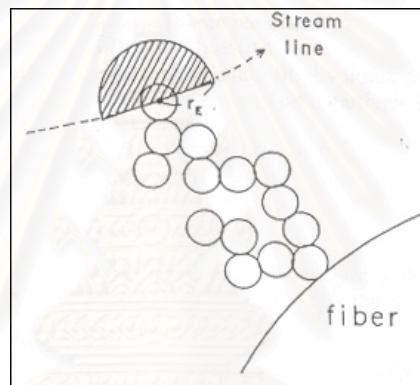
Figure 4.3 Region of high gradient electrostatic field

4. However, if an oncoming particle is not in radius of hemisphere of influence, then the model of diffusion mechanism is used to check that particle has collided on the fiber surface or with any of the previously captured particles. If collision has occurred the coordinates of the location of capture is stored, and step 5 is executed next. If no collision has occurred, step 2, 3 and 4 are repeated until the particle either is captured or moves out of the boundary of Kuwabara's cell.

5. Steps 1, 2, 3 and 4 are repeated until one of the dendrites on the fiber surface grows up to a predetermined height of given-particle layer.

6. Steps 1, 2, 3, 4 and 5 are repeated for a number of samples to yield enough information for stochastic analysis.

       7. For the case of non-electret fiber, the equations in step 2 are replaced by equation (3.32) for Brownian diffusion and (3.35) and (3.36) for inertial impaction process. Moreover, step 3 will be omitted in the case of ordinary fiber.

       A flow chart of the computational procedure is given in Figure 4.4. Monte Carlo simulations are carried out under various filtration conditions. However, the packing density of the filter α and the particle density ρ_p are fixed at 0.06 and 1000 respectively. Time step Δt and fiber length Z are the two most important parameters which control the accuracy and computational time of the simulation. A short time step and a longer fiber length would enhance accuracy but consume very large computer memory and much computational time. Their suitable values in previous study (Kanaoka et al., 2001 and Hiragi, 1995) are adopted in this study. A compromise of 50 samples is selected in this study.

Figure 4.4 Flow chart of the stochastic simulation procedure

CHAPTER 5
VALIDATION OF STOCHASTIC MODEL

In this chapter, the importance of various kinds of mechanisms is taken into account case by case. Mechanisms considered here are composed of convective diffusion, inertial impaction, electrical deposition, electrical deposition plus convective diffusion and electrical deposition including inertial impaction.
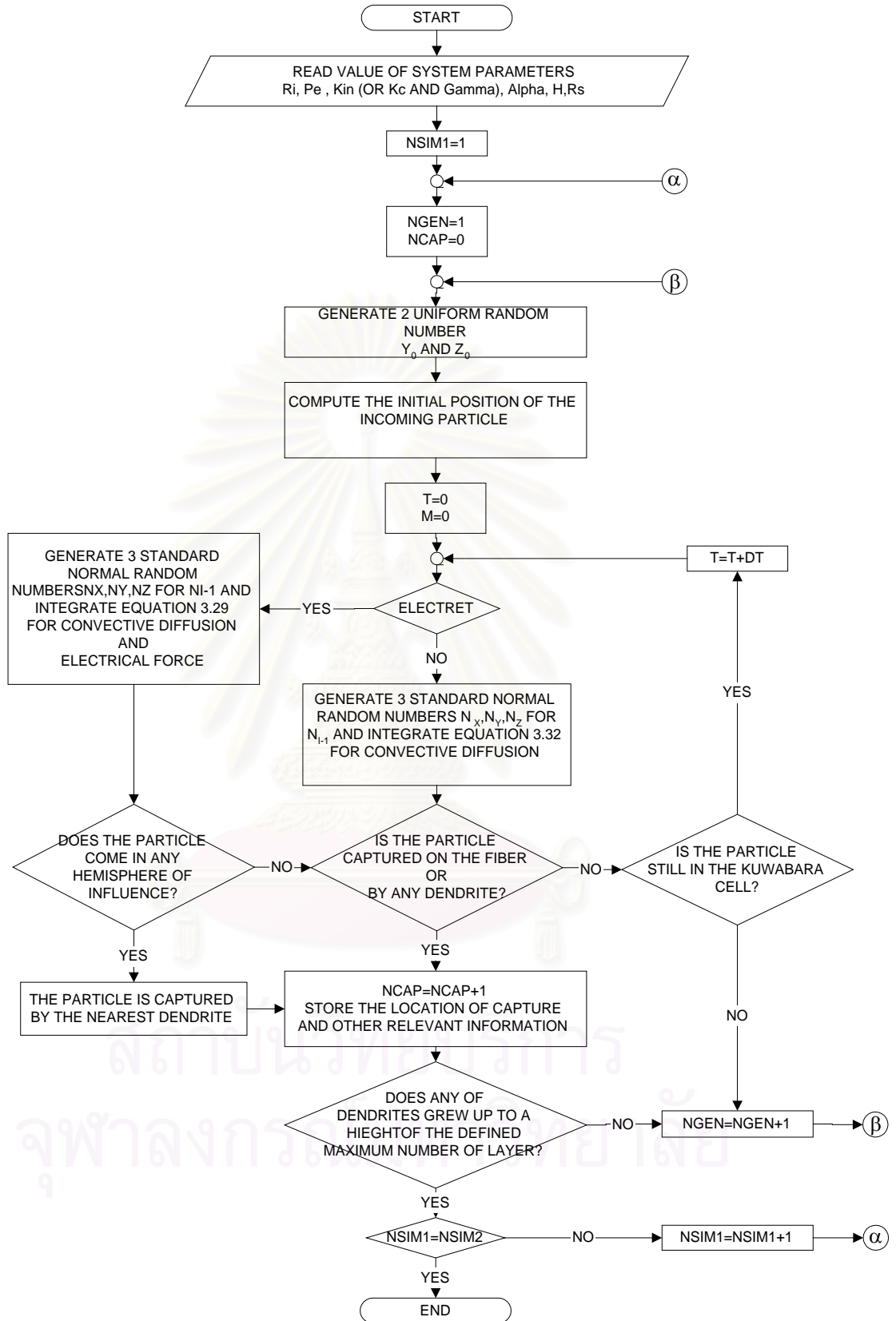
5.1 Case of Diffusion Mechanism

The Brownian motion of small particles is sufficient to greatly enhance the probability of their hitting a fiber while traveling past it on streamline for non-electret fiber mentioned in section 3.1.3. The single fiber collection efficiency is expressed in equation (3.16) and (3.17) based on correlation of Stechkina and Fuchs (1966) and shown in Table 5.1.

In this section, Morphology and clean fiber collection efficiency are discussed. Figure 5.1 is a sample of simulation results to show the typical morphology of the dendrites of diffusion mechanism for the case of Ri=0.05 and Pe=1000, referred as basis condition. The configuration of dendrites is densely packed all over the entire fiber surface.

Table 5.1 Clean fiber efficiency for convective diffusion for case of Ri = 0.05 and Pe=1000

Mechanism	Clean Fiber Efficiency (%)	
	Correlation	Simulation
Diffusion	3.93	3.78

Clean fiber collection efficiencies are shown in Table 5.1. These results derived from correlation and simulation have included interception mechanism. It is obvious that the values are slightly different. The discrepancy between the experiment and the simulation can be understood by considering the following facts (Kanaoka, 1980):

1) the microstructures of filter are different, one by one, even if the packing densities of the filters are the same

2) the structure of a real filter is more complicated than that of a filter assumed in the simulation and

3) re-entrainment of captured particles from fibers in the filter has not occurred in the simulation.
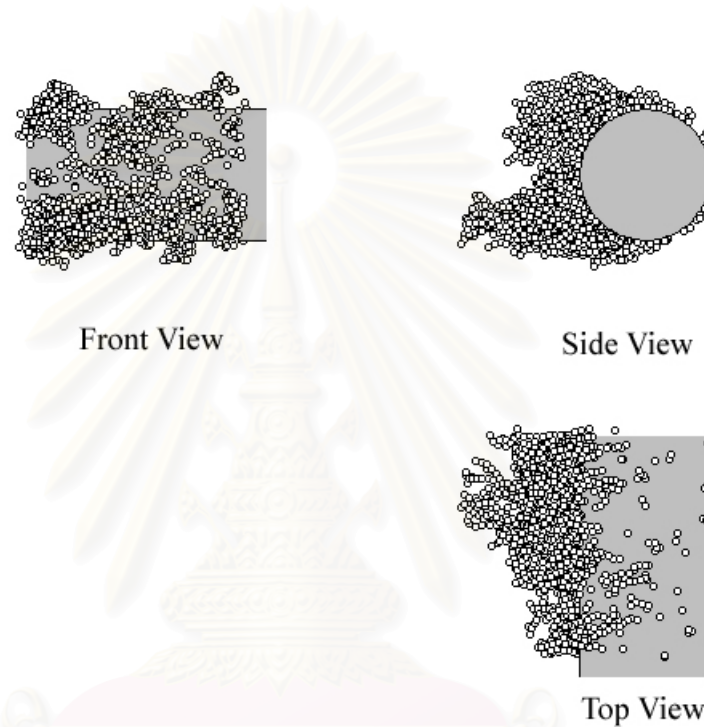
Figure 5.1 Typical configuration of dendrite for the case of Ri = 0.05 and
Pe= 1000

5.2 Case of Inertial Impaction Mechanism

Inertial impaction of a particle on a fiber occurs when the particle, because of its inertia, is unable to adjust quickly enough to the abruptly changing streamlines near the fiber and crosses those streamlines to hit the fiber. The clean fiber collection efficiency, stated in section 3.1.3, derived from Stechkina's correlation, is shown in Table 5.2 including effect interception parameter. Equations of collection efficiency of this mechanism are equation (3.18) and (3.19).

Table 5.2 Clean fiber efficiency for inertial impaction for case of Ri= 0.05
and Stk=0.1

Mechanism	Clean Fiber Efficiency (%)	
	Correlation	Simulation
Inertial impaction	0.59	0.61

Sample of typical configuration of inertial impaction is illustrated in Figure 5.2 for
the case of Ri=0.05 and Stk= 0.1. It is clear that particles are captured only on the front
surface of the fiber or near the stagnation point and dendrites are tall.
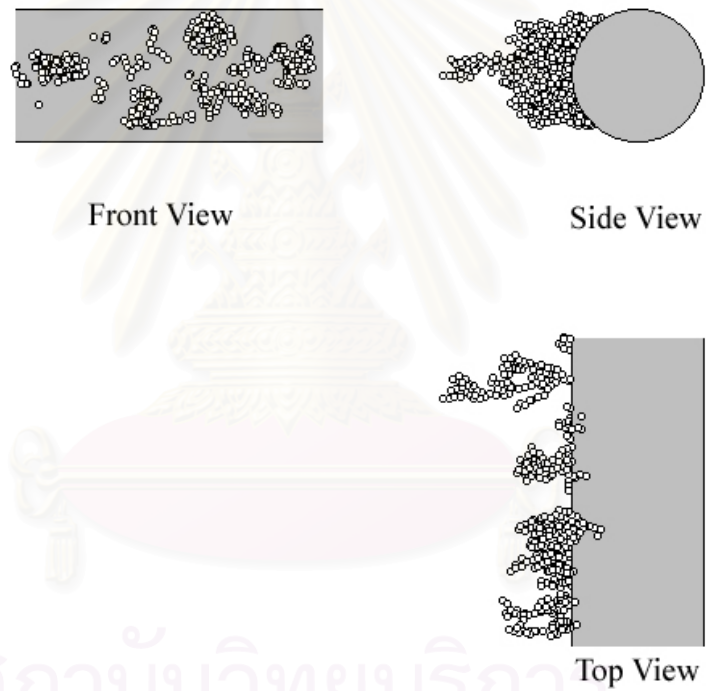

Front View   Side View

Top View

Figure 5.2 Typical configuration of dendrite for the case of Ri = 0.05 and
Stk= 1000

5.3 Case of Electrical Deposition Mechanism

Electrical deposition mechanism is the main mechanism in this study and is categorized into 2 parts, namely, induced force deposition for uncharged particle and coulombic force deposition for charged particle. Electrical deposition is extremely momentous but difficult to quantify because it requires knowing the charge on the particles and on the fiber. As mentioned in section 3.1.3, for electret fiber, the clean fiber collection efficiency can be obtained from equation (3.22) for uncharged particle and equation (3.23) for charged particle and equation (3.24) for considering both electrical forces simultaneously and can be seen in Table 5.3 including interception parameter effect. These equations are based on Emi's correlation (Emi, 1987).

In this section, morphology and clean fiber collection efficiency of deposited particles are discussed. Figure 5.3 and 5.4 are illustrations of simulation results to show the typical morphology of the dendrites of electrical deposition mechanism for the case of uncharged and charged particle respectively. The conditions used in this section are Ri=0.03 K_{In}=0.004, K_C=0.016 and Gamma = 90.

Table 5.3 Clean fiber efficiency for electrical deposition for case of Ri = 0.03,
K_{In}=0.004, K_C=0.016 and Gamma = 90

Mechanism	Clean Fiber Efficiency (%)	
	Correlation	Simulation
Induced force	2.09	1.16
Coulombic force	1.02	1.25

From Figure 5.3, for the case of uncharged particles, the configurations of dendrites are collected on the fiber surface and form chainlike agglomerates. The rear area of fiber is still clean, that means, no particles are captured on this area. However, these phenomena quite disagree the experimental results on which particles are captured all over surface of fiber. For Figure 5.4, the coulombic effect is concerned. It is so apparent that the agglomerates concentrate in a limiting area of opposite polarity to the fiber.
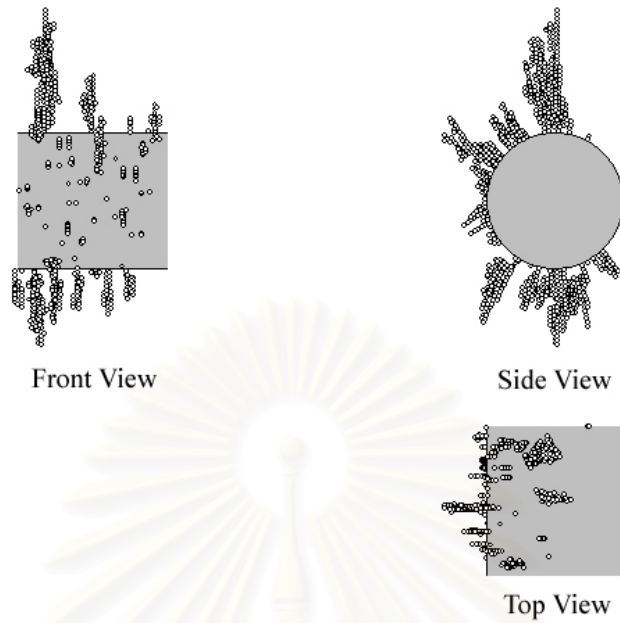
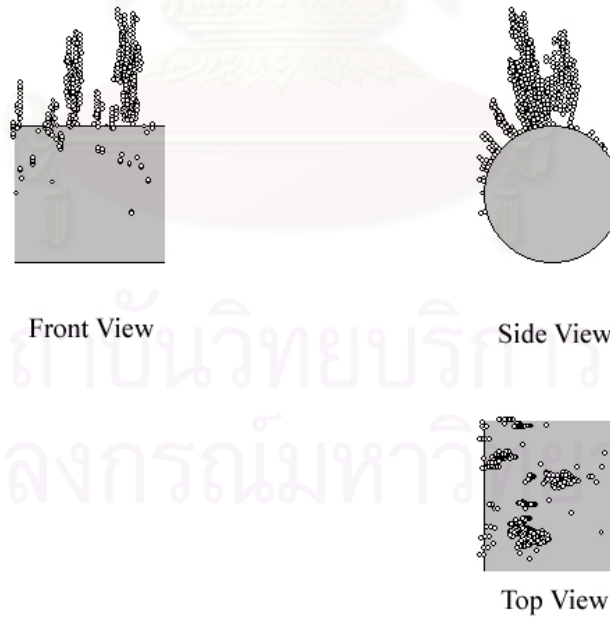Figure 5.3 Typical configuration of dendrite for the case of Ri = 0.03 and
K_{In}=0.004

Figure 5.4 Typical configuration of dendrite for the case of Ri = 0.03,
K_C=0.016 and Gamma = 90

5.4 Case of Electrical Deposition and Diffusion Mechanism

From section 5.3 considering only the electrical effect, the simulated results do not agreed well with experimental results because of morphology of the dendrites. However, when convective diffusional deposition mechanism is included in the model, the simulated results are more realistic and agree well with experimental results especially those with lower Peclet number.

In this section, morphology and clean fiber collection efficiency of deposited particles are discussed. Figure 5.5 and 5.6 are illustrations of simulation results to show the typical morphology of the dendrites of electrical deposition mechanism plus convective diffusional deposition for the case of uncharged and charged particle respectively. In addition, Figure 5.7 and 5.8 show the configuration of the dendritic growth with respect to time. The conditions used in this section are the same that used in Prof. Kanaoka's experiment, those are, Pe=50000, K_{In}=0.004, K_C=0.05 and Gamma = 90 except for interception parameter Ri=0.013.

Collection efficiencies shown in Table 5.4 are based on Emi's theory plus not only diffusion effect but also interception parameter effect. Clean fiber efficiency for induced force effect derived from correlation is higher than that from simulation because at Pe =50000, velocity calculated from equation (3.15) is more than experimental condition limited in the paper (Emi, 1987) ranging from 5-200 cm/s.

Table 5.4 Clean fiber efficiency for electrical deposition and convective
diffusion for case of Ri = 0.03, Pe=50000, K_{In}=0.004, K_C=0.016
and Gamma = 90

Mechanism	Clean Fiber Efficiency (%)	
	Correlation	Simulation
Induced force and Diffusion	2.33	1.22
Coulombic force and Diffusion	1.26	1.28

Morphology shown in Figure 5.5 and 5.6 are slightly different from Figure 5.3 and 5.4. because of low Peclet number. The lower Peclet number is, the more realistic morphology of simulated results becomes. This fact can be seen in chapter 6.
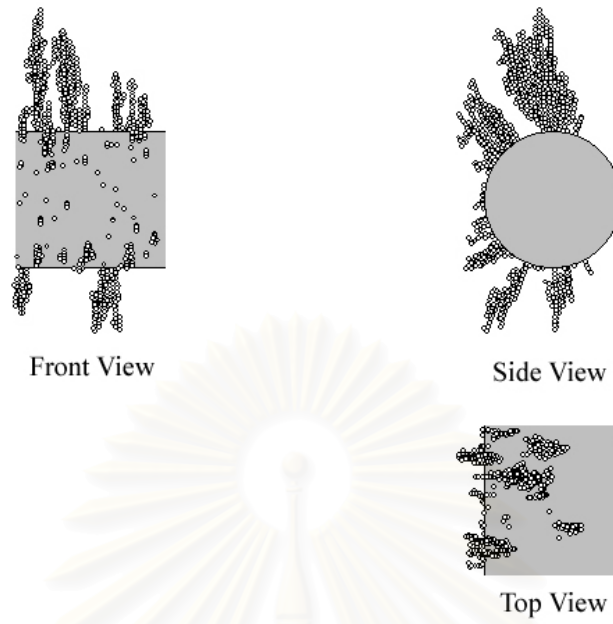
Figure 5.5 Typical configuration of dendrite for the case of Ri = 0.03,
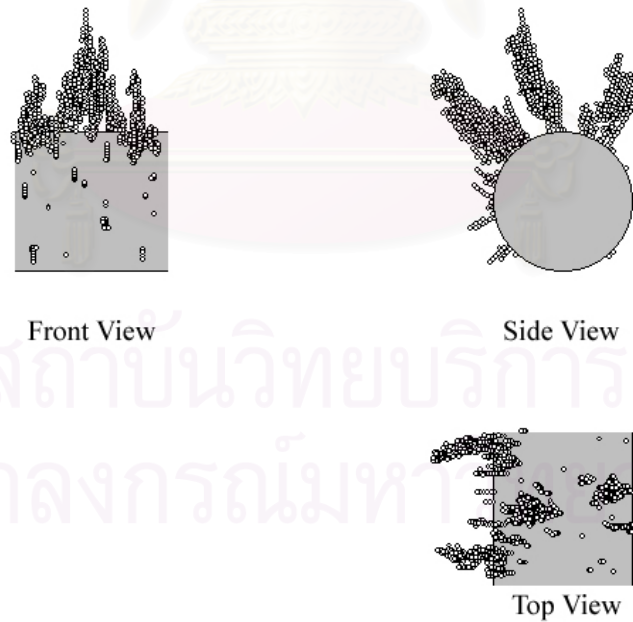K_{In}=0.004 and Pe = 50000

Figure 5.6 Typical configuration of dendrite for the case of Ri = 0.03,
K_C=0.016, Gamma = 90 and Pe = 50000

Front View   Side View

Ngen = 3000
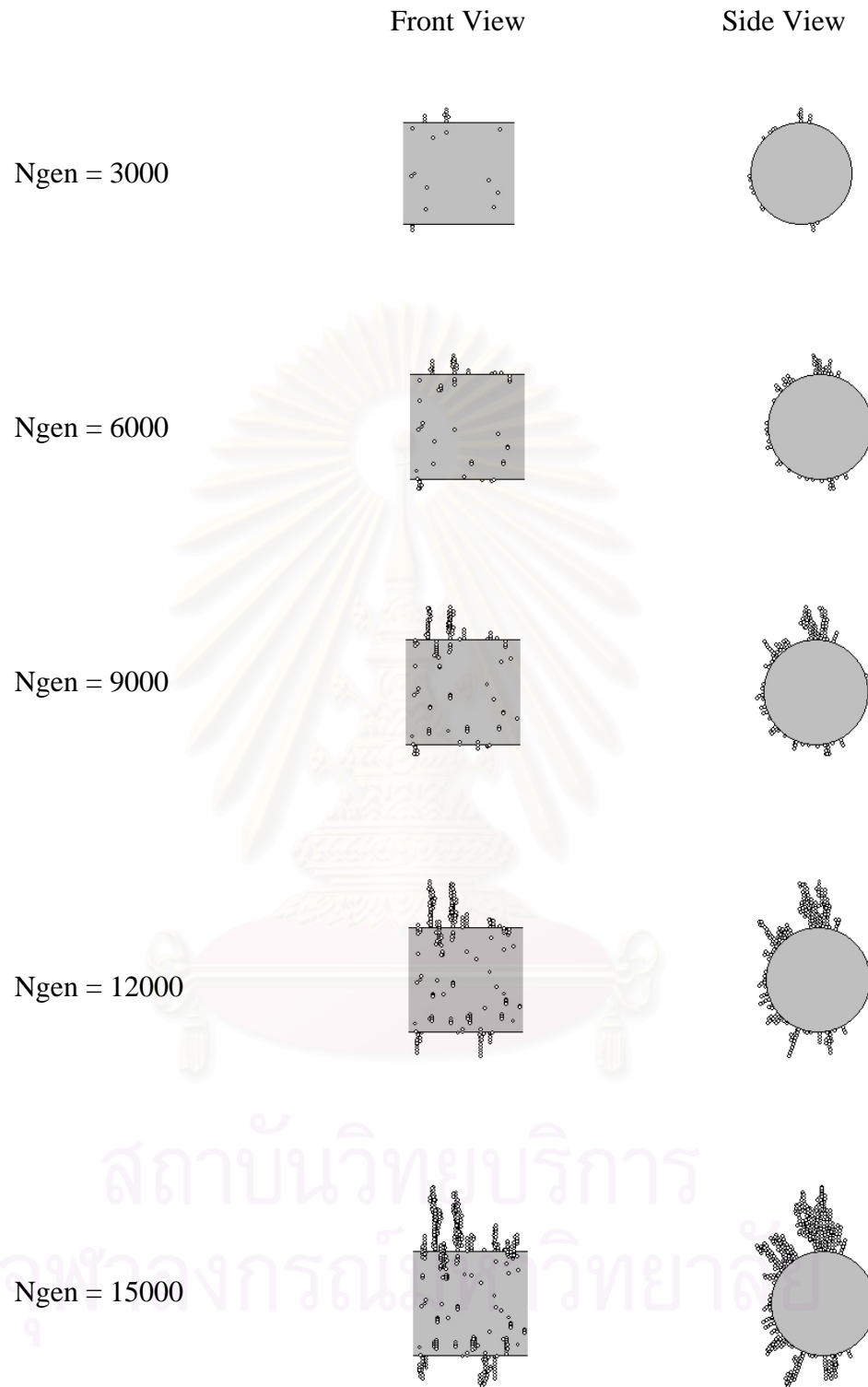
Ngen = 6000

Ngen = 9000

Ngen = 12000

Ngen = 15000

Figure 5.7 Time dependency of particles agglomerates on a fiber for the
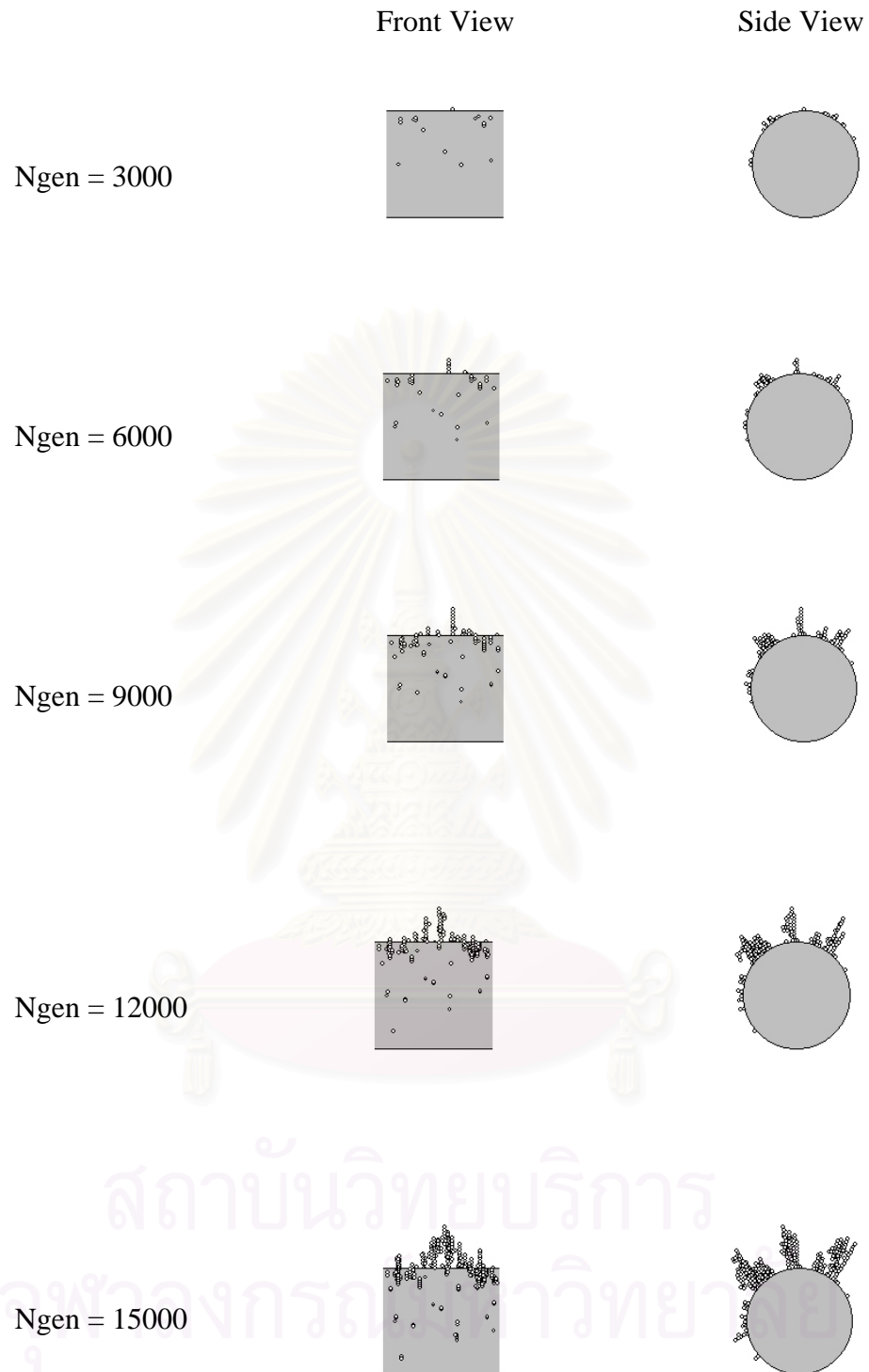
case of Ri=0.03, K_{In} = 0.004 and Pe= 50000

Figure 5.8 Time dependency of particles agglomerates on a fiber for the
case of Ri=0.03, K_C = 0.016, Gamma = 90 and Pe= 50000

5.5 Case of Electrical Deposition and Inertial Impaction Mechanism

Like section 5.4, section 5.3 considering exclusively the electrical effect, the simulated results do not agreed well with experimental results because of morphology of the dendrites. For this section, inertial impaction mechanism is incorporated to compare with experimental results. The clean fiber efficiency and morphology are investigated shown in Table 5.5, Figure 5.9 and 5.10 respectively with experimental conditions except for Ri=0.013. There is previous work for this blending mechanism run by Prof. Kanaoka. He assumed that Stoke number has negligible effect and can be ignored. However, for the sake of completion, these mechanisms have to be proved.

Table 5.5 Clean fiber efficiency for electrical deposition and inertial
impaction for case of Ri = 0.03, Stk= 0.015, K_{In}=0.004,
K_C=0.016 and Gamma = 90

Mechanism	Clean Fiber Efficiency (%)	
	Correlation	Simulation
Induced force and Inertial impaction	2.11	1.05
Coulombic force and Inertial impaction	1.04	1.16

Compared with Table 5.3, Table 5.5 has slightly different values for both induced and coulombic force. Furthermore, morphologies of dendrites for both in Figure 5.3 and 5.9 for induced force and in 5.4 and 5.10 for coulombic force look the same, in that particles are captured only on the limiting area on opposite polarity to the fiber for the case of charge particles and for the case of uncharged particles, they deposit almost all around fiber with chainlike form. For this reason, we can conclude that the effect of inertial impaction is negligible compared with electrical deposition mechanism.
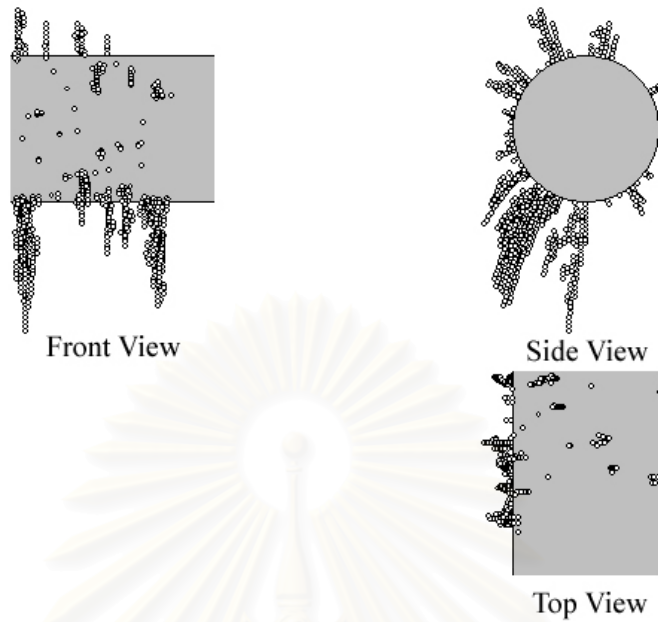
Figure 5.9 Typical configuration of dendrite for the case of Ri = 0.03,
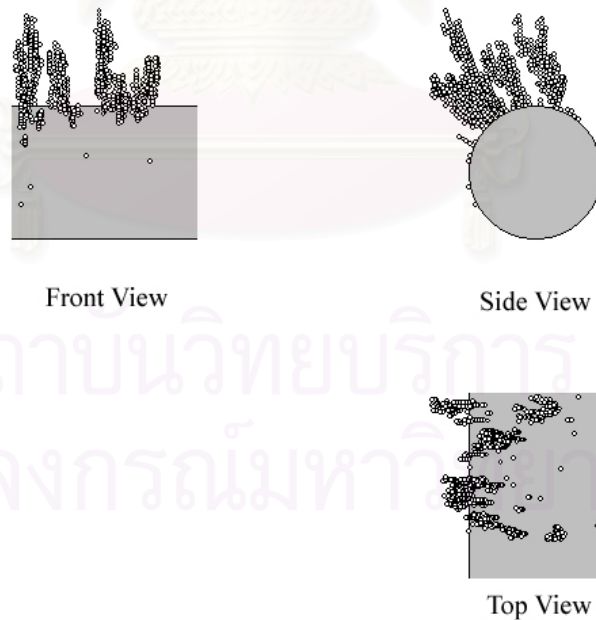K_{In}=0.004 and Stk = 0.015

Figure 5.10 Typical configuration of dendrite for the case of Ri = 0.03,
K_C=0.016, Gamma = 90 and Stk = 0.015

5.6 Selection of Present Stochastic Model

Prior to the conclusion which model is suitable for simulation on an electret fiber, first experimental results done by Prof. Kanaoka will be discussed. Figure 5.11 and 5.12 are results for uncharged particles at low and high dust load, respectively. And Figure 5.13 and 5.14 are the results for charged particles with at low and high dust load (Kanaoka et al., 2001 and Hiragi, 1995).

Figure 5.11 and 5.12 show the deposition pattern of particle on an electret fiber by induced force effect. When induced force dominates, i.e., uncharged particles are collected, they are uniformly collected all around the fiber surface regardless of charge distribution on the fiber at the initial stage and most of them form chainlike agglomerates and grows almost perpendicular to the surface until certain height. Then the shape of agglomerates becomes random and complicated, probably because induced force is no more effective at higher region, but shading effect of agglomerates increases.

Figure 5.13 and 5.14 illustrate the deposition pattern of particle on an electret fiber by induced force effect. When coulombic force is prevailing, i.e., charged particles are collected, the shape of agglomerates itself is similar to the case of induced force effect but chain length is much longer than the former.

From this section and section 5.1 to 5.5, we can conclude from the results of clean fiber efficiency especially the morphology that

1. inertial impaction can be negligible
2. diffusion is significant and prevailing when particles are small
3. the lower Peclet number is, the more realistic morphology of simulated results becomes
4. clean fiber efficiency is slightly different but morphology is evidently distinctive.
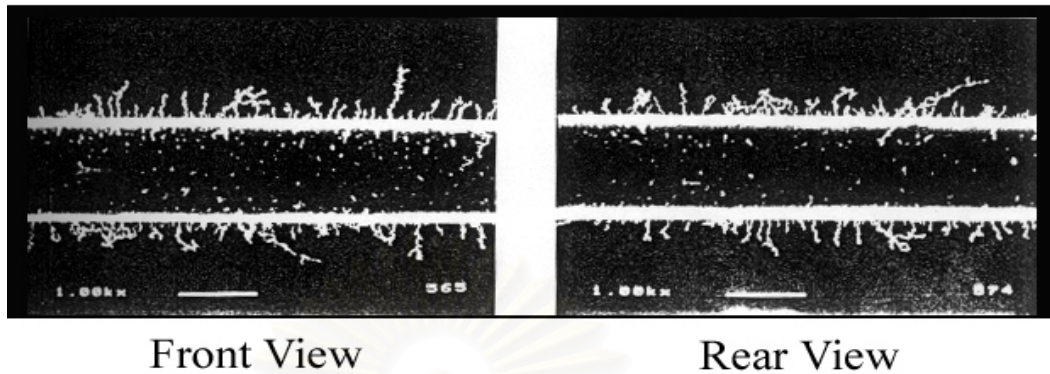
Front View   Rear View
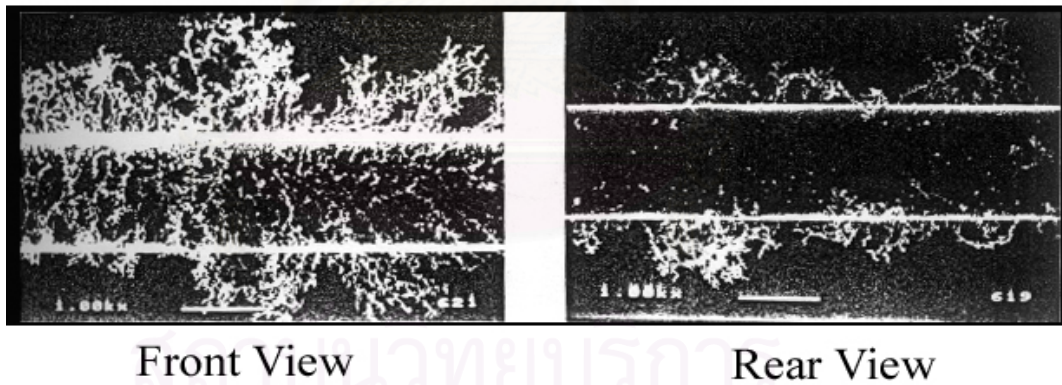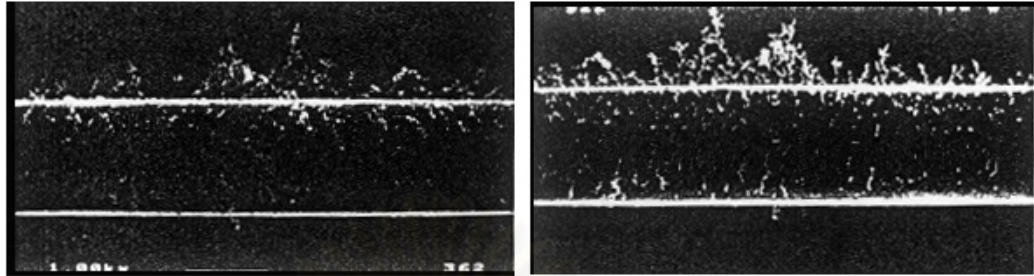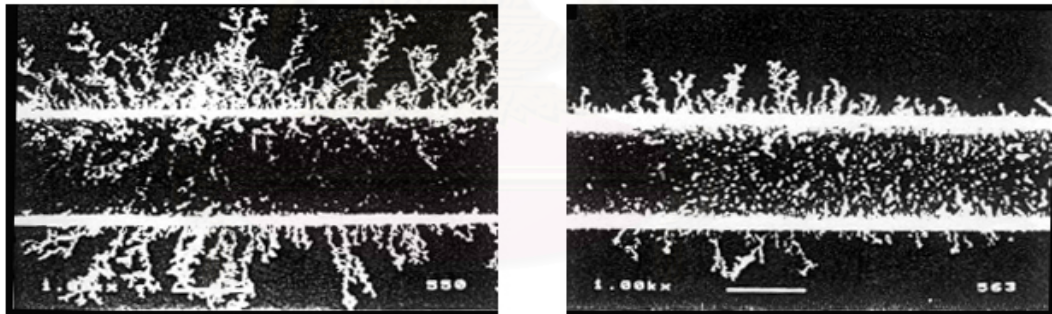
Figure 5.11 Experimental results of dendrite on an electret fiber for uncharged
particles with low dust load at conditions : d_f =30 μm,
d_p= 0.039 μm, Ri = 0.013, u=15 cm/s, ρ_p=2.33 g/cm^3, K_{In}=0.004,
Pe= 50000 and Stk = 0.015

Front View   Rear View

Figure 5.12 Experimental results of dendrite on an electret fiber for uncharged
particles with high dust load at conditions : d_f =30 μm,
d_p= 0.039 μm, Ri = 0.013, u=15 cm/s, ρ_p=2.33 g/cm^3, K_{In}=0.004,
Pe= 50000 and Stk = 0.015

Front View   Rear View

Figure 5.13 Experimental results of dendrite on an electret fiber for charged
particles with low dust load at conditions : d_f =30 μm,
d_p= 0.039 μm, Ri = 0.013, u=15 cm/s, ρ_p=2.33 g/cm^3, K_C=0.016,
Pe= 50000 and Stk = 0.015

Front View   Rear View

Figure 5.14 Experimental results of dendrite on an electret fiber for charged
particles with high dust load at conditions : d_f =30 μm,
d_p= 0.039 μm, Ri = 0.013, u=15 cm/s, ρ_p=2.33 g/cm^3, K_C=0.016,
Pe= 50000 and Stk = 0.015

CHAPTER 6
RESULTS AND DISCUSSION

The process of dendritic deposition is very complex and difficult to predict. The particle deposition process has been stochastically simulated using Monte-Carlo technique, under various filtration conditions of electrostatic deposition as well as convective Brownian diffusion.

6.1 Effects of Important parameters

The effects of important parameters such as step size, sample size, fiber length and radius of hemisphere of influence on morphology collection efficiency and collection efficiency raising factor are discussed here in section 6.1.

6.1.1 Effect of step size

Step size is one of the most important parameters in this work. There are 3 step sizes used here, those are, 0.025, 0.05 and 0.075. In theory, the smaller the step size is used, the better the estimates become. However, if the smaller step size is used, it has to take more computational time and memory. Consequently, it is very vital to choose the right value of step size. And the useful information to select the right value is below.

Table 6.1 Clean fiber efficiency and collection efficiency raising factor for
various step size for the case of Ri=0.05, K_{In}=0.05 and Pe 1000

Step size	Clean Fiber Efficiency (%)		Lamda	Varience
	Correlation	Simulation		
0.025	8.95	8.38	3.75	0.9
0.05	8.95	8.58	3.83	0.94
0.075	8.95	8.45	3.66	0.91

Table 6.1 and Figure 6.1 show the clean fiber collection efficiency and collection efficiency raising factor, λ at each step size. It is obvious from the table that the values are not much different.
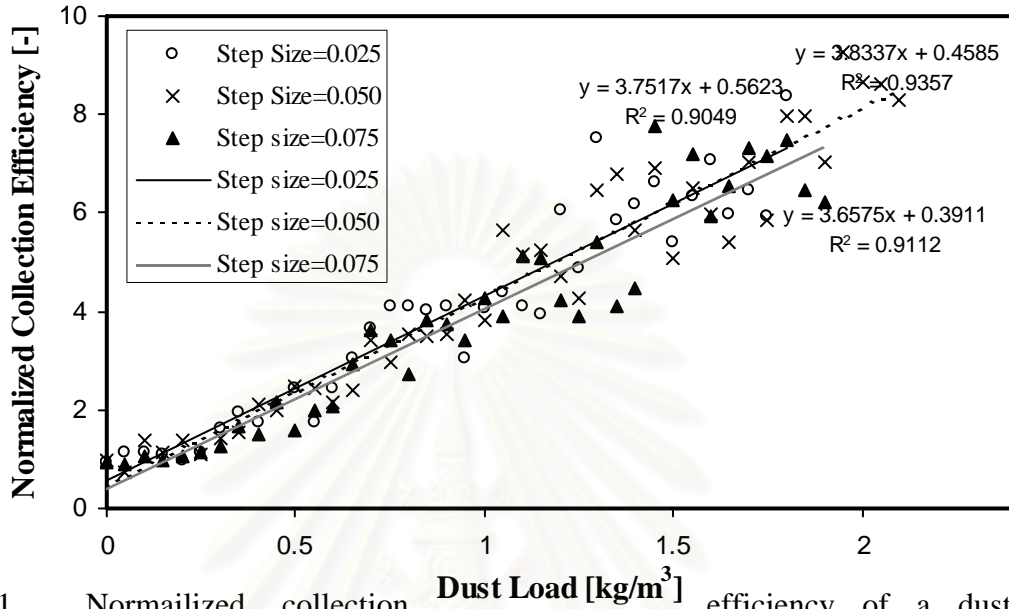

Figure 6. 1 Normailized collection efficiency of a dust-loaded fiber at each

step size for the case of Ri=0.05, K_{In}=0.05 and Pe=1000

From Figure 6.2-6.4, the morphologies of various step sizes are shown. It is so apparent that the configurations look the same. And Figure 6.5-6.7 and 6.8 are angular distribution of number of deposited particles and time dependency of number of dendrite in a unit fiber length, respectively. It is also clear that they are slightly different.

From the above information, it can be concluded that the most suitable value of step size is 0.05 because it takes a reasonable computational time and memory to obtain the precise solution.
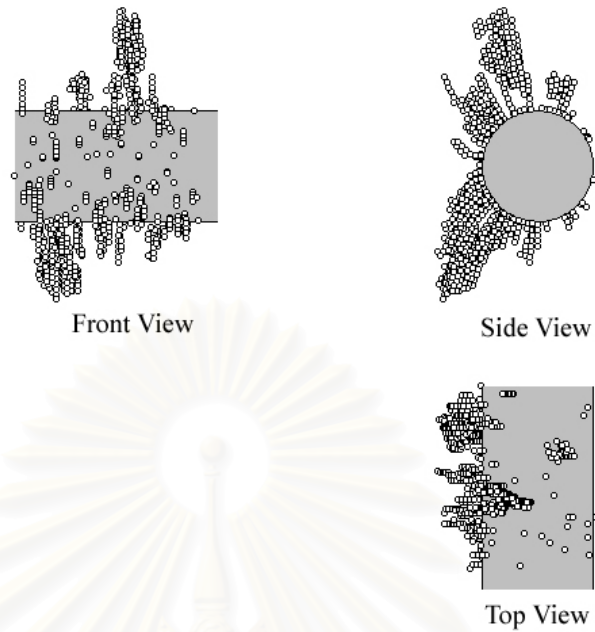
Figure 6.2 Typical configuration of dendrite at step size= 0.025 for the case of
Ri = 0.05, Kin=0.05 and Pe= 1000
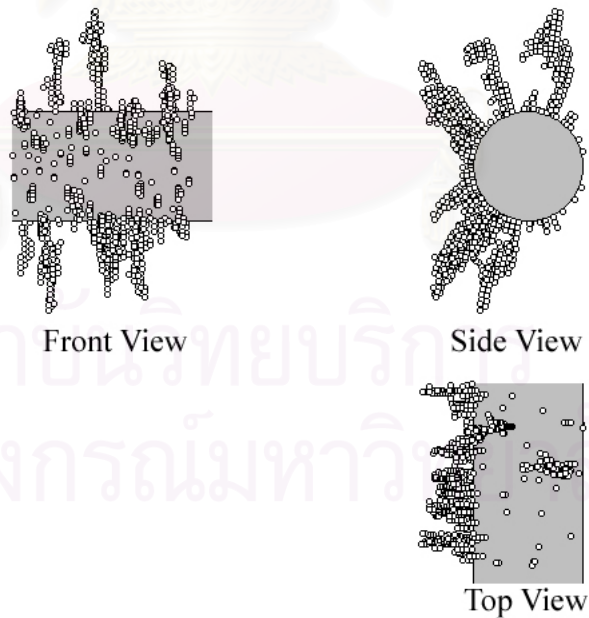
Figure 6.3 Typical configuration of dendrite at step size= 0.05 for the case of
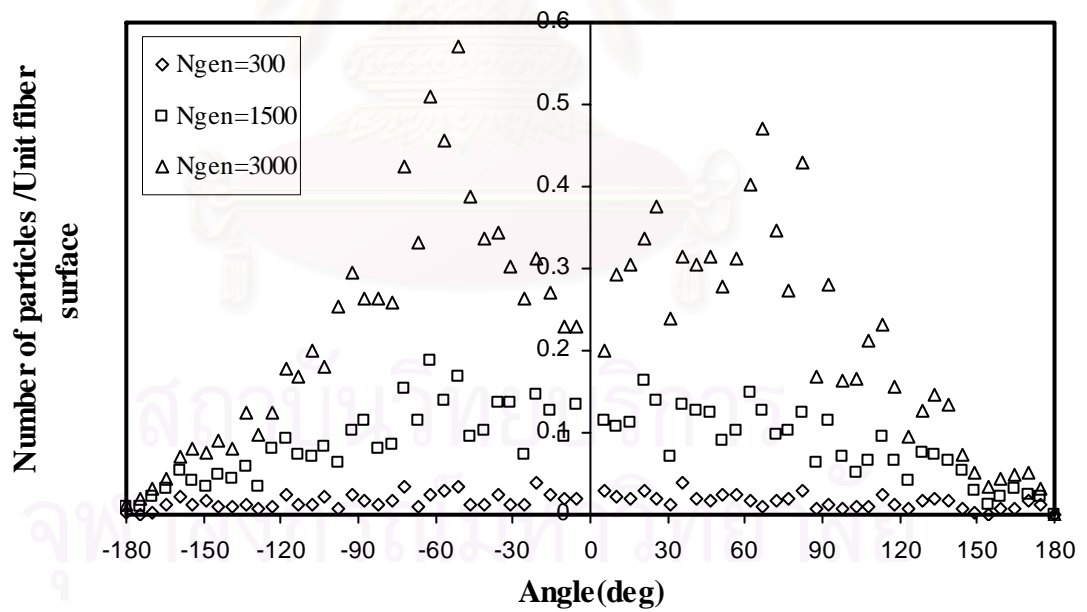Ri = 0.05, Kin=0.05 and Pe= 1000

Front View   Side View

Top View
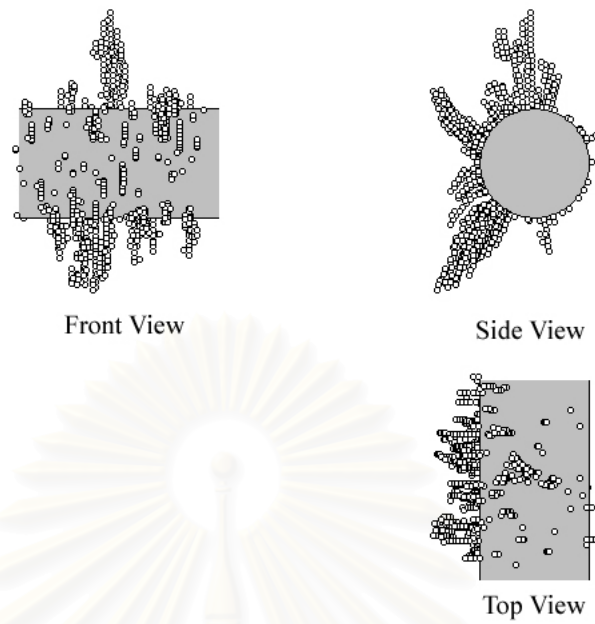
Figure 6.4 Typical configuration of dendrite at step size= 0.075 for the case of
Ri = 0.05, Kin=0.05 and Pe= 1000

Figure 6.5 Angular distribution of number of deposited particles on a fiber at
step size=0.025 for the case of Ri=0.05, Kin=0.05 and Pe=5000
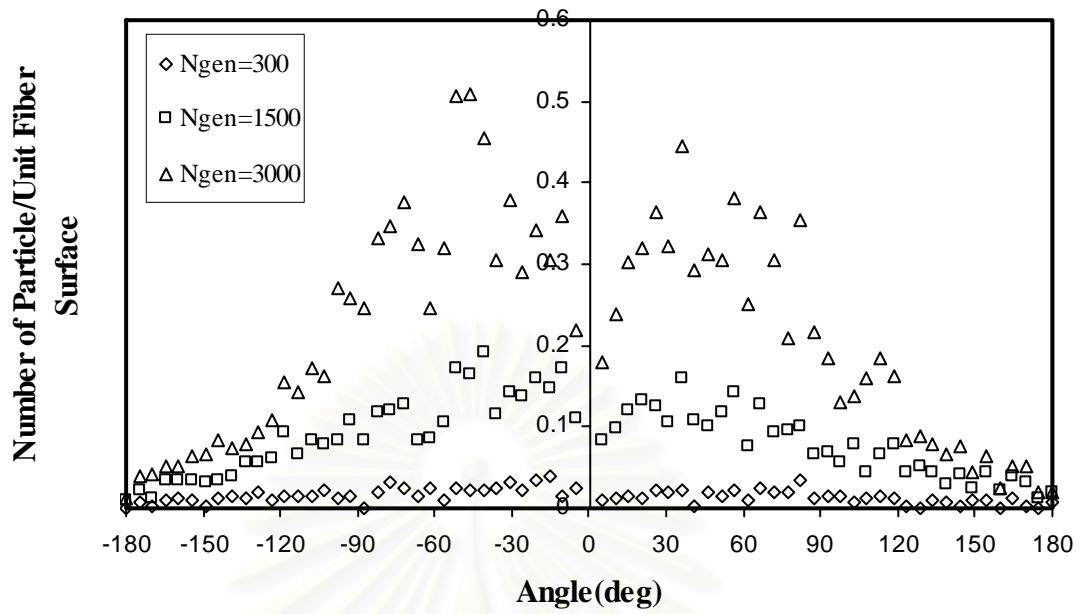
Figure 6.6 Angular distribution of number of deposited particles on a fiber at
step size=0.05 for the case of Ri=0.05, Kin=0.05 and Pe=5000
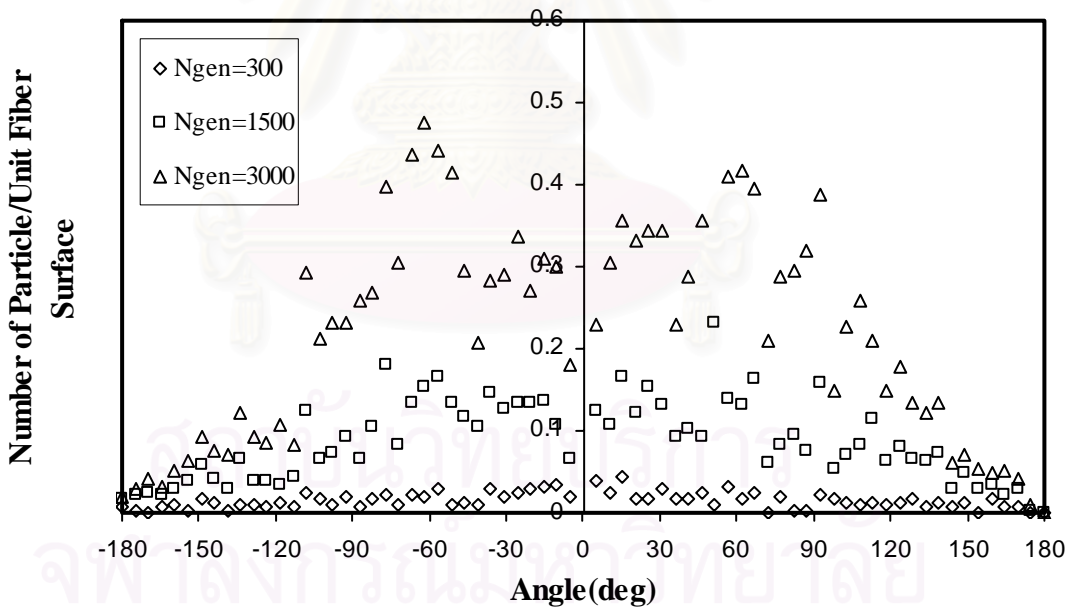
Figure 6.7 Angular distribution of number of deposited particles on a fiber at
step size=0.075 for the case of Ri=0.05, Kin=0.05 and Pe=5000
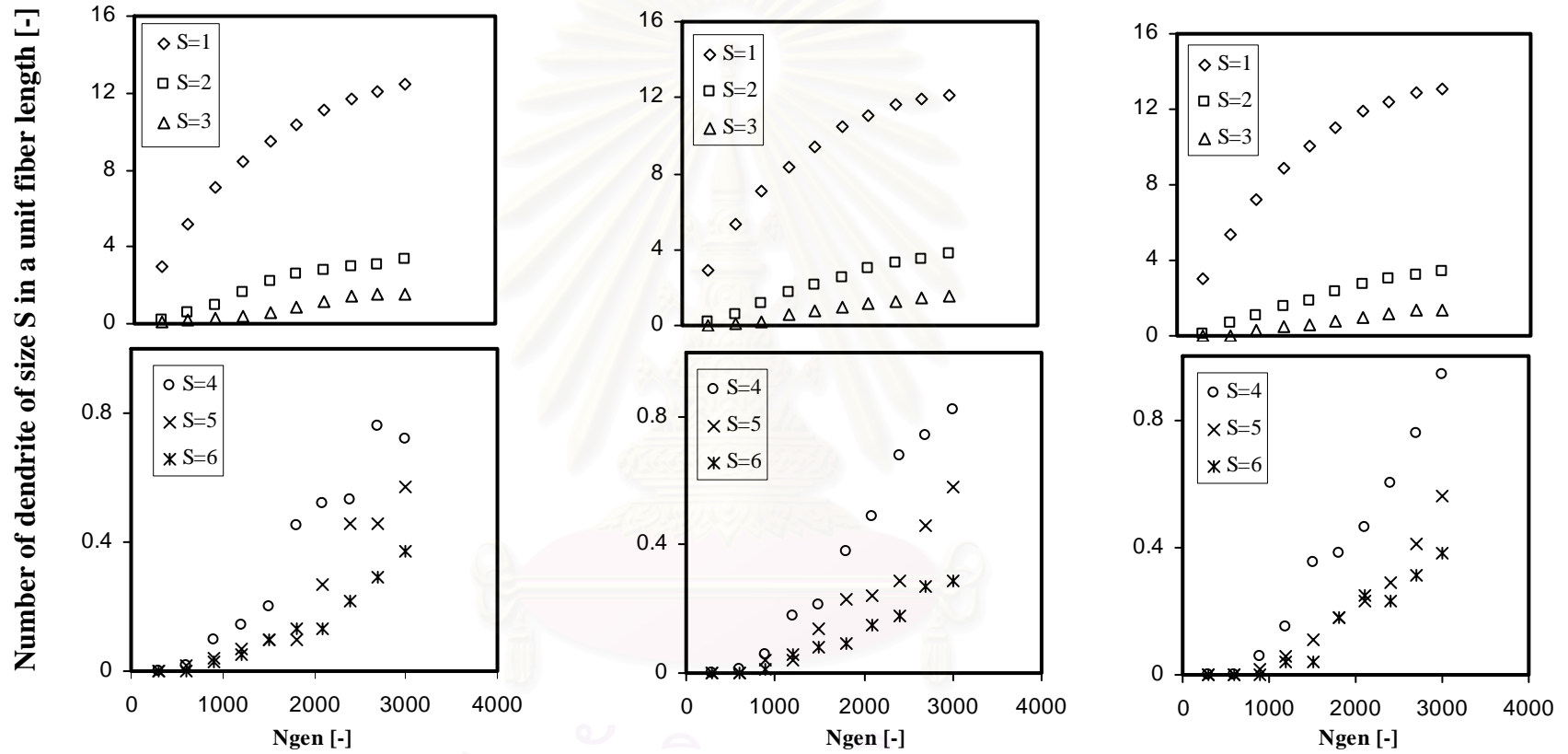
Figure 6.8 Time dependency of number of dendrites in a unit fiber length at each step size for the case of Ri=0.05, Kin=0.05 and Pe=5000

6.1.2   Effect of sample size

The sample size here refers to the number of independent samples obtained via Monte Carlo simulation technique for a given filtration condition. Theoretically, the larger sample size is used, the better the estimates of the ensemble statistics of the outputs of interest will acquire. Obviously, there exists an upper limit for the sample size beyond which little improvement in the precision of these estimates could be obtained. And sample sizes used here are 50 and 100.

Table 6.2 Clean fiber efficiency and collection efficiency raising factor for various sample size for the case of Ri=0.05, K_{In}=0.05 and Pe 1000

Sample size	Clean Fiber Efficiency (%)		Lamda	Varience
	Correlation	Simulation		
50	8.95	8.58	3.91	0.95
100	8.95	8.43	3.97	0.94

Table 6.2 and Figure 6.9 show the clean fiber collection efficiency and collection efficiency raising factor, λ at each sample size. It is obvious from the table that the values are not much different.

Figure 6.10 is the sample of morphology at sample size = 50 and the other is identical. And Figure 6.11-6.12 and 6.13 are angular distribution of number of deposited particles and time dependency of number of dendrite in a unit fiber length, respectively. It is also patent that they are slightly different.

Because of saving amount of computational time and memory to obtain each sample of the present stochastic process and gaining accurate simulation results, a compromise of 50 samples is selected as the sample size in this study.
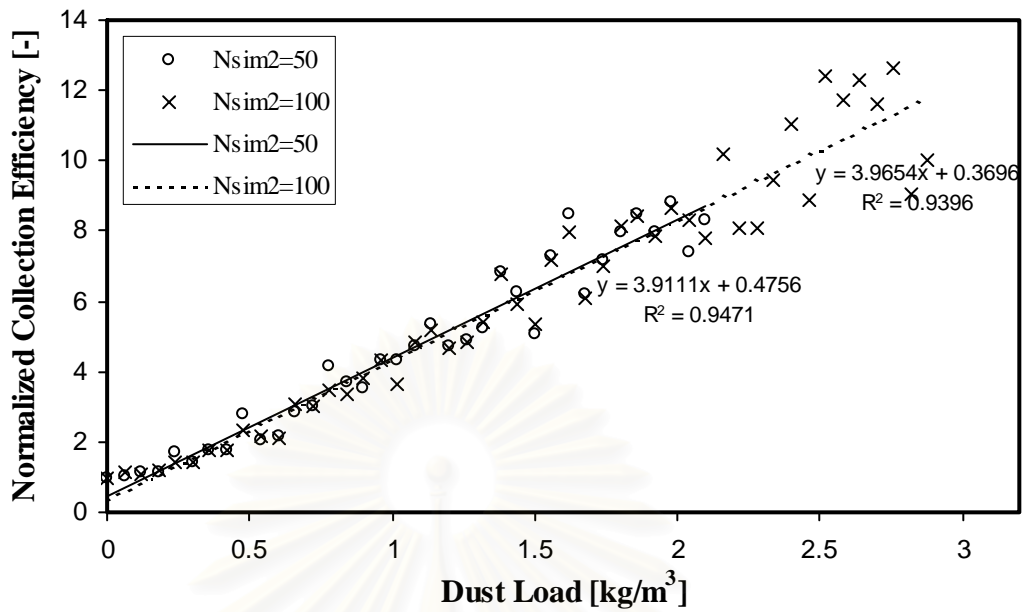
Figure 6.9 Normalized collection efficiency of a dust-loaded fiber at sample
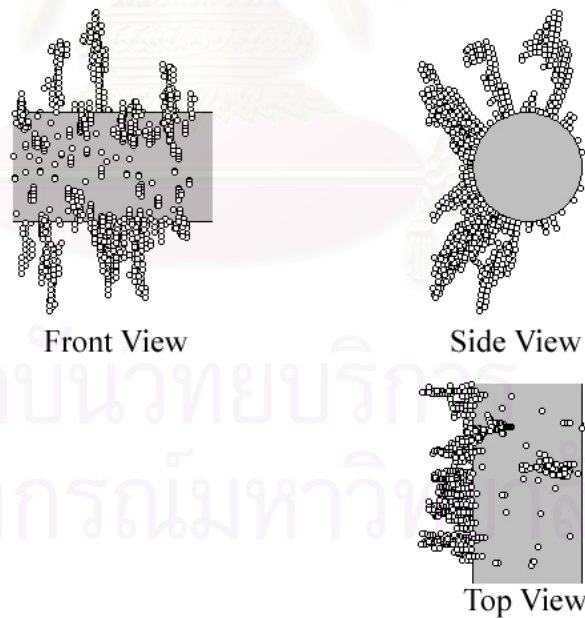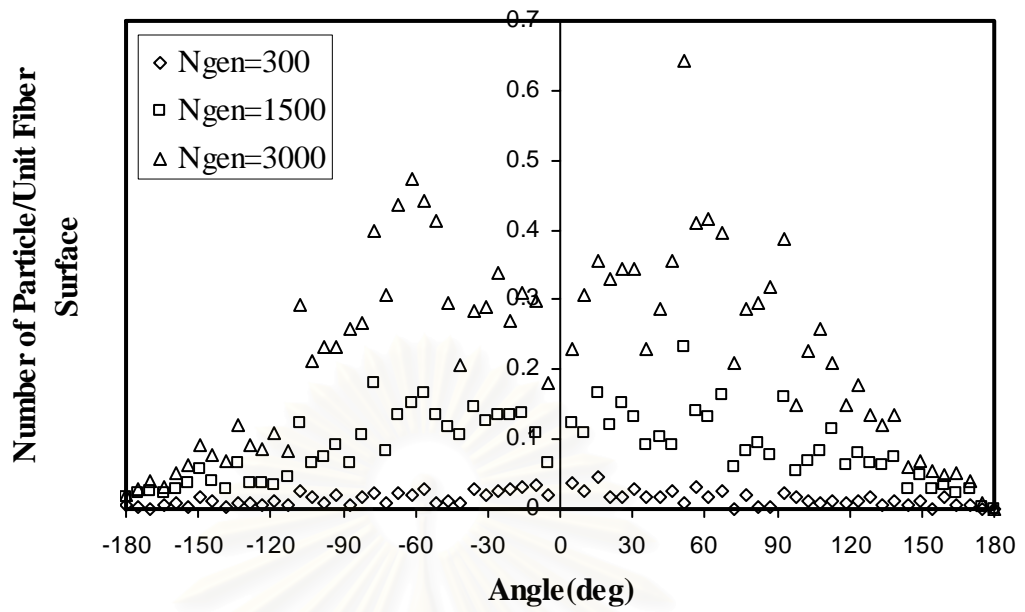size= 50 and 100 for the case of Ri=0.05, K_{In}=0.05 and Pe=1000

Front View   Side View

Top View

Figure 6.10 Typical configuration of dendrite at sample size= 50 for the case
of Ri = 0.05, Kin=0.05 and Pe= 1000

Figure 6.11 Angular distribution of number of deposited particles on a fiber at
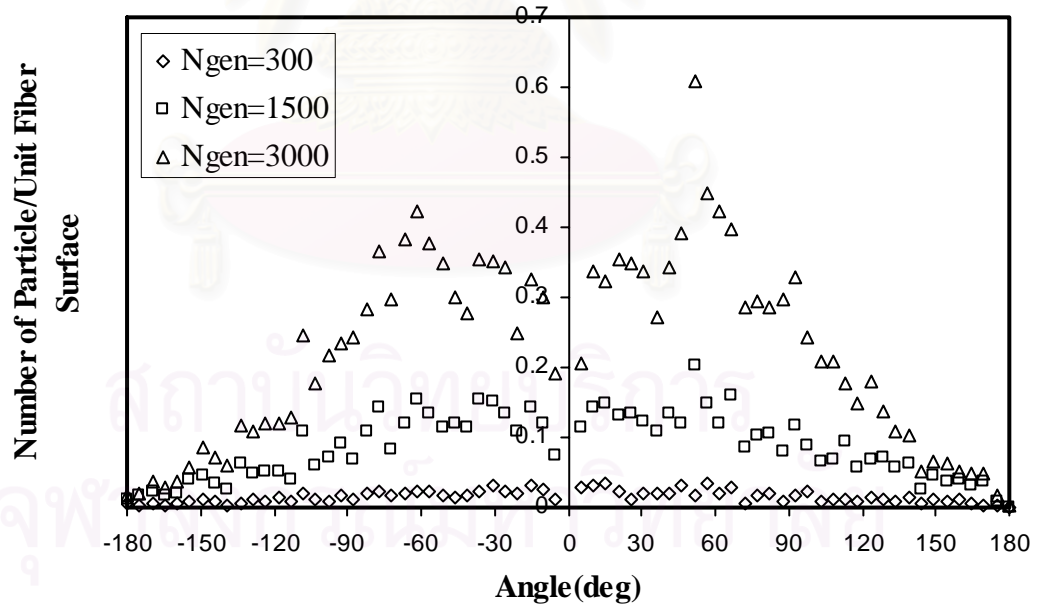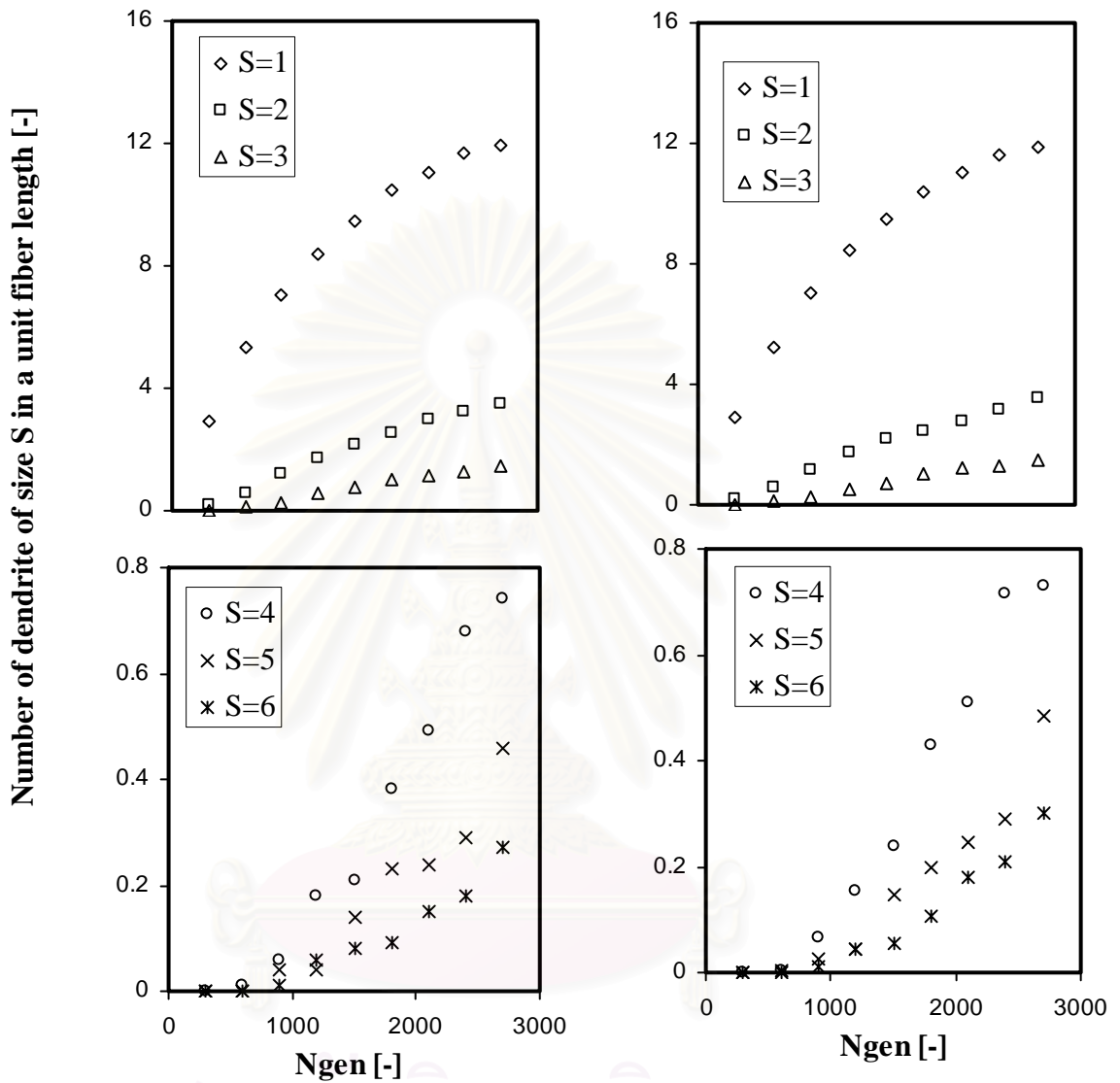sample size=50 for the case of Ri=0.05, Kin=0.05 and Pe=5000

Figure 6.12 Angular distribution of number of deposited particles on a fiber at
sample size=100 for the case of Ri=0.05, Kin=0.05 and Pe=5000

Figure 6.13 Time dependency of number of dendrites in a unit fiber length at
sample size = 50 and 100, respectively for the case of Ri=0.05,
Kin=0.05 and Pe=5000

6.1.3 Effect of fiber length

Fiber length is one of the most significant parameters in this work. Now the effect of fiber length is investigated. There are 2 values of fiber length, 20dp and 40dp. In consideration, the entire fiber is divided into five subsections, I, II, III, IV and V, of length Z_1, Z_2, Z_3 , Z_4 and Z_5, respectively. Moreover, to reduce end effect, generation of particles will take place over the entire length Z and Z_3 is flanked by two relatively wide buffer zones Z_2 and Z_4 for free diffusion and flanked again by two comparatively broad buffer zones Z_1 and Z_5. This fiber length and subsectors are shown in Figure 4.1. In this way, the shapes of dendrites within Z_3 are made relatively free from end effect because dendrites are also allowed to flourish in the buffer regions.

In this part, as mentioned above, the effect of fiber length is investigated by morphology, clean fiber efficiency and λ as in Table 6.3 and Figure 6.14. It can be seen that collection efficiency and λ are comparatively not different. Furthermore, the morphologies for both values look the same in Figure 6.15 and 6.16.

Table 6.3 Clean fiber efficiency and collection efficiency raising factor for

various fiber length for the case of Ri=0.05, K_{In}=0.05 and Pe 1000

Length	Clean Fiber Efficiency (%)		Lamda	Varience
	Correlation	Simulation		
20dp	8.95	8.58	3.91	0.95
40dp	8.95	8.62	3.98	0.92

From Figure 6.17 to 6.19, the angular distribution and dendrite distribution on fiber at various fiber length are shown. It is so apparent that the distributions seem to be the same.

Judging from these considerations, it can be concluded that the fiber length = 20dp is adopted in this investigation since it uses a reasonable computational time and memory to obtain the accurate solution.
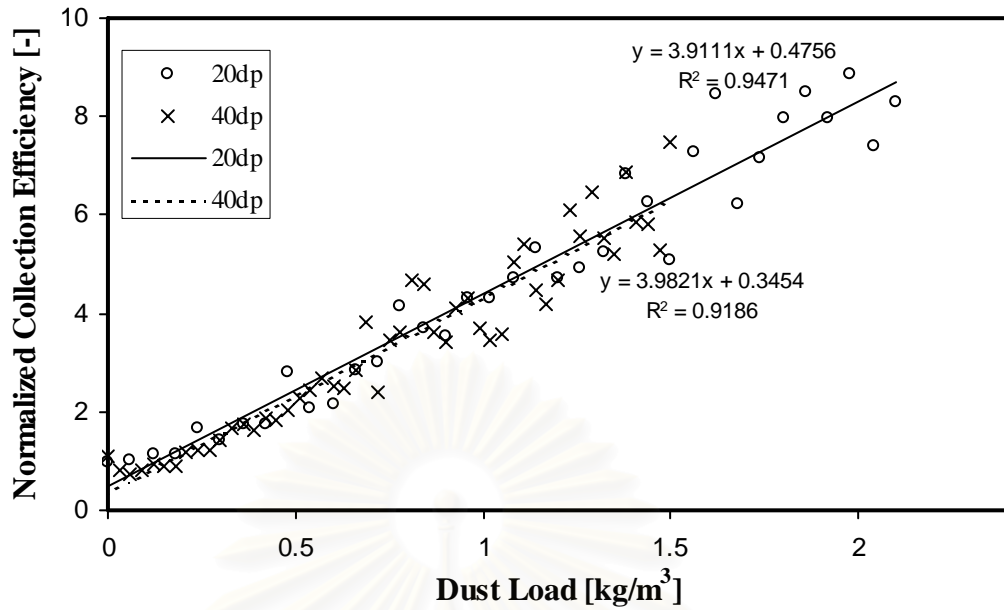
Figure 6.14 Normalized collection efficiency of a dust-loaded fiber at fiber
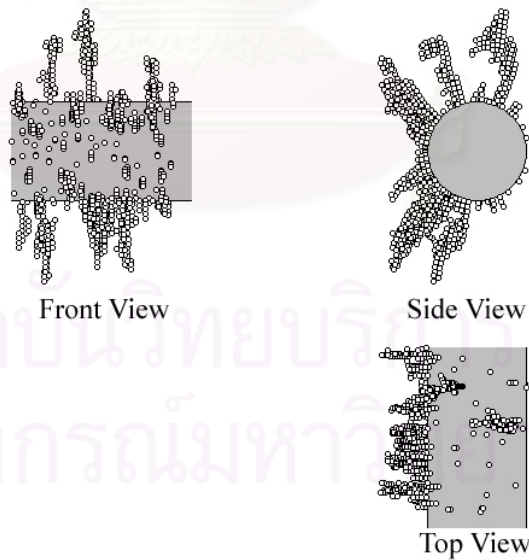length = 20dp and 40dp for the case of Ri=0.05, K_{In}=0.05
and Pe=1000

Figure 6.15 Typical configuration of dendrite at fiber length = 20dp for the
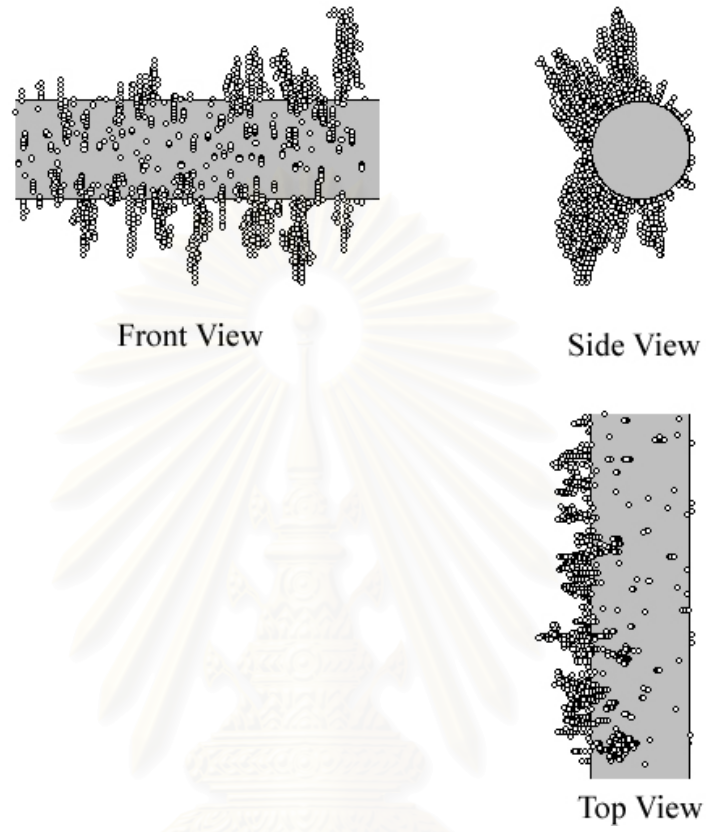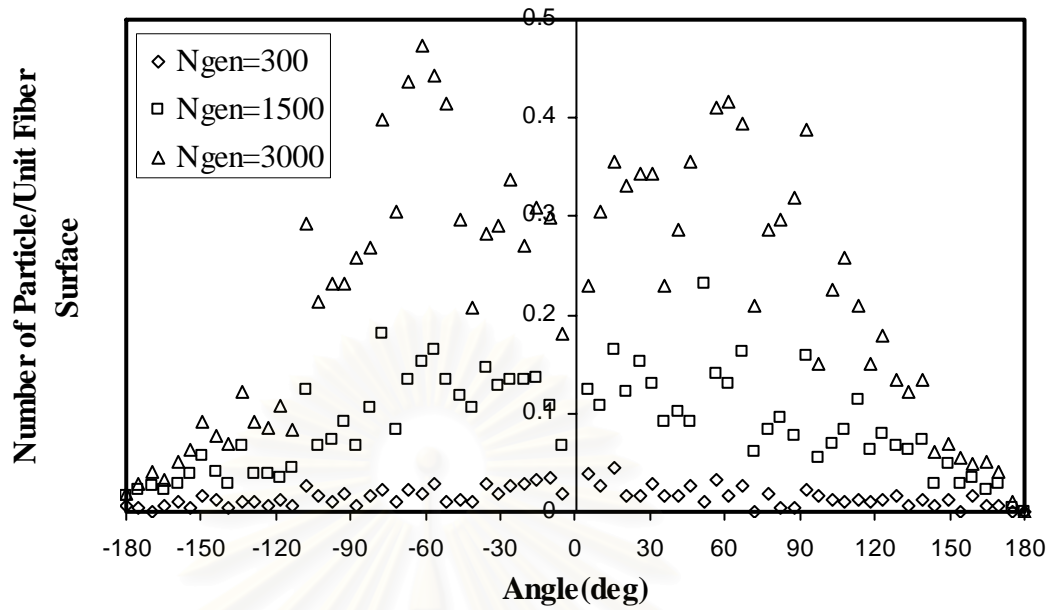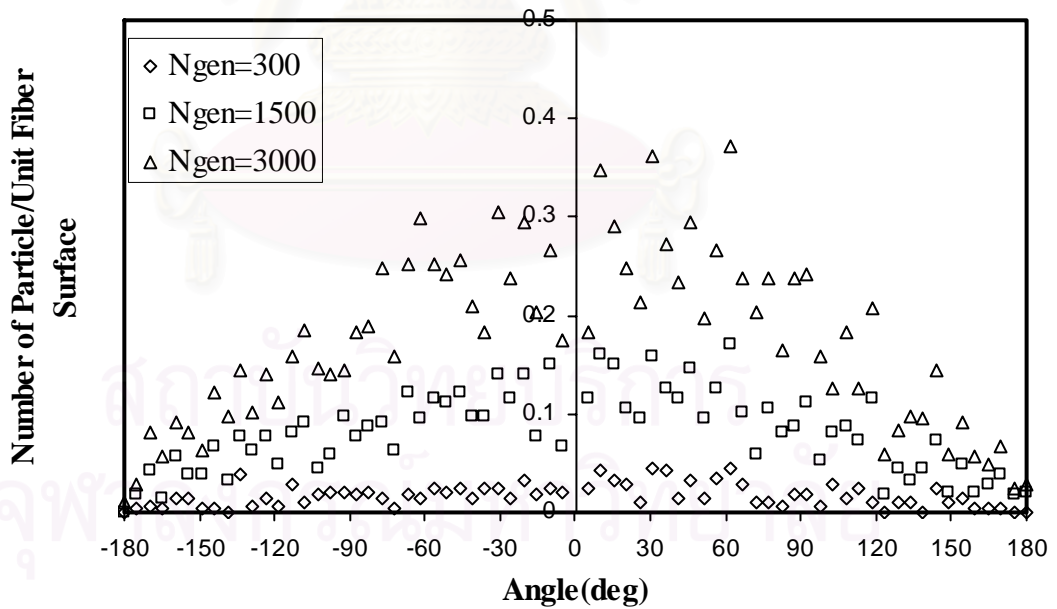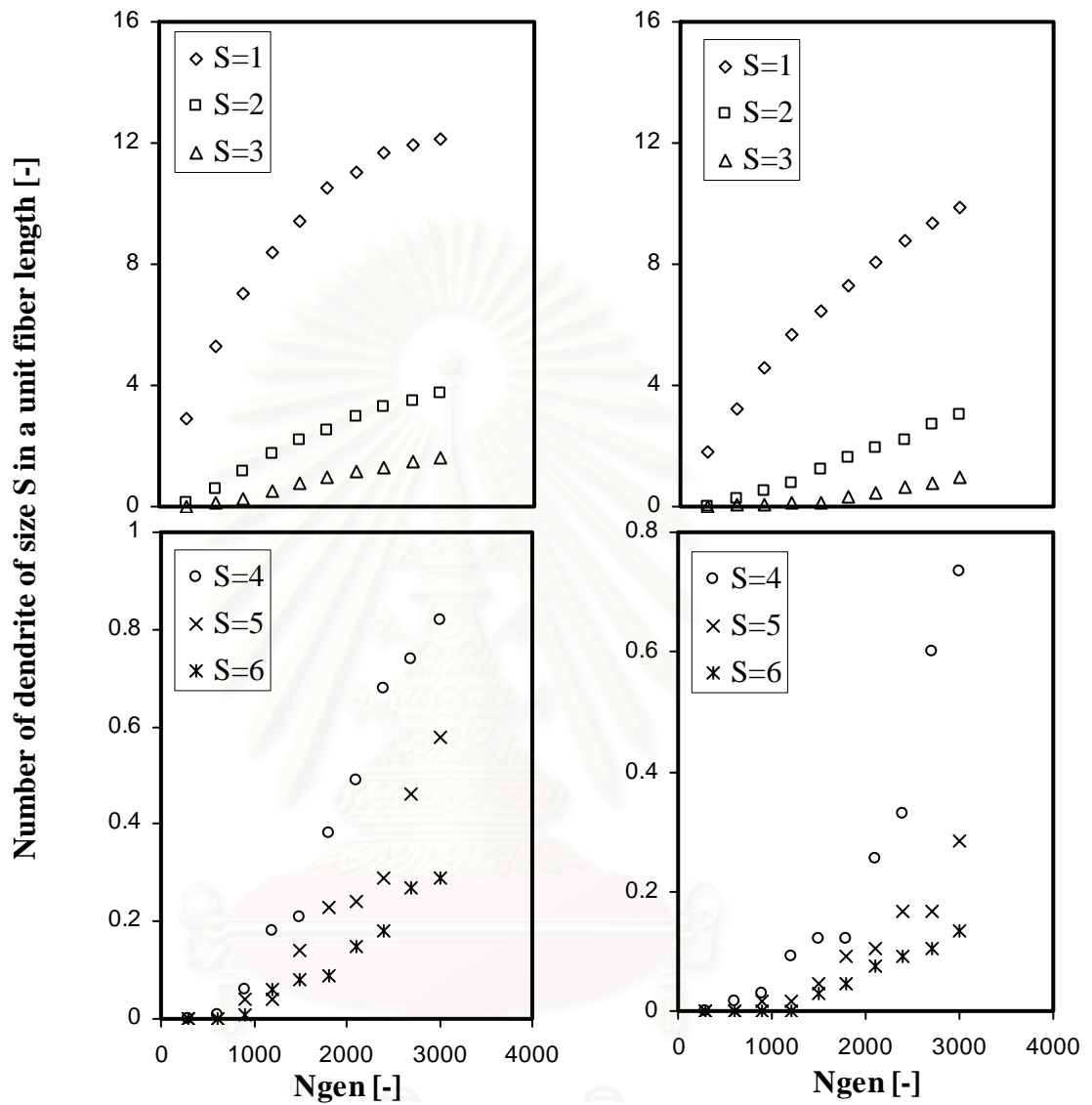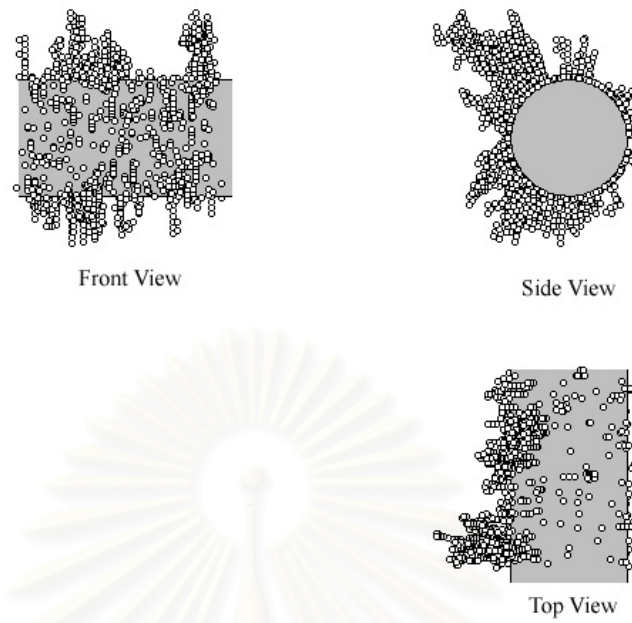case of Ri = 0.05, Kin=0.05 and Pe= 1000

Figure 6.16 Typical configuration of dendrite at fiber length = 40dp for the
case of Ri = 0.05, Kin=0.05 and Pe= 1000

Figure 6.17 Angular distribution of number of deposited particles on a fiber at
fiber length = 20dp for the case of Ri=0.05, Kin=0.05 and
Pe=5000

Figure 6.18 Angular distribution of number of deposited particles on a fiber at
fiber length = 40dp for the case of Ri=0.05, Kin=0.05 and
Pe=5000

Figure 6.19 Time dependency of number of dendrites in a unit fiber length at fiber

length = 20dp and 40dp, respectively for the case of Ri=0.05,

Kin=0.05 and Pe=5000

6.1.4 Effect of sphere of influence on morphology

The crucial parameter that has to be concerned is the radius of hemisphere of influence and the effect of this parameter is shown in Figure 4.3.

For this part, only the morphology of dendrites will be accentuated shown in Figure 6.20 to 6.26. Figure 6.20 to 6.22 are the samples of configuration at Re = 1.0, 1.5 and 2.0,respectively. For Re=1.0, the configuration looks bushy and short and sticks together all over the entire surface. For Re=2.0 in Figure 22, unlike that of Re=1.0, the morphology looks tall and slender like straight line and covers some areas like a patch on fiber surface. For Re=1.5, it seems slightly different from those of Re=1.0 and Re=2.0. It is in the middle of them, that is, it looks tall, slender but relatively not straight. Furthermore, it disperses on fiber surface more than that of Re=2.0 but less than that of Re=1.0.

And Figure 6.23 to 6.25 and 6.26 are angular distribution of number of deposited particles and time dependency of number of dendrite in a unit fiber length, respectively. It is also evident that they are comparatively different.

For these reasons, it can be inferred that the most appropriate value of radius of hemisphere of influence is 1.5 because it sounds reasonable and more realistic compared with the experimental results in Figure 5.11 to 5.14 in chapter 5.

Figure 6.20 Typical configuration of dendrite at Re= 1.0 for the case
of Ri = 0.05, Kin=0.05 and Pe= 1000
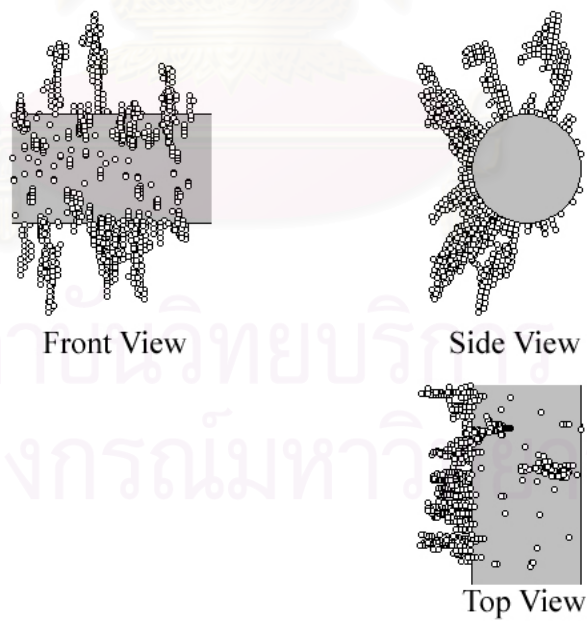
Figure 6.21 Typical configuration of dendrite at Re= 1.5 for the case
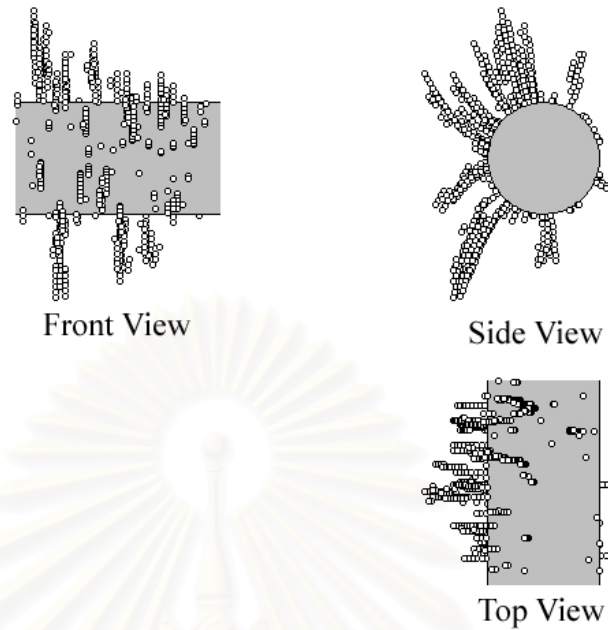of Ri = 0.05, Kin=0.05 and Pe= 1000

Figure 6.22 Typical configuration of dendrite at Re= 2.0 for the case
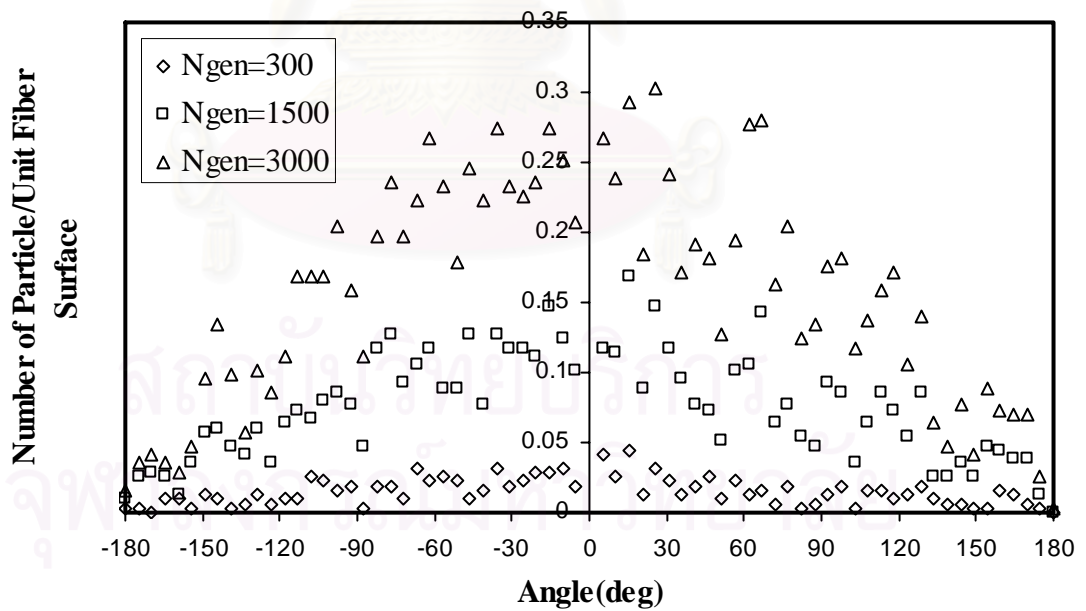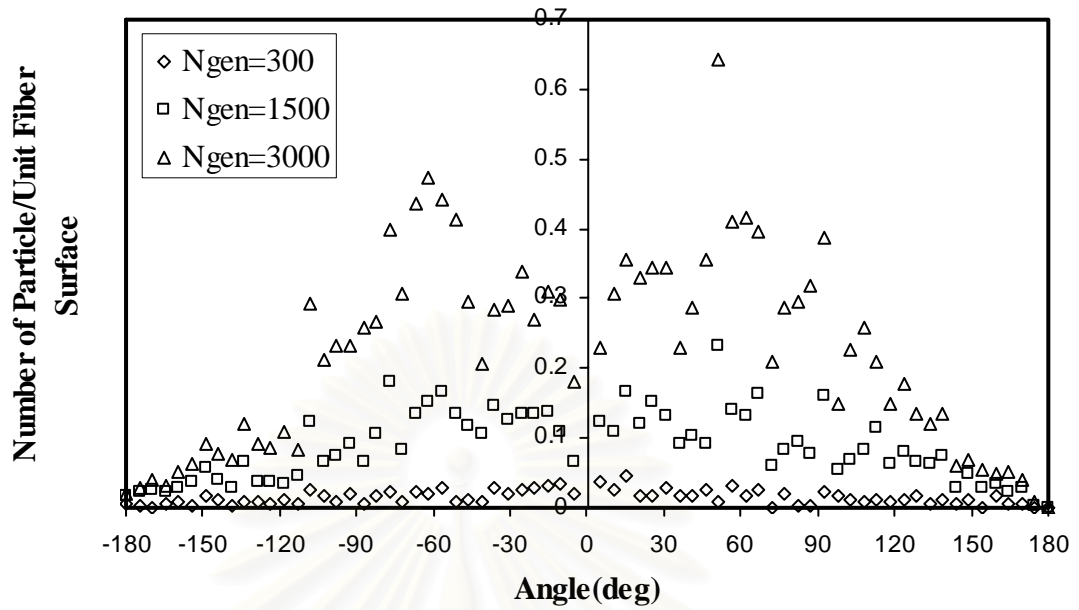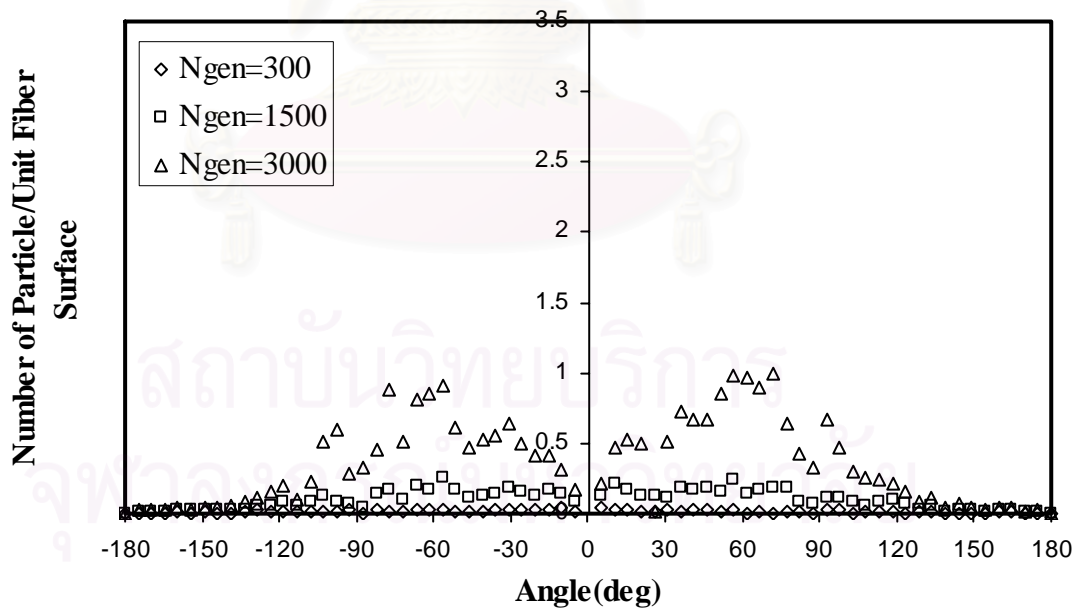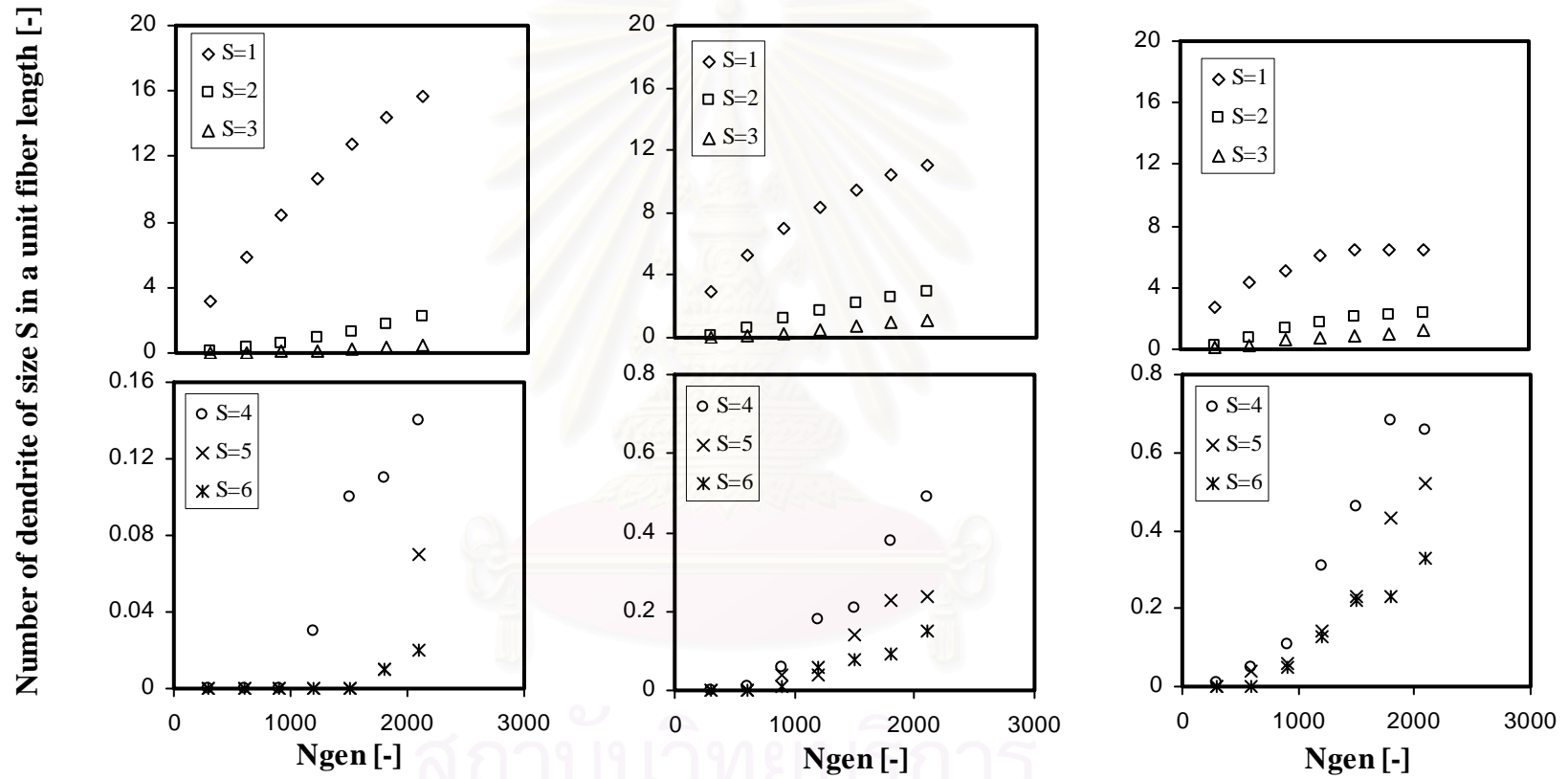
of Ri = 0.05, Kin=0.05 and Pe= 1000

Figure 6.23 Angular distribution of number of deposited particles on a fiber at

Re = 1.0 for the case of Ri=0.05, Kin=0.05 and Pe=5000

Figure 6.24 Angular distribution of number of deposited particles on a fiber at
Re = 1.5 for the case of Ri=0.05, Kin=0.05 and Pe=5000

Figure 6.25 Angular distribution of number of deposited particles on a fiber at
Re = 2.0 for the case of Ri=0.05, Kin=0.05 and Pe=5000

Figure 6.26 Time dependency of number of dendrites in a unit fiber length at Re = 1.0, 1.5 and 2.0, respectively for the case of Ri=0.05, Kin=0.05 and Pe=5000

6.2 Simulation Conditions

Monte Carlo simulations are achieved under various filtration conditions. However, the packing density of the filter and the particle density are fixed at 0.06 and $1g/cm^3$, respectively. The investigated conditions are listed in Table 6.4. As mentioned before, the value of step size adopted in this study is 0.05. Furthermore, this study is concerned with convective diffusional deposition of aerosols on a dust-loaded fiber and this work studied here is an extension of Prof. Kanaoka's work.

Table 6.4 Stochastic simulation conditions for convective diffusion on an electret fiber

Interception parameter R_i (-)		0.03, 0.05 and 0.1
Peclet number P_e (-)		200, 1000, 5000 and 50000
Packing density of filter α (-)		0.06
Electrical parameter		
Induced force K_{In} (-)		0.004, 0.05 and 0.1
Coulombic force K_C (-)		0.016, 0.05 and 0.1
Length of fiber section		
I	Z_1 (-)	3 dp
II	Z_2 (-)	5 dp
III	Z_3 (-)	20 dp
IV	Z_4 (-)	5 dp
V	Z_5 (-)	3 dp
Radius of fiber R_f (-)		1
Half height of generation plane H (-)		2
Step size Δt (-)		0.05
Number of simulation N_{sim2} (-)		50
Maximum layer of captured particles		
for $R_i = 0.03$		30
for $R_i = 0.05$		20
for $R_i = 0.1$		10
Radius of hemisphere of influence R_e (-)		1.5

6.3 Stochastic Simulation Results

6.3.1   General shape of particle accumulates on the fiber surface

The morphology of dendrites is complex and hard to explain. Then, for the sake of simplicity, the shape of accumulates for the case of non-electret fiber is discussed first. Subsequently, the shape of accumulates for the case of electret fiber is investigated.

Shapes of accumulates on a non-electret fiber surface

When fiber is clean, particles are collected directly on it, but once a particle is collected, the flow pattern change, and this enhances the collection of particles because of the existence of captured particles. Figure 6.27 based on experimental observation shows the general features of the deposition pattern by diffusion, inertial impaction and effect of interception parameter.
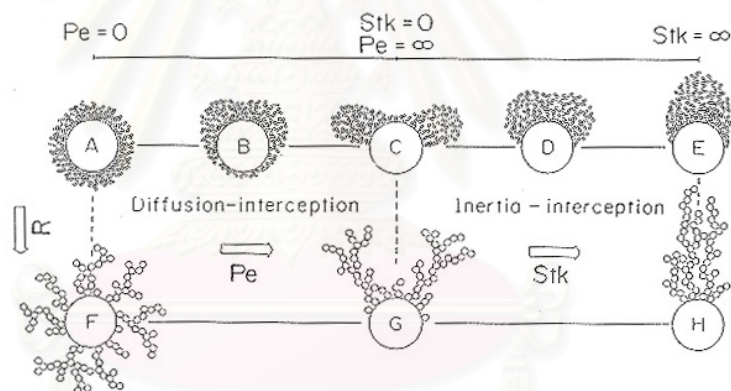
Figure 6.27 Shape of particle accumulates by the change of collection
                      mechanism

From this figure, it can be concluded that at low Pe number, particles are captured all over the entire surface and densely packed. But when Pe number increases, the maximum deposition appears on the stagnation point and gradually becomes separated and shifted away from the stagnation point.

Furthermore, when particle is large, the captured particle becomes more porous but the effect of Pe is the same, namely, particles are captured all over the entire surface at low Pe number and locates around stagnation point at high Pe number.

Unlike diffusion mechanism, for the case of inertial impaction, at low Stk, configuration of dendrite seems like that of high Pe number. However, when Stk increases, particles are densely captured near the stagnation point. But when particles become larger, configuration of dendrite looks the same that of small size except for more porosity.

Shapes of accumulates on an electret fiber surface

Figure 6.28 to 6.31 show the configuration of the dendritic growth with respect to time for the case of Ri=0.03, Pe=5000, K_{In}=0.1 K_C=0.1 and Gamma=90, 135 and 180, respectively. At beginning, the dendrite grows slowly but when the number of captured particles are large enough to form agglomerates, the dendrite accumulating on the fiber grows faster.

In addition, the morphologies of accumulates on an electret fiber by the present model become realistic compared with the experimental results in Figure 5.11-5.14.

Table 6.5– 6.8 show typical configuration of dendrites for the case of Ri=0.03 and 0.1, K_{In}=0.004 and 0.1 K_C=0.016 and 0.1. These figures will be discussed in detail such as effect of K_{In} and /or K_C and the polarization direction, γ, effect of Pe number and effect of Ri.

Effect of K_{In}

When induced force is prevailing, uncharged particles are collected uniformly all around the entire fiber surface and form chainlike agglomerates, which subsequently become irregular and complicated. Furthermore, these agglomerates grow almost perpendicular to the surface until a given height. For the low K_{In}, the shape of dendrite is fatter and shorter than that of high K_{In} . In contrast, for high K_{In}, the dendrite becomes taller and more slender and looks straighter. Moreover, the number of dendrites dispersed all around the surface for the high K_{In}, becomes more in quantity than that of the low K_{In}. And these can be seen in the figure.

Effect of K_C

Like the effect of K_{In}, the effect of high K_C on morphology makes the dendrite taller, straighter and more slender and can capture more particles than that of low K_C which can be seen that there are more scattered dendrites on the fiber surface. However, regarding of limited area of opposite polarity, the effect of low K_C can collect more particles than that of high K_C on this surface area because of the weaker in K_C. This can be noticed in the figure. In consideration of polarization direction, γ, when angle increases, particles can be more captured. But the effect of γ on the average shape of dendrites is hard to elucidate because it is necessary to fully understand how the electrical charges on the deposited particles are transferred among themselves and between them and the electret fiber.

Effect of Pe

At low Pe, the configuration of dendrite looks comparatively tall, slim and straight for both uncharged and charged particles. And it is remarkable that the fiber with low Pe can capture more particles especially the rear side of the surface shown in the side view and has more small-size of dendrites scattering all around the fiber. At high Pe, the dendrites look shorter and fatter and the fiber has more space area.

Effect of Ri

For both induced and coulombic force, when Ri is low, captured particles are densely packed. But when Ri increases, morphology has more vacant area and looks more porous just like the case of non-elecrtret fiber. For the case of electrical deposition plus diffusional mechanism, when Ri increases, the electret fiber can collect more particles.
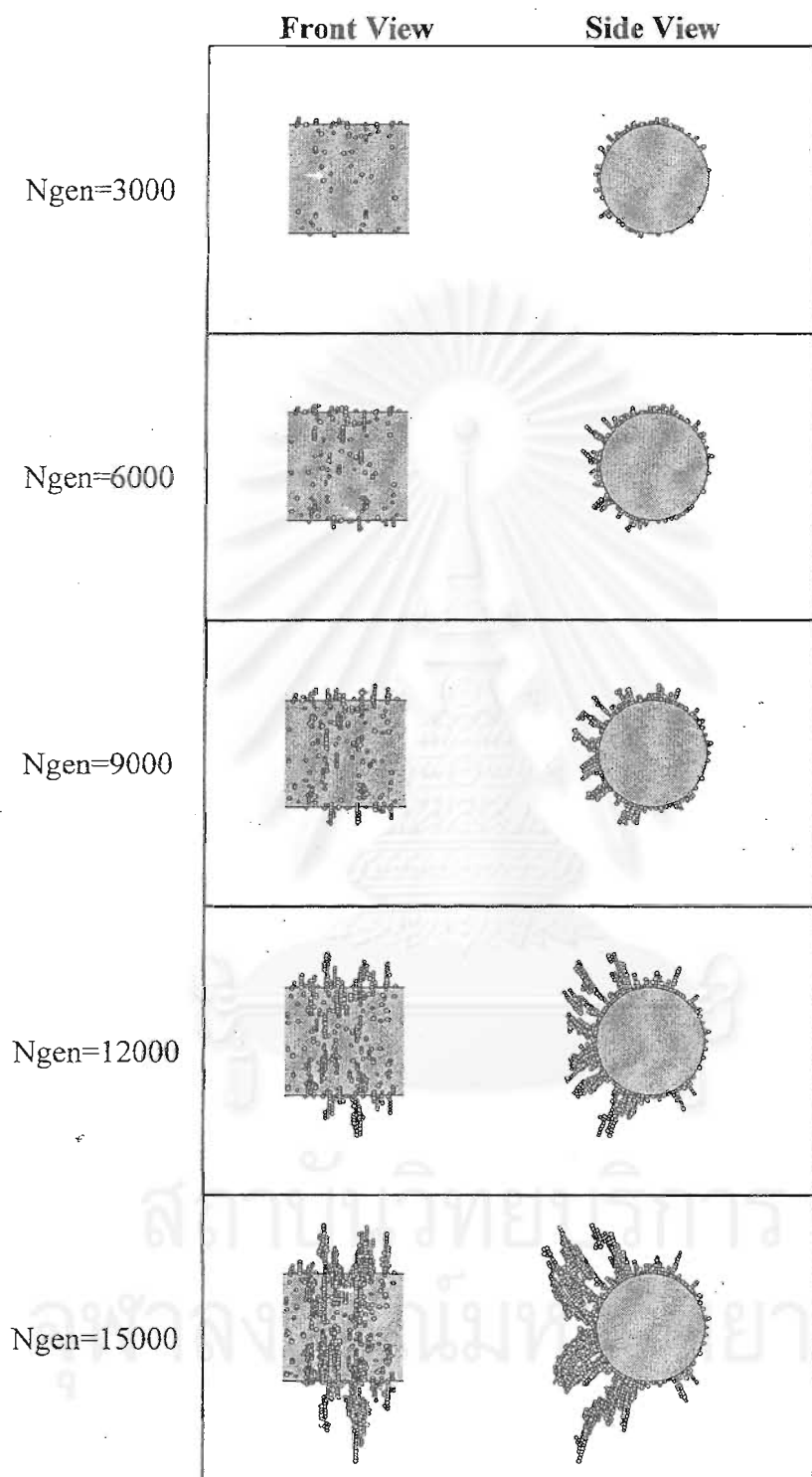
Figure 6.28 Time dependency of particles agglomerates on a fiber for the case of Ri=0.03, K_{In} = 0.1 and Pe= 5000
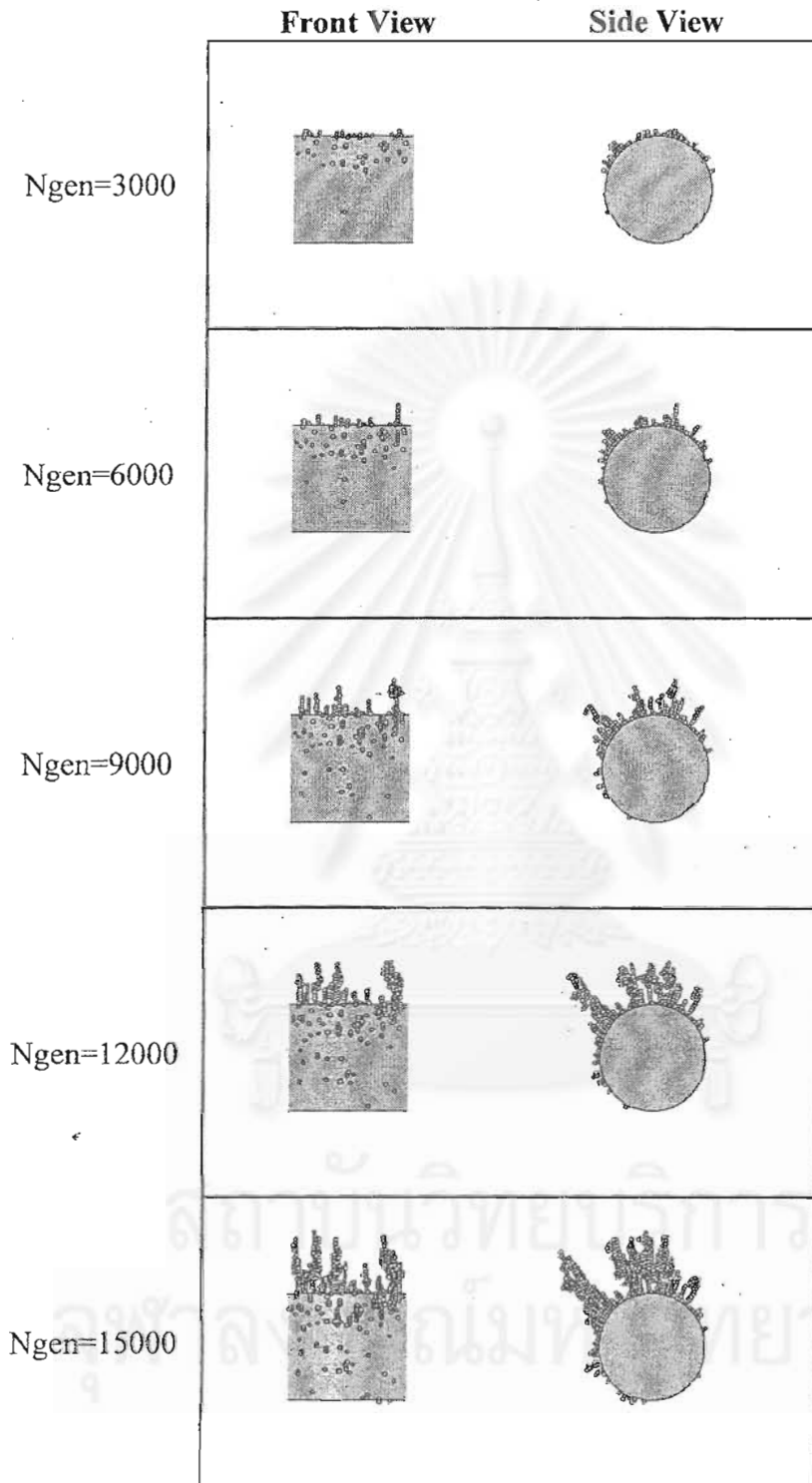
Figure 6.29 Time dependency of particles agglomerates on a fiber for the case
of Ri=0.03, K_C = 0.1, Gamma = 90 and Pe= 5000

	Front View	Side View
Ngen=3000		
Ngen=6000		
Ngen=9000		
Ngen=12000		
Ngen=15000		
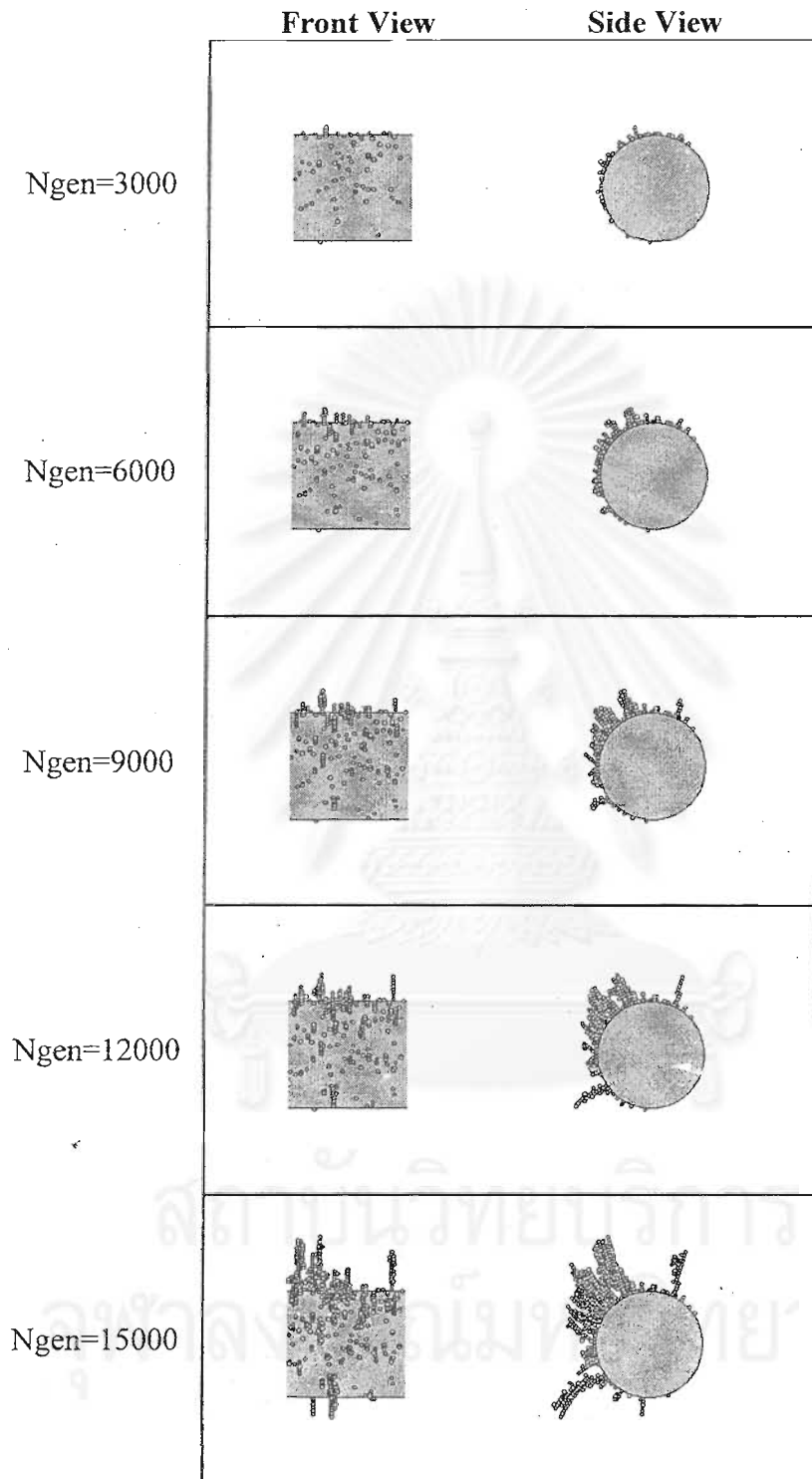
Figure 6.30 Time dependency of particles agglomerates on a fiber for the case
of Ri=0.03, K_C = 0.1, Gamma = 135 and Pe= 5000
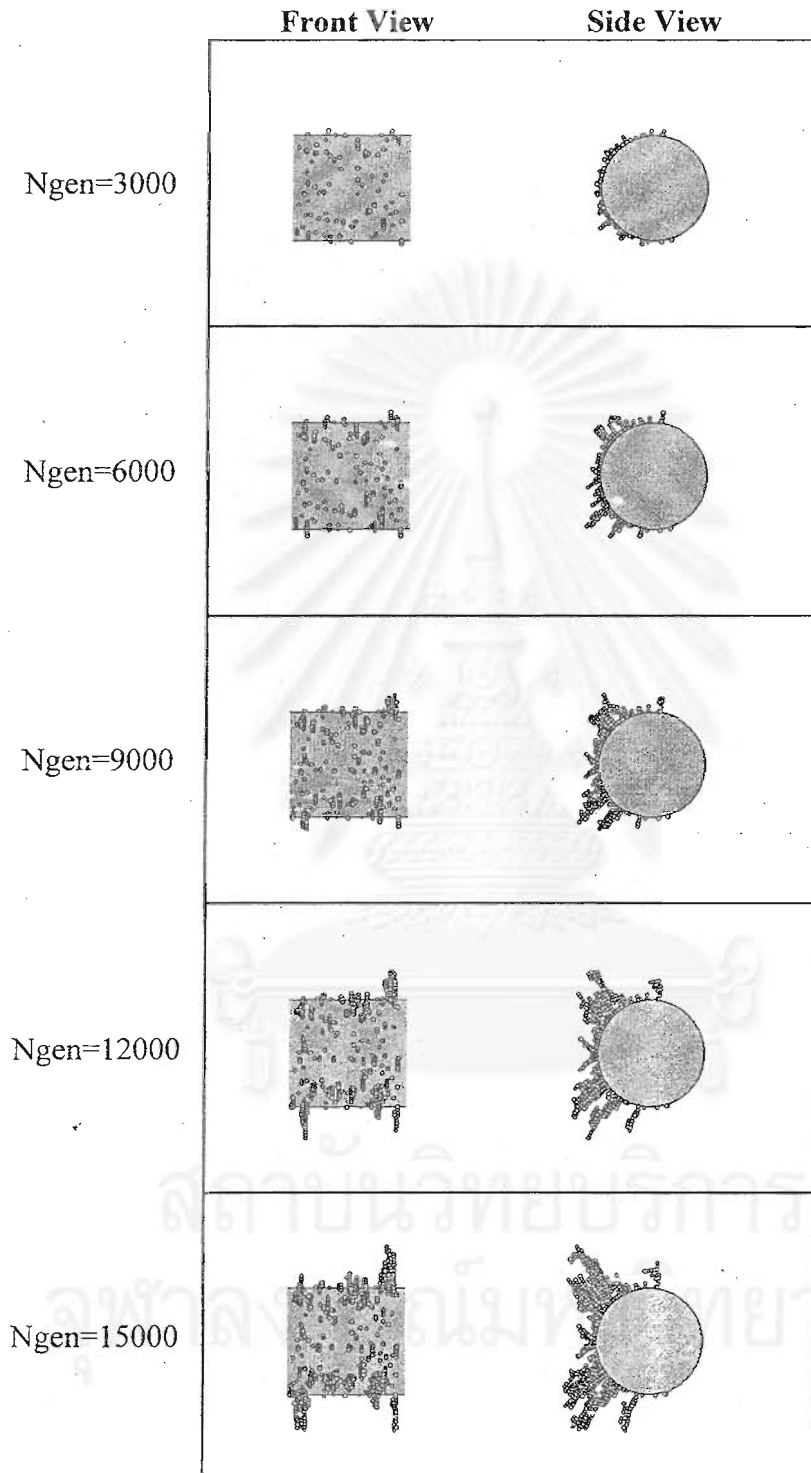
Figure 6.31 Time dependency of particles agglomerates on a fiber for the case of Ri=0.03, K_C = 0.1, Gamma = 180 and Pe= 5000
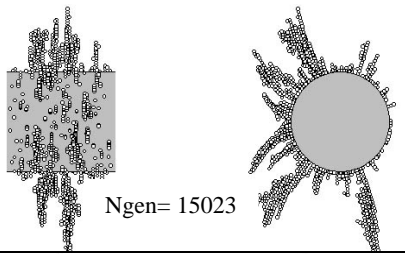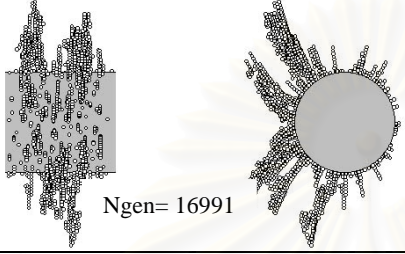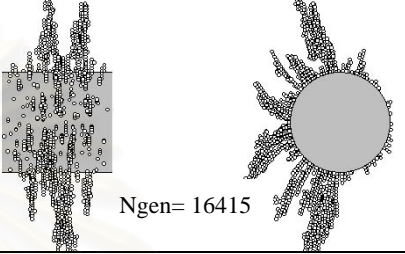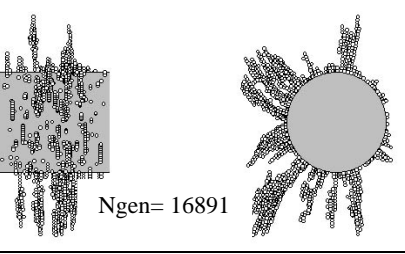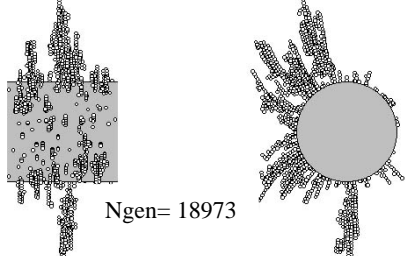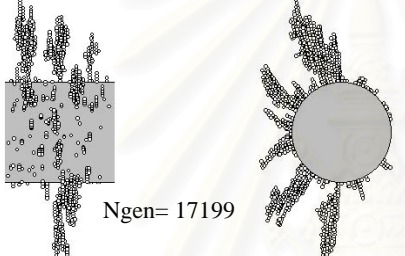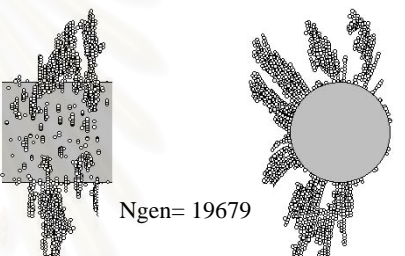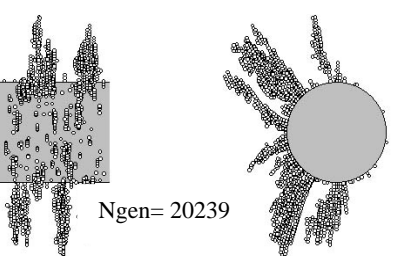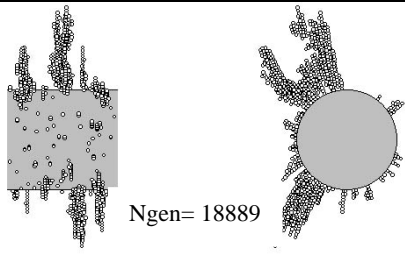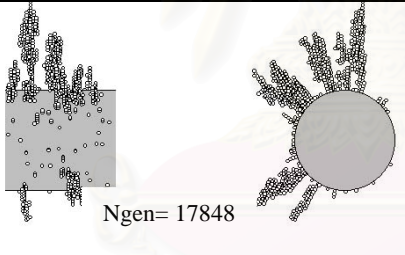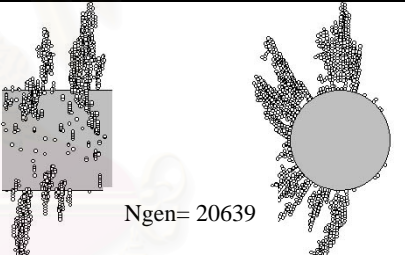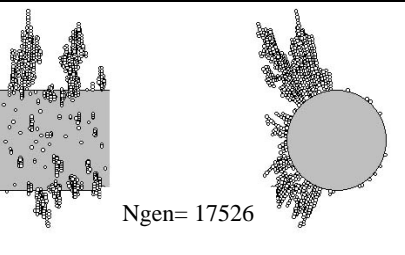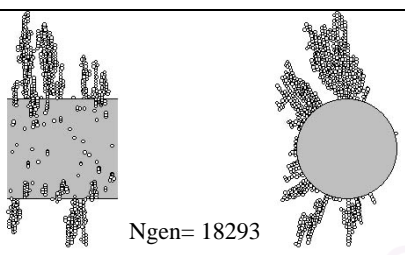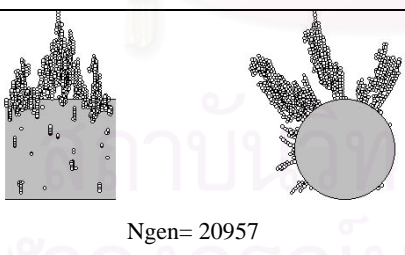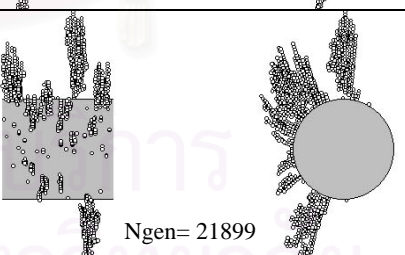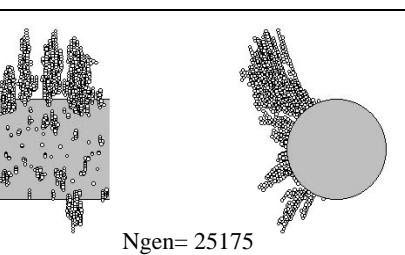
Pe	$K_{In}=0.004$	Kc=0.016		
		$\gamma=90°$	$\gamma=135°$	$\gamma=180°$
200	Ngen= 15023	Ngen= 16991	Ngen= 16415	Ngen= 16891
1000	Ngen= 18973	Ngen= 17199	Ngen= 19679	Ngen= 20239
5000	Ngen= 18889	Ngen= 17848	Ngen= 20639	Ngen= 17526
50000	Ngen= 18293	Ngen= 20957	Ngen= 21899	Ngen= 25175

Table 6.5 Typical dendrites configurations for the case of Ri = 0.03, K_{In} =0.004 and K_C = 0.016

Pe	KIn=0.004	Kc=0.016		
		γ=90°	γ=135°	γ=180°
200	Ngen= 1567	Ngen= 1589	Ngen= 1279	Ngen= 1527
1000	Ngen= 1839	Ngen= 1610	Ngen= 1436	Ngen= 1684
5000	Ngen= 2429	Ngen= 1755	Ngen= 2078	Ngen= 1813
50000	Ngen= 1783	Ngen= 1893	Ngen= 1459	Ngen= 1882

Table 6.6 Typical dendrites configurations for the case of Ri = 0.1, K_{In} =0.004 and K_C = 0.016
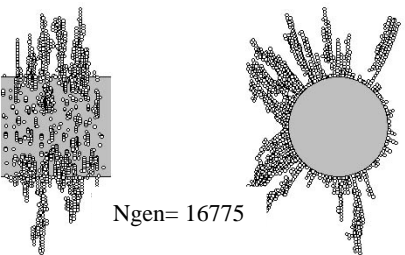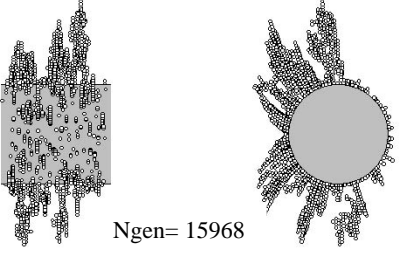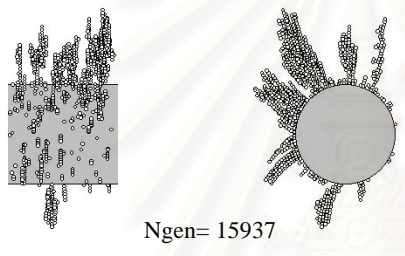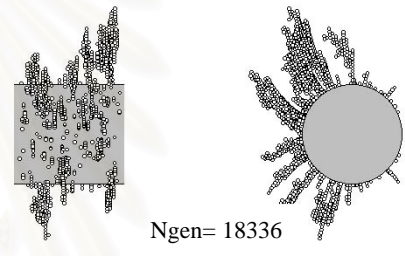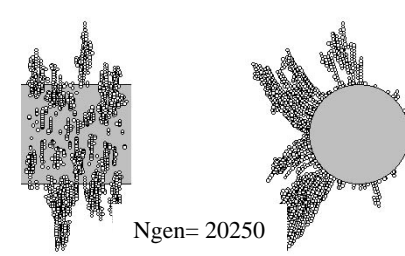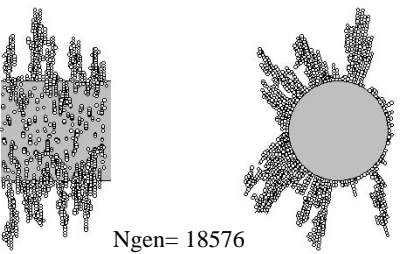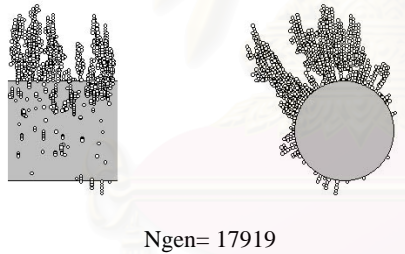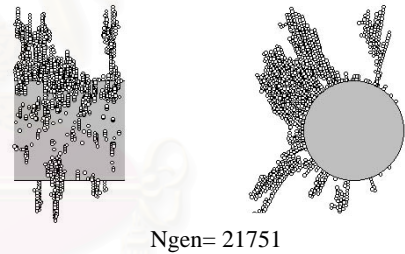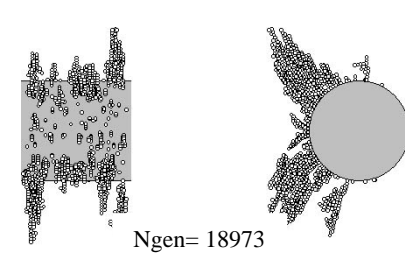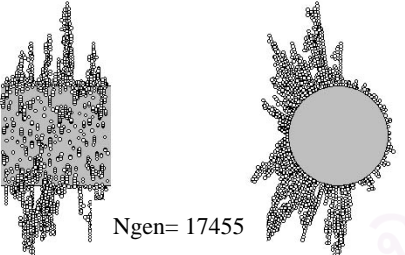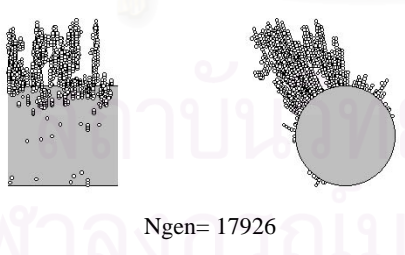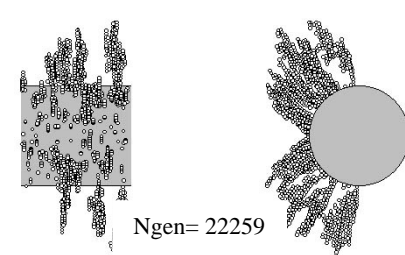
Pe	K_{In}=0.1	Kc=0.1		
		γ=90°	γ=135°	γ=180°
200	Ngen= 16775	Ngen= 14334	Ngen= 14714	Ngen= 16070
1000	Ngen= 15968	Ngen= 15937	Ngen= 18336	Ngen= 20250
5000	Ngen= 18576	Ngen= 17919	Ngen= 21751	Ngen= 18973
50000	Ngen= 17455	Ngen= 17926	Ngen= 23335	Ngen= 22259

Table 6.7 Typical dendrites configurations for the case of Ri = 0.03, K_{In} =0.1 and K_C = 0.1
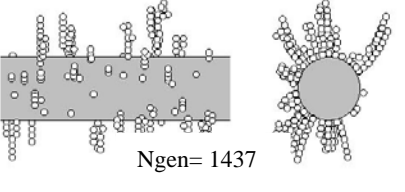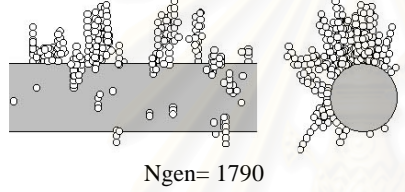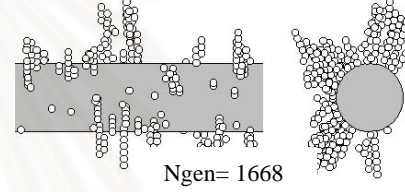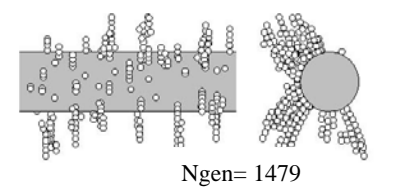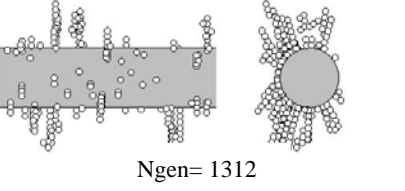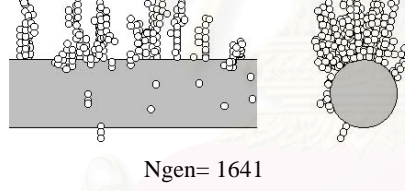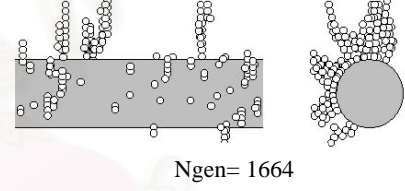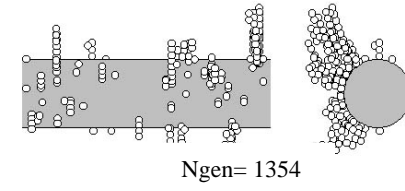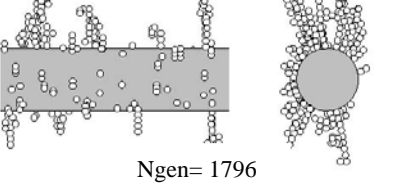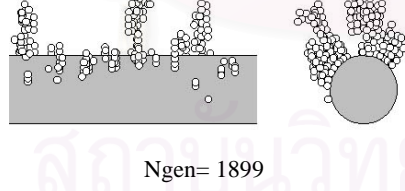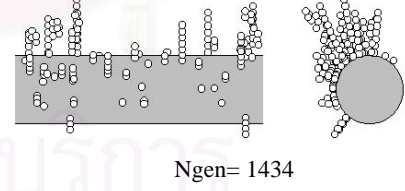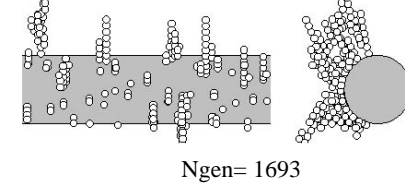
Pe	KIn=0.1	Kc=0.1		
		γ=90°	γ=135°	γ=180°
200	Ngen= 1591	Ngen= 1438	Ngen= 1273	Ngen= 1191
1000	Ngen= 1437	Ngen= 1790	Ngen= 1668	Ngen= 1479
5000	Ngen= 1312	Ngen= 1641	Ngen= 1664	Ngen= 1354
50000	Ngen= 1796	Ngen= 1899	Ngen= 1434	Ngen= 1693

Table 6.8 Typical dendrites configurations for the case of Ri = 0.1, K_{In} =0.1 and K_C = 0.1
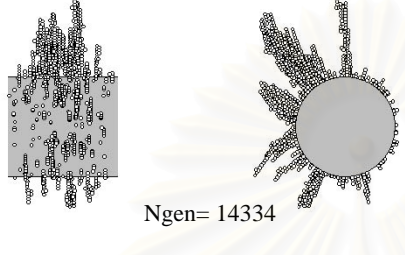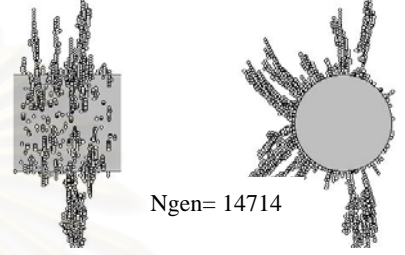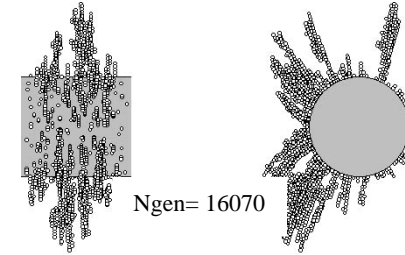
6.3.2 Aerosol deposition by induced force with diffusional effect

In this section, the simulation results of aerosol deposition by induced force are discussed in detail about angular distribution on a fiber, dendrite distribution, average dendrite size with age, initial collection efficiency, normalized collection efficiency and collection efficiency raising factor.

Angular distribution of number of deposited particles in a fiber

An angular distribution of particles on a fiber seems like figures in section 6.3.1 but for this section, this calculated from 50 sample sizes shown in Figure 6.32 to 6.43. At low Pe, captured particles are sporadic all over the entire surface even large and small-size of dendrites. But when Pe increases, a number of large-size of dendrite become reduced and locate around the stagnation point. This result agrees well with that in section 6.3.1. However when Ri increases, captured particles are dispersed in the front of stagnation point about 20-45 degree, which can be seen clearly in the figure. For the increase of K_{In}, there are more captured particles than that of low K_{In} at the same Ngen, but angular distribution look slightly different. However, the maximum Ngen for both of these are different and can be up to 23000.
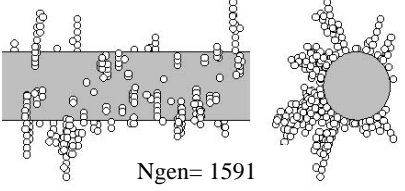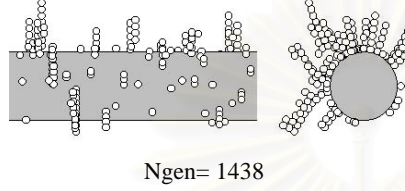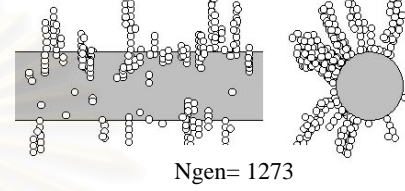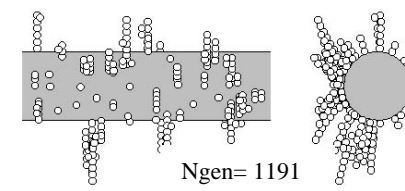
Dendrite Distribution on the fiber

Figure 6.44 to 6.49 show dendrite of size 1-6 that distribute on the fiber. Like the effect of Ri, the concentration of small dendrites decreases when Pe increases because diffusion is more favorable on small particle. However, for an increase of K_{In}, the concentration becomes larger because of a strong effect of K_{In}.

Average dendrite size with age

At low K_{In}, the results are slightly different at various Pe. Due to the fact that at low K_{In}, many particles can be captured then there are so many small-size dendrites. Consequently, average dendrite size can grow slowly. For the case of high Pe, fiber can collect fewer particles but there are few dendrites on the fiber. That's a reason why the results look slightly different. However, the results can be seen obviously at high K_{In}. This means that, at high K_{In}, the electrical effect dominates and fiber can collect more particles. And this can discriminate the results at various Pe. For the constant Pe and Ri, at high K_{In}, the results are lower than that of low K_{In} because at high K_{In}, there are so many small-size

dendrites, thus average dendrite becomes lower. The results of this can be seen in Figure 6.89-6.91.

Collection efficiency

Collection efficiency, η, can be seen in Table B1-B3 in Appendix B or in the Figure 119-120. In consideration of collection efficiency, η decreases with increasing Pe because of a decrease in diffusion effect. Furthermore, η increases with an increase of Ri because the particles are bigger. Then they are captured more easily. Finally, when electrical force is dominant, η increases with an increase of K_{In}.

Normalized collection efficiency

Figure 6.50-6.58 show the value of normalized collection efficiency with dust load. It is clear from the figure that this function is linear. The initial value of normalized collection for each condition is not equal to one because the simulated value partially deviate from that of the Emi's correlation obtained from experiment. This error can explain in 3 aspects:

1. The shape of fiber used in Emi's experiment is rectangular while the shape of this study corresponds to cylindrical fiber.

2. The range of particle size is 0.01-0.4 μm (Ri= 0.002-0.08) which is not appropriate for the case of Ri =0.1.

3. At high Pe, the air velocity is so high calculated by Equation (3.15). But in an Emi's experiment, this velocity is quite low about 0.05-2 m/s

When K_{In} becomes higher, the curve is not a perfectly linear function, which is different from the case of an ordinary filtration (non-electret fiber) but normalized collection efficiency gradually increases at low dust load. After a period of time, the number of captured particles are large enough to form agglomerates, so collection efficiency linearly increases and slope is steeper. It can be said that, at high K_{In} the normalized collection efficiency, η/η_0, can be represented by two linear correlations: the initial stage and the later stage, respectively. The former is represented by $\eta/\eta_0 = a_I + \lambda_I m$ and the latter by $\eta/\eta_0 = a + \lambda m$, respectively. As seen in the figure, the collection efficiency raising factor of the initial stage, λ_I, is smaller than that of the later or overall dust-loaded period, λ. This is due to the fact that at the initial stage or low dust load, the

effect of electrical parameter is prevailing. But at higher dust load or overall stage, dust load is dominant.

Collection efficiency raising factor

This can be concluded from Table C1-C3 in Appendix C or Figure 121-123 that collection efficiency raising factor, λ, increases with increasing Pe because of a decrease in η_0. Furthermore, λ increases with a decrease of Ri because η_0 increases. Eventually, λ increases with a decrease of K_{In}. Because η_0 increases.
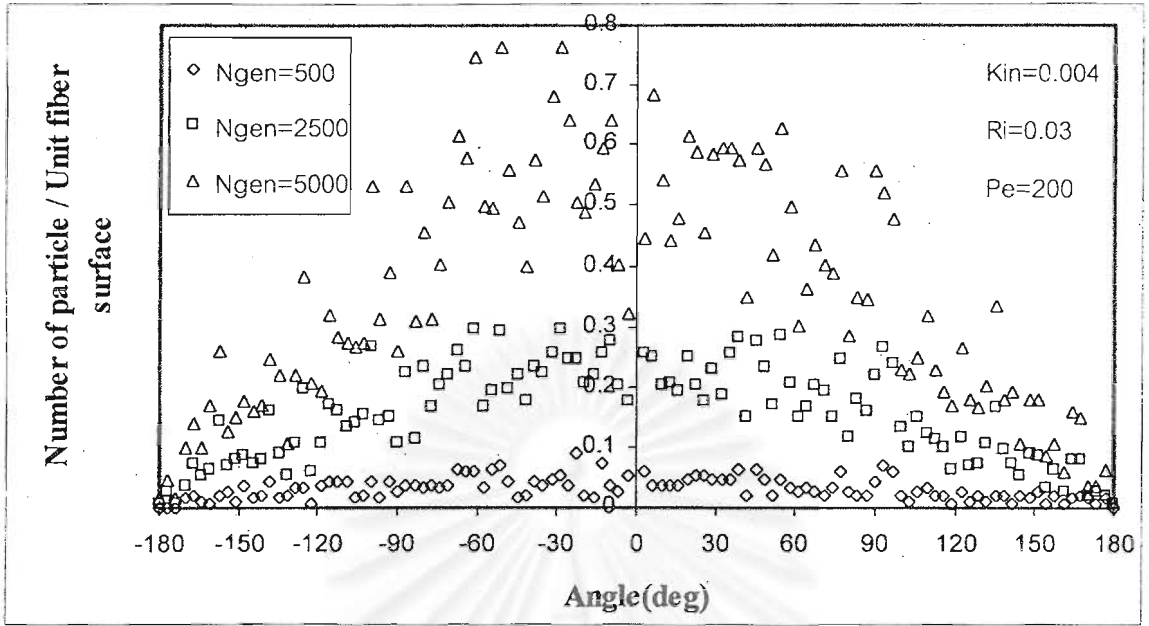
Figure 6.32 Angular distribution of number of deposited particles on a fiber
for the case of Ri=0.03, K$_{In}$=0.004 and Pe=200
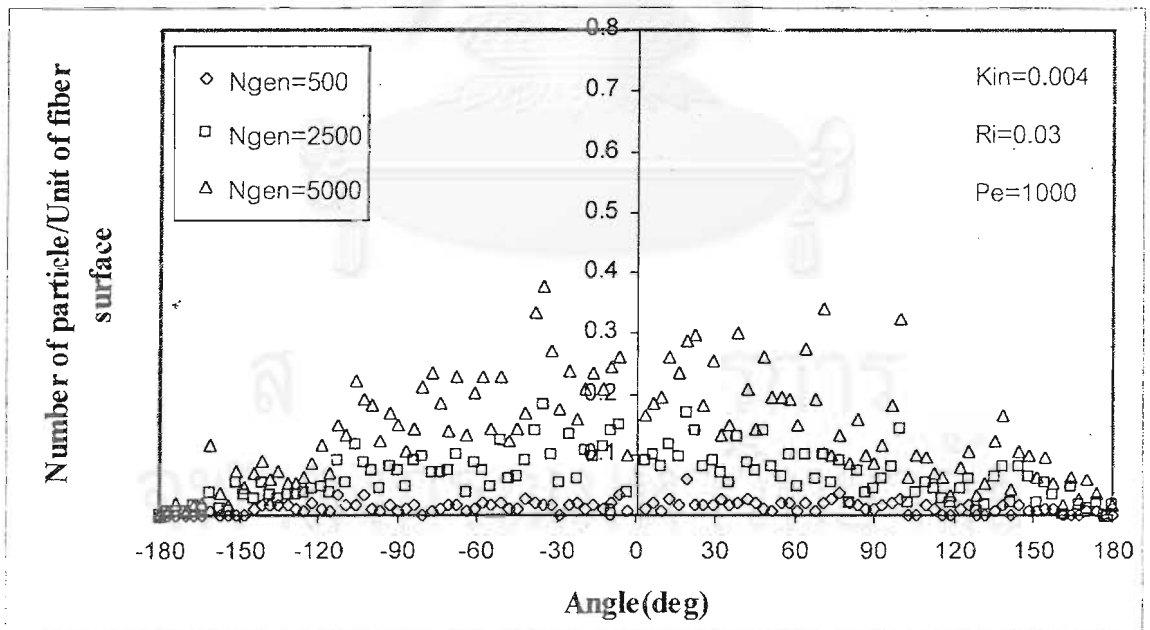
Figure 6.33 Angular distribution of number of deposited particles on a fiber
for the case of Ri=0.03, K$_{In}$=0.004 and Pe=1000
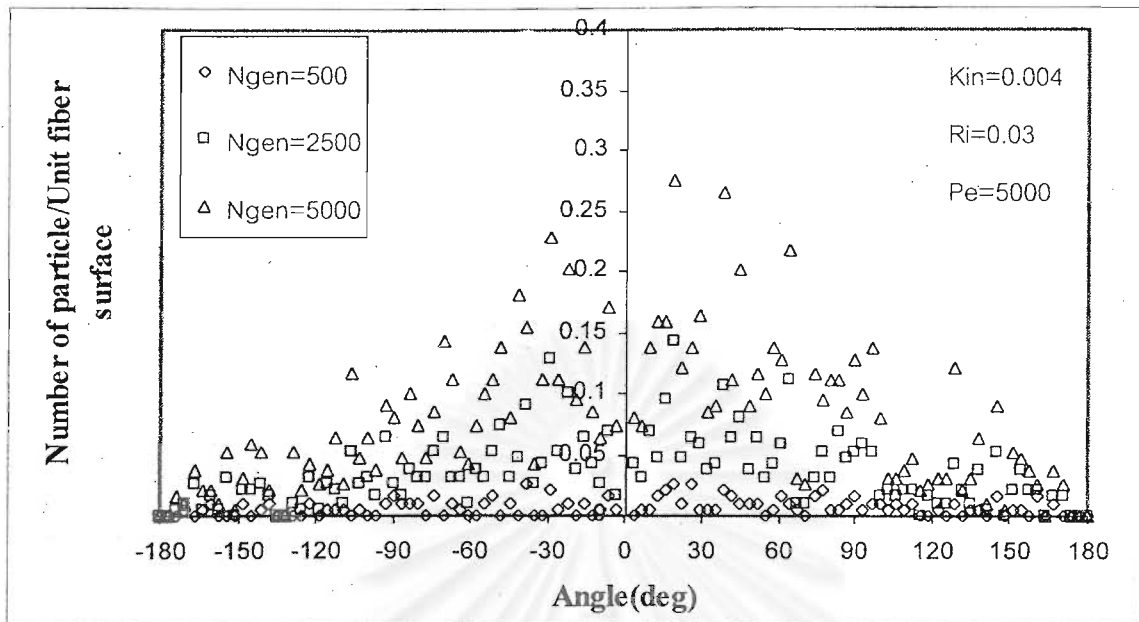
Figure 6.34 Angular distribution of number of deposited particles on a fiber
for the case of Ri=0.03, K_{In}=0.004 and Pe=5000
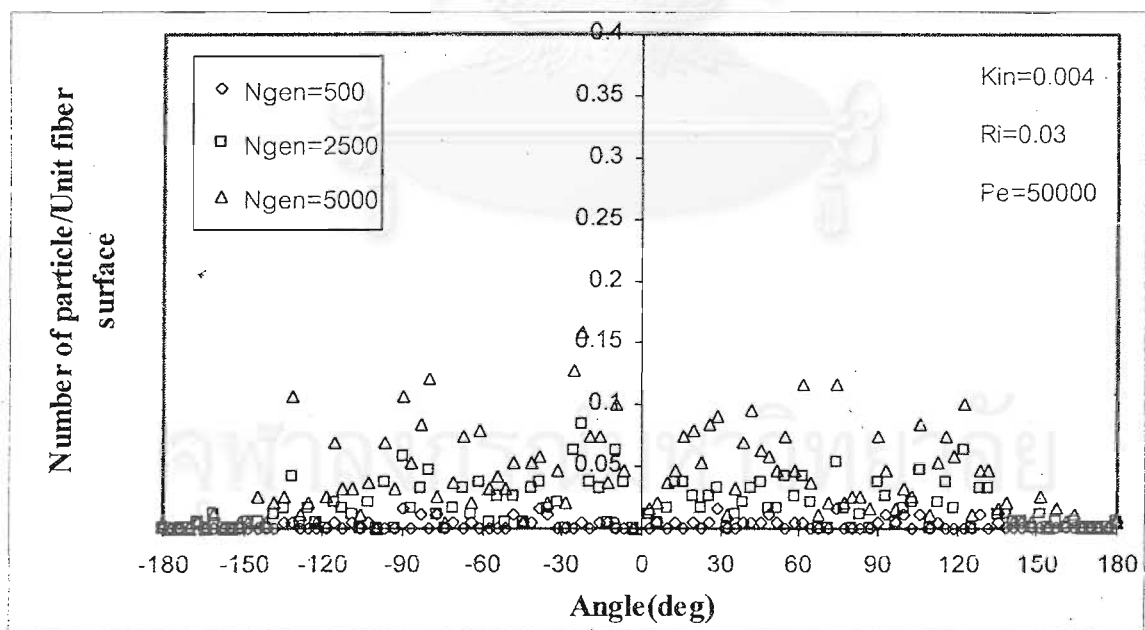
Figure 6.35 Angular distribution of number of deposited particles on a fiber
for the case of Ri=0.03, K_{In}=0.004 and Pe=50000
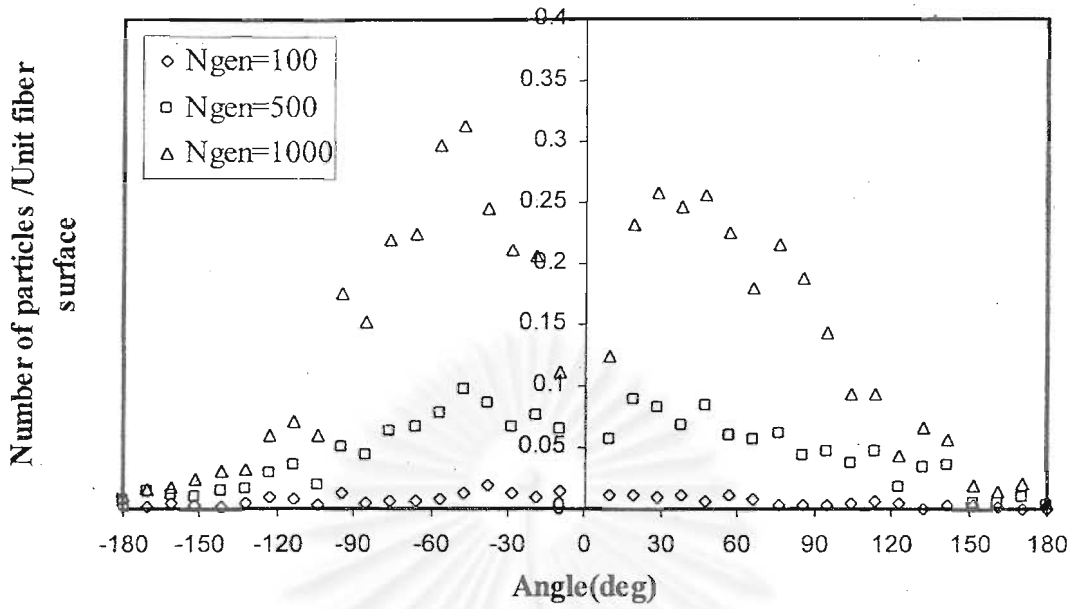
Figure 6.36 Angular distribution of number of deposited particles on a fiber
for the case of Ri=0.1, K_{In}=0.004 and Pe=200
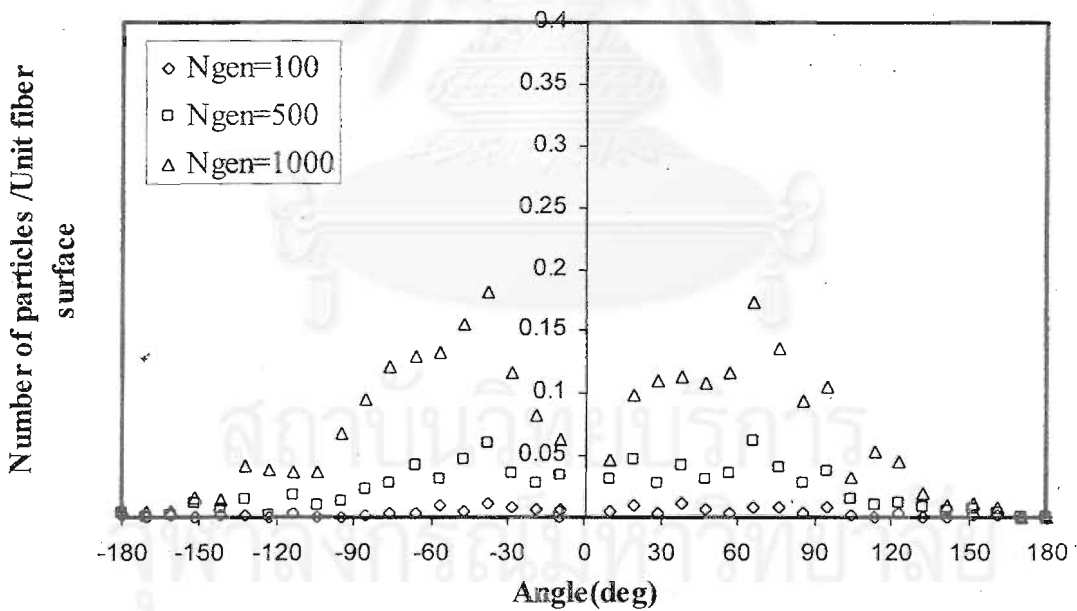
Figure 6.37 Angular distribution of number of deposited particles on a fiber
for the case of Ri=0.1, K_{In}=0.004 and Pe=1000
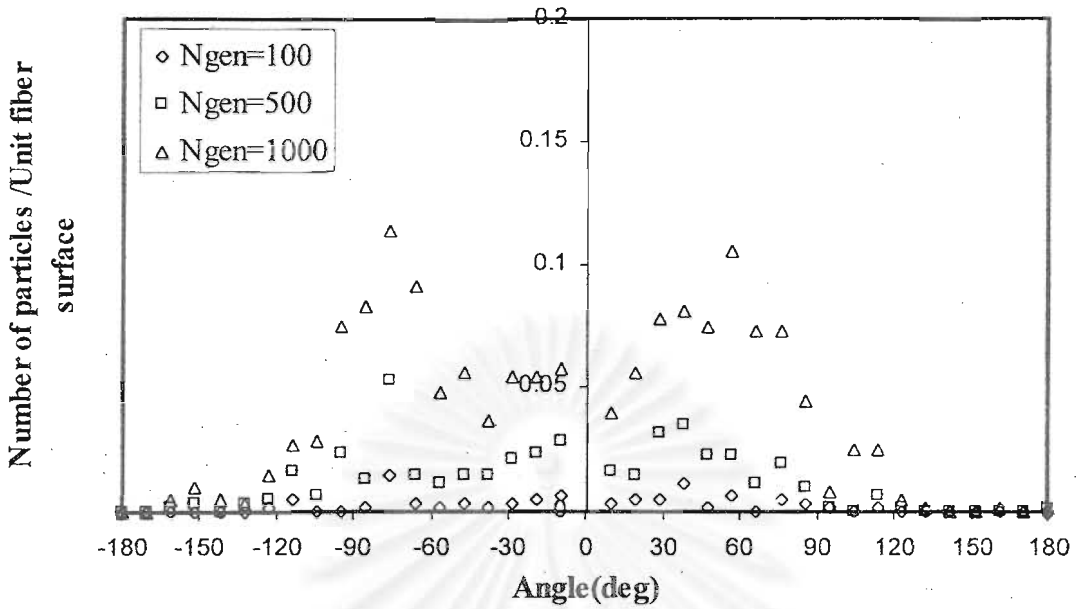
Figure 6.38 Angular distribution of number of deposited particles on a fiber
for the case of $Ri=0.1$, $K_{In}=0.004$ and $Pe=5000$
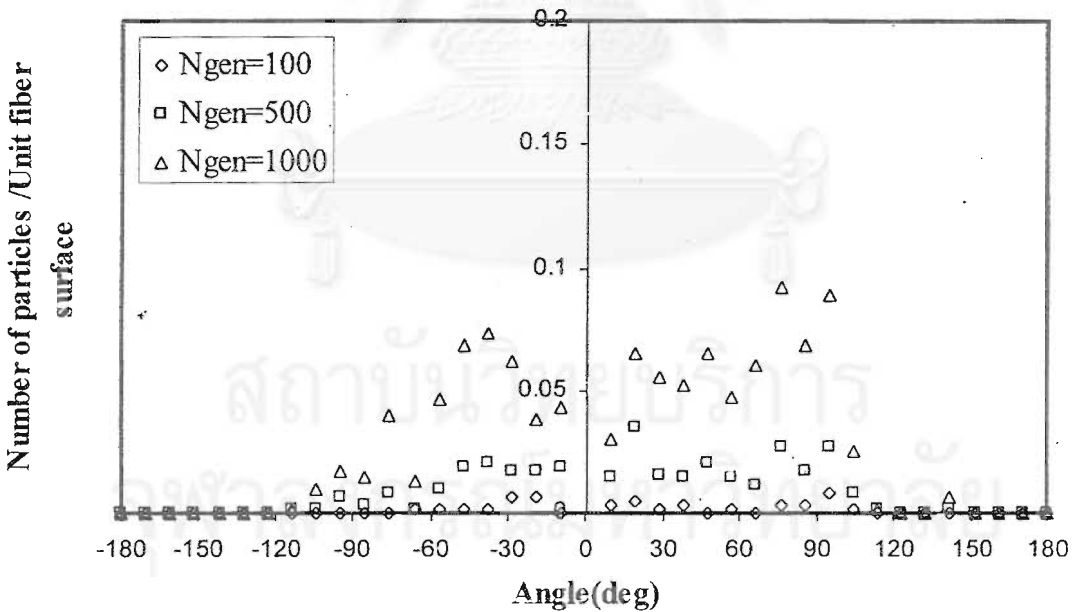
Figure 6.39 Angular distribution of number of deposited particles on a fiber
for the case of $Ri=0.1$, $K_{In}=0.004$ and $Pe=50000$
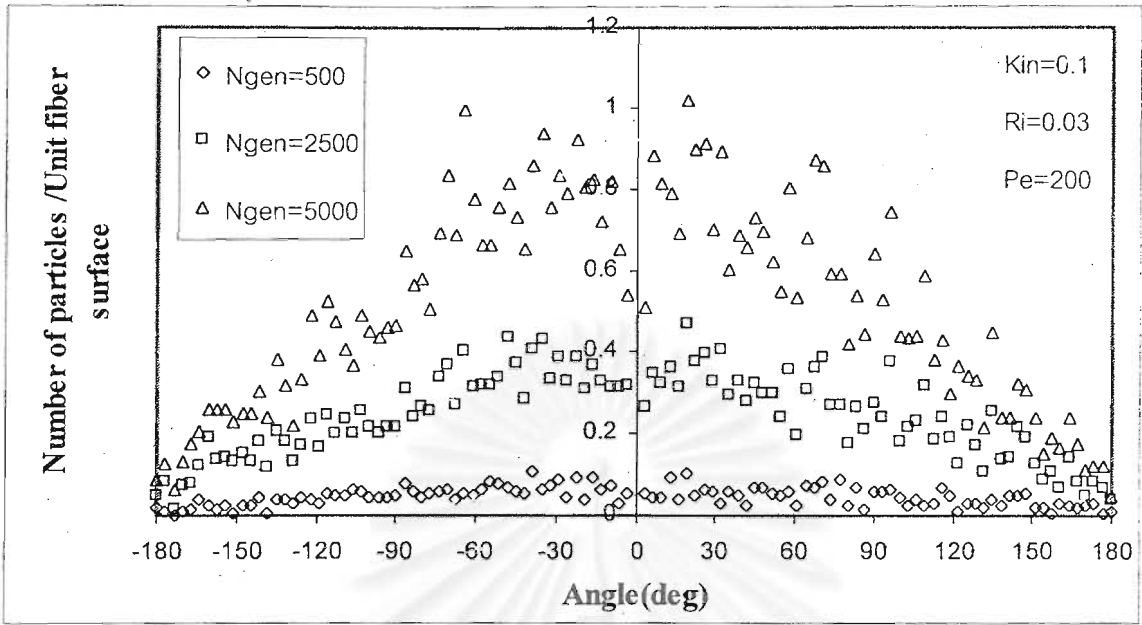
Figure 6.40 Angular distribution of number of deposited particles on a fiber

for the case of Ri=0.03, K_{In}=0.1 and Pe=200
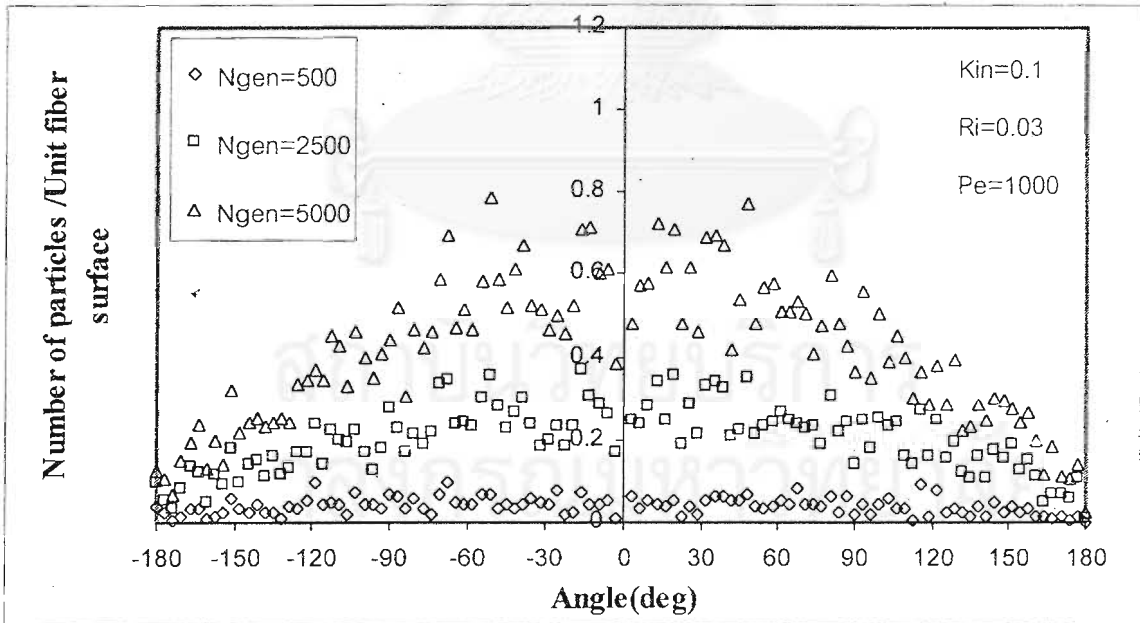
Figure 6.41 Angular distribution of number of deposited particles on a fiber

for the case of Ri=0.03, K_{In}=0.1 and Pe=1000
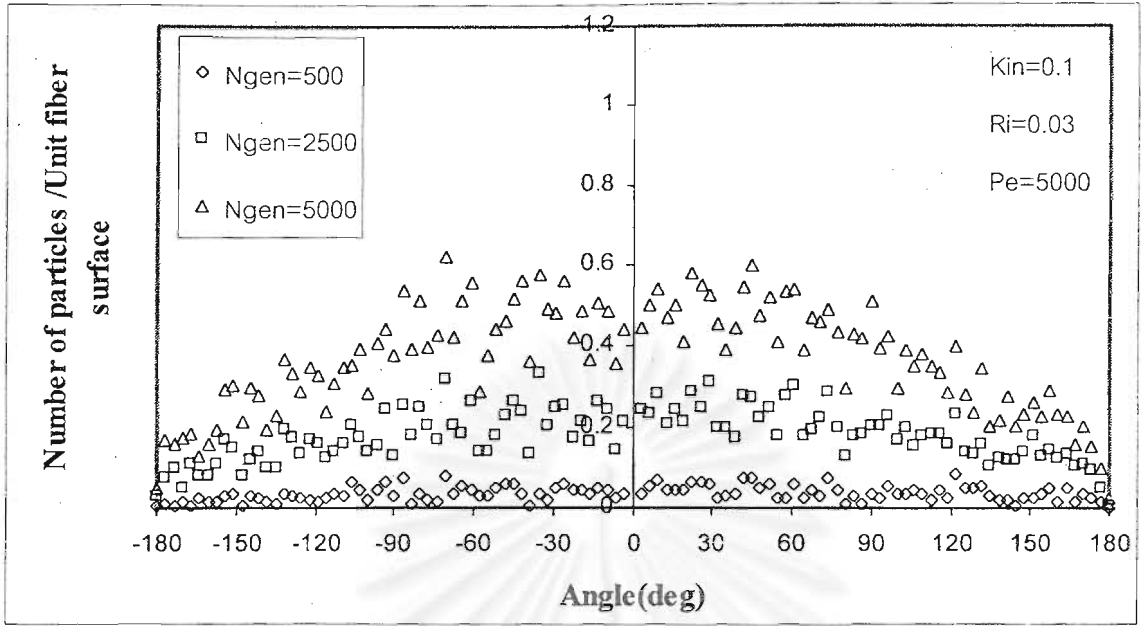
Figure 6.42 Angular distribution of number of deposited particles on a fiber
for the case of Ri=0.03, K_{In}=0.1 and Pe=5000
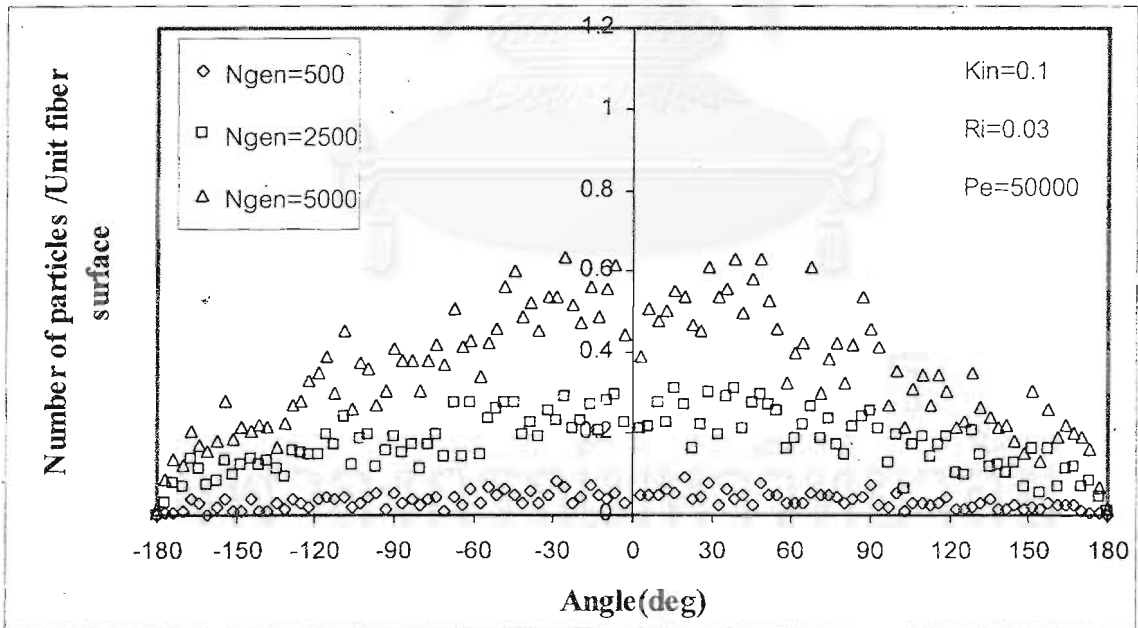
Figure 6.43 Angular distribution of number of deposited particles on a fiber
for the case of Ri=0.03, K_{In}=0.1 and Pe=50000
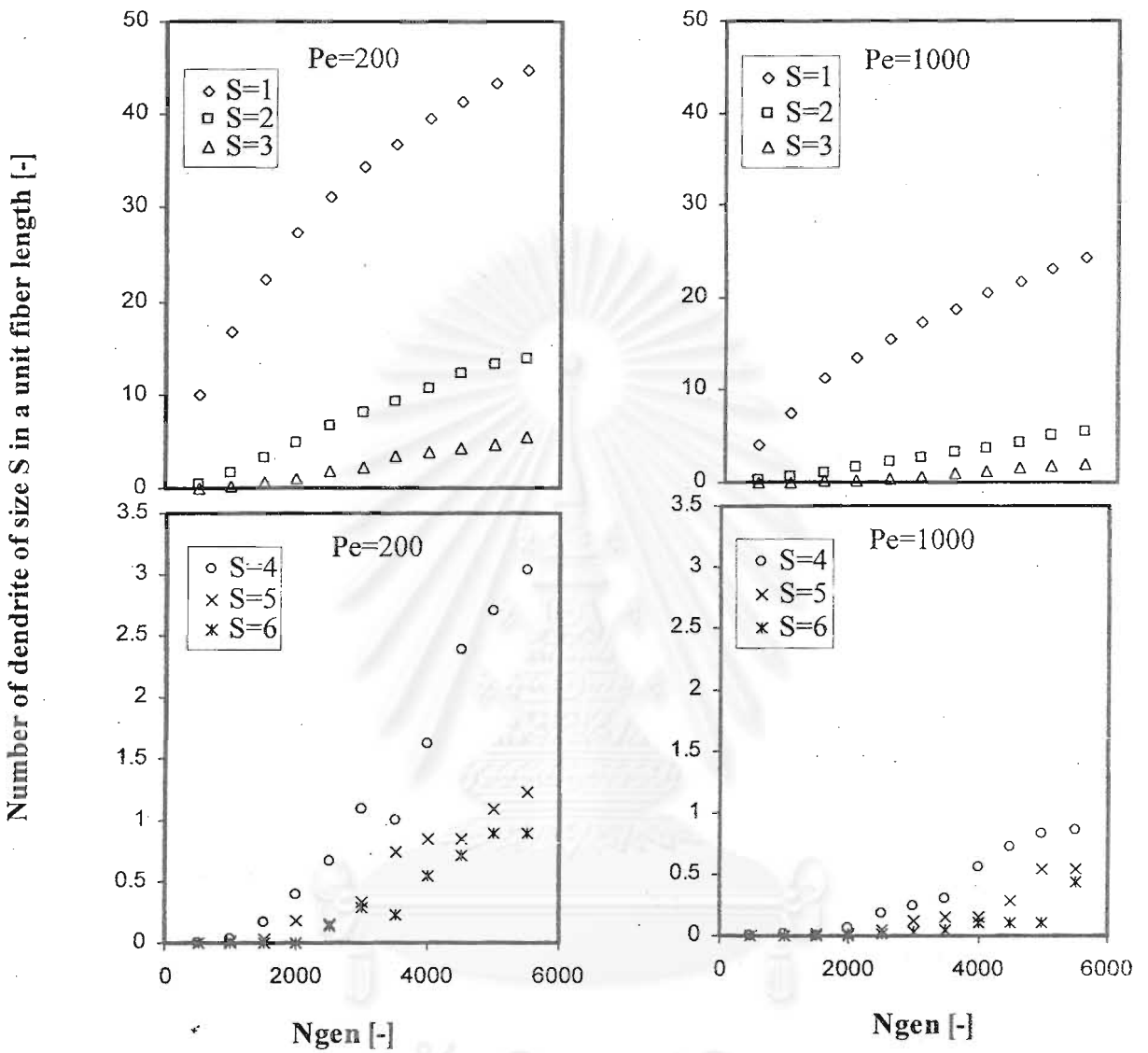
Figure 6.44 Time dependency of number of dendrite in a unit fiber length for
the case of Ri=0.03 and K$_{In}$=0.004 (Pe=200 and 1000)
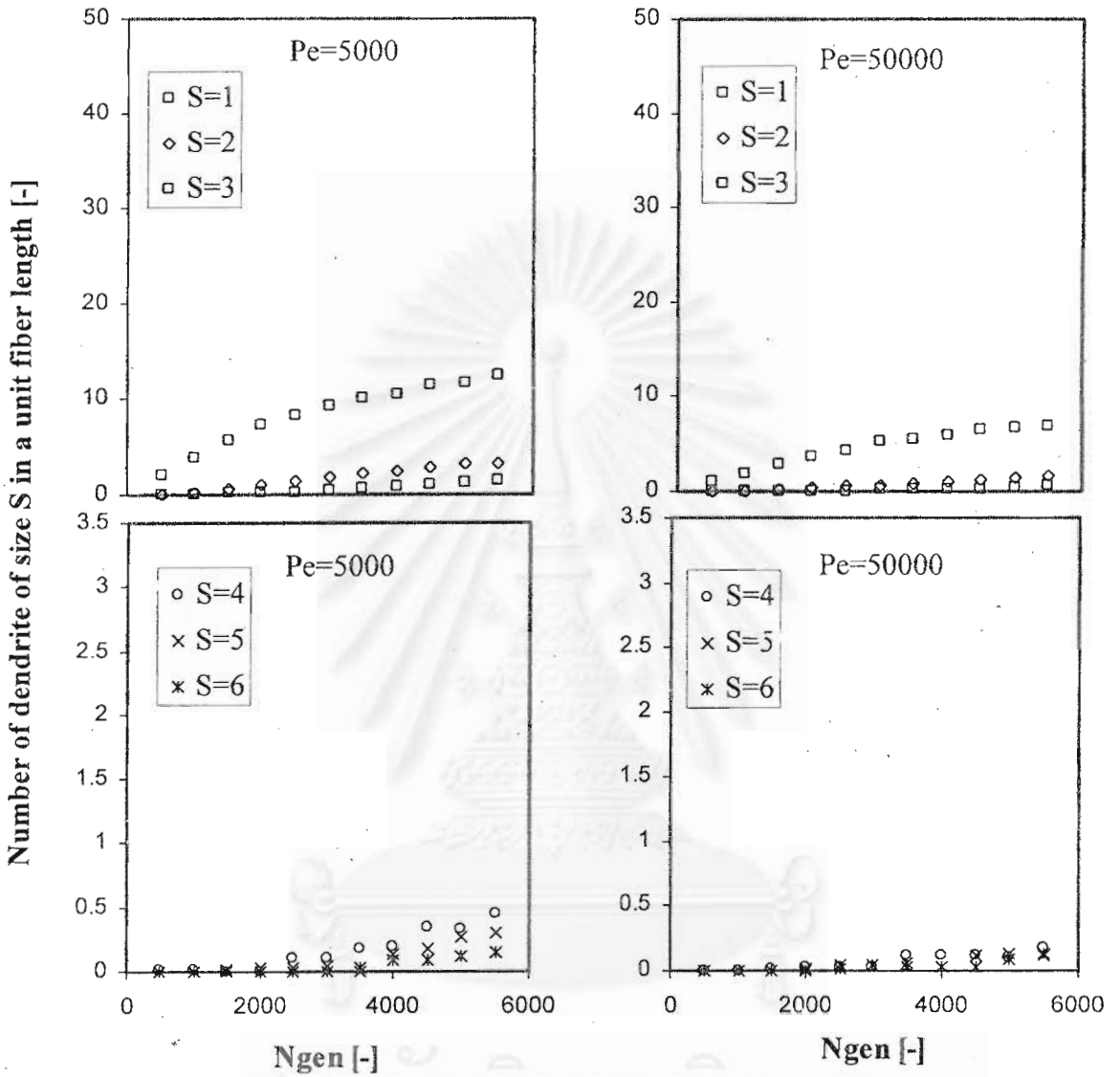
Figure 6.45 Time dependency of number of dendrite in a unit fiber length for
the case of Ri=0.03 and K_{In}=0.004 (Pe=5000 and 50000)
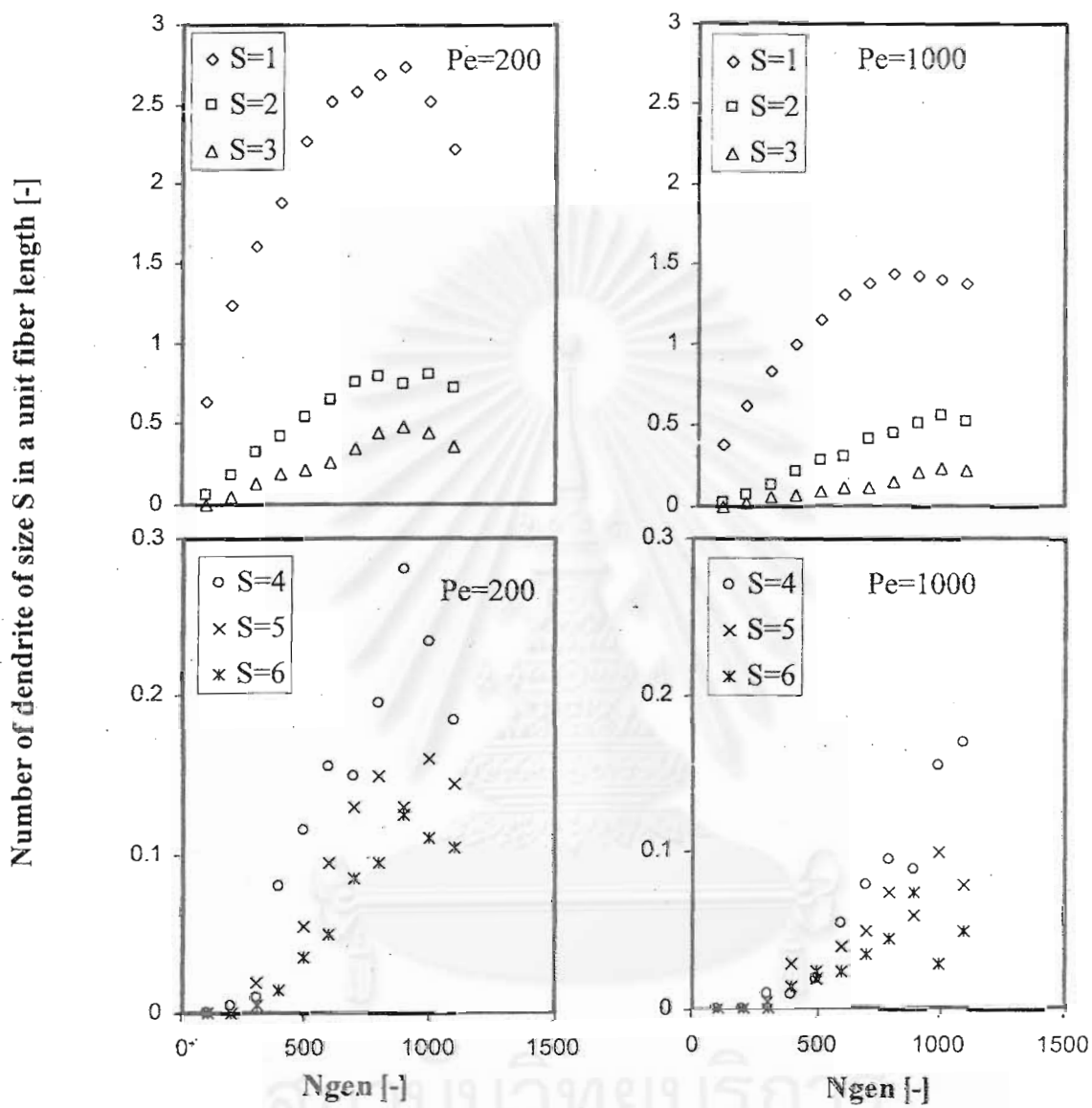
Figure 6.46 Time dependency of number of dendrite in a unit fiber length for the case of Ri=0.1 and K$_{fn}$=0.004 (Pe=200 and 1000)
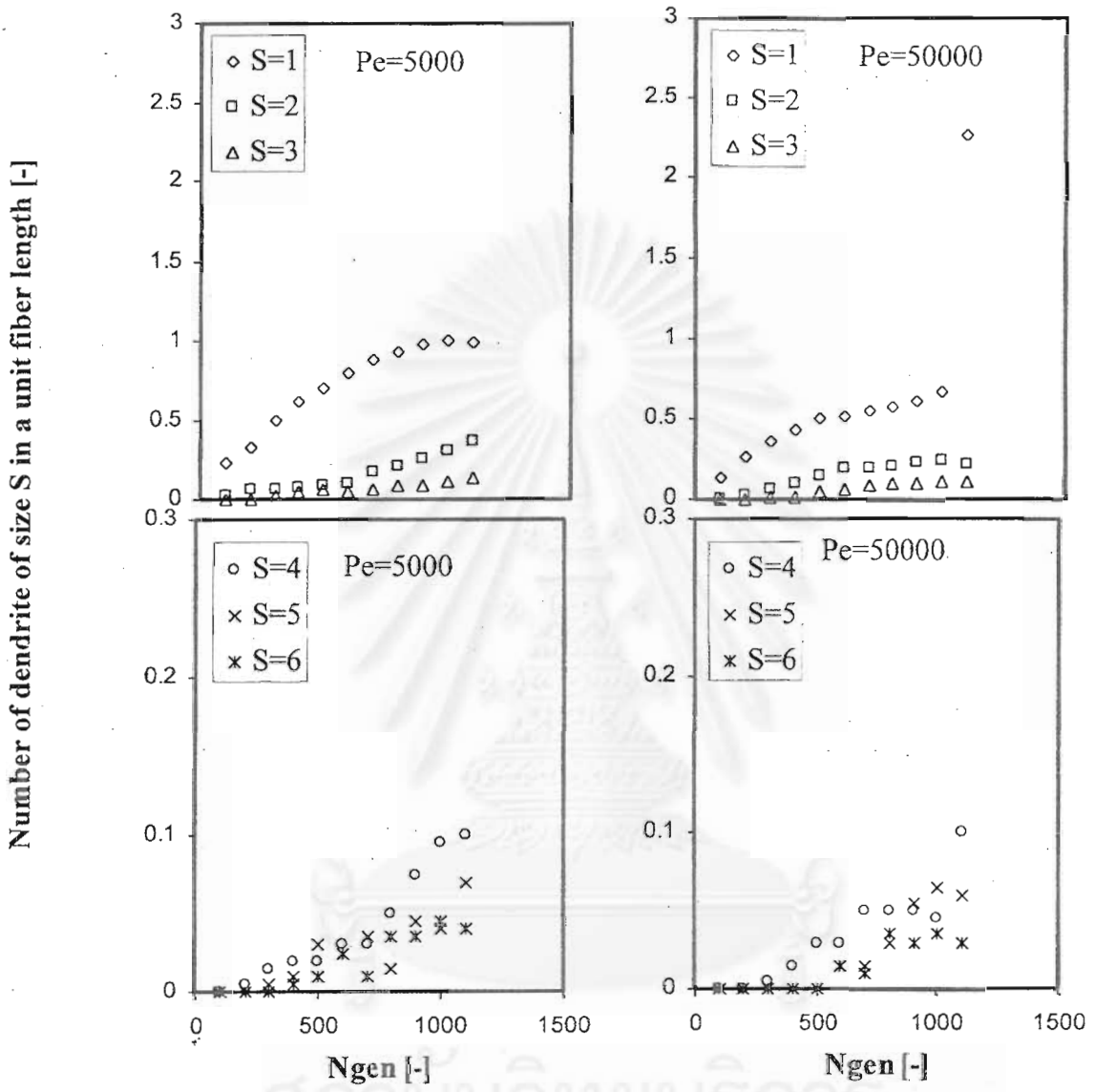
Figure 6.47 Time dependency of number of dendrite in a unit fiber length for

the case of Ri=0.1 and K_{In}=0.004 (Pe=5000 and 50000)
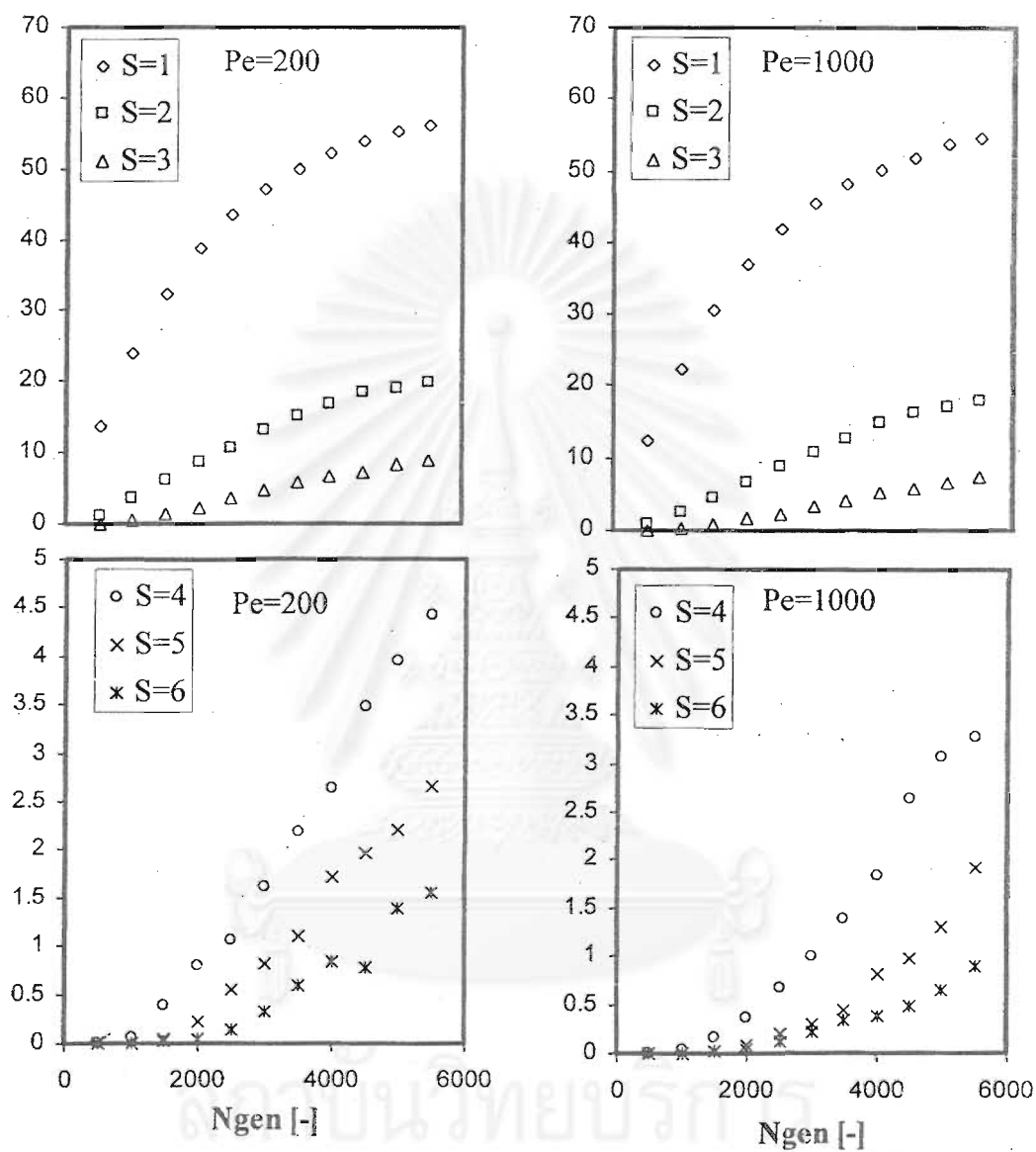
Figure 6.48 Time dependency of number of dendrite in a unit fiber length for the case of $R_i=0.03$ and $K_{In}=0.1$ (Pe=200 and 1000)
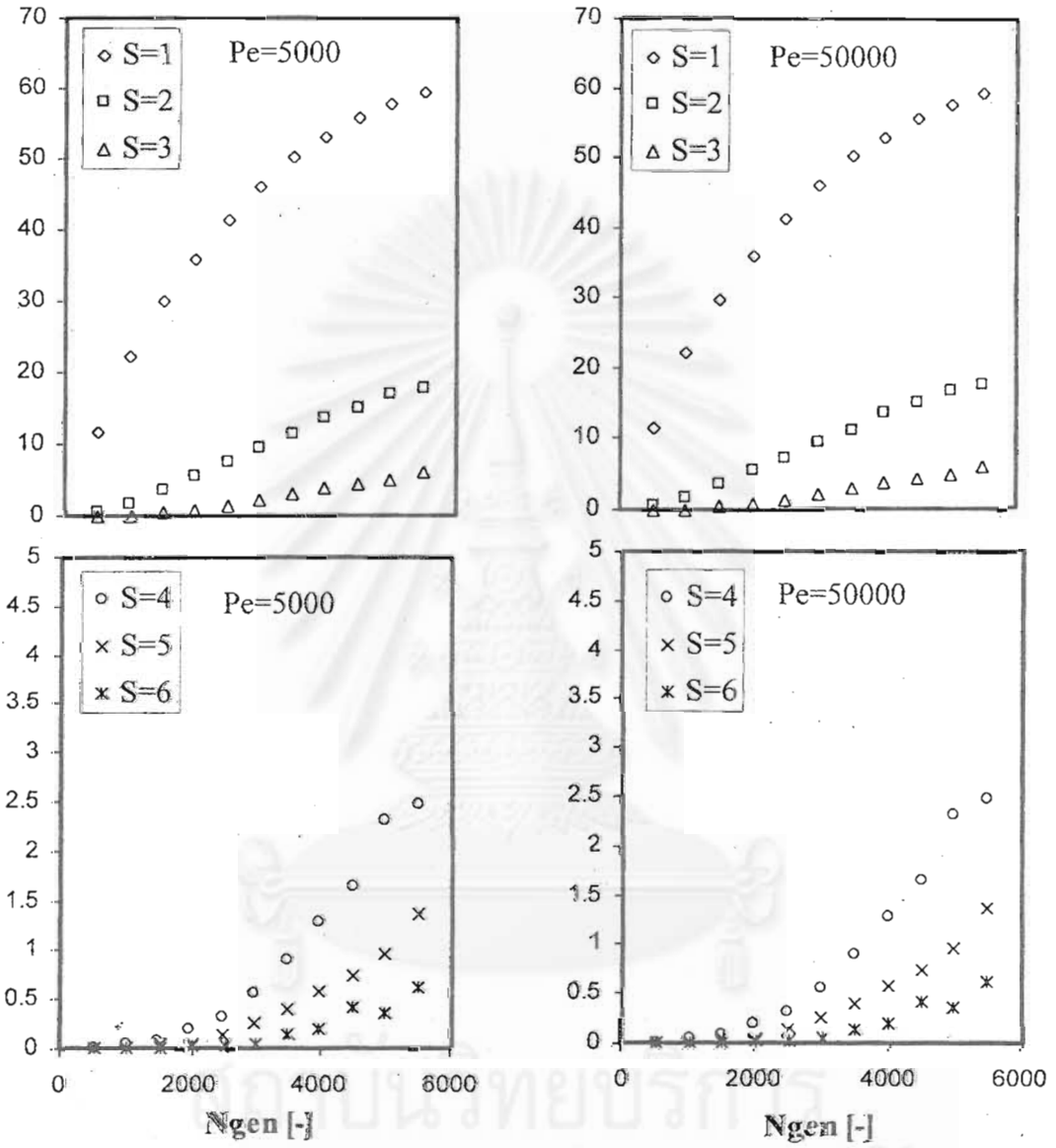
Figure 6.49 Time dependency of number of dendrite in a unit fiber length for the case of Ri=0.03 and K_{In}=0.1 (Pe=5000 and 50000)
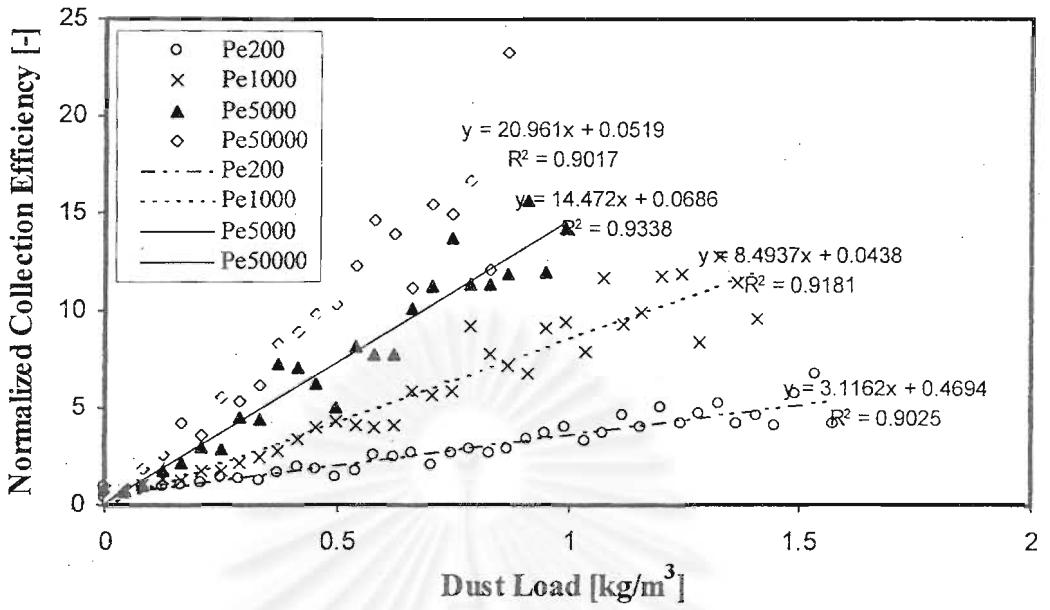
Figure 6.50 Normalized collection efficiency of a dust-loaded fiber for the
case of Ri=0.03 and K_{In} = 0.004
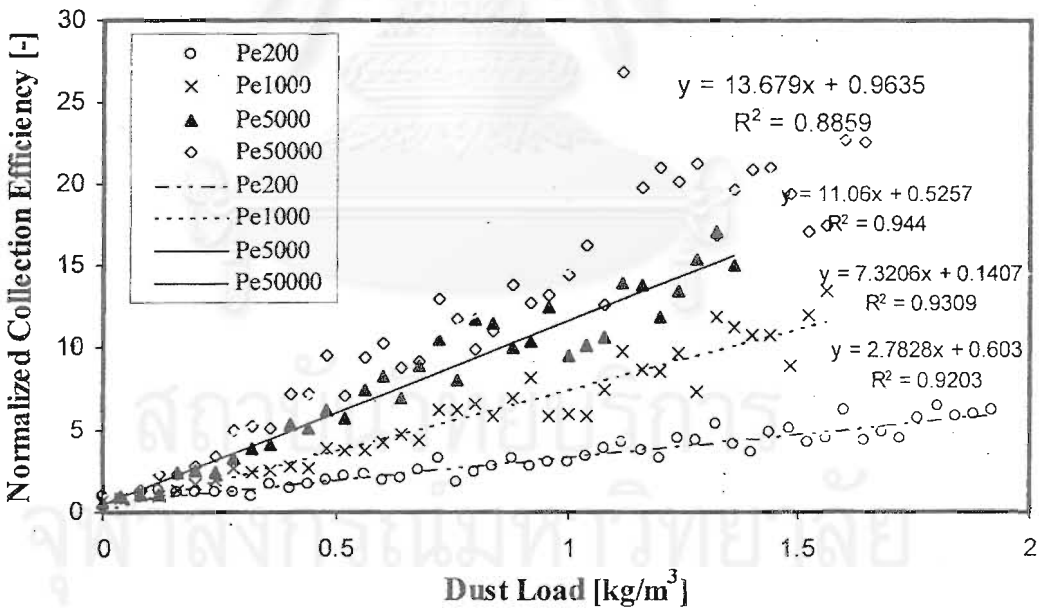
Figure 6.51 Normalized collection efficiency of a dust-loaded fiber for the
case of Ri=0.05 and K_{In} = 0.004
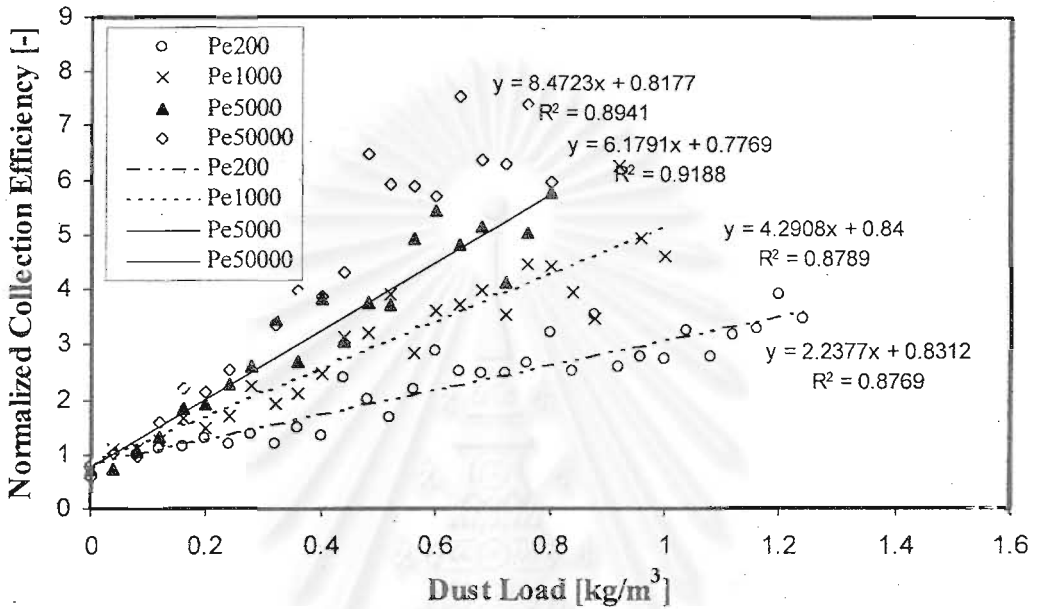
Figure 6.52 Normalized collection efficiency of a dust-loaded fiber for the
case of Ri=0.1 and K_{In} = 0.004
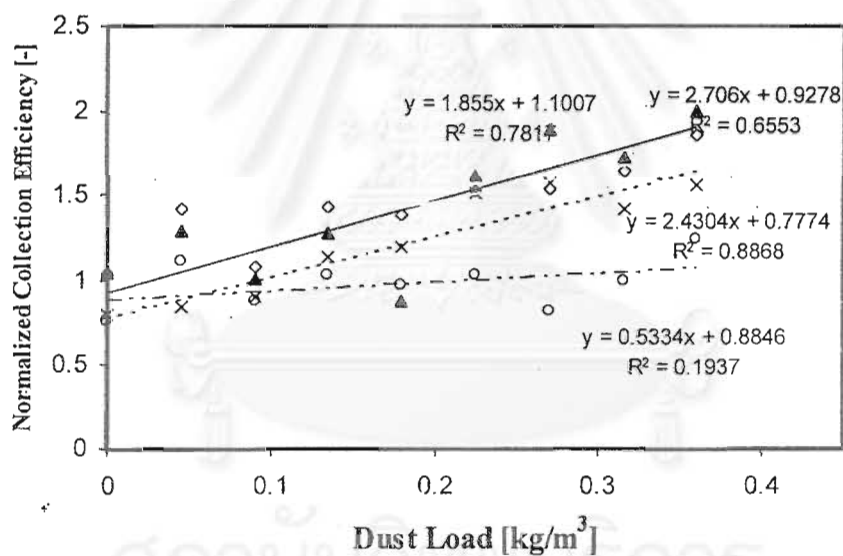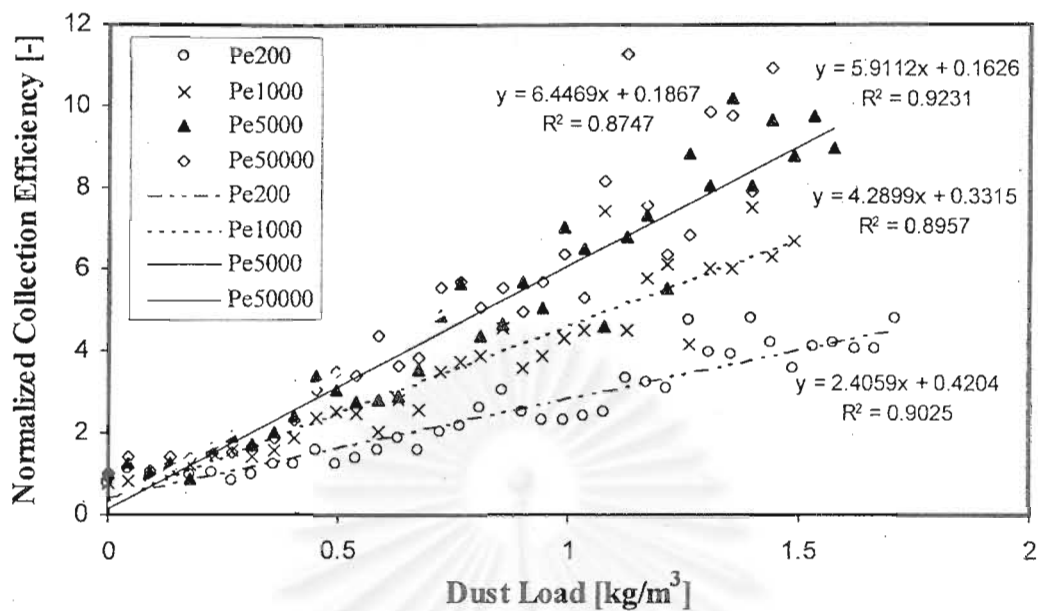
Figure 6.53 Normalized collection efficiency of a dust-loaded fiber for the

case of Ri=0.03 and K_{In} = 0.05

(above : overall dust load period, below : initial dust load period)
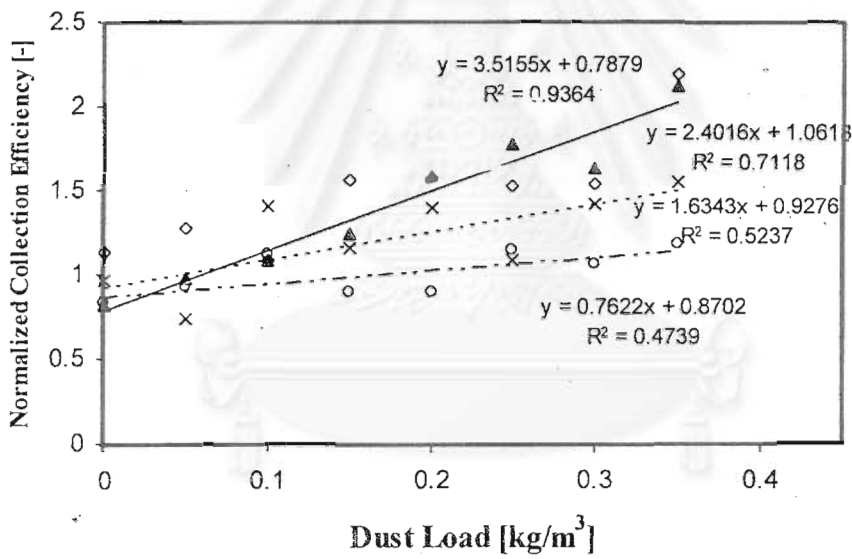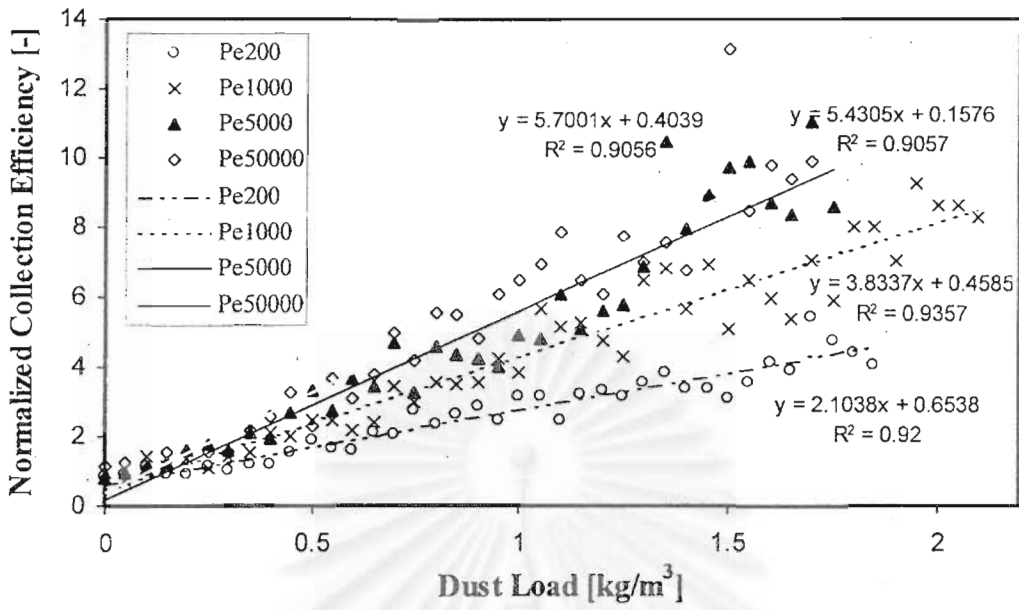
Figure 6.54 Normalized collection efficiency of a dust-loaded fiber for the

case of Ri=0.05 and $K_{In} = 0.05$

(above : overall dust load period, below : initial dust load period)
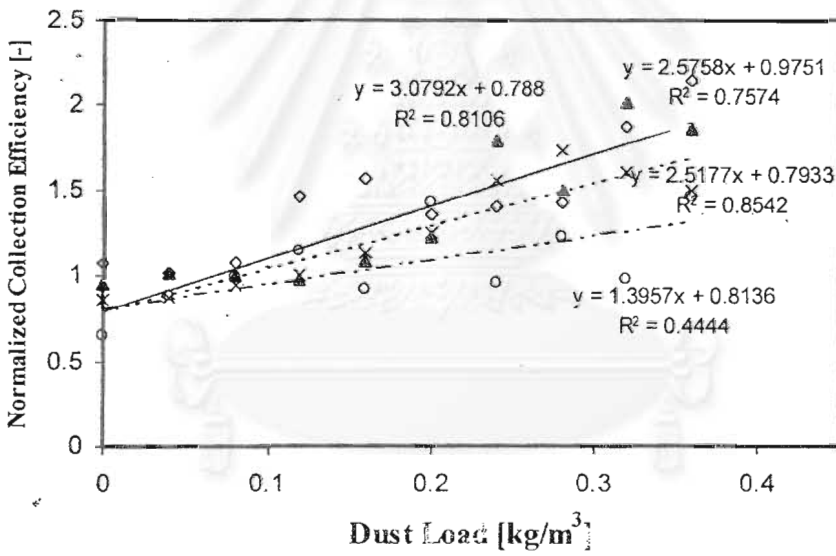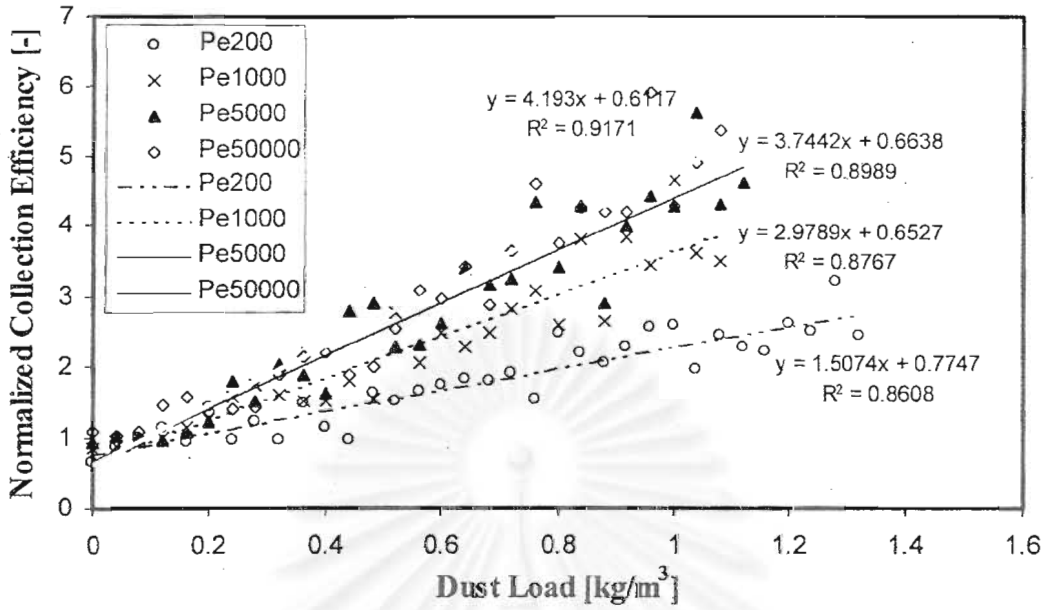
Figure 6.55 Normalized collection efficiency of a dust-loaded fiber for the
case of Ri=0.1 and $K_{In} = 0.05$
(above : overall dust load period, below : initial dust load period)
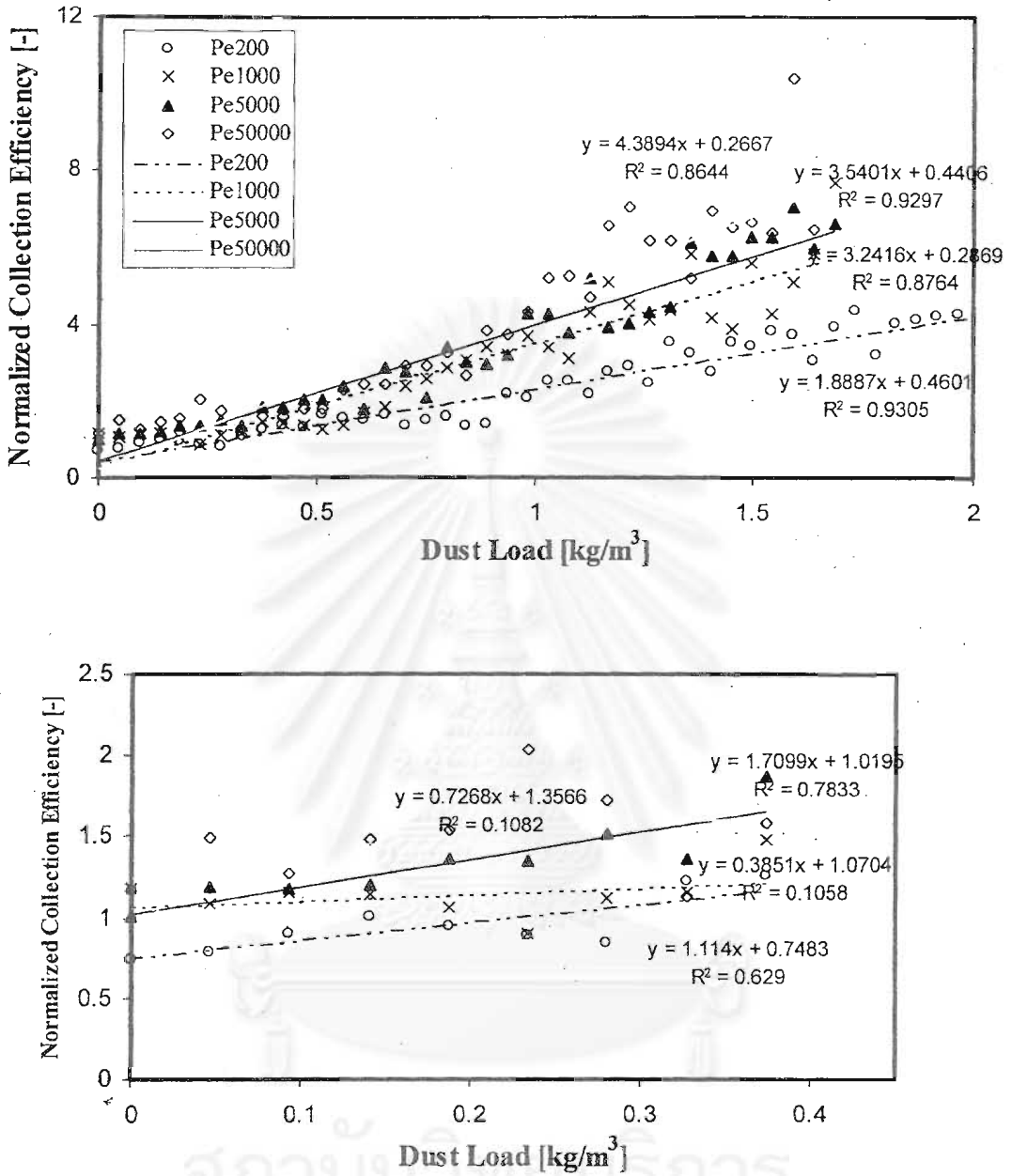
Figure 6.56 Normalized collection efficiency of a dust-loaded fiber for the

case of Ri=0.03 and K_{In} = 0.1

(above : overall dust load period, below : initial dust load period)
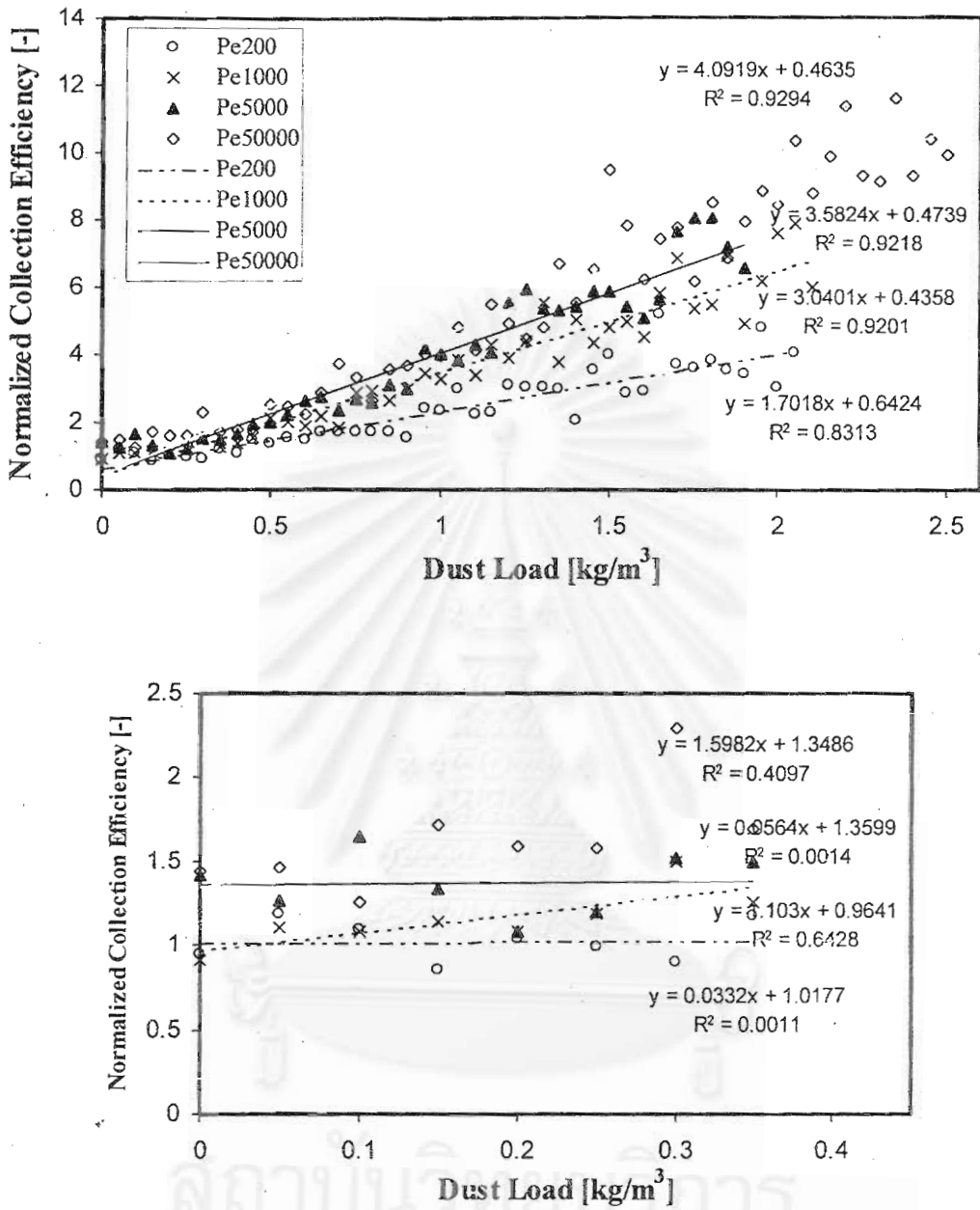
Figure 6.57 Normalized collection efficiency of a dust-loaded fiber for the
case of Ri=0.05 and K_{in} = 0.1

(above : overall dust load period, below : initial dust load period)
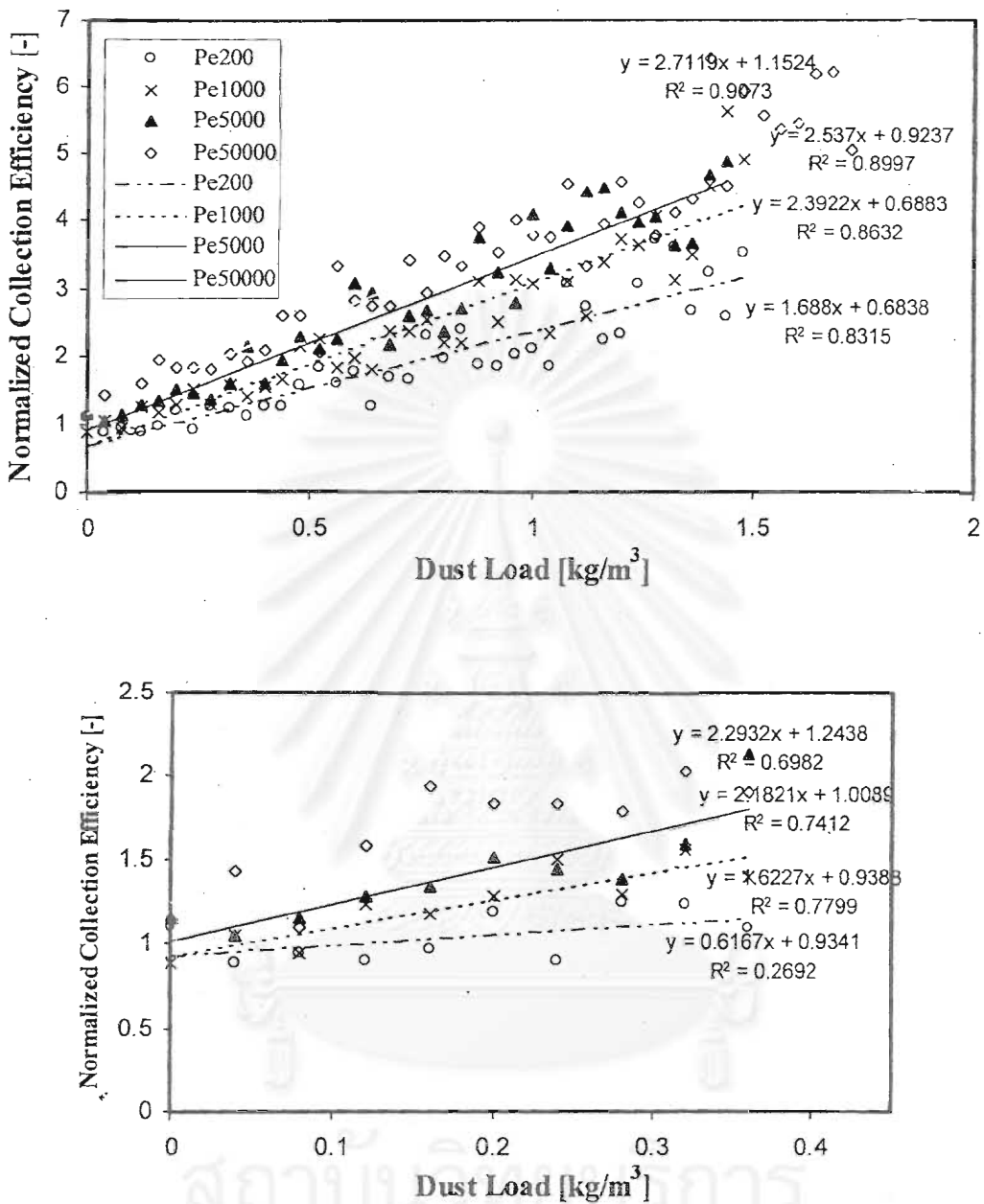
Figure 6.58 Normalized collection efficiency of a dust-loaded fiber for the
case of Ri=0.1 and K_{In} = 0.1

(above : overall dust load period, below : initial dust load period)

6.3.3 Aerosol deposition by coulombic force with diffusional effect

Like the results of aerosol deposition by induced force, in this section, the simulation results of aerosol deposition by coulombic force are discussed in detail about angular distribution on a fiber, dendrite distribution, average dendrite size with age, initial collection efficiency, normalized collection efficiency and collection efficiency raising factor. And the effect of twist angle of an electret fiber is also studied.

Angular distribution of number of deposited particles in a fiber

The angular distributions of particles on a fiber for various conditions are shown in Figure 6.59 to 6.78. At low Pe, captured particles are scattered almost all over the whole surface even large and small-size of dendrites. But when Pe increases, a number of large-size of dendrite become reduced and locate only around the stagnation point. This result agrees well with that in section 6.3.1. Furthermore, at twist angle, γ, equal to 90 degree, particles are captured only on the limited area of opposite polarity and stay densely at angle about 90 degree. On the contrary, when γ increases up to 180 degree, the densely captured area is shifted near a stagnation point. However when Ri increases, captured particles are dispersed in the front of stagnation point about 30-60 degree and dendrites are smaller than that at low Ri, which can be seen clearly in the figure. For the increase of K_C, there are more captured particles than that of low K_C at the same Ngen, but angular distribution look slightly different especially the rear side and shift to the opposite polarity area.

Dendrite Distribution on the fiber

Figure 6.79 to 6.88 show dendrite of size 1-6 that distribute on the fiber. Like the effect of Ri, the concentration of small dendrites decreases when Pe increases because diffusion is more favorable on small particle. However, for an increase of K_C, the concentration becomes larger because of a strong effect of K_C. In the twist angle's point of view, dendrite distributions of various angles are the same at low Pe, but look slightly different at high Pe.

Average dendrite size with age

At low K_C, the results are slightly different at various Pe and γ. Due to the fact that at low K_C, many particles can be captured then the many small-size dendrites occur. As a result, average dendrite size can grow slowly. For the case of high Pe, fiber can collect fewer particles but there are few dendrites on the fiber. That's a reason why the results look slightly different. However, the results can be seen obviously at high K_C except for γ= 90 degree. This means that, at high K_C, the electrical effect dominates and fiber can collect more particles. And this can discriminate the results at various Pe. For the constant Pe and Ri, at high K_C, the results are lower than that of low K_C because at high K_C, there are so many small-size dendrites, thus average dendrite becomes lower. The results of this can be seen in Figure 6.89-6.91.

Collection efficiency

Collection efficiency, η, can be seen in Table B1-B3 in Appendix B or in the Figure 119-120. In consideration of collection efficiency, η decreases with increasing Pe due to a decrease in diffusion effect. Furthermore, η increases with an increase of Ri because the particles are bigger. Consequently, they are captured more easily. In addition, η increases slightly as γ increases. Finally, when electrical force is dominant, η increases with an increase of K_C.

Normalized collection efficiency

Figure 6.92-6.118 show the value of normalized collection efficiency with dust load. It is apparent from the figure that this function is linear. The initial value of normalized collection for each condition is not equal to one because the simulated value partially deviate from that of the Emi's correlation obtained from experiment. This error can explain as mentioned in 6.3.2.

Like the results in the case of K_{In}, when K_C becomes higher, the curve is not a perfectly linear function, which is different from the case of an ordinary filtration (non-electret fiber) but normalized collection efficiency gradually increases at low dust load. After a period of time, the number of captured particles are significant enough to form agglomerates, so collection efficiency linearly increases and slope is precipitous. It can be said that, at high K_C the normalized collection efficiency, $η/η_0$, can be represented by two

linear correlations: the initial stage and the subsequent stage, respectively. The former is represented by $\eta/\eta_0 = a_I + \lambda_I m$ and the latter by $\eta/\eta_0 = a + \lambda m$, respectively. As seen in the figure, the collection efficiency raising factor of the initial stage, λ_I, is smaller than that of the later or overall dust-loaded period, λ. This is due to the fact that at the initial stage or low dust load, the effect of electrical parameter is prevailing. But at higher dust load or overall stage, dust load is dominant. From the figures, the effect of γ on the normalized collection efficiency is not different and hard to clarify because it is necessary to fully understand how the electrical charges on the deposited particles are transferred among themselves and between them and the electret fiber.

Collection efficiency raising factor

This can be deduced from Table C1-C3 in Appendix C or Figure 121-123 that collection efficiency raising factor, λ, increases with increasing Pe owing to a decrease in η_0. Furthermore, λ increases with a decrease of Ri because η_0 increases. Eventually, λ increases with a decrease of K_C. Because η_0 increases. In consideration of γ, γ increases but λ because the effect of is not thoroughly understand yet as stated above.

Figure 6.59 Angular distribution of number of deposited particles on a fiber
for the case of Ri=0.03, K_C=0.016, Gamma = 90 and Pe=200

Figure 6.60 Angular distribution of number of deposited particles on a fiber
for the case of Ri=0.03, K_C=0.016 Gamma = 90and Pe=50000
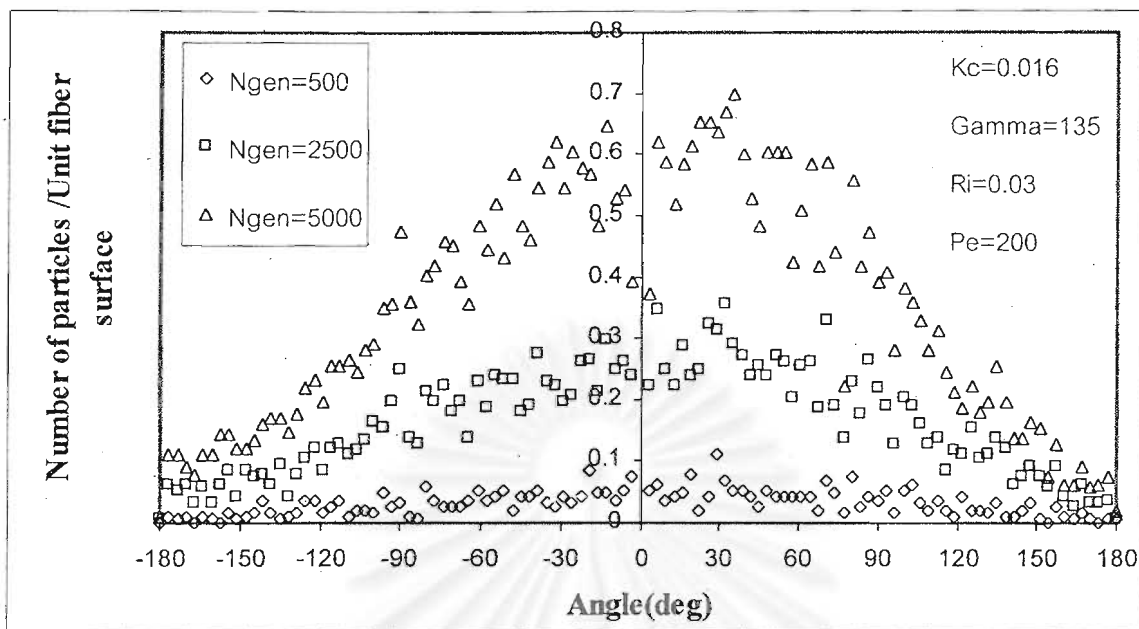
Figure 6.61 Angular distribution of number of deposited particles on a fiber
for the case of Ri=0.03, K$_C$=0.016, Gamma = 135 and Pe=200
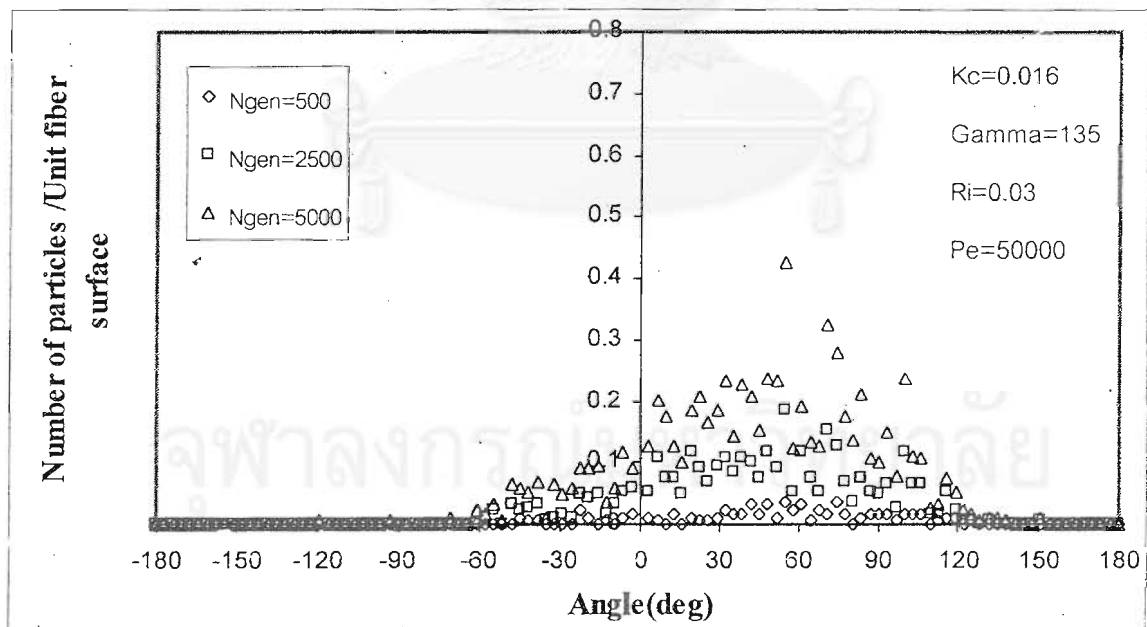
Figure 6.62 Angular distribution of number of deposited particles on a fiber
for the case of Ri=0.03, K$_C$=0.016 Gamma = 135 and Pe=50000
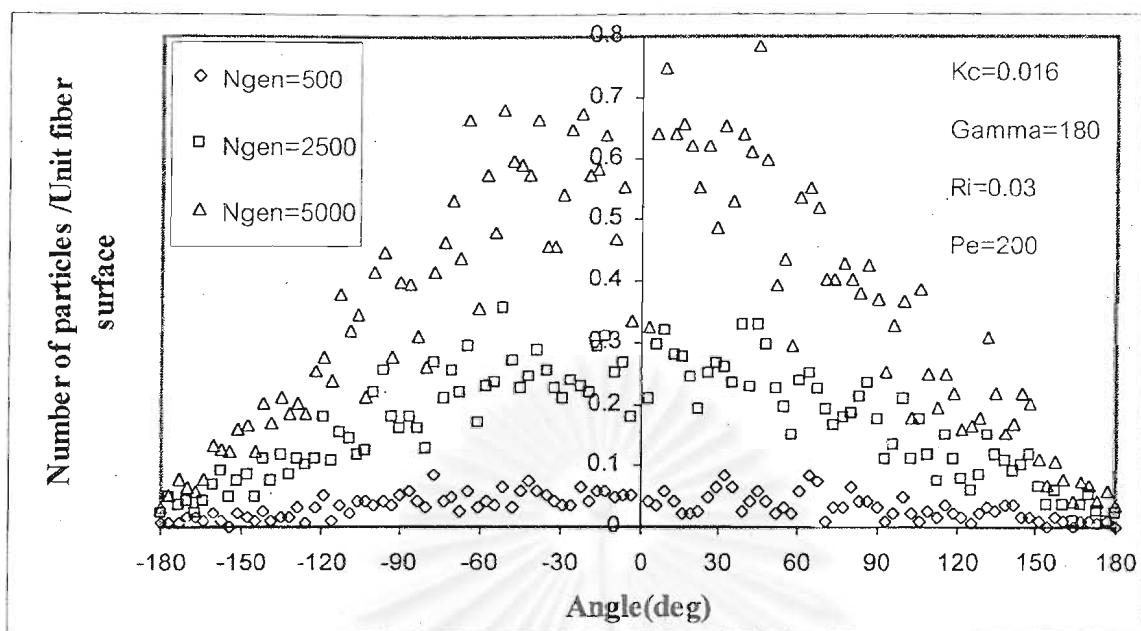
Figure 6.63 Angular distribution of number of deposited particles on a fiber
for the case of Ri=0.03, K_C=0.016, Gamma = 180 and Pe=200
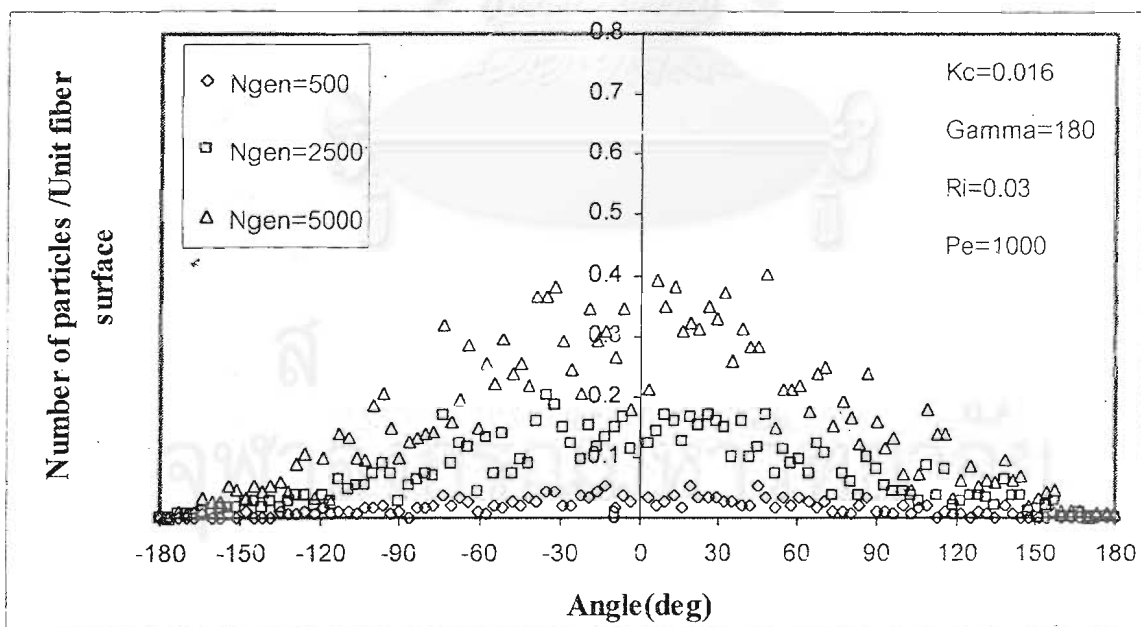
Figure 6.64 Angular distribution of number of deposited particles on a fiber
for the case of Ri=0.03, K_C=0.016, Gamma = 180 and Pe=1000
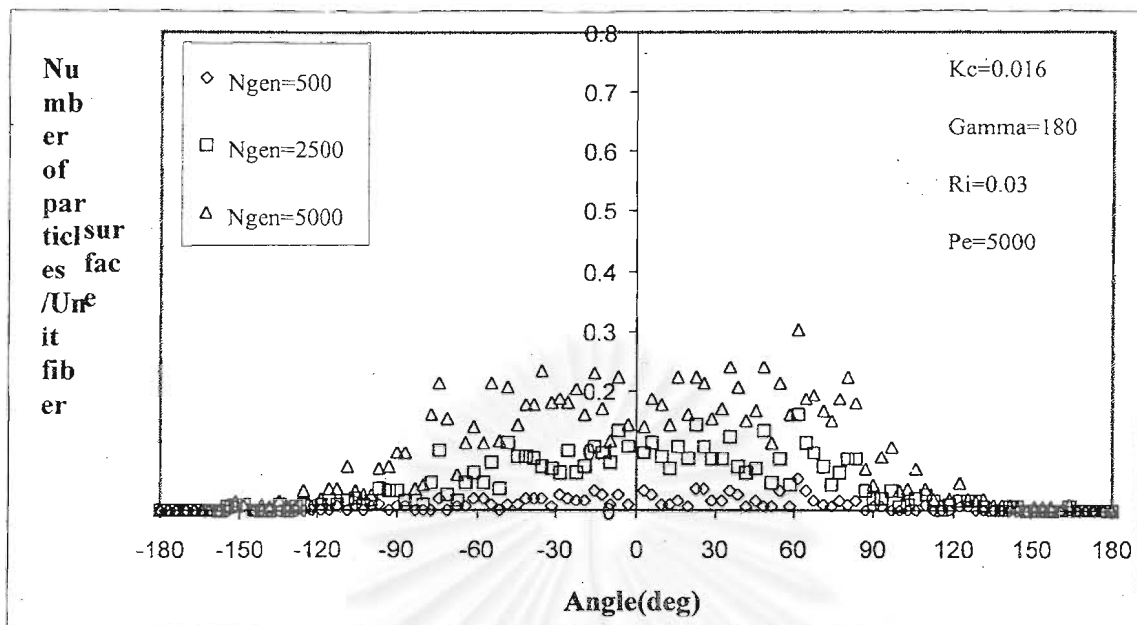
Figure 6.65 Angular distribution of number of deposited particles on a fiber
for the case of Ri=0.03, K_C=0.016, Gamma = 180 and Pe=5000
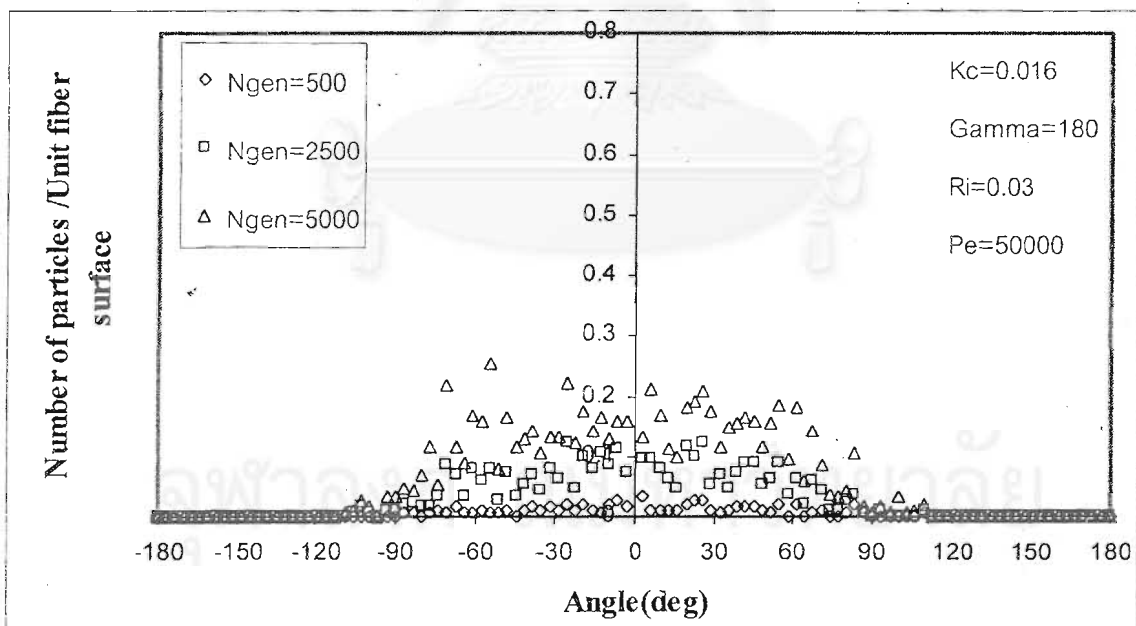
Figure 6.66 Angular distribution of number of deposited particles on a fiber
for the case of Ri=0.03, K_C=0.016, Gamma = 180 and Pe=50000
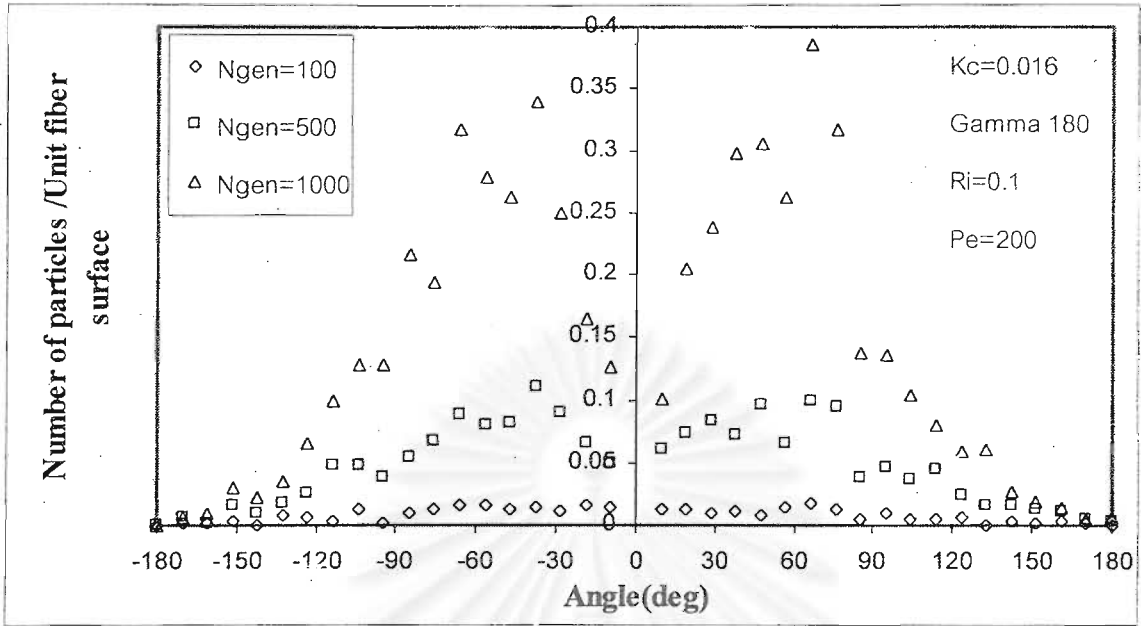
Figure 6.67 Angular distribution of number of deposited particles on a fiber
for the case of Ri=0.1, K_C=0.016, Gamma = 180 and Pe=200
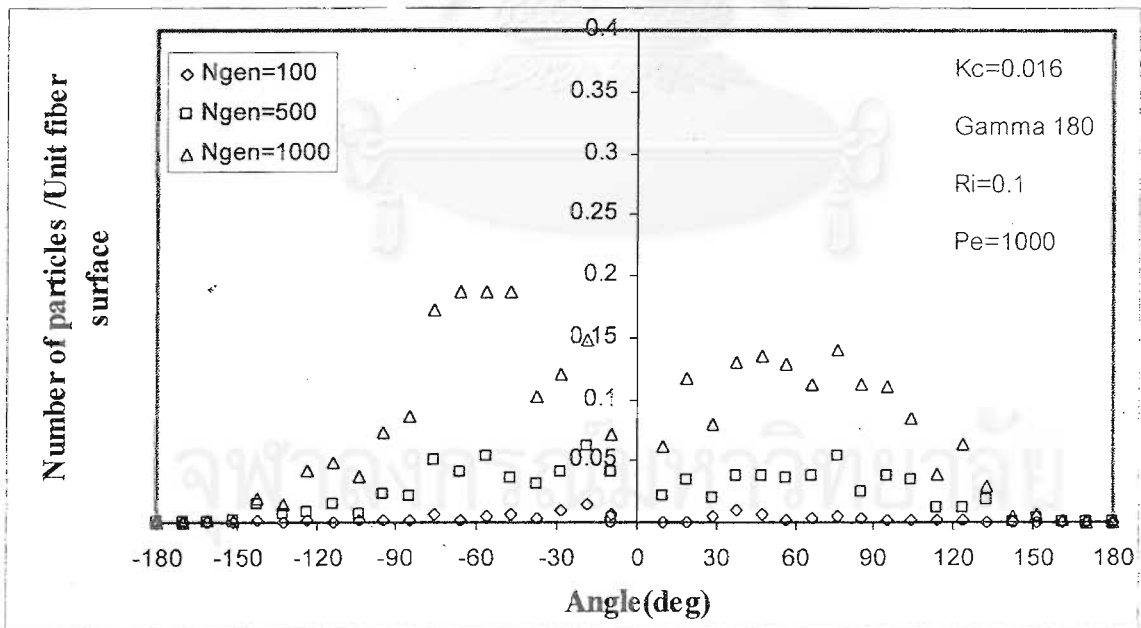
Figure 6.68 Angular distribution of number of deposited particles on a fiber
for the case of Ri=0.1, K_C=0.016, Gamma = 180 and Pe=1000
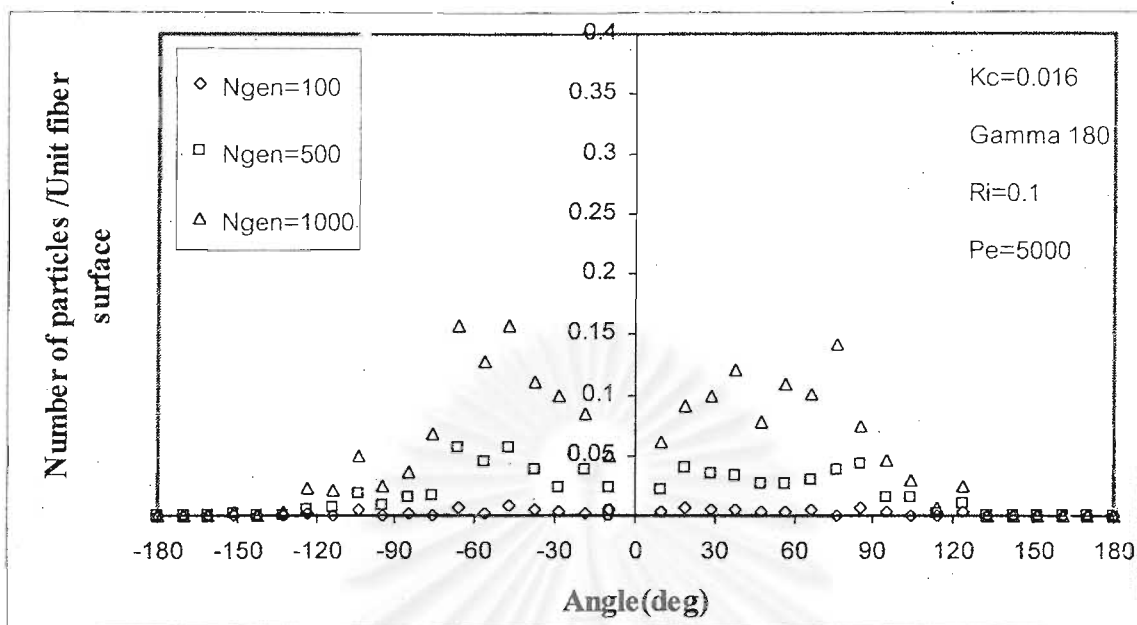
Figure 6.69 Angular distribution of number of deposited particles on a fiber

for the case of Ri=0.1, K_C=0.016, Gamma = 180 and Pe=5000
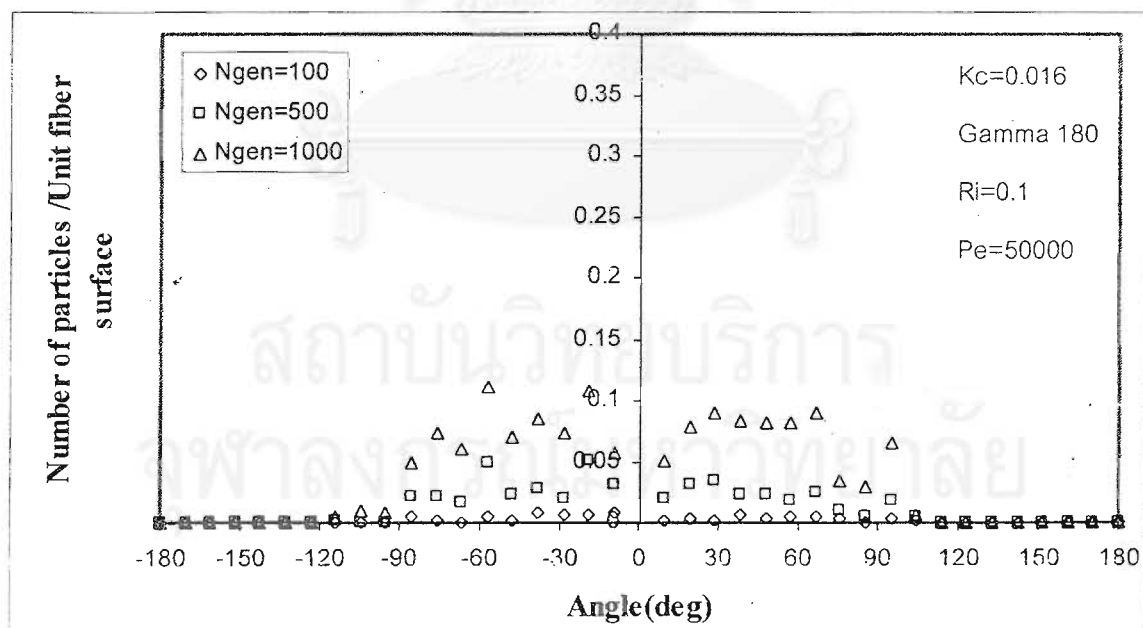
Figure 6.70 Angular distribution of number of deposited particles on a fiber

for the case of Ri=0.1, K_C=0.016, Gamma = 180 and Pe=50000
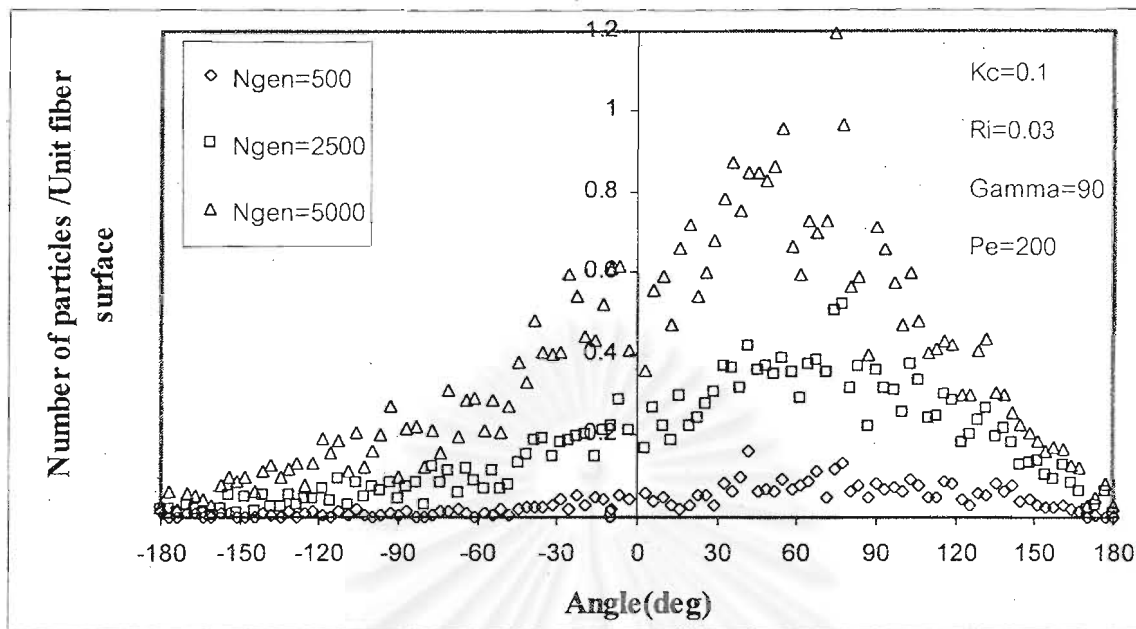
Figure 6.71 Angular distribution of number of deposited particles on a fiber
for the case of Ri=0.03, K_C=0.1, Gamma = 90 and Pe=200
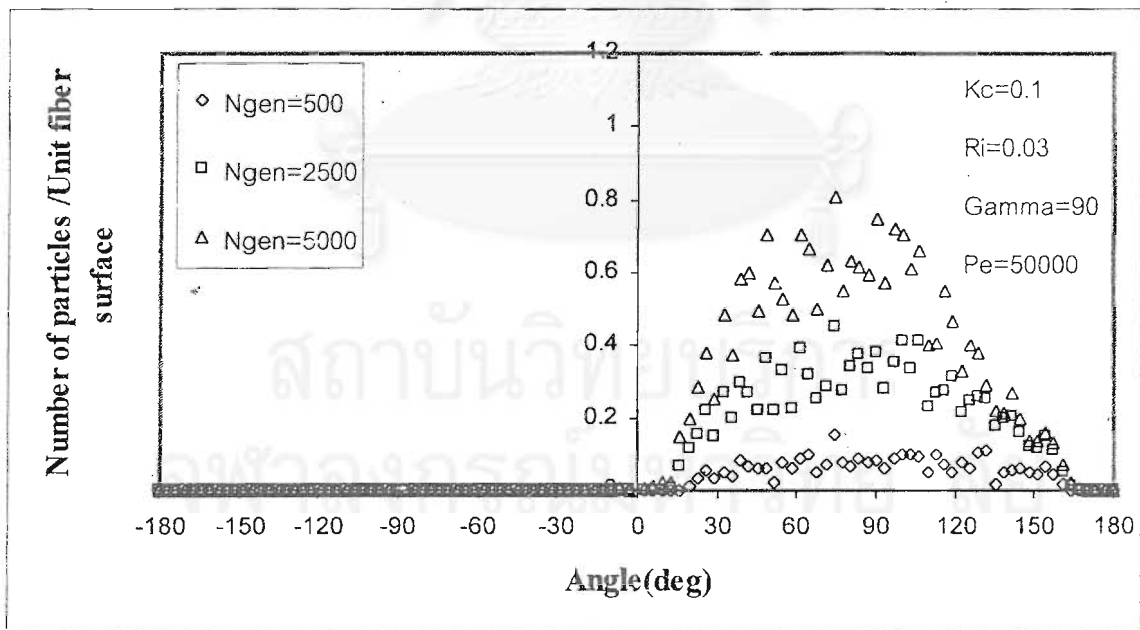
Figure 6.72 Angular distribution of number of deposited particles on a fiber
for the case of Ri=0.03, K_C=0.1, Gamma = 90 and Pe=50000
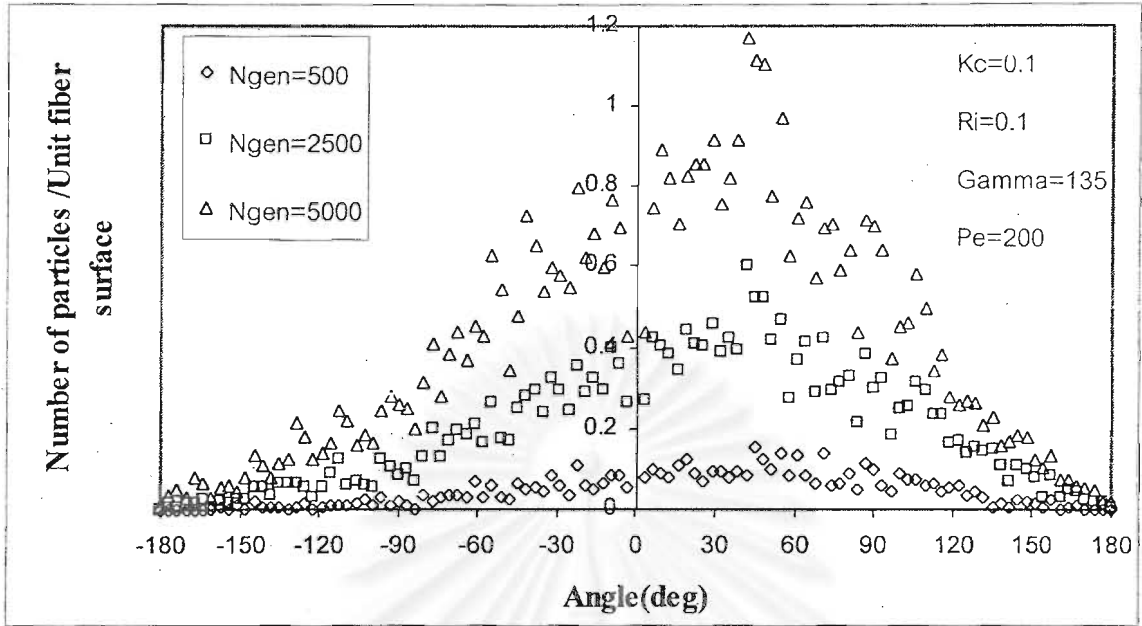
Figure 6.73 Angular distribution of number of deposited particles on a fiber
for the case of Ri=0.03, K$_C$=0.1, Gamma = 135 and Pe=200
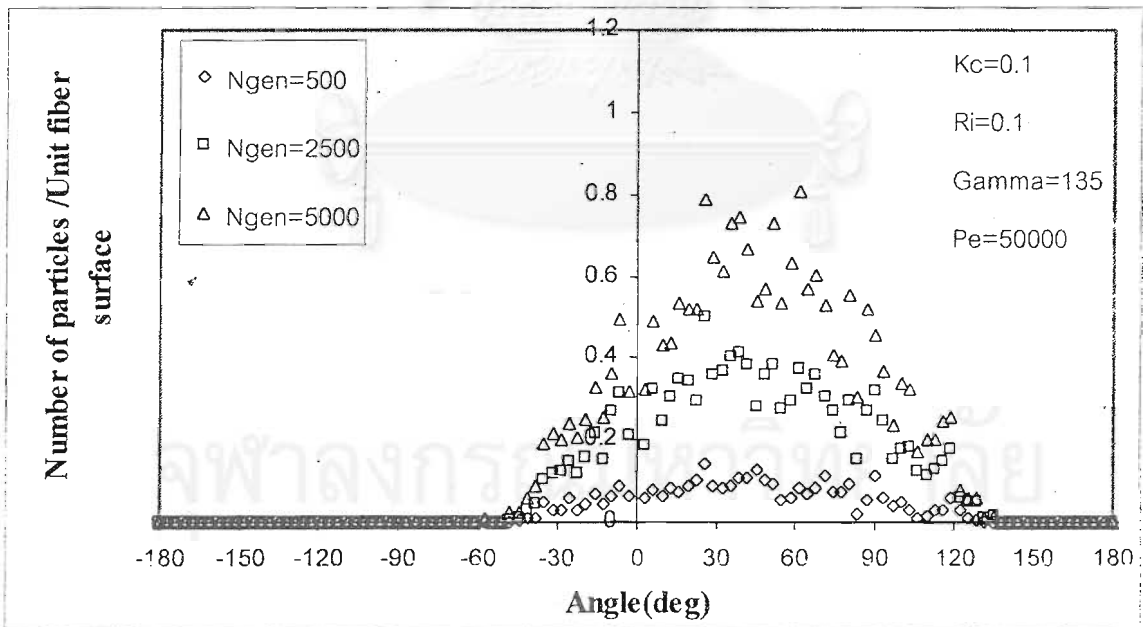
Figure 6.74 Angular distribution of number of deposited particles on a fiber
for the case of Ri=0.03, K$_C$=0.1, Gamma = 135 and Pe=50000
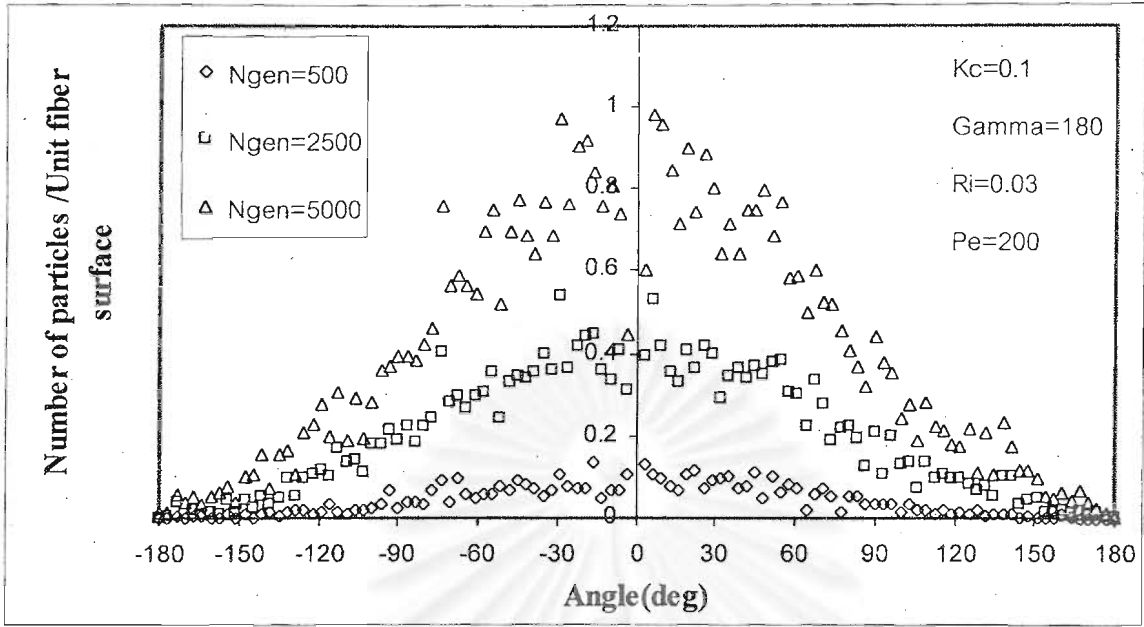
Figure 6.75 Angular distribution of number of deposited particles on a fiber
for the case of Ri=0.03, K_C=0.1, Gamma = 180 and Pe=200
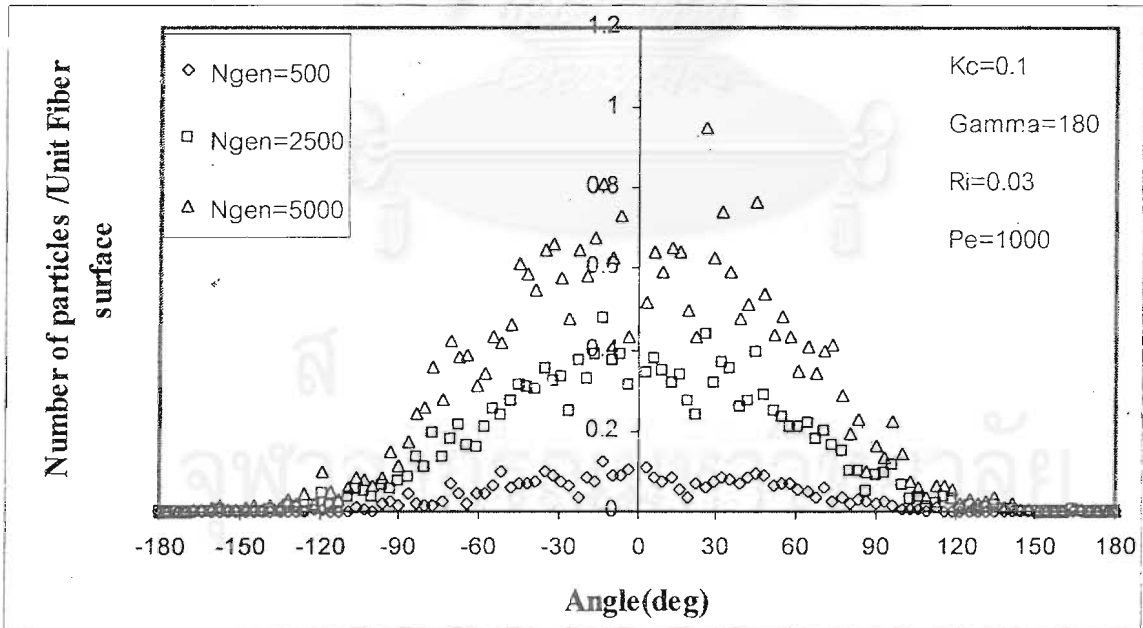
Figure 6.76 Angular distribution of number of deposited particles on a fiber
for the case of Ri=0.03, K_C=0.1, Gamma = 180 and Pe=1000
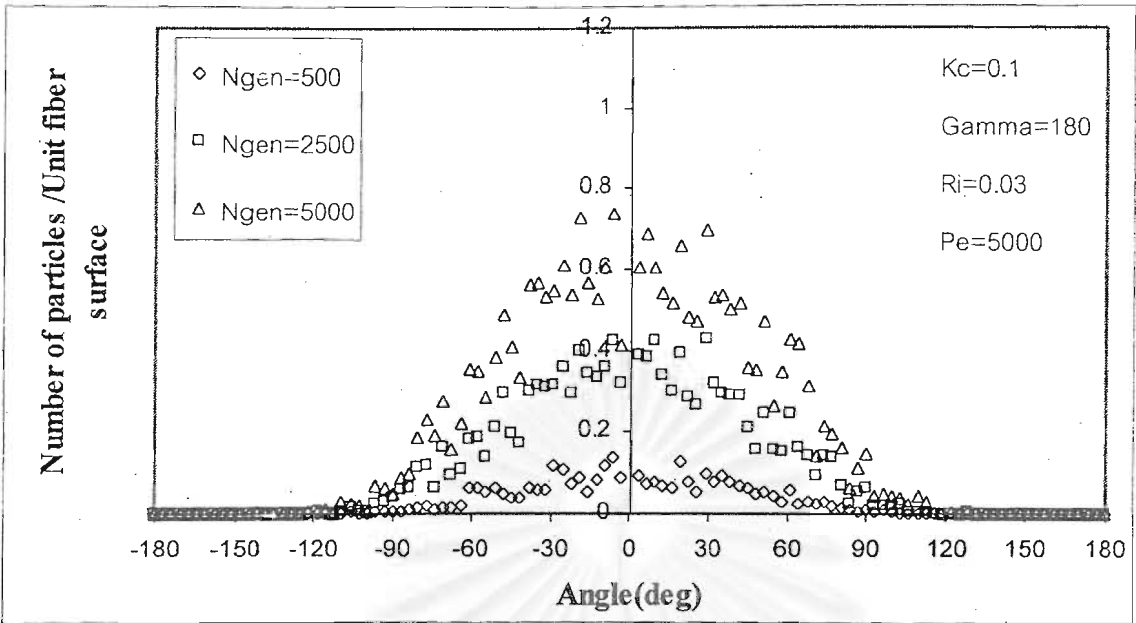
Figure 6.77 Angular distribution of number of deposited particles on a fiber
for the case of Ri=0.03, K_C=0.1, Gamma = 180 and Pe=5000

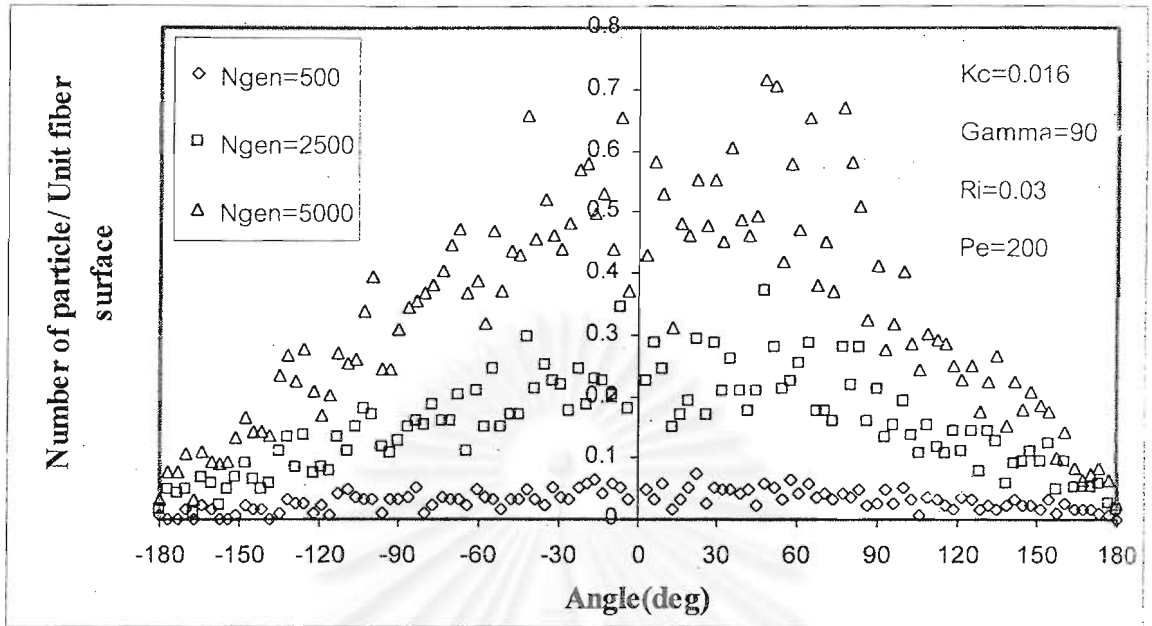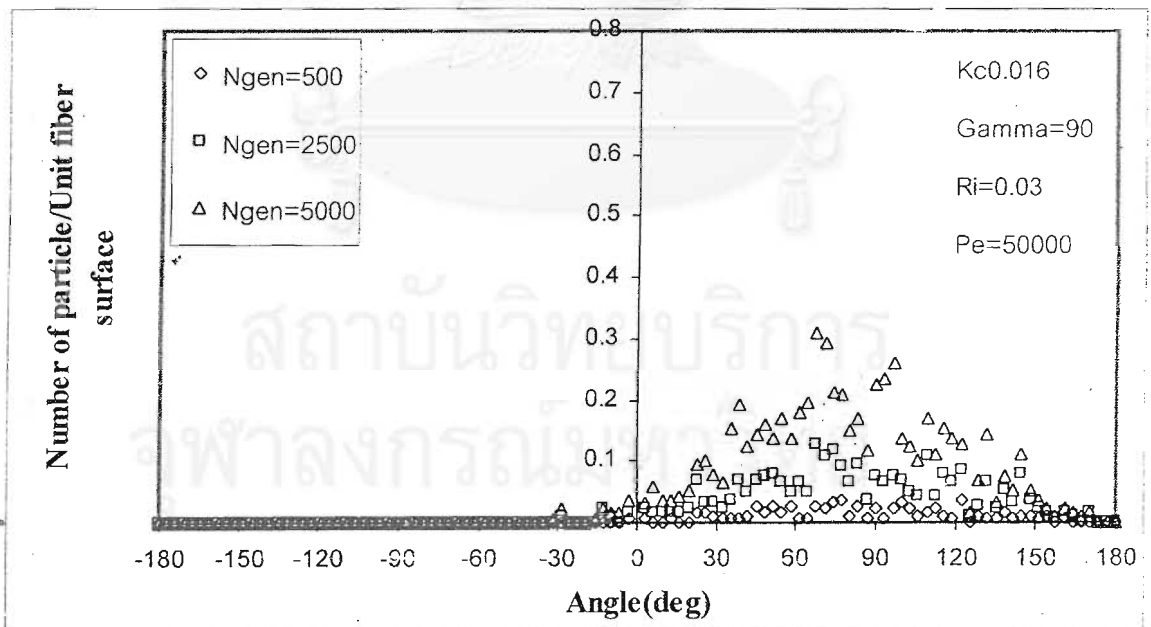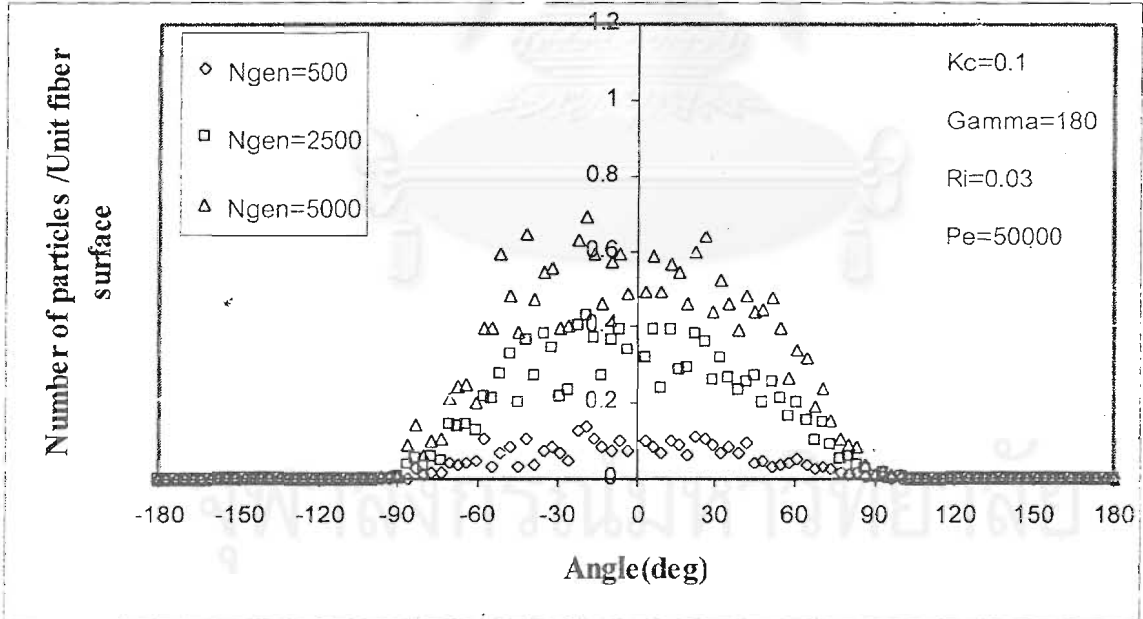Figure 6.78 Angular distribution of number of deposited particles on a fiber
for the case of Ri=0.03, K_C=0.1, Gamma = 180 and Pe=50000
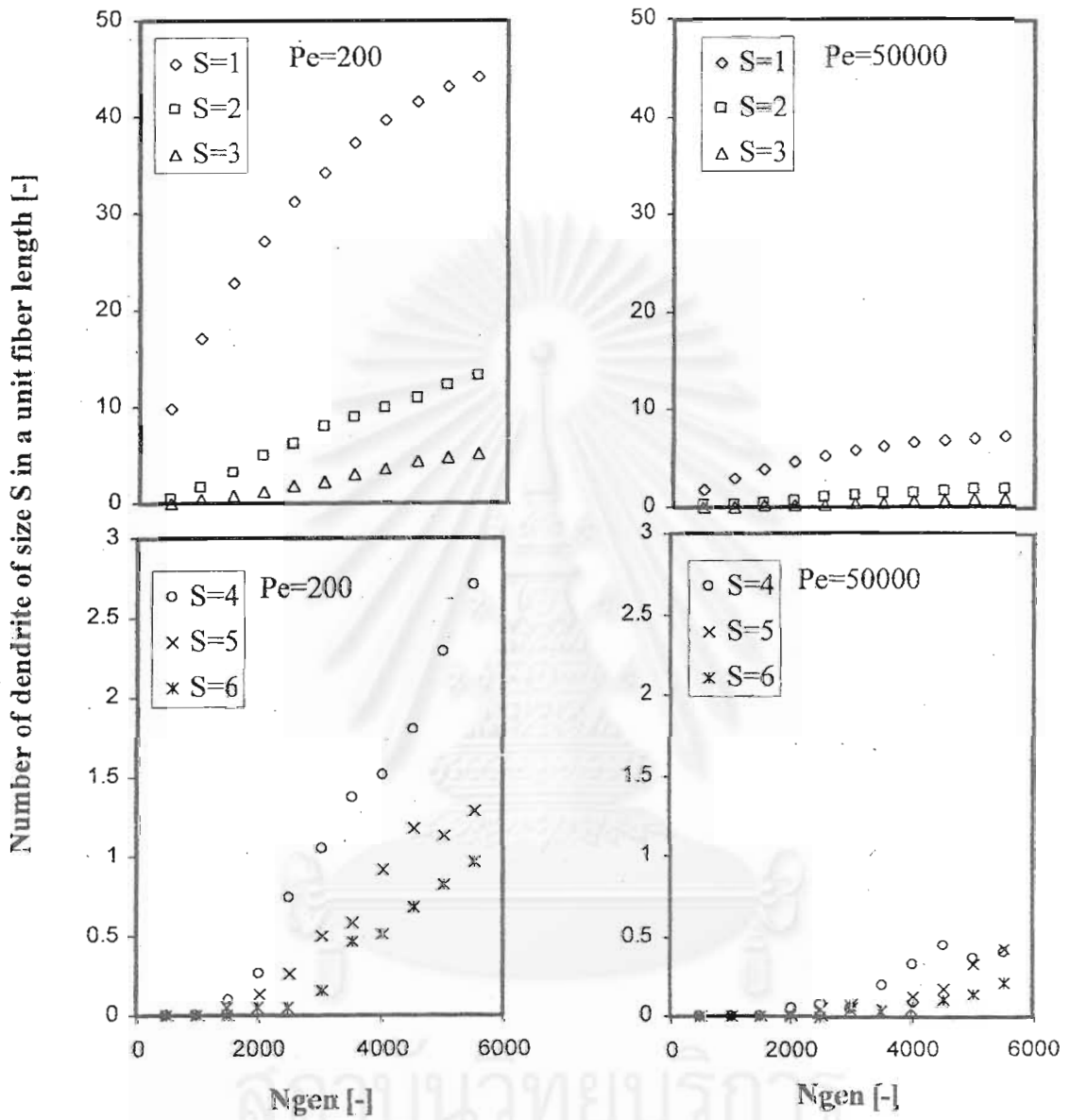
Figure 6.79 Time dependency of number of dendrite in a unit fiber length for
the case of Ri=0.03, K_C=0.016 and Gamma = 90 (Pe=200 and 50000)
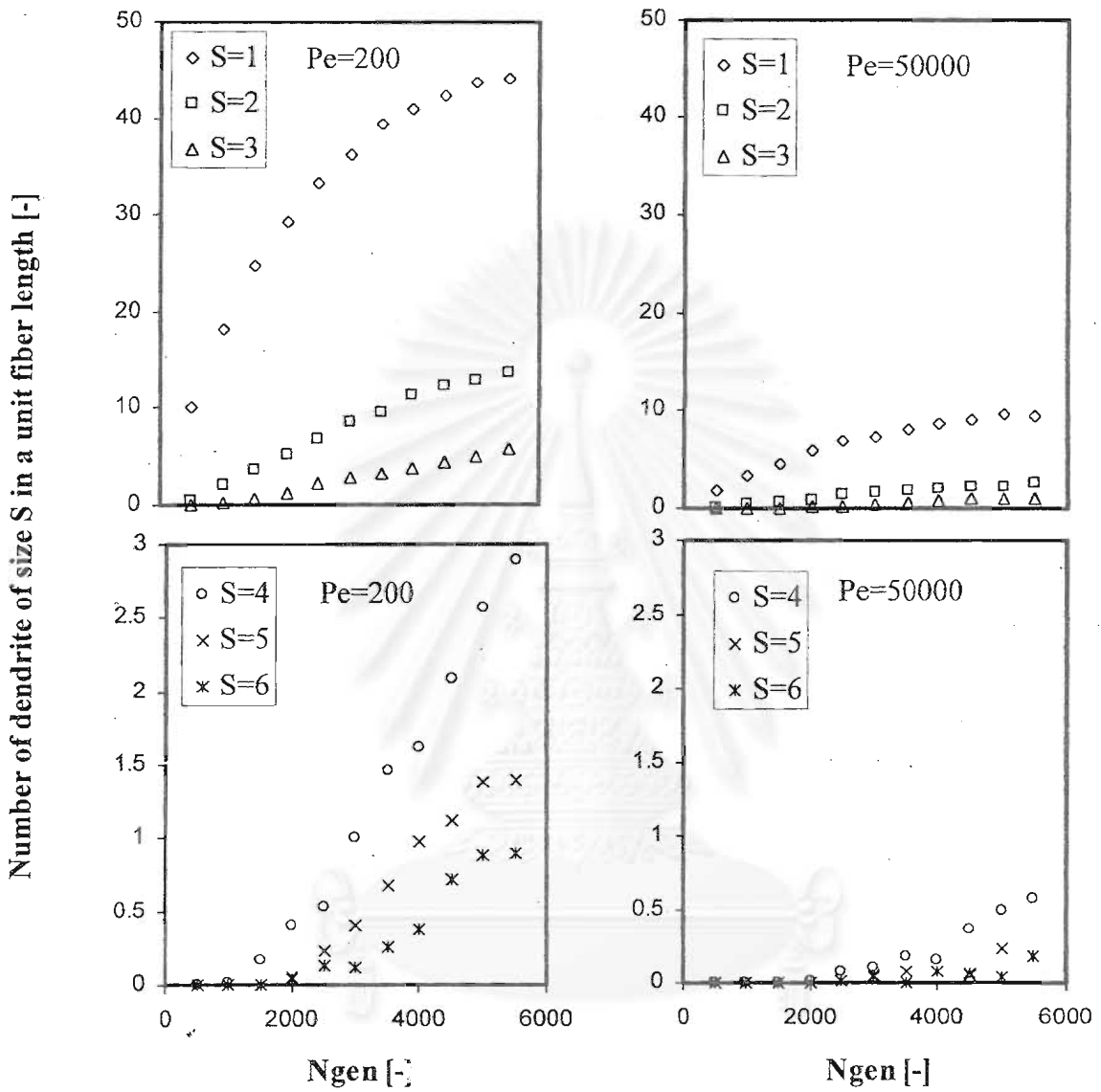
Figure 6.80 Time dependency of number of dendrite in a unit fiber length for
the case of Ri=0.03, K_C=0.016 and Gamma = 135(Pe=200 and 50000)
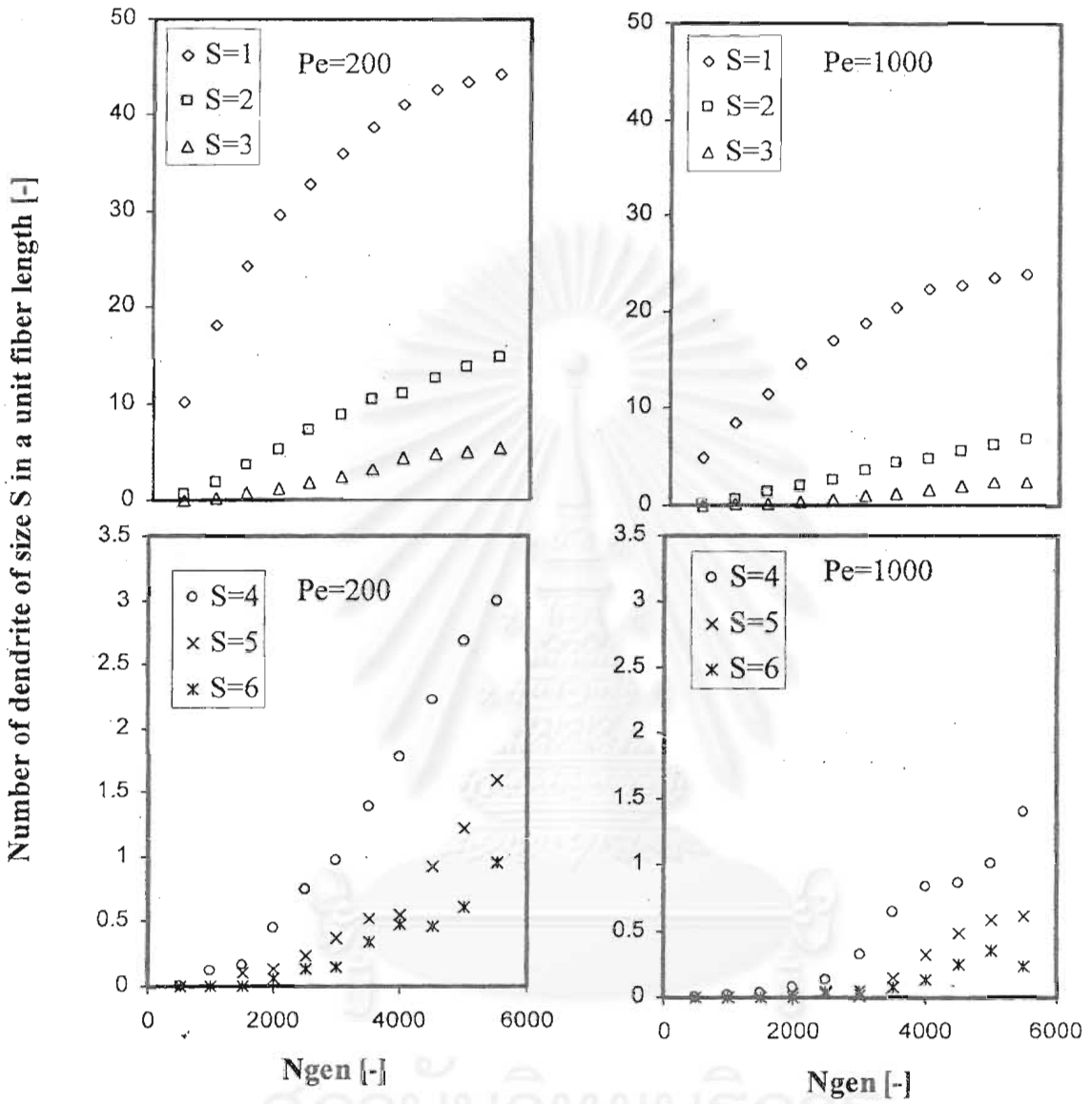
Figure 6.81 Time dependency of number of dendrite in a unit fiber length for the case of Ri=0.03, K_C=0.016 and Gamma = 180 (Pe=200 and 1000)
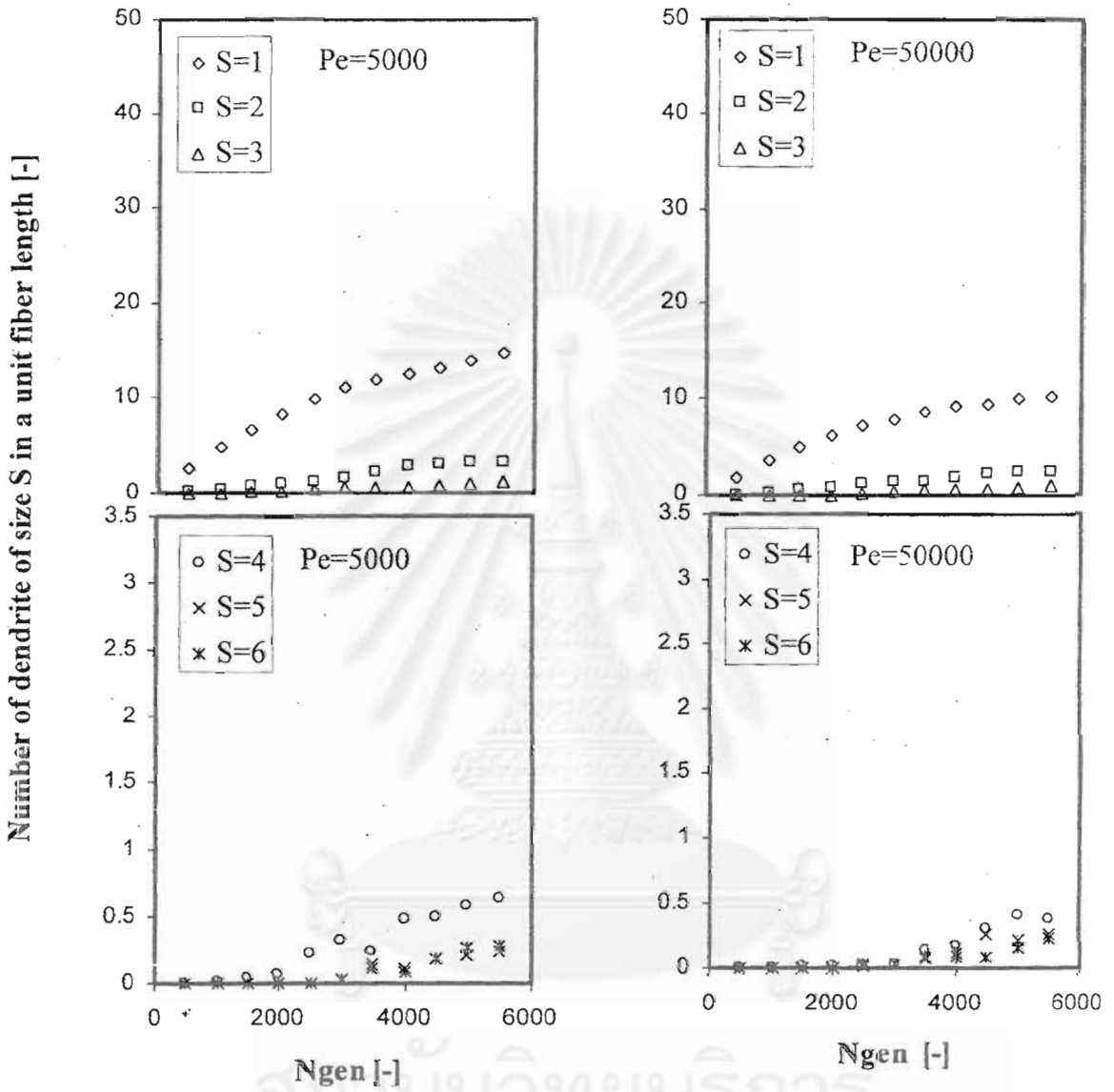
Figure 6.82 Time dependency of number of dendrite in a unit fiber length for the case of R_i=0.03, K_C=0.016 and Gamma = 180 (Pe=5000 and 50000)
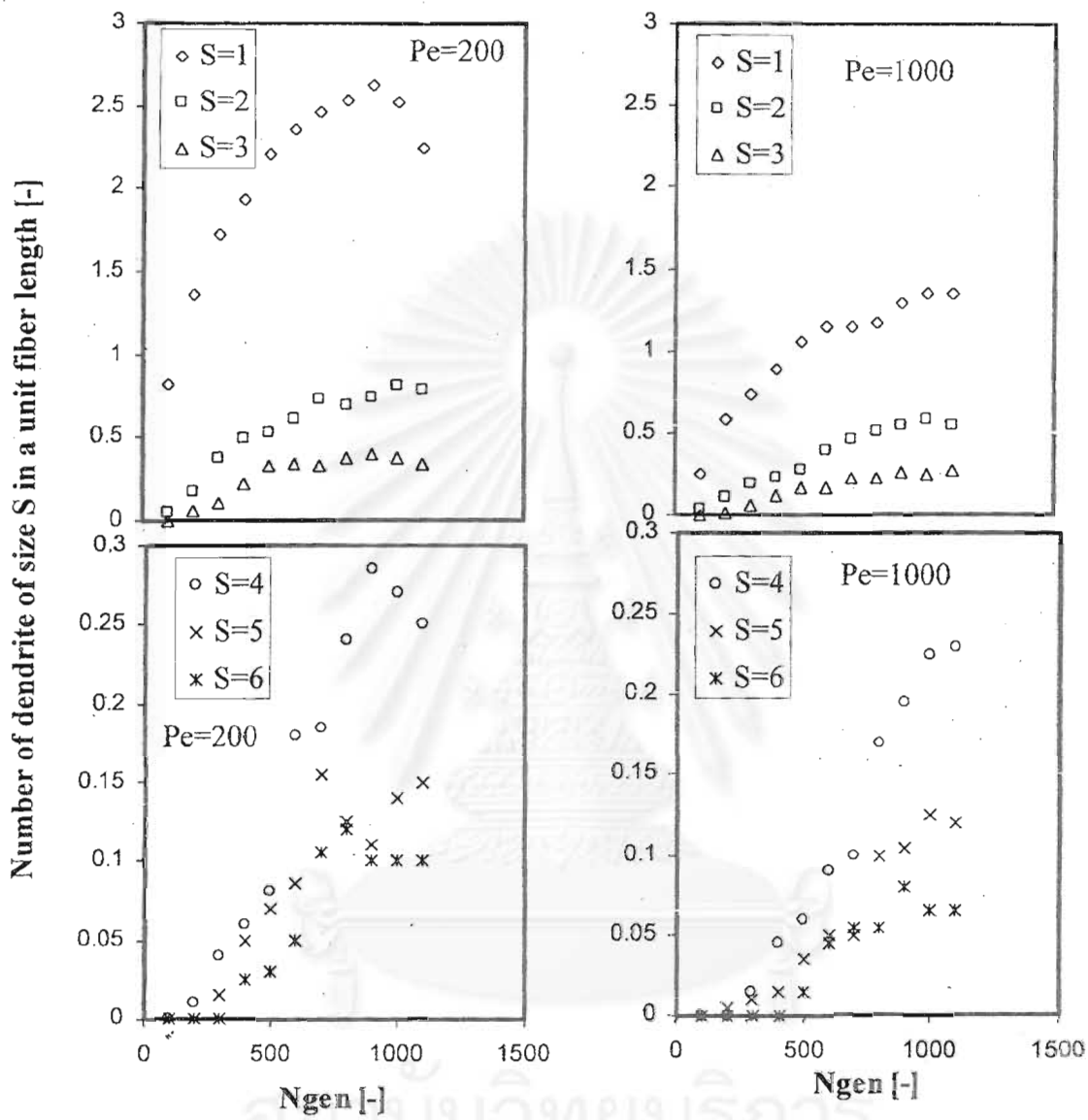
Figure 6.83 Time dependency of number of dendrite in a unit fiber length for
the case of Ri=0.1, K_C=0.016 and Gamma = 180 (Pe=200 and 1000)
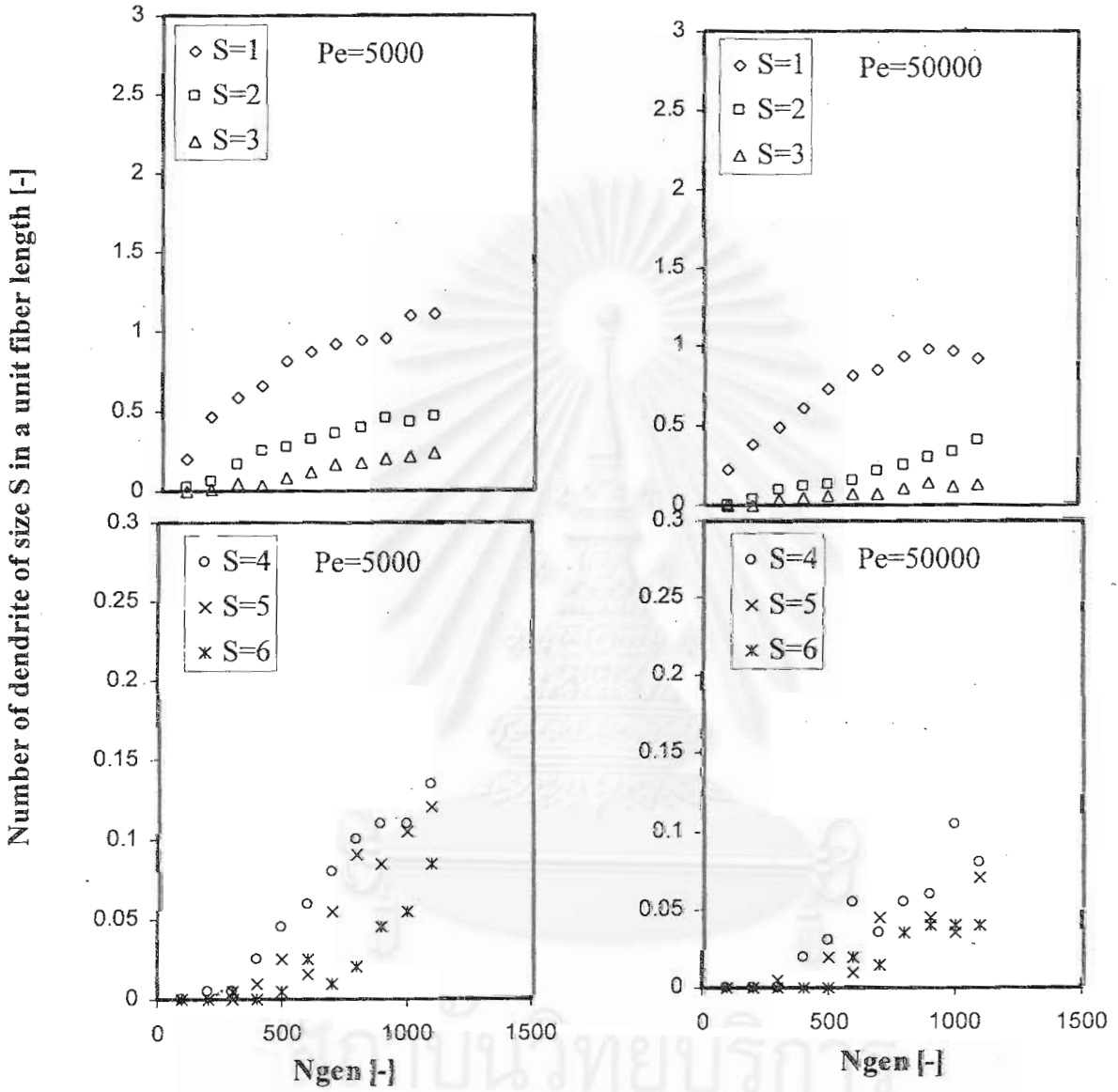
Figure 6.84 Time dependency of number of dendrite in a unit fiber length for the case of Ri=0.1, K_C=0.016 and Gamma = 180 (Pe=5000 and 50000)
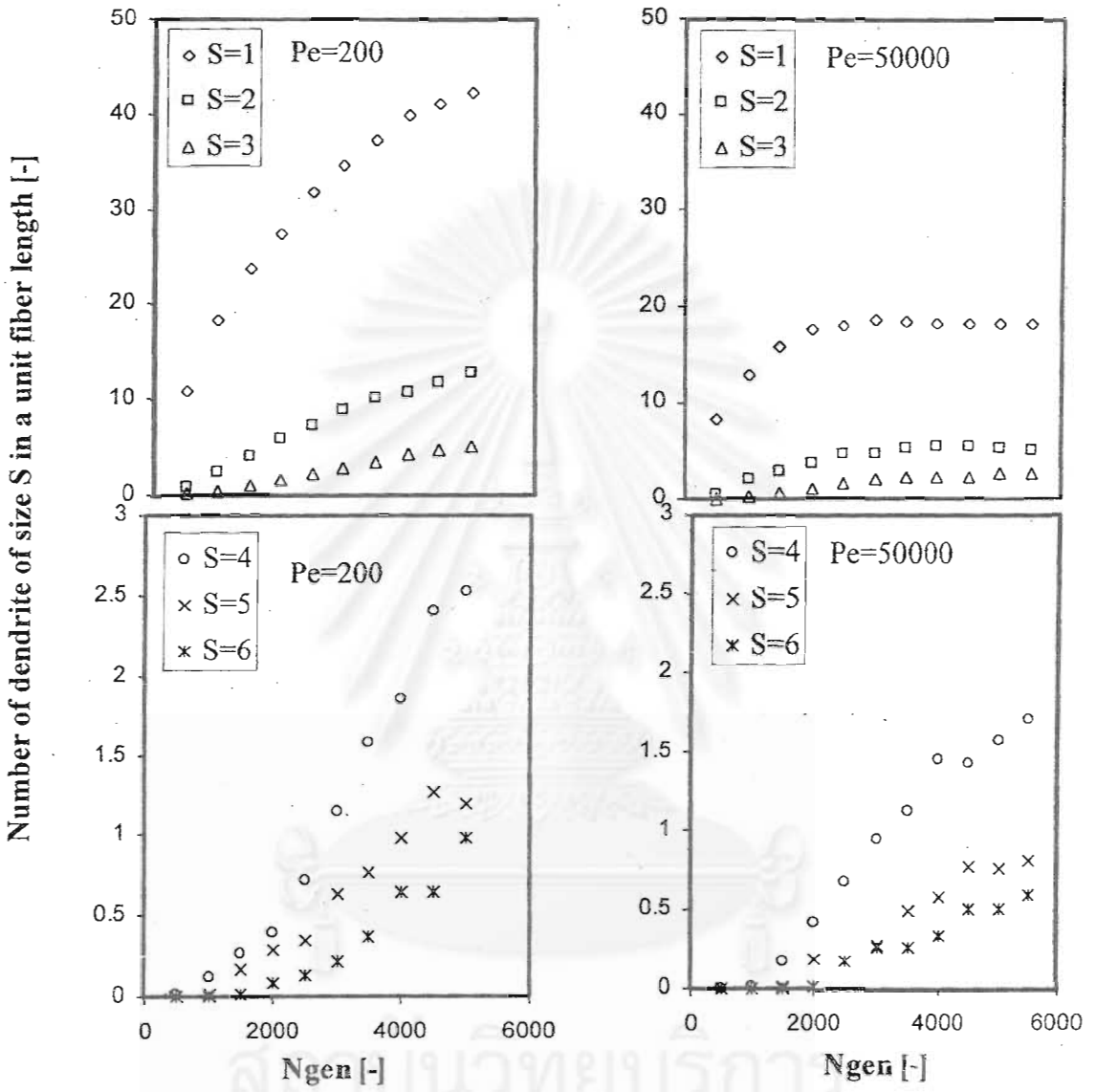
Figure 6.85 Time dependency of number of dendrite in a unit fiber length for the case of Ri=0.03, K_C=0.1 and Gamma = 90 (Pe=200 and 50000)
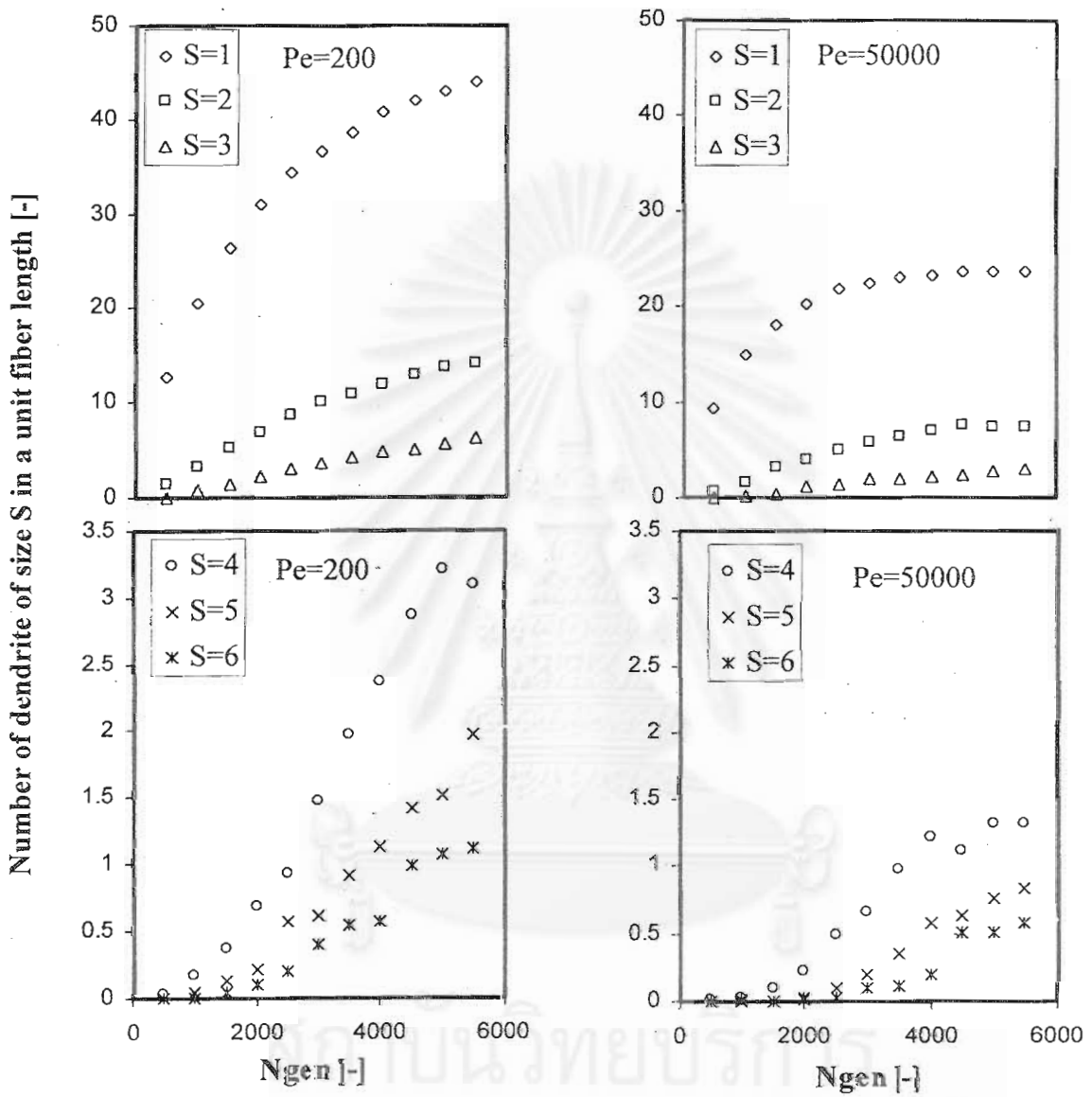
Figure 6.86 Time dependency of number of dendrite in a unit fiber length for the case of Ri=0.03, K_C=0.1 and Gamma = 135 (Pe=200 and 50000)
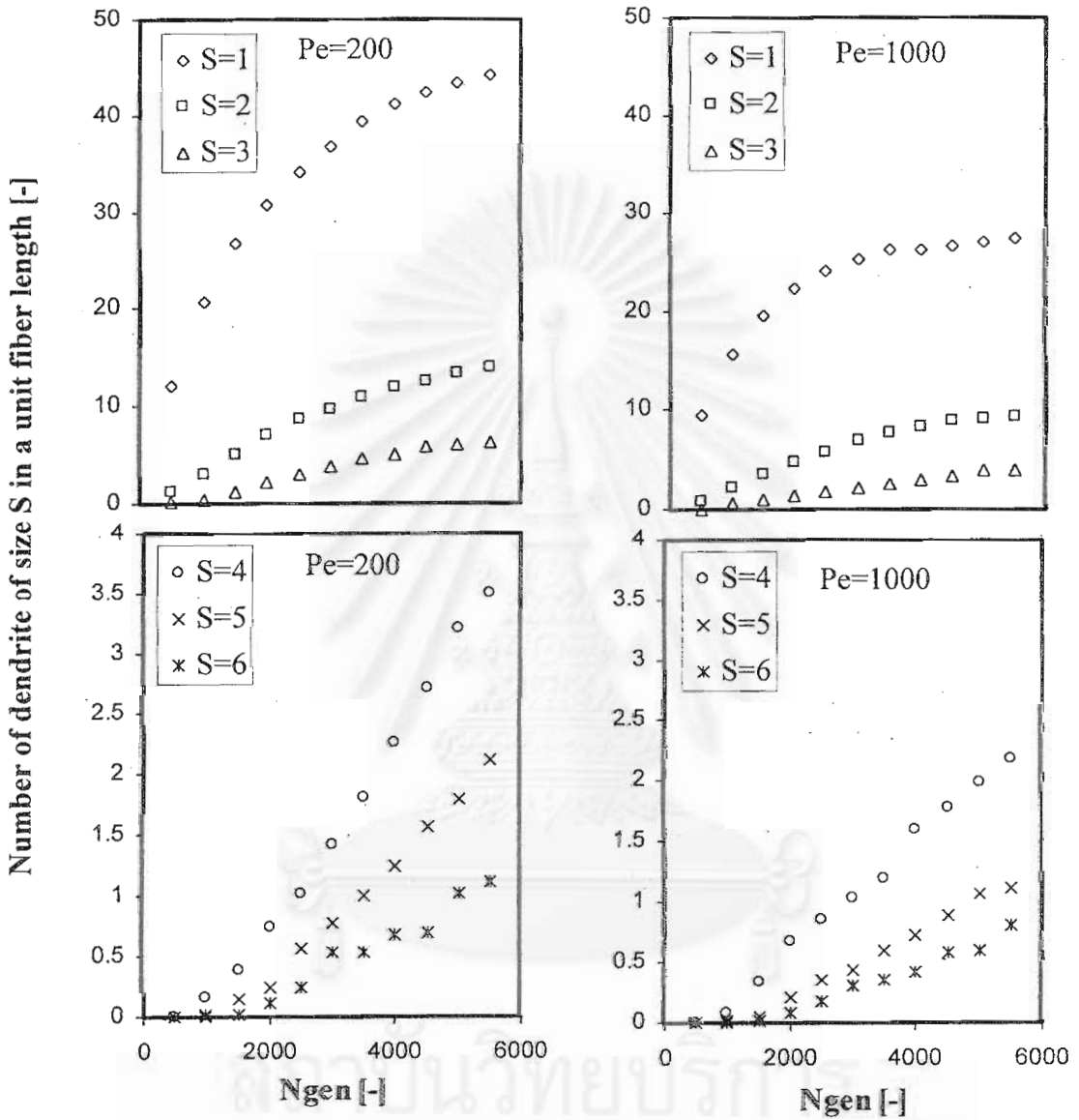
Figure 6.87 Time dependency of number of dendrite in a unit fiber length for the case of Ri=0.03, K_C=0.1 and Gamma = 180 (Pe=200 and 1000)
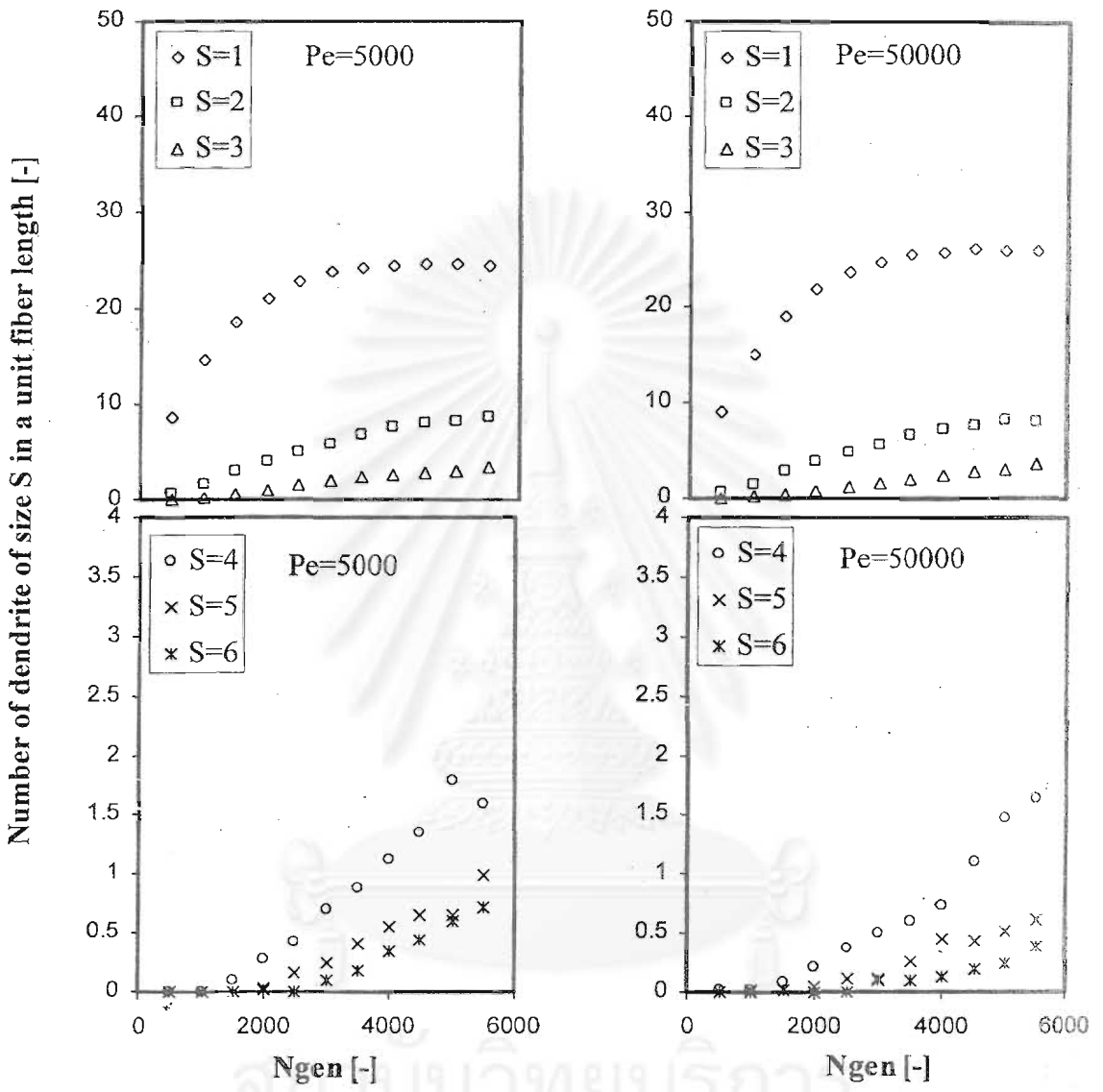
Figure 6.88 Time dependency of number of dendrite in a unit fiber length for
the case of Ri=0.03, K_C=0.1 and Gamma = 180 (Pe=5000 and 50000)
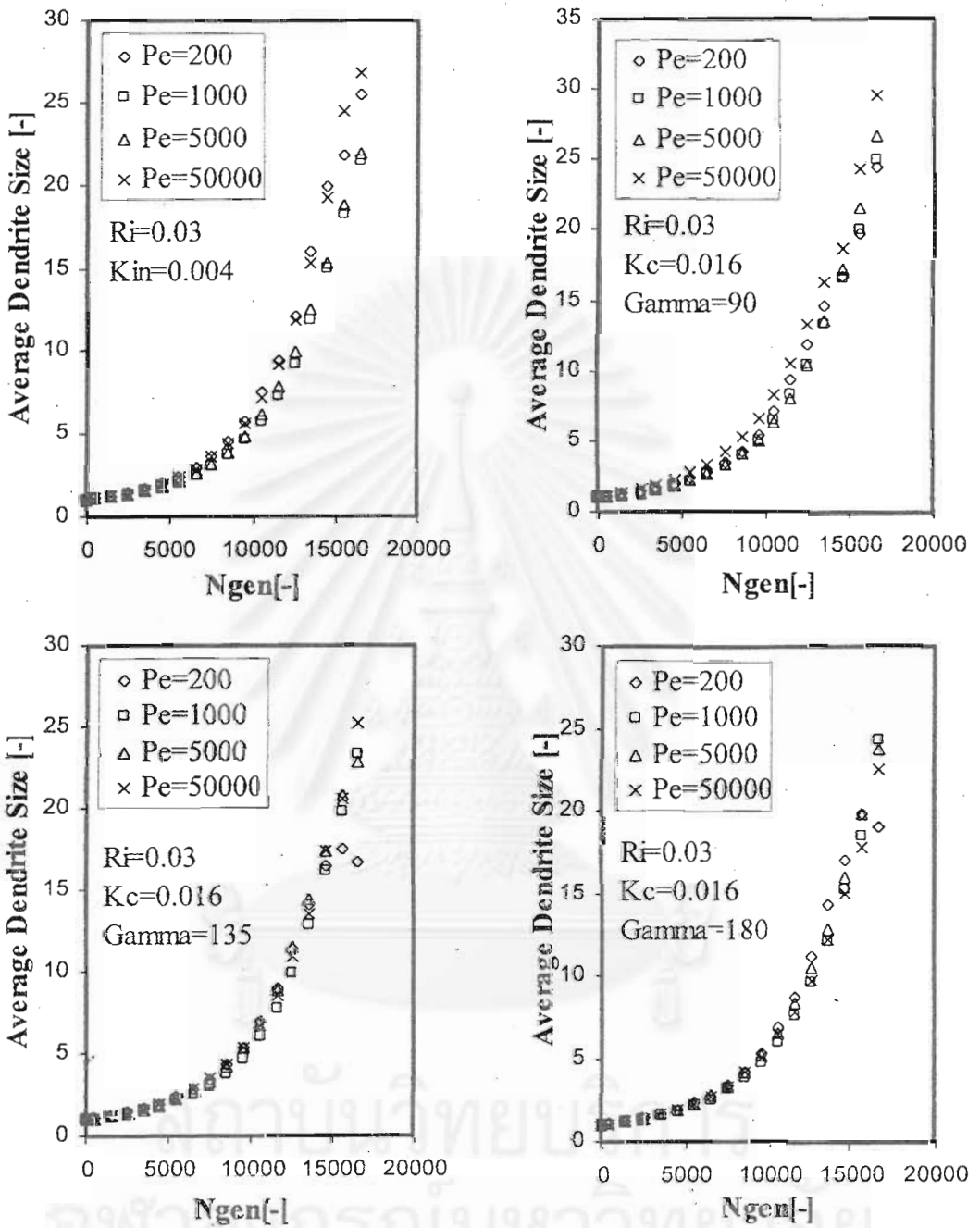
Figure 6.89 Age dependency of average dendrite size for the case of

Ri=0.03, K_{In}= 0.004 and K_C= 0.016
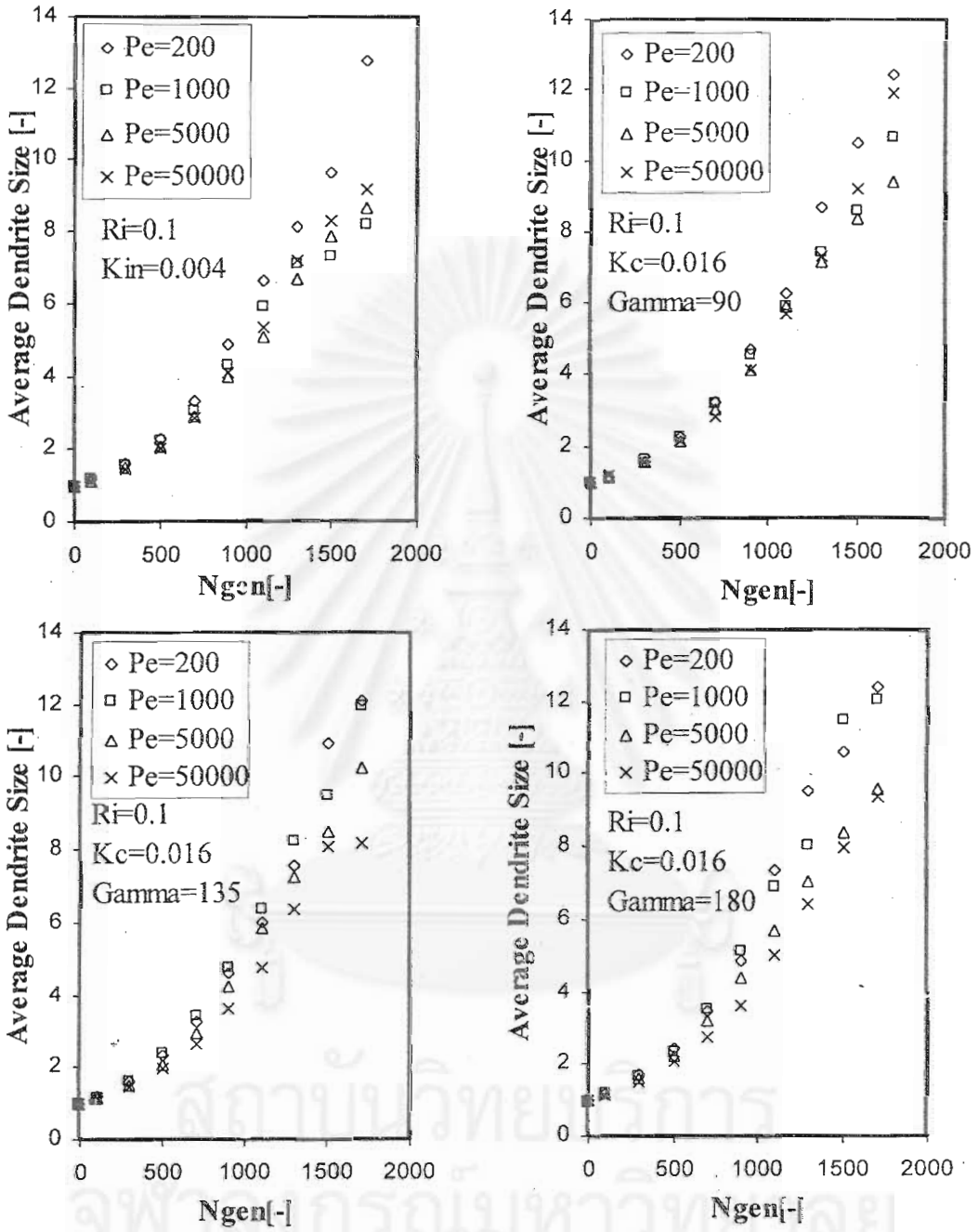
Figure 6.90 Age dependency of average dendrite size for the case of
Ri=0.1, K_{In}= 0.004 and K_C= 0.016
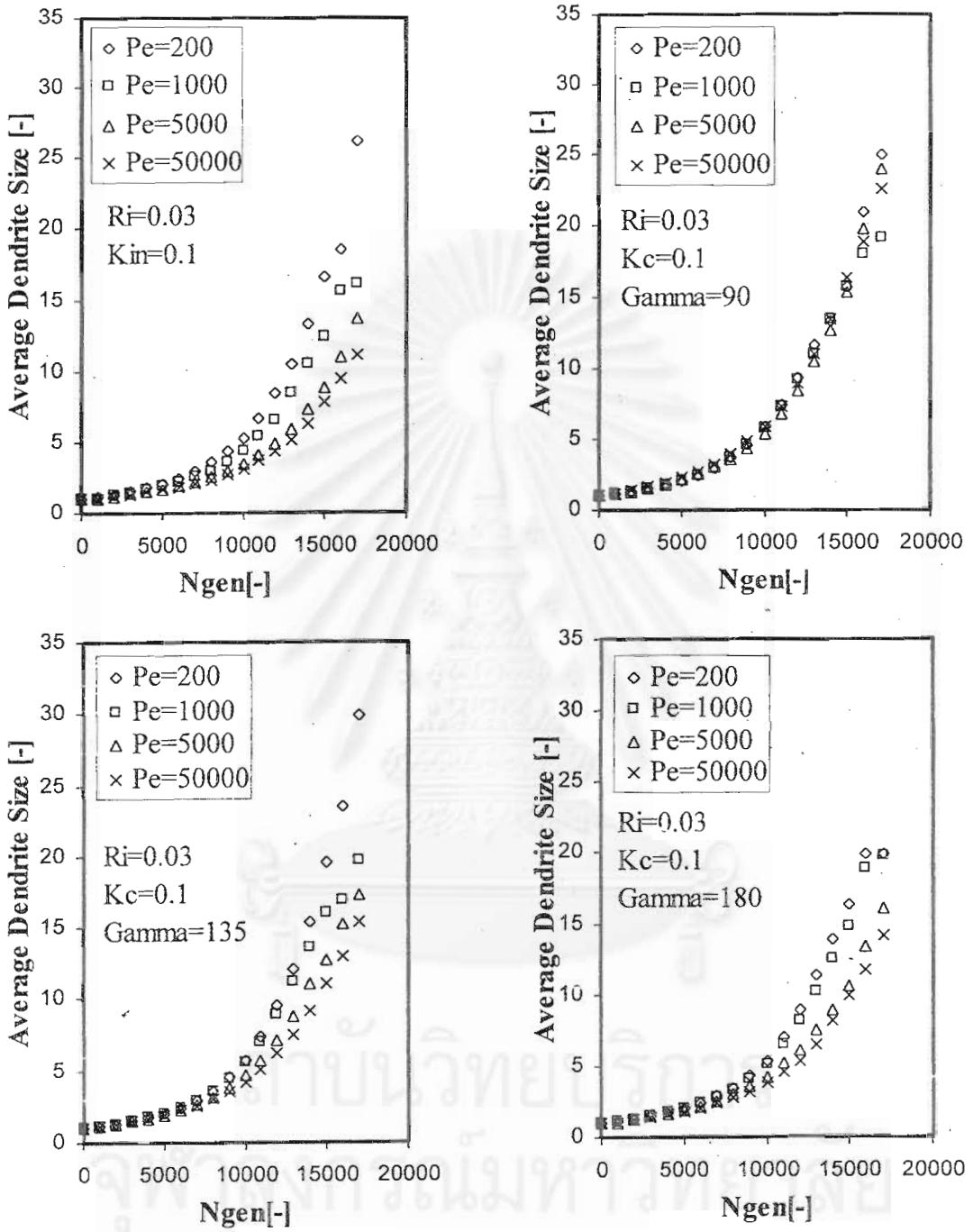
Figure 6.91 Age dependency of average dendrite size for the case of
Ri=0.03, K_{In}= 0.1 and K_C= 0.1
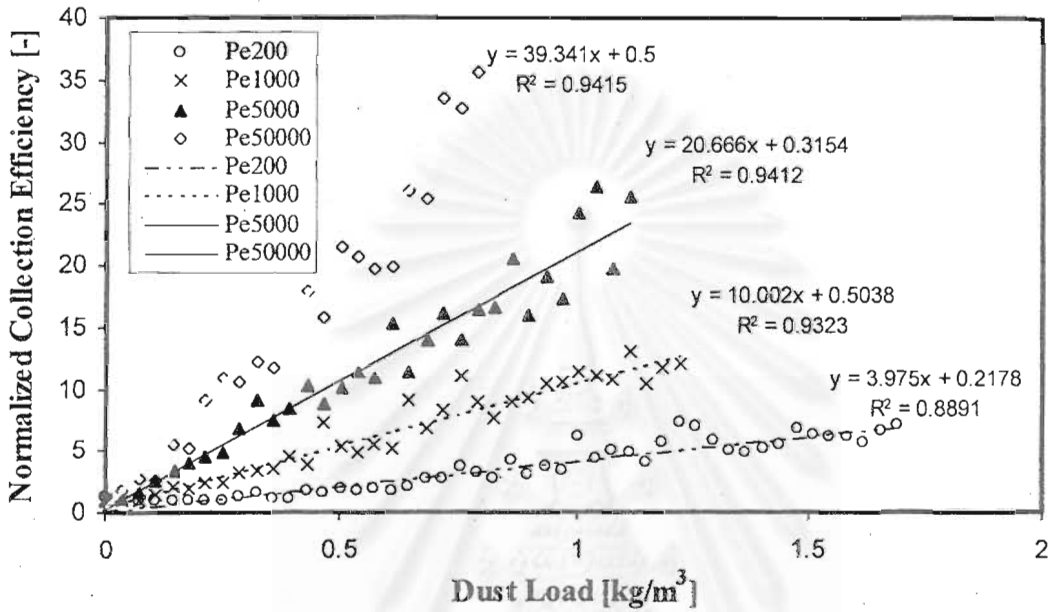
Figure 6.92 Normalized collection efficiency of a dust-loaded fiber for the case of Ri=0.03, Kc = 0.016 and Gamma = 90
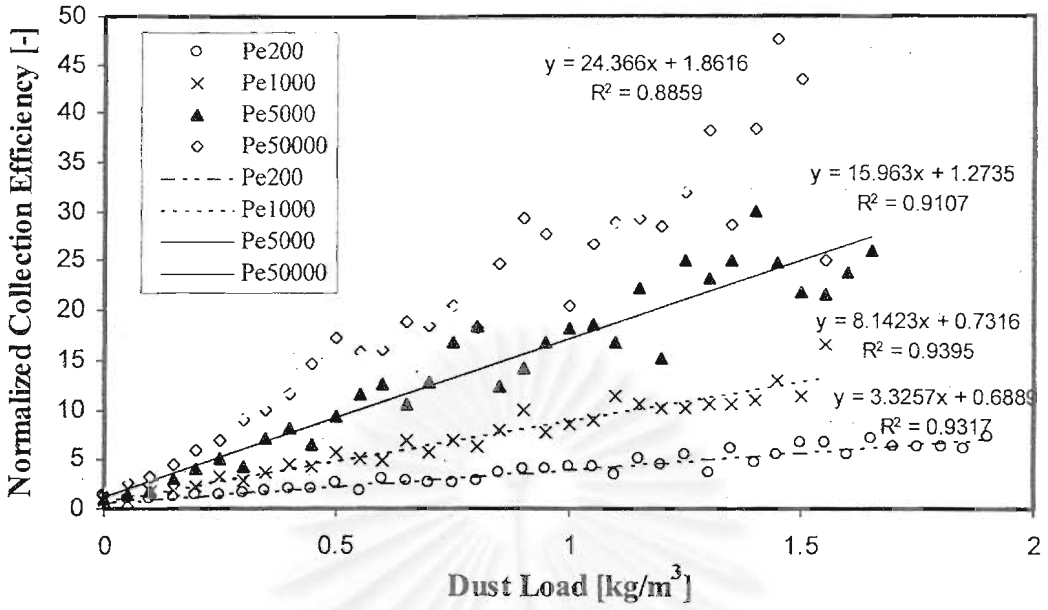
Figure 6.93 Normalized collection efficiency of a dust-loaded fiber for the
case of Ri=0.05, Kc = 0.016 and Gamma = 90
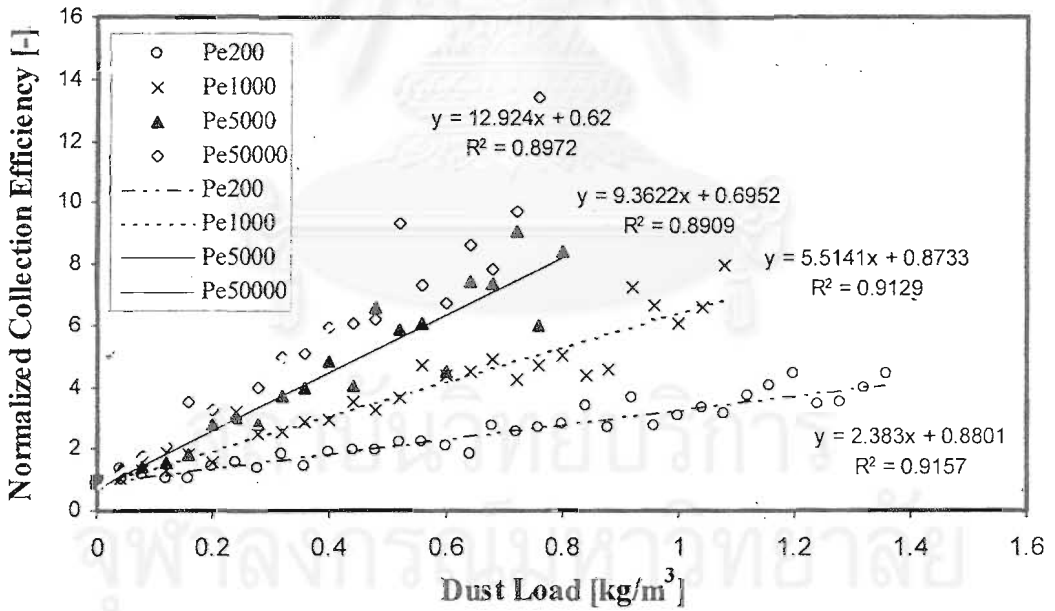
Figure 6.94 Normalized collection efficiency of a dust-loaded fiber for the
case of Ri=0.1, Kc = 0.016 and Gamma = 90
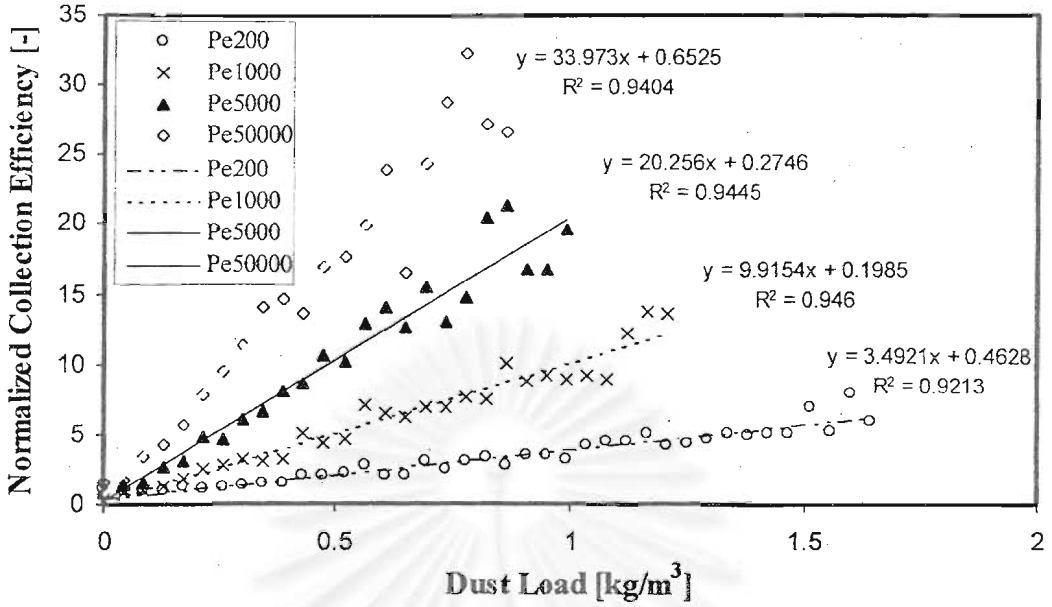
Figure 6.95 Normalized collection efficiency of a dust-loaded fiber for the case of Ri=0.03, Kc = 0.016 and Gamma = 135
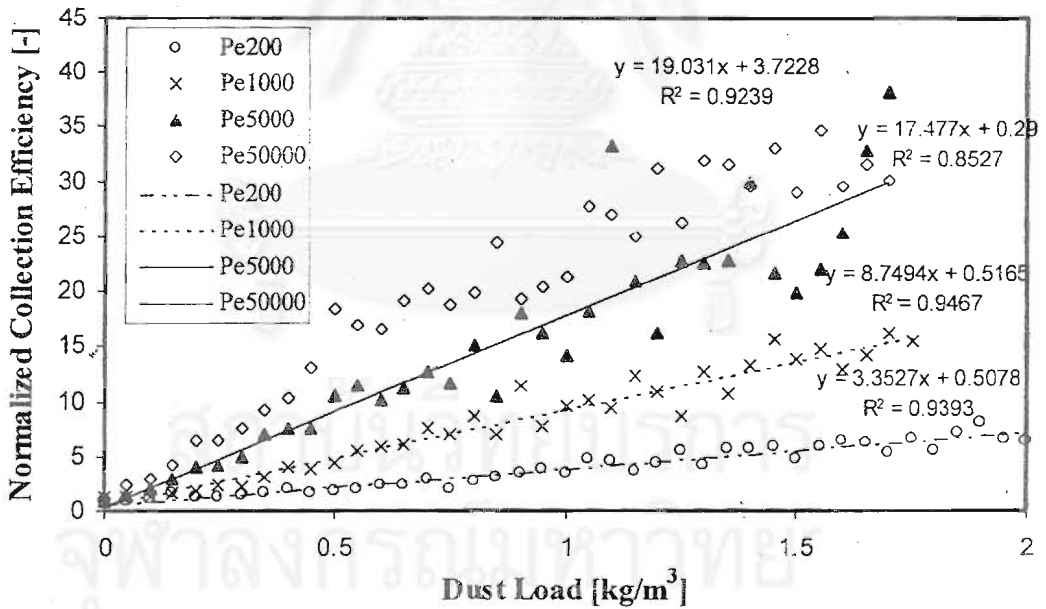
Figure 6.96 Normalized collection efficiency of a dust-loaded fiber for the case of Ri=0.05, Kc = 0.016 and Gamma = 135
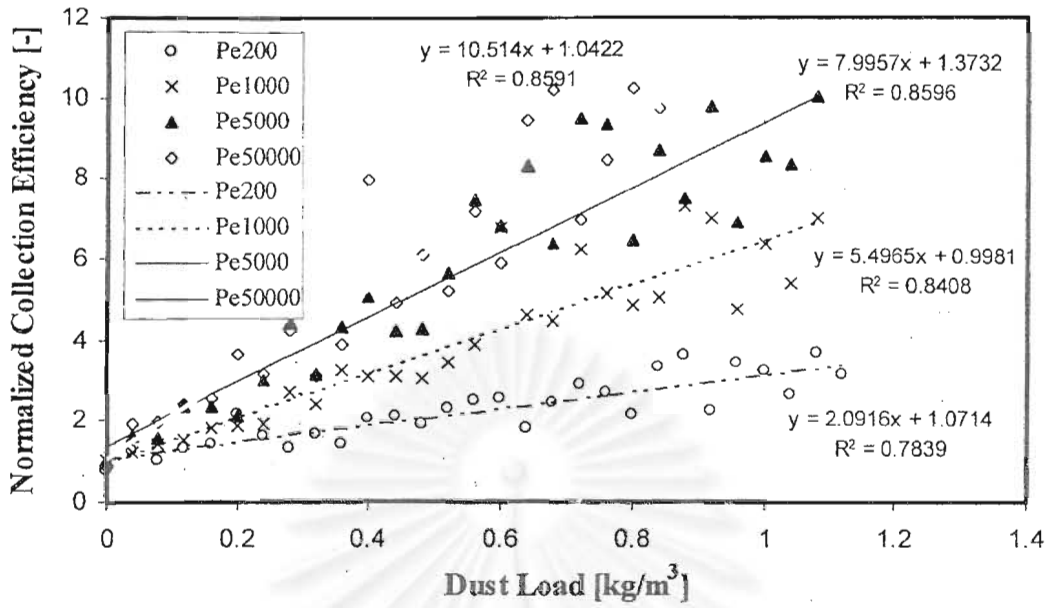
Figure 6.97 Normalized collection efficiency of a dust-loaded fiber for the
case of Ri=0.1, Kc = 0.016 and Gamma = 135
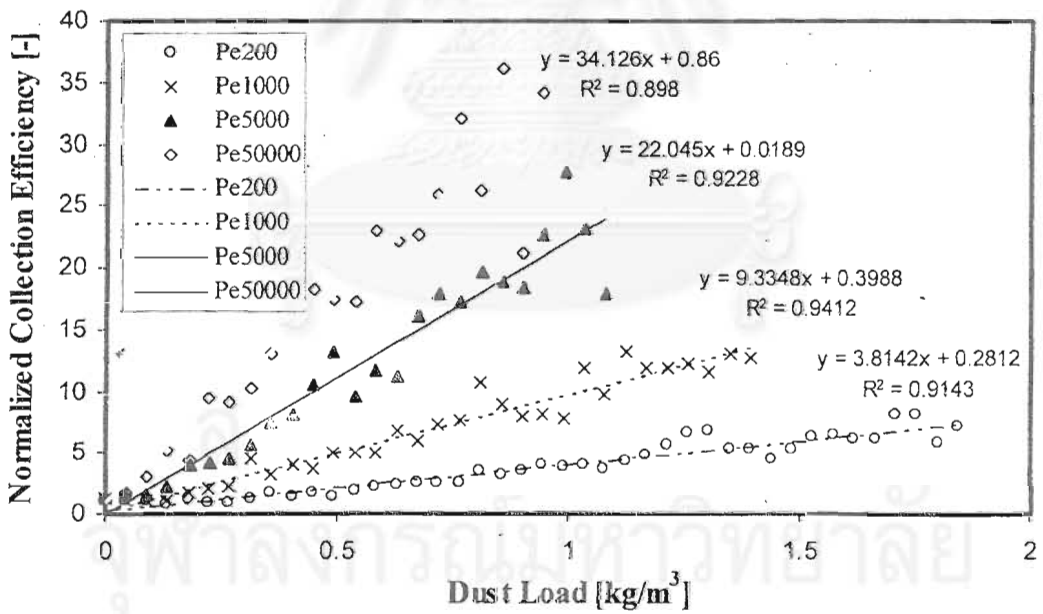
Figure 6.98 Normalized collection efficiency of a dust-loaded fiber for the
case of Ri=0.03, Kc = 0.016 and Gamma = 180
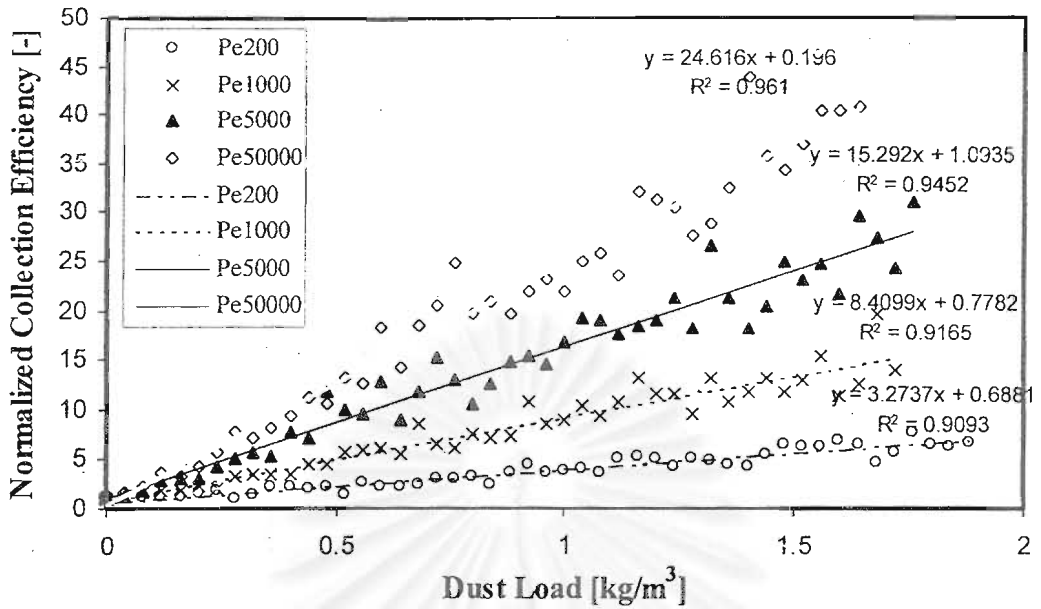
Figure 6.99 Normalized collection efficiency of a dust-loaded fiber for the
case of Ri=0.05, Kc = 0.016 and Gamma = 180
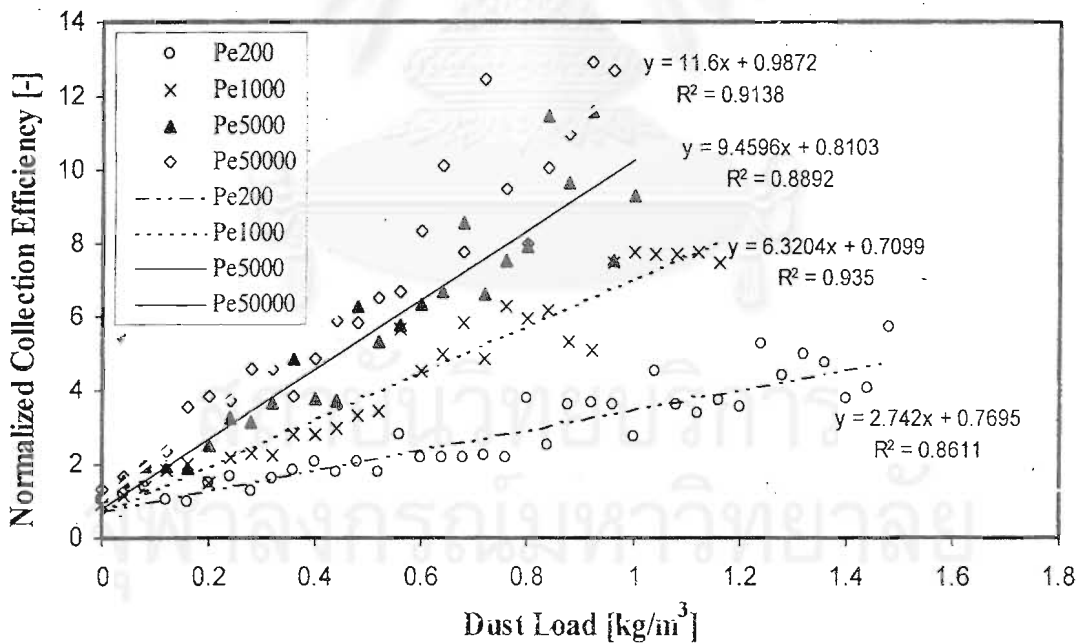
Figure 6.100 Normalized collection efficiency of a dust-loaded fiber for the
case of Ri=0.1, Kc = 0.016 and Gamma = 180
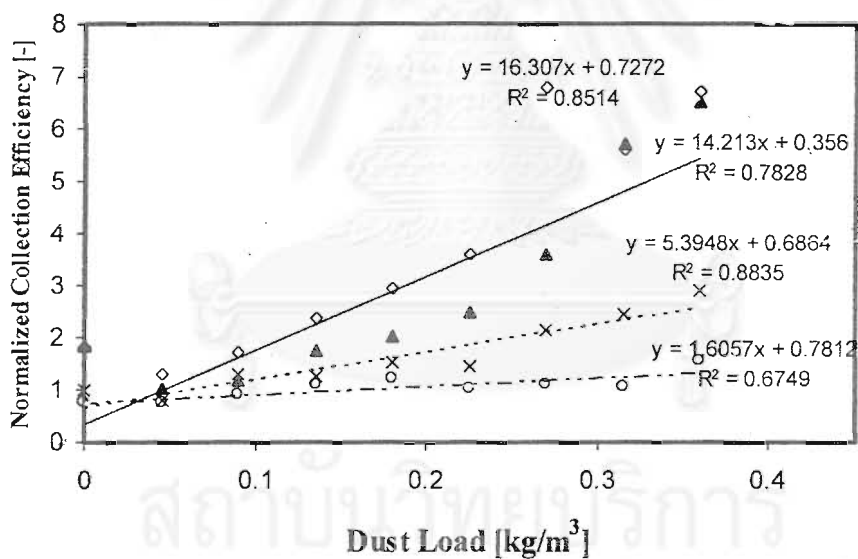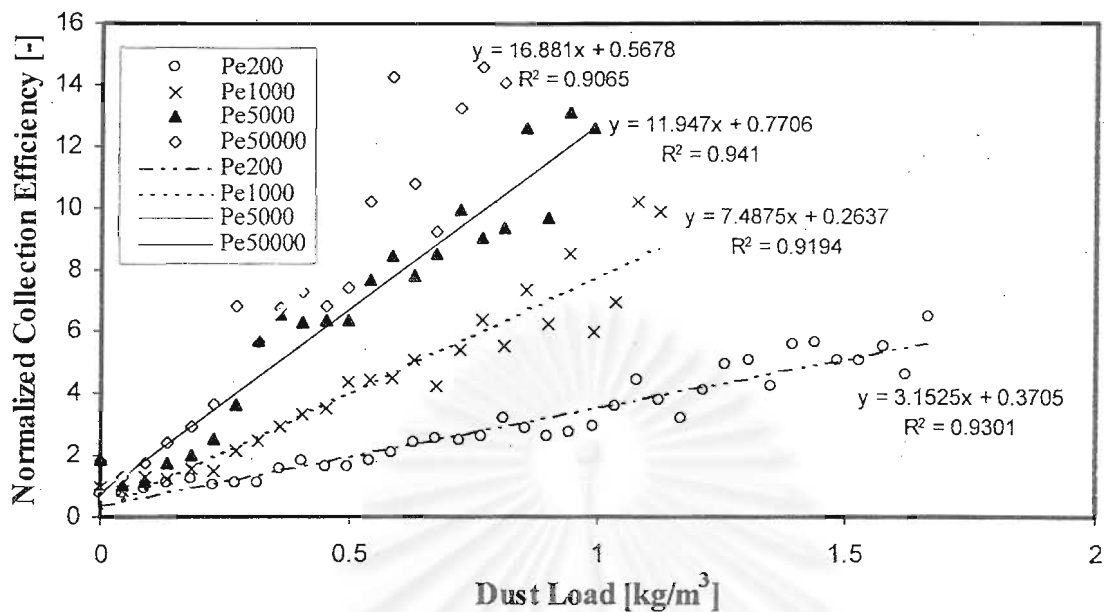
Figure 6.101 Normalized collection efficiency of a dust-loaded fiber for the

case of Ri=0.03 and K_C = 0.05 and Gamma = 90

(above : overall dust load period, below : initial dust load period)
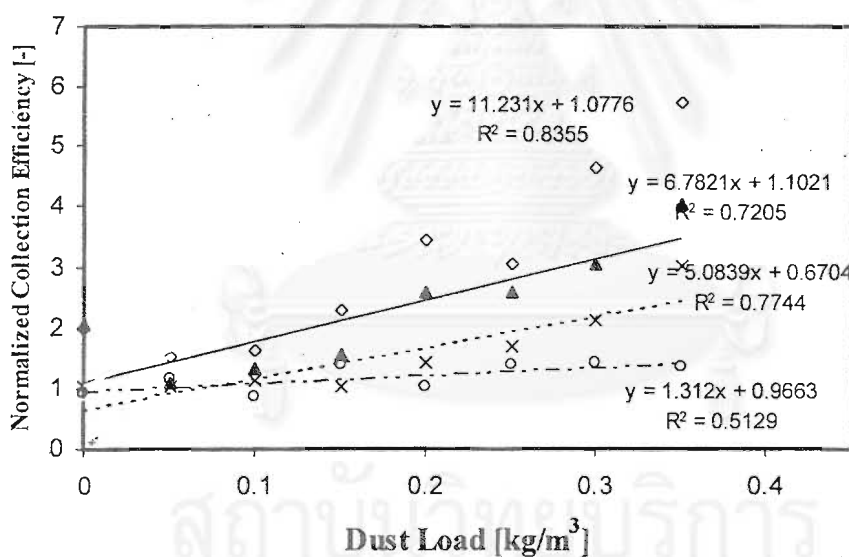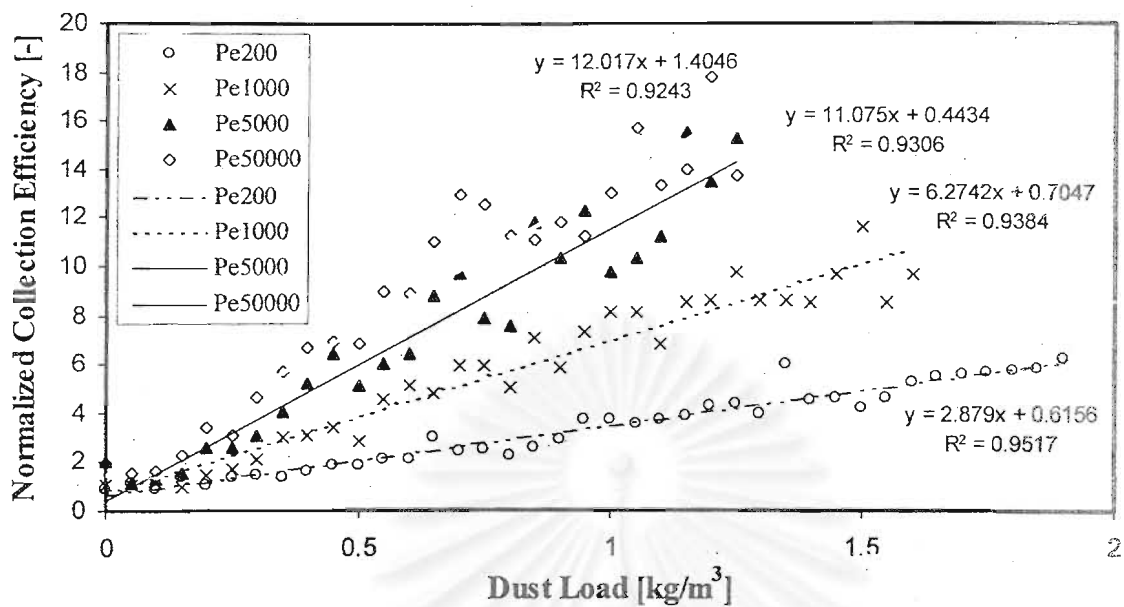
Figure 6.102 Normalized collection efficiency of a dust-loaded fiber for the
case of Ri=0.05 and K_C = 0.05 and Gamma = 90
(above : overall dust load period, below : initial dust load period)
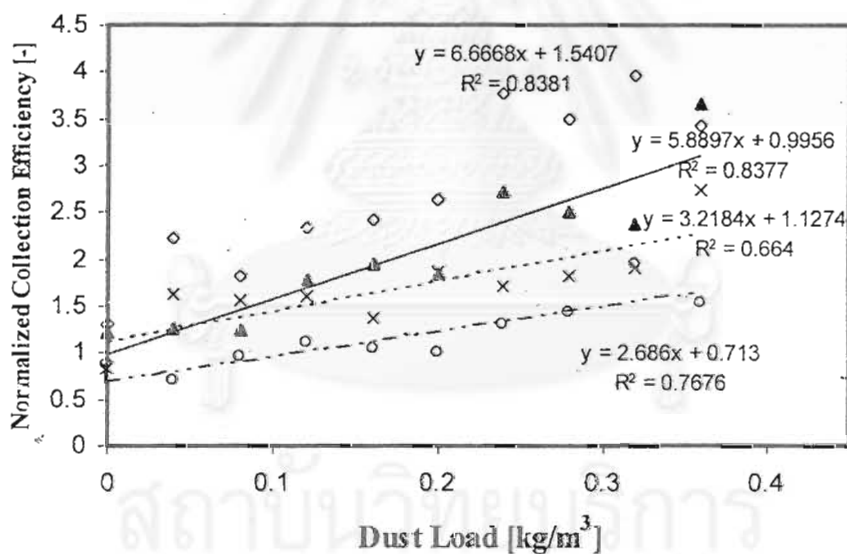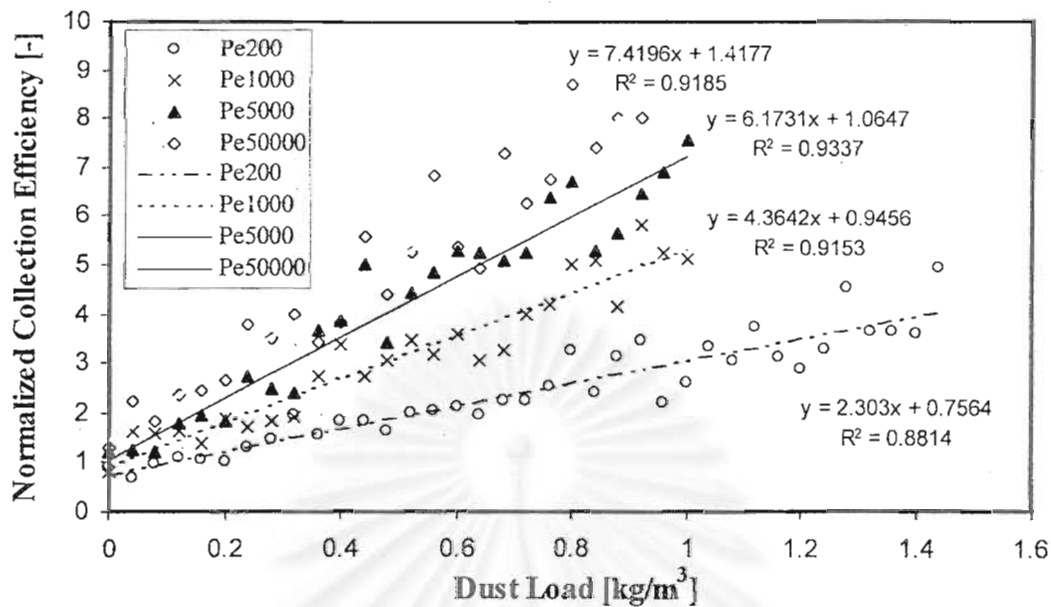
Figure 6.103 Normalized collection efficiency of a dust-loaded fiber for the

case of Ri=0.1 and K_C = 0.05 and Gamma = 90

(above : overall dust load period, below : initial dust load period)
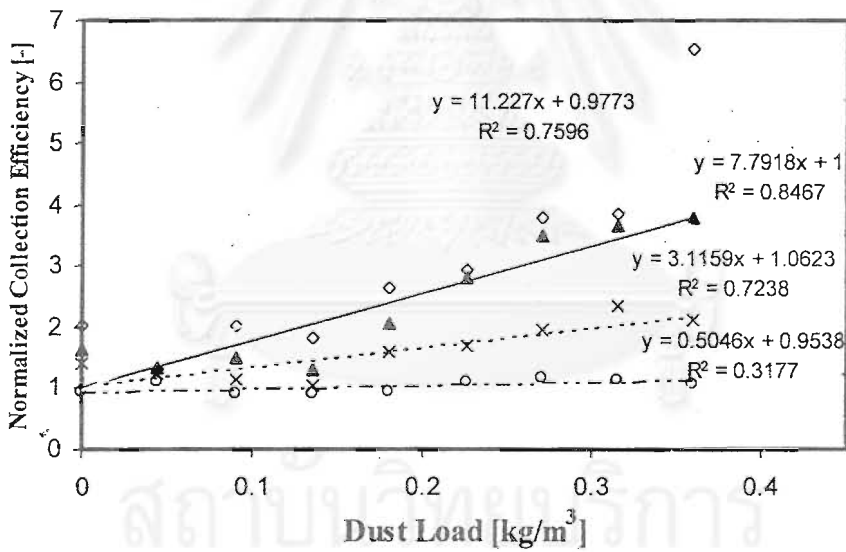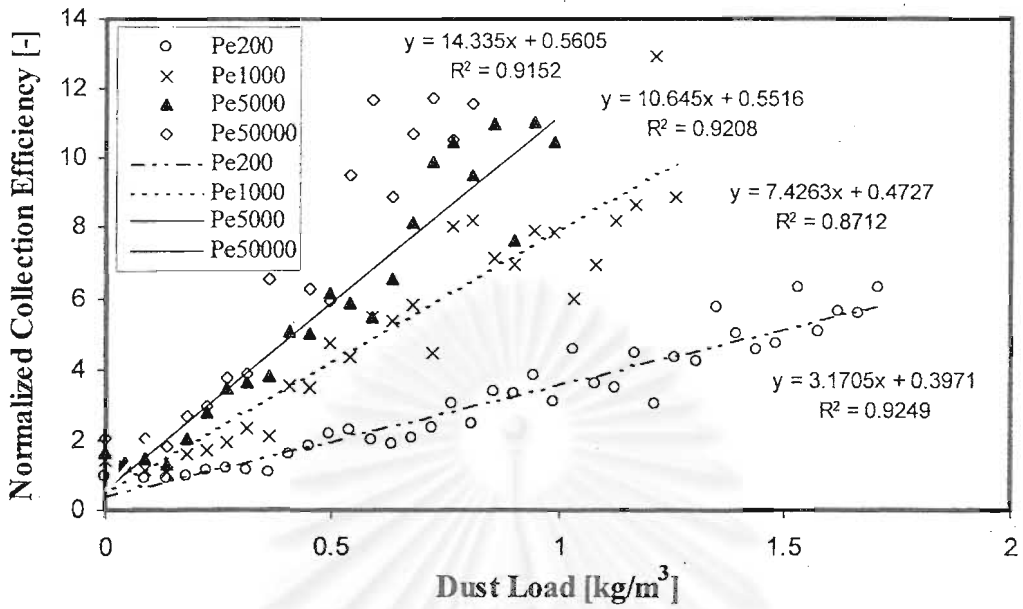
Figure 6.104 Normalized collection efficiency of a dust-loaded fiber for the
case of Ri=0.03 and K_C = 0.05 and Gamma = 135
(above : overall dust load period, below : initial dust load period)
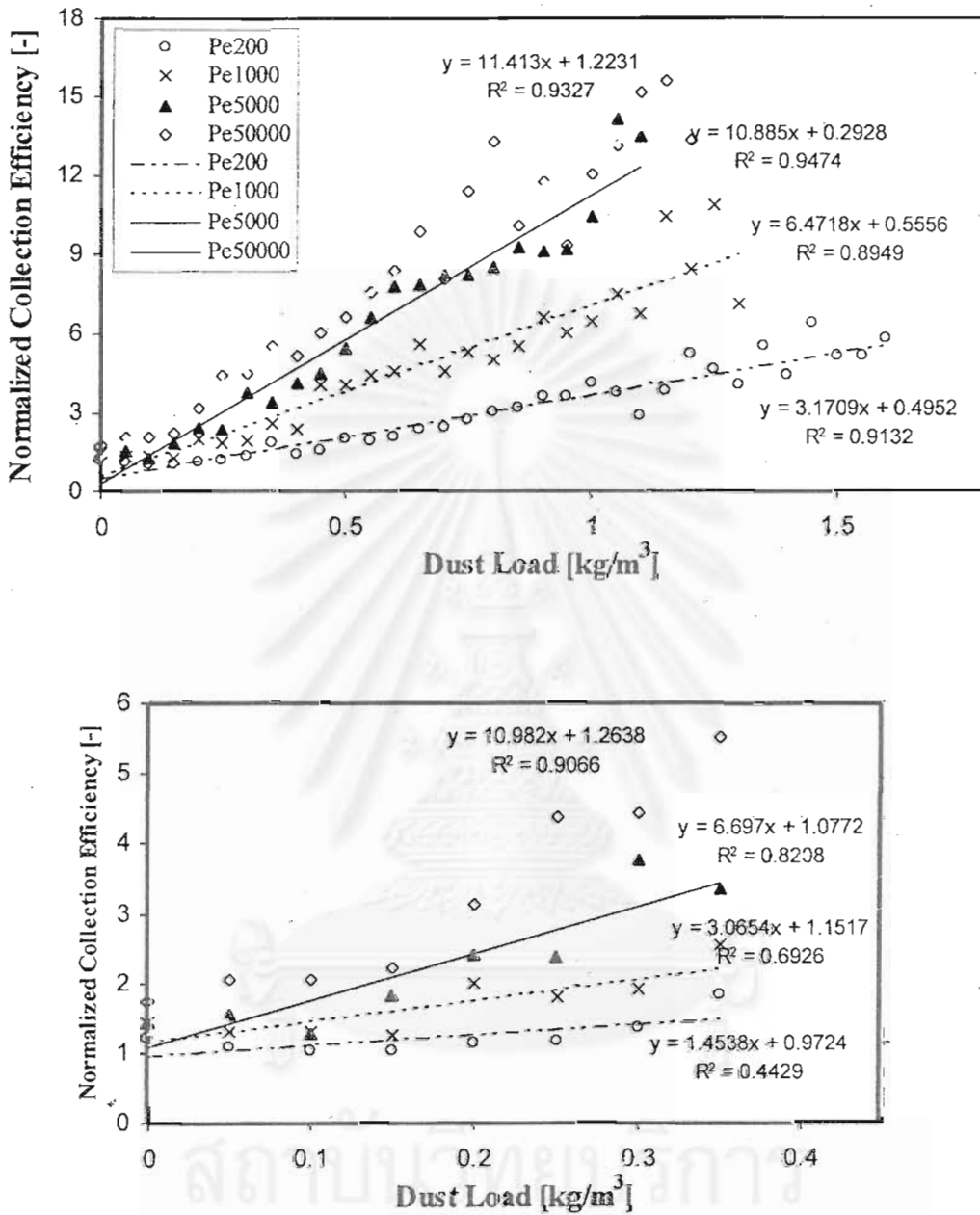
Figure 6.105 Normalized collection efficiency of a dust-loaded fiber for the
case of Ri=0.05 and K_C = 0.05 and Gamma = 135

(above : overall dust load period, below : initial dust load period)
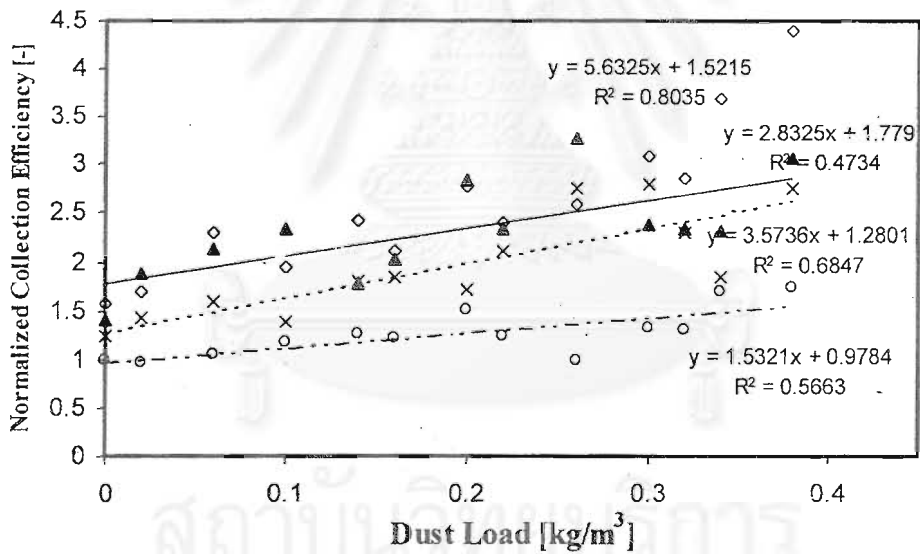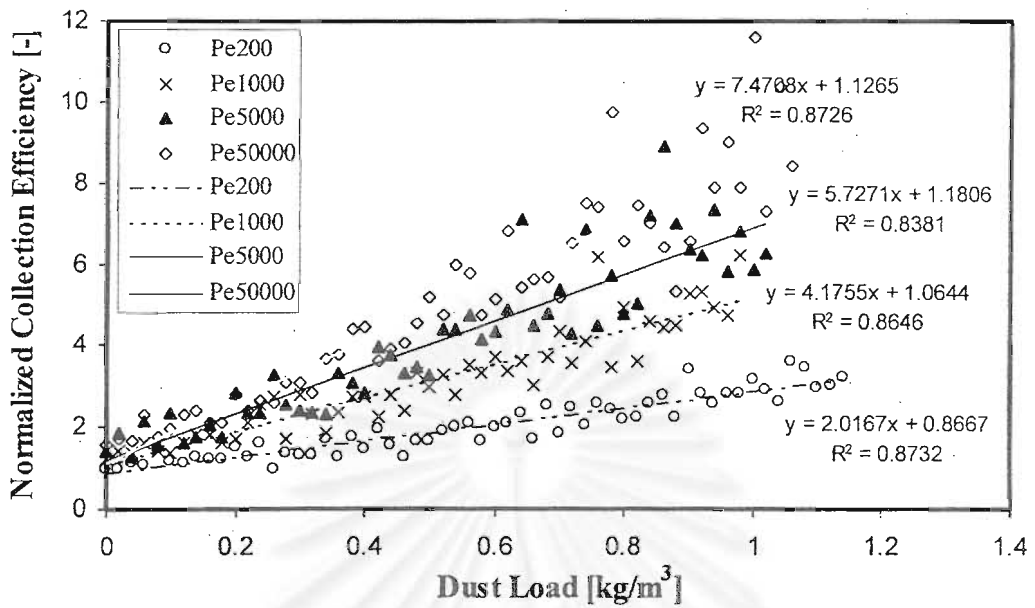
Figure 6.106 Normalized collection efficiency of a dust-loaded fiber for the
case of Ri=0.1 and K_C = 0.05 and Gamma = 135

(above : overall dust load period, below : initial dust load period)
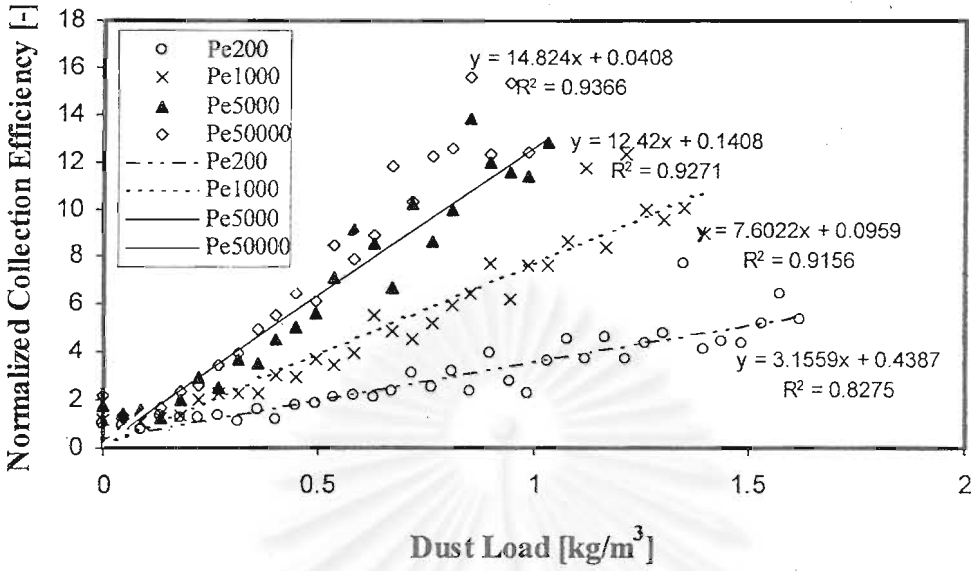
Figure 6.107 Normalized collection efficiency of a dust-loaded fiber for the case of Ri=0.03 and $K_C = 0.05$ and Gamma = 180
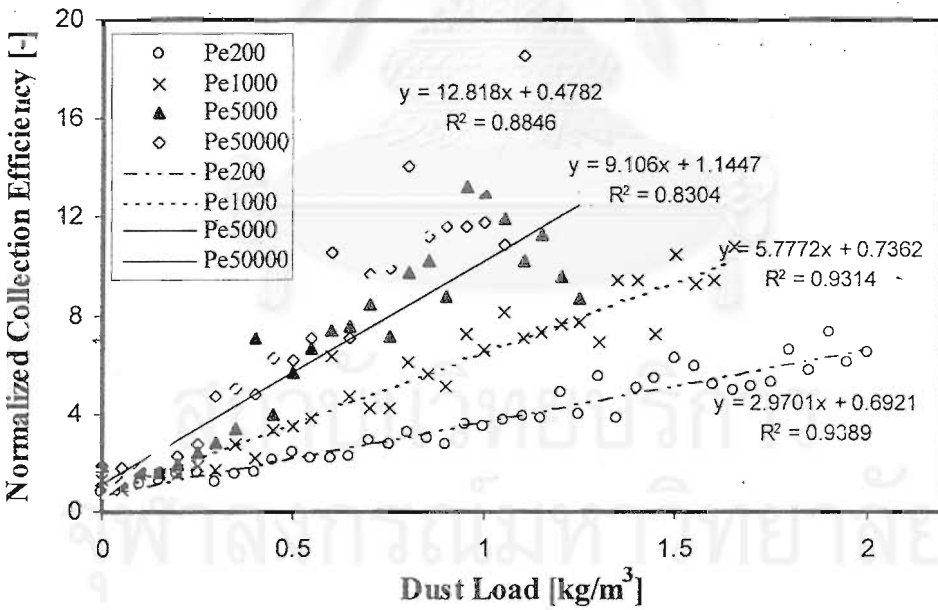
Figure 6.108 Normalized collection efficiency of a dust-loaded fiber for the case of Ri=0.05 and $K_C = 0.05$ and Gamma = 180
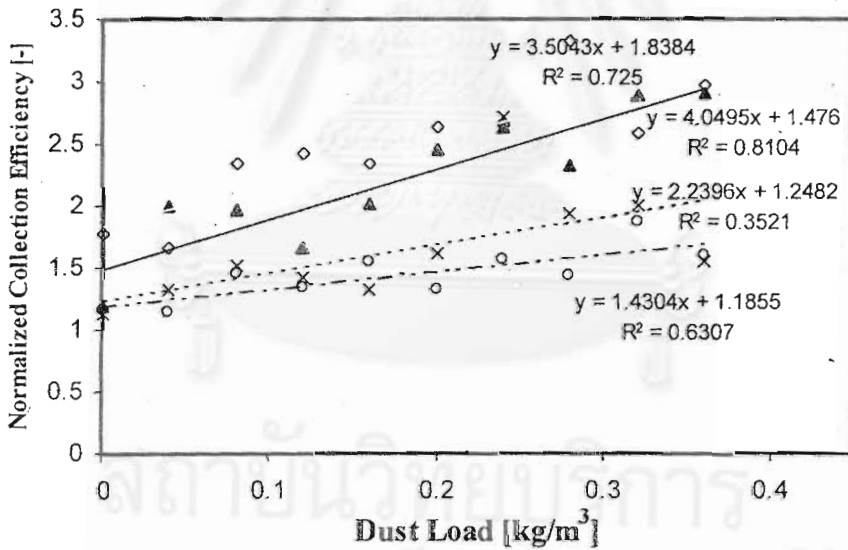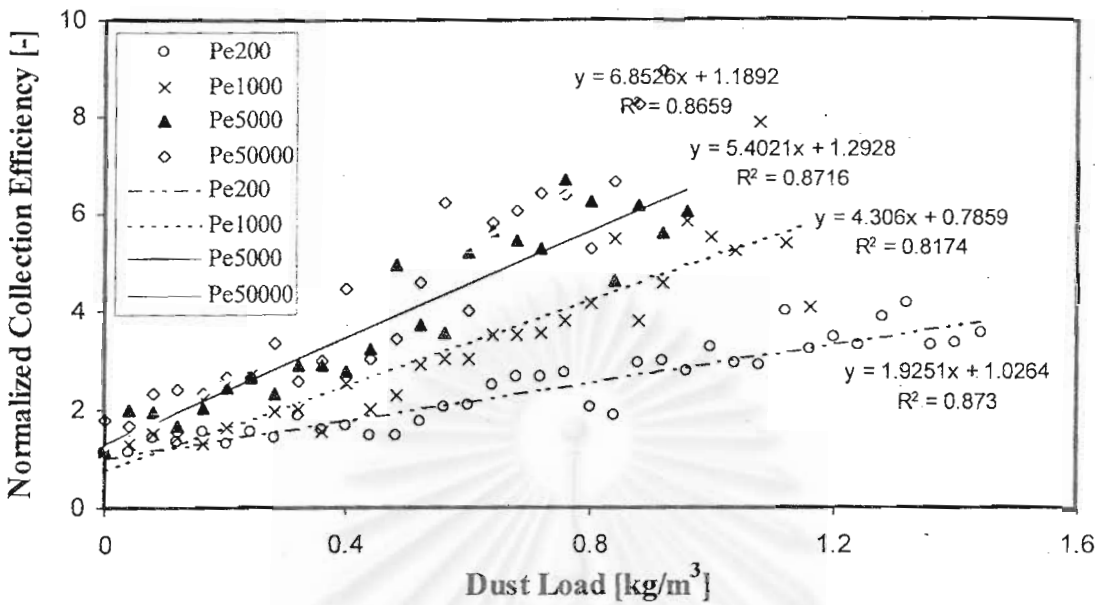
Figure 6.109 Normalized collection efficiency of a dust-loaded fiber for the

case of Ri=0.1 and K_C = 0.05 and Gamma = 180

(above : overall dust load period, below : initial dust load period)
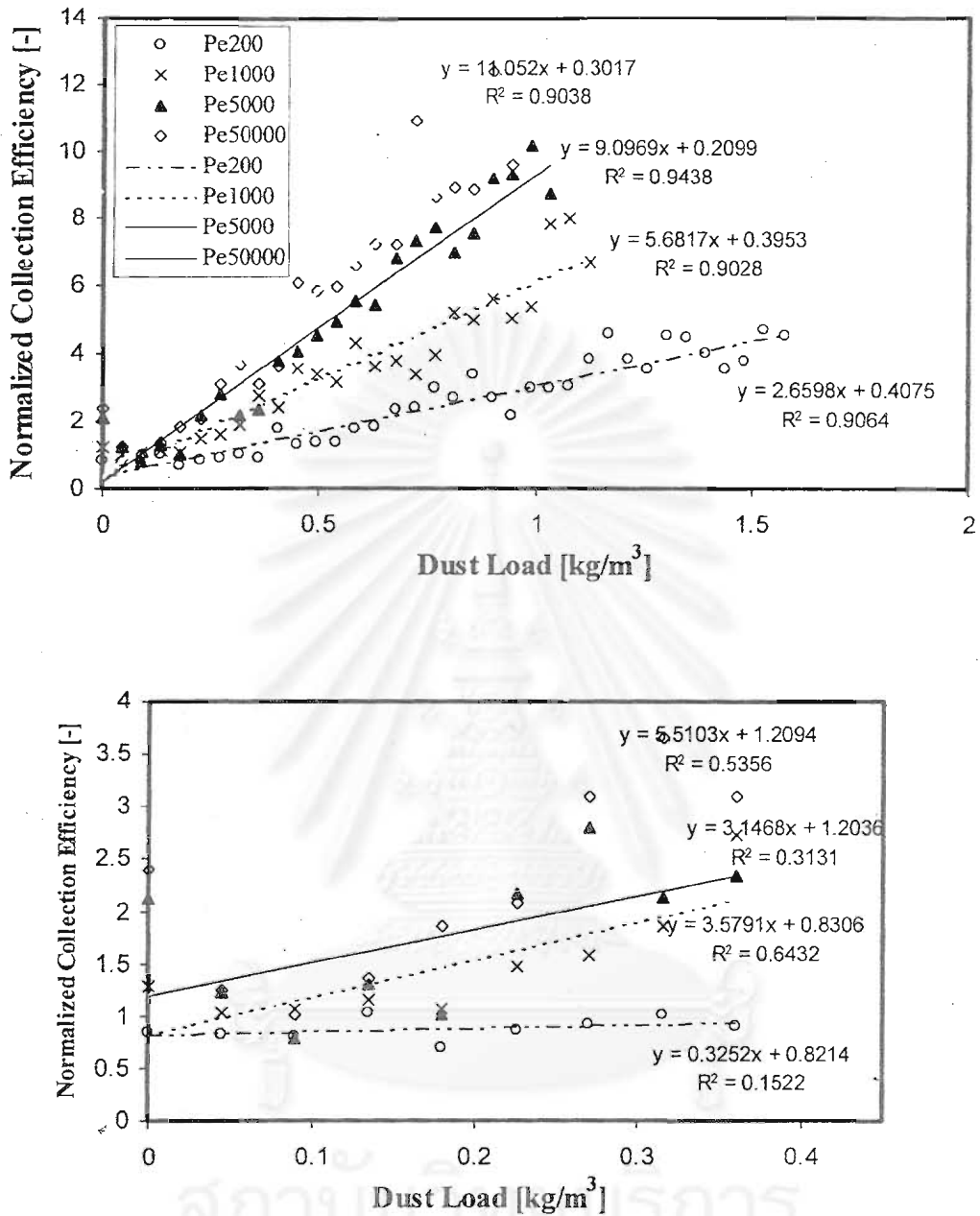
Figure 6.110 Normalized collection efficiency of a dust-loaded fiber for the

case of Ri=0.03, K_C = 0.1 and Gamma = 90

(above : overall dust load period, below : initial dust load period)
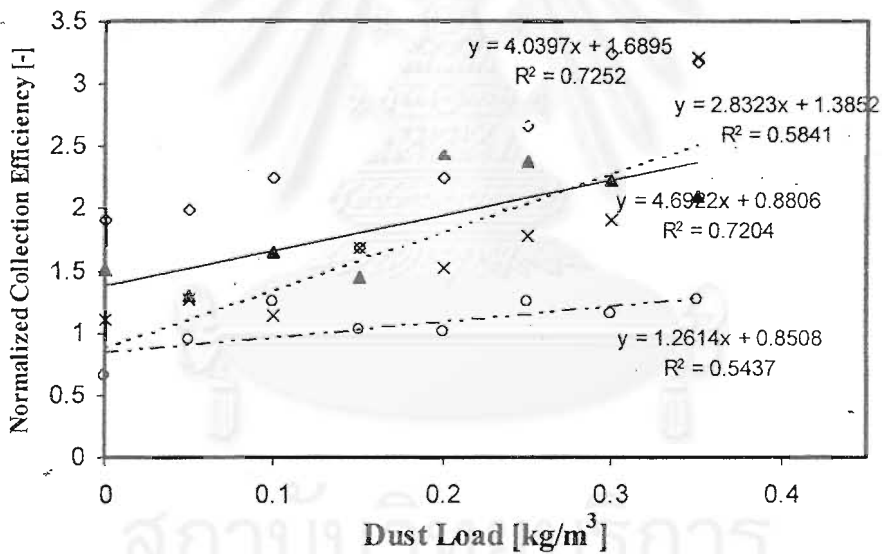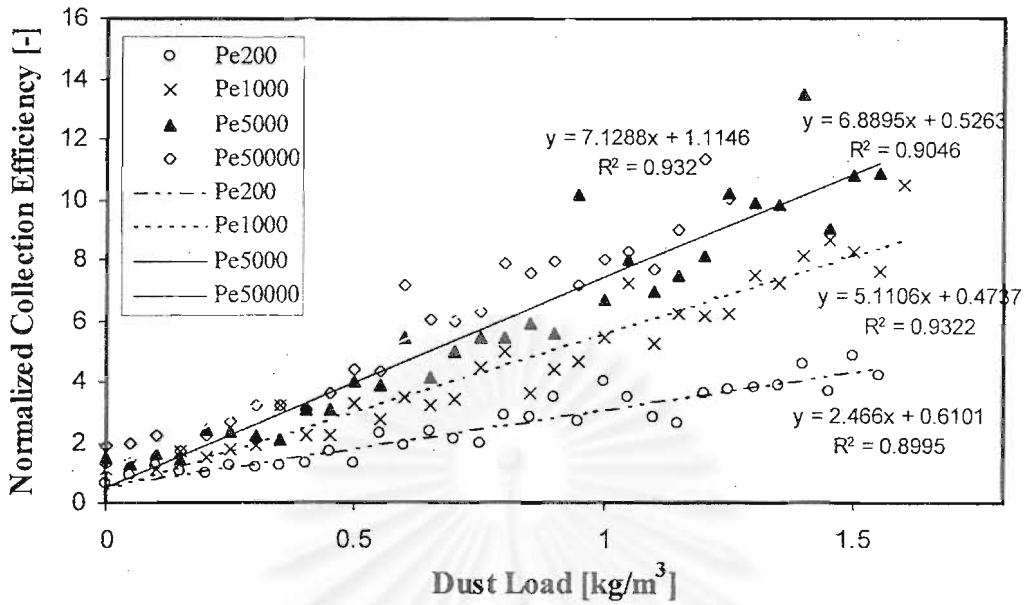
Figure 6.111 Normalized collection efficiency of a dust-loaded fiber for the
case of Ri=0.05, K_C = 0.1 and Gamma = 90

(above : overall dust load period, below : initial dust load period)
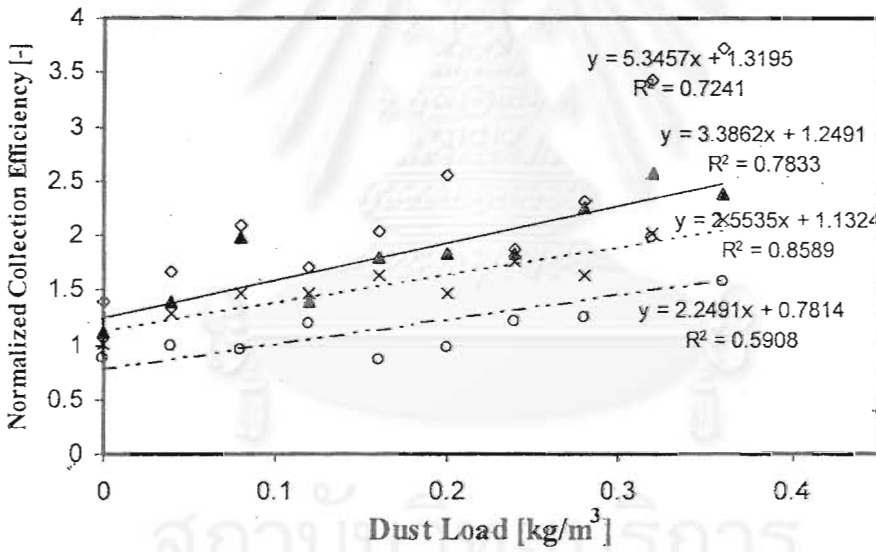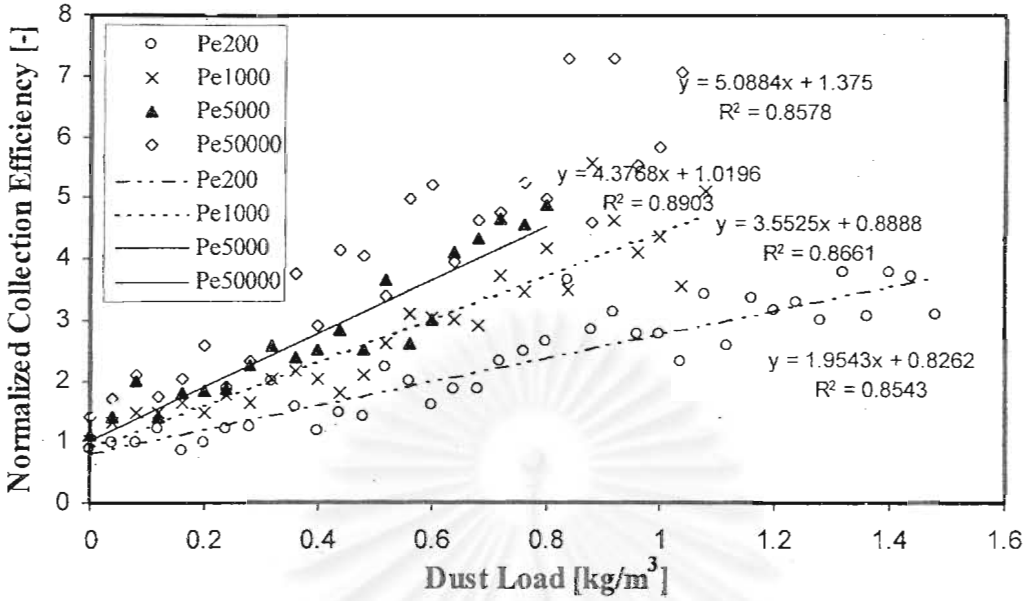
Figure 6.112 Normalized collection efficiency of a dust-loaded fiber for the

case of Ri=0.1, K_C = 0.1 and Gamma = 90

(above : overall dust load period, below : initial dust load period)
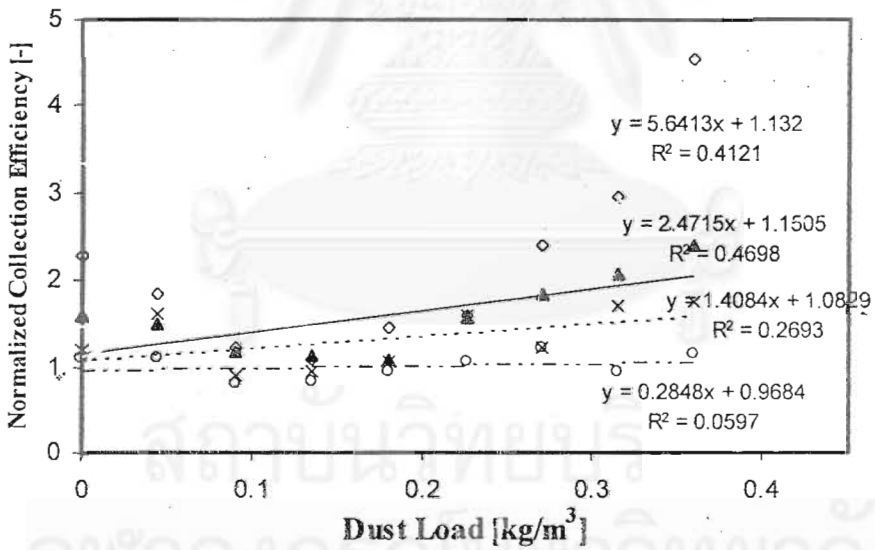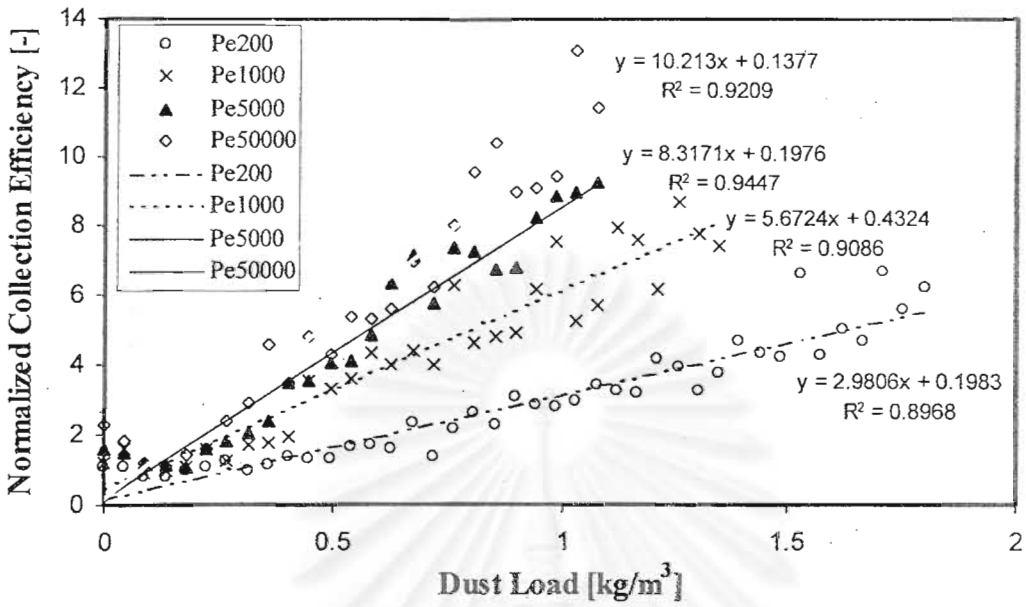
Figure 6.113 Normalized collection efficiency of a dust-loaded fiber for the
case of Ri=0.03, $K_C = 0.1$ and Gamma = 135
(above : overall dust load period, below : initial dust load period)
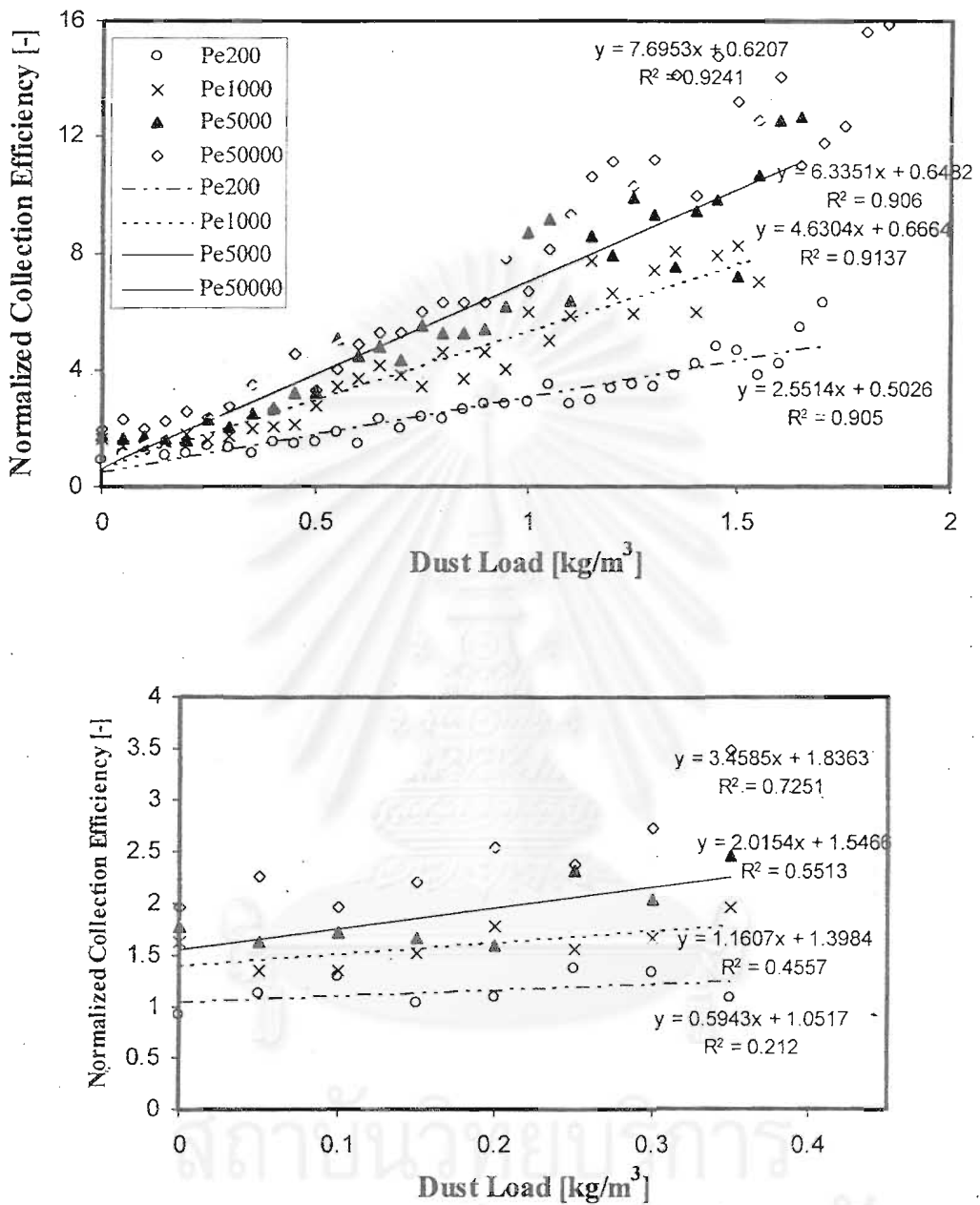
Figure 6.114 Normalized collection efficiency of a dust-loaded fiber for the

case of Ri=0.05, $K_C = 0.1$ and Gamma = 135

(above : overall dust load period, below : initial dust load period)
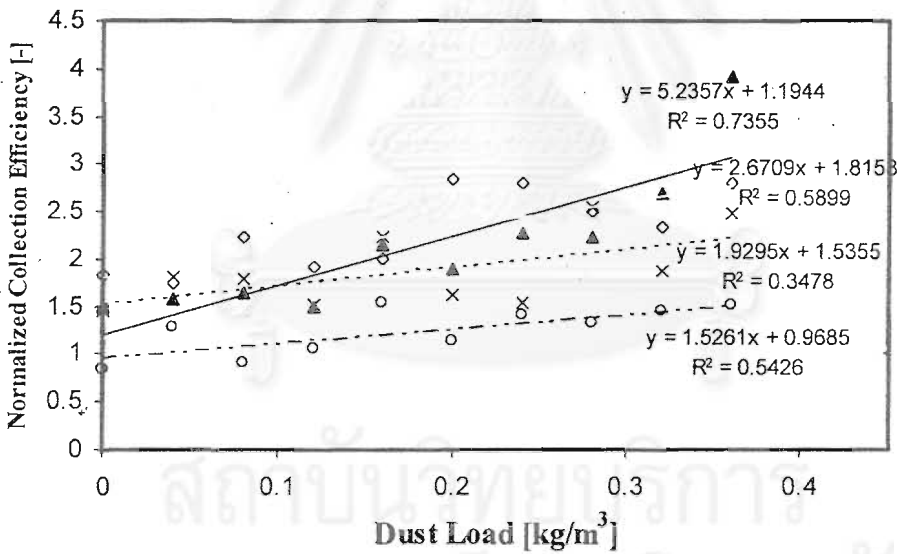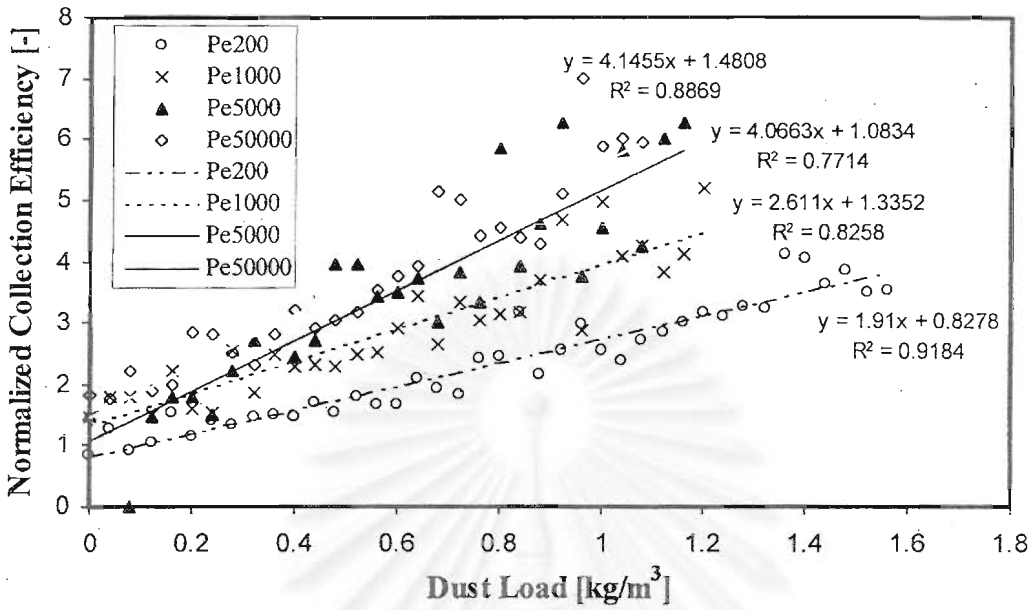
Figure 6.115 Normalized collection efficiency of a dust-loaded fiber for the

case of Ri=0.1, $K_C = 0.1$ and Gamma = 135

(above : overall dust load period, below : initial dust load period)
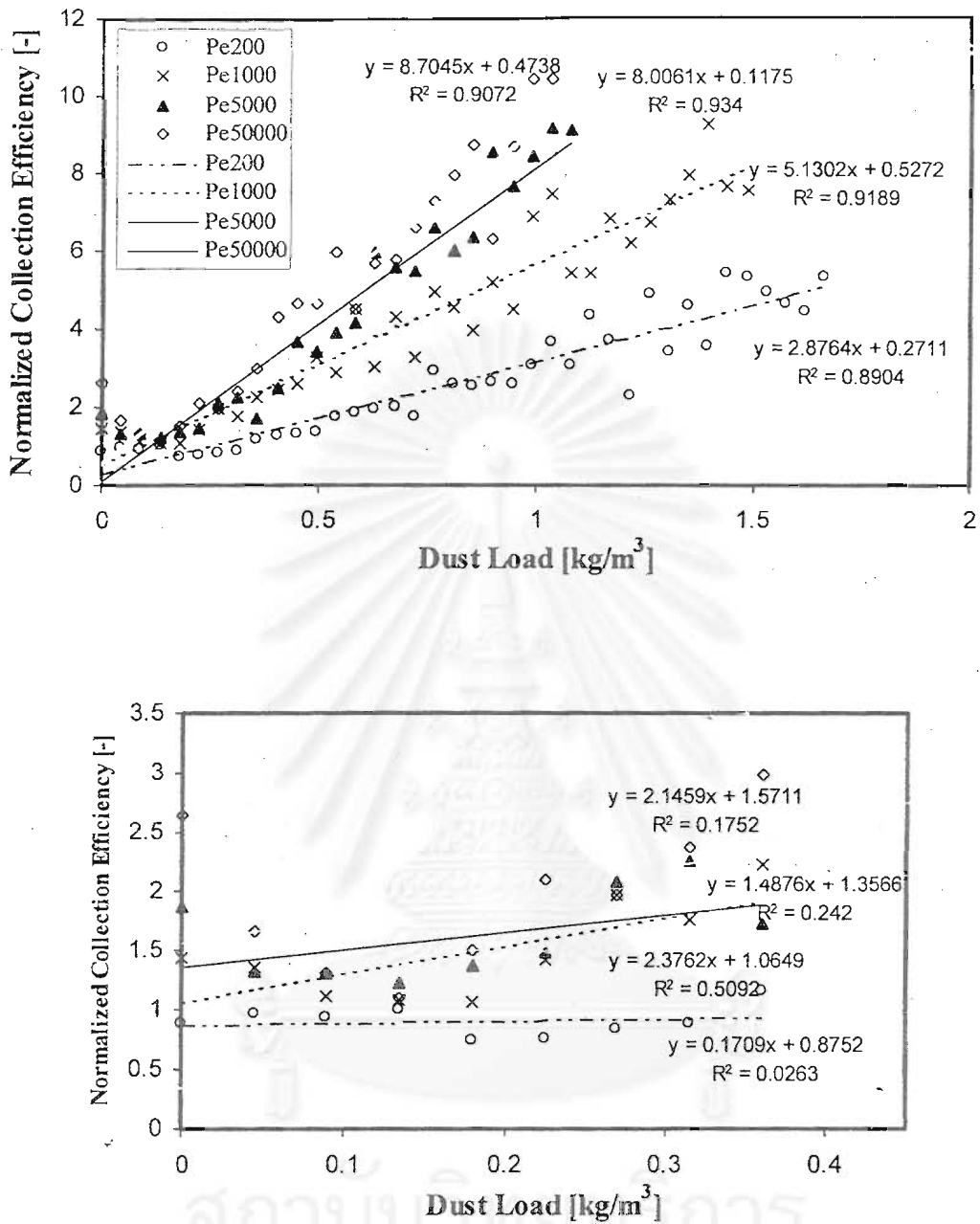
Figure 6.116 Normalized collection efficiency of a dust-loaded fiber for the
case of Ri=0.03, K_C = 0.1 and Gamma = 180
(above : overall dust load period, below : initial dust load period)
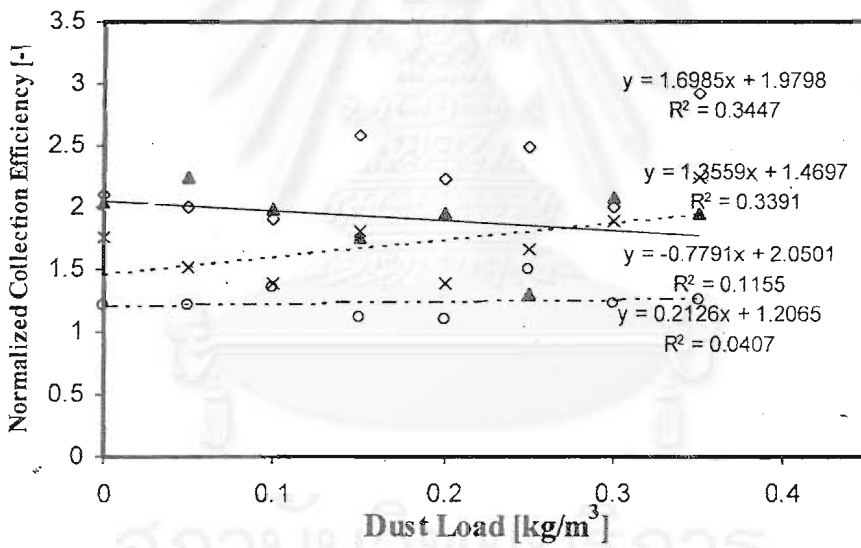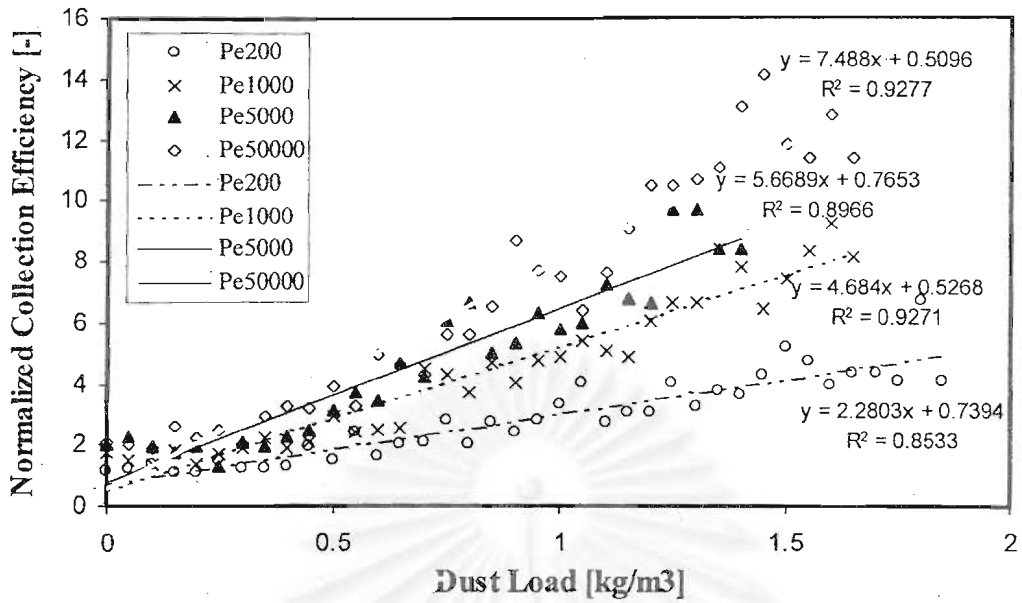
Figure 6.117 Normalized collection efficiency of a dust-loaded fiber for the
case of Ri=0.05, $K_C = 0.1$ and Gamma = 180
(above : overall dust load period, below : initial dust load period)
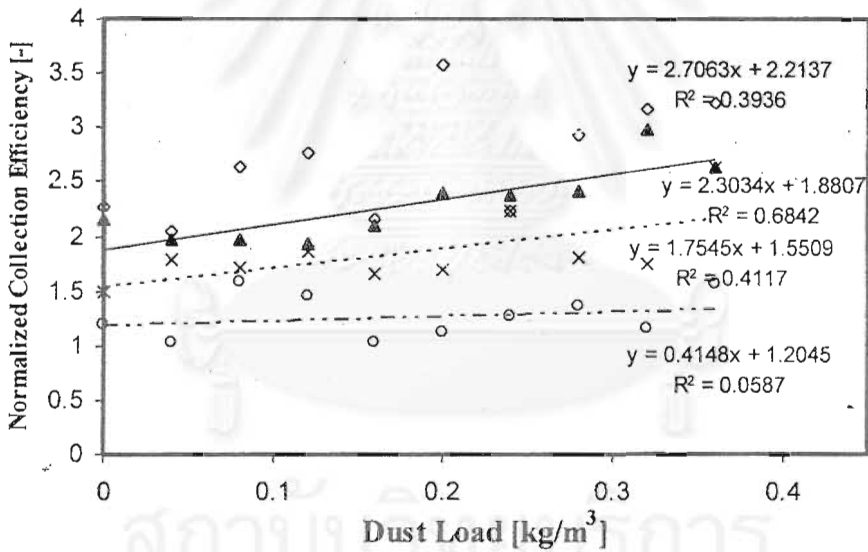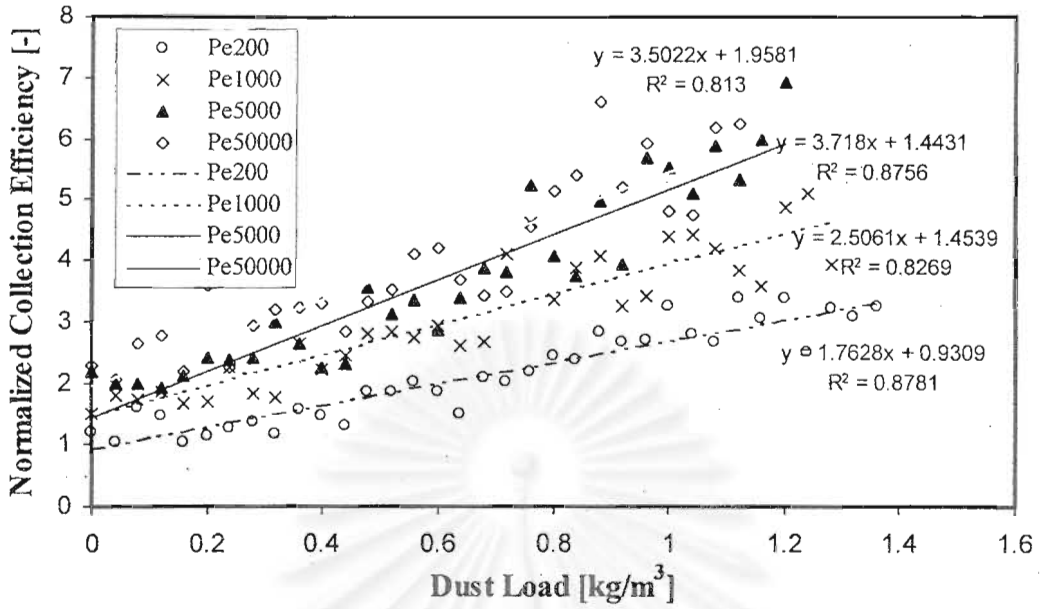
Figure 6.118 Normalized collection efficiency of a dust-loaded fiber for the

case of Ri=0.1, $K_C = 0.1$ and Gamma = 180

(above : overall dust load period, below : initial dust load period)
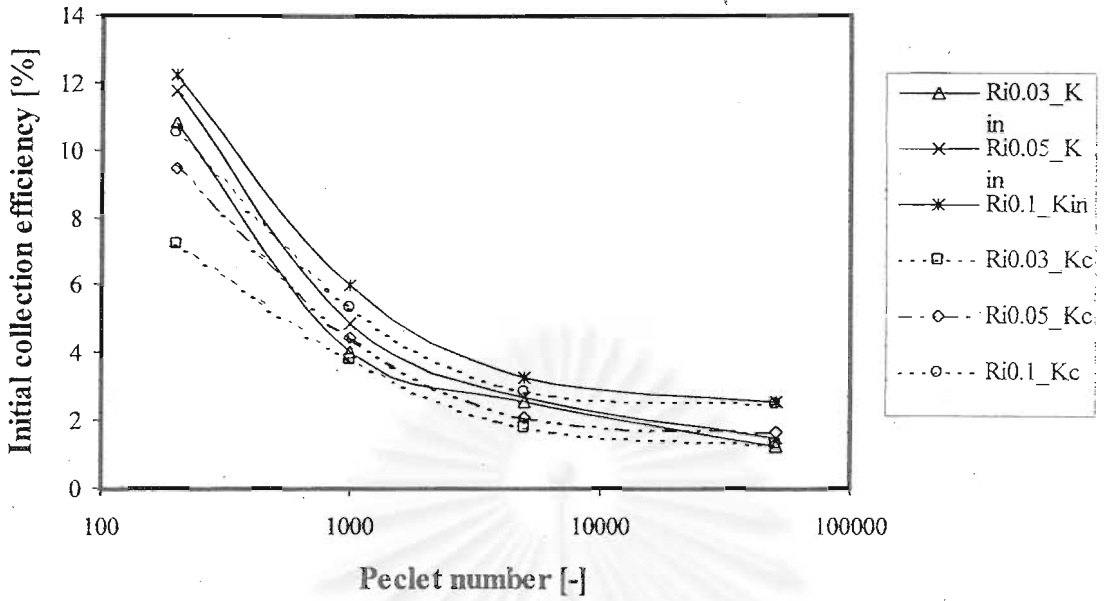
Figure 6.119 Relation between collection efficiency and Pe number

(K$_{In}$= 0.004, K$_C$=0.016 and Gamma=90)
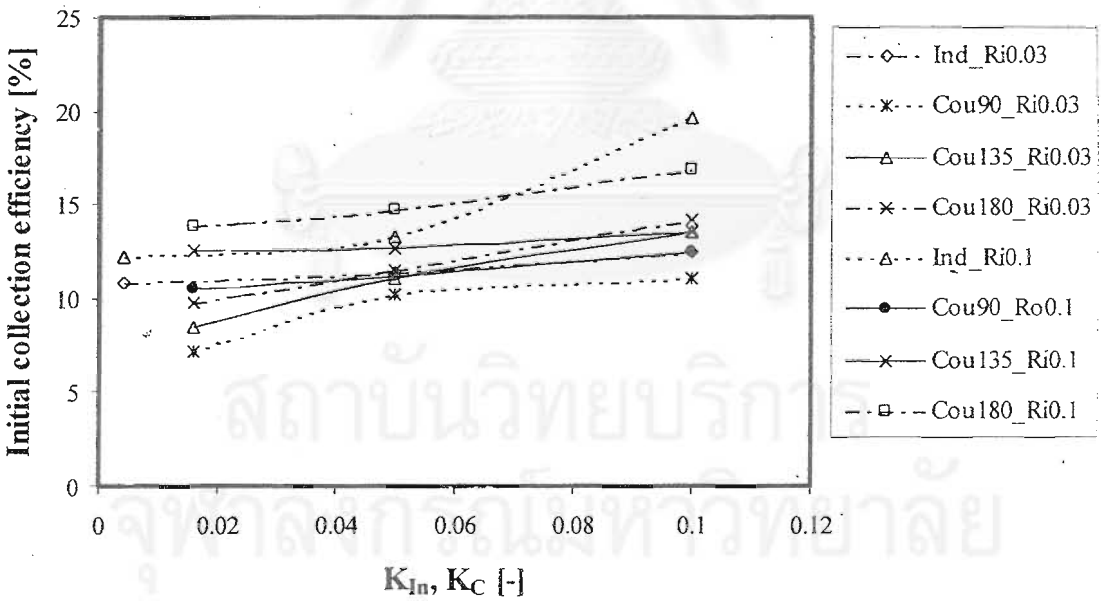
Figure 6.120 Relation between collection efficiency and K$_{In}$ or K$_C$ and

Gamma (Pe=200)
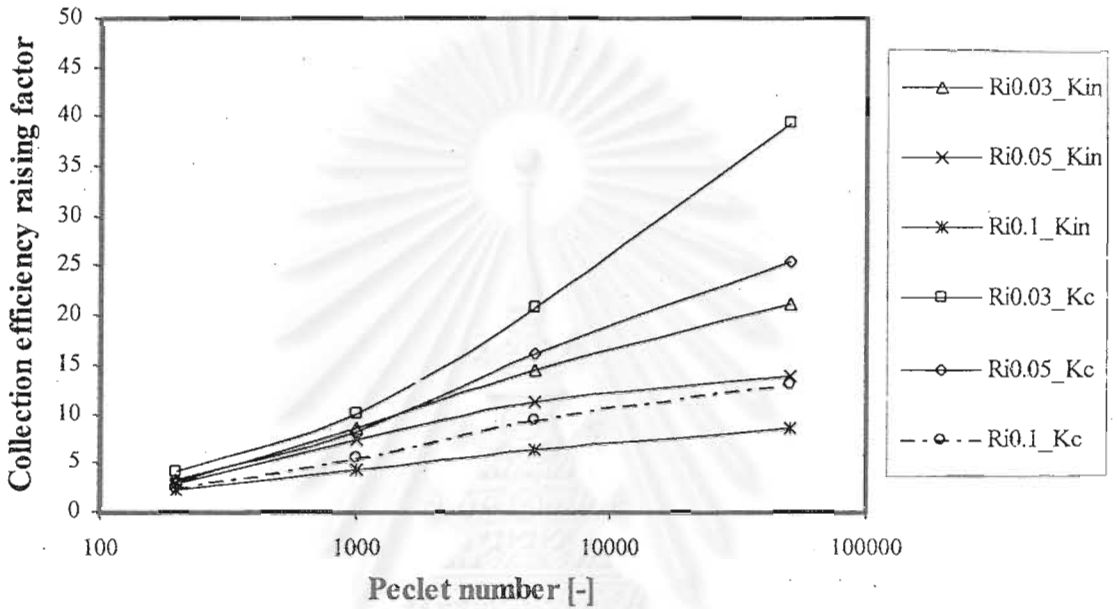
Figure 6.121 Relation between collection efficiency raising factor and Pe

number (K_{In}= 0.004, K_C=0.016 and Gamma=90)

149
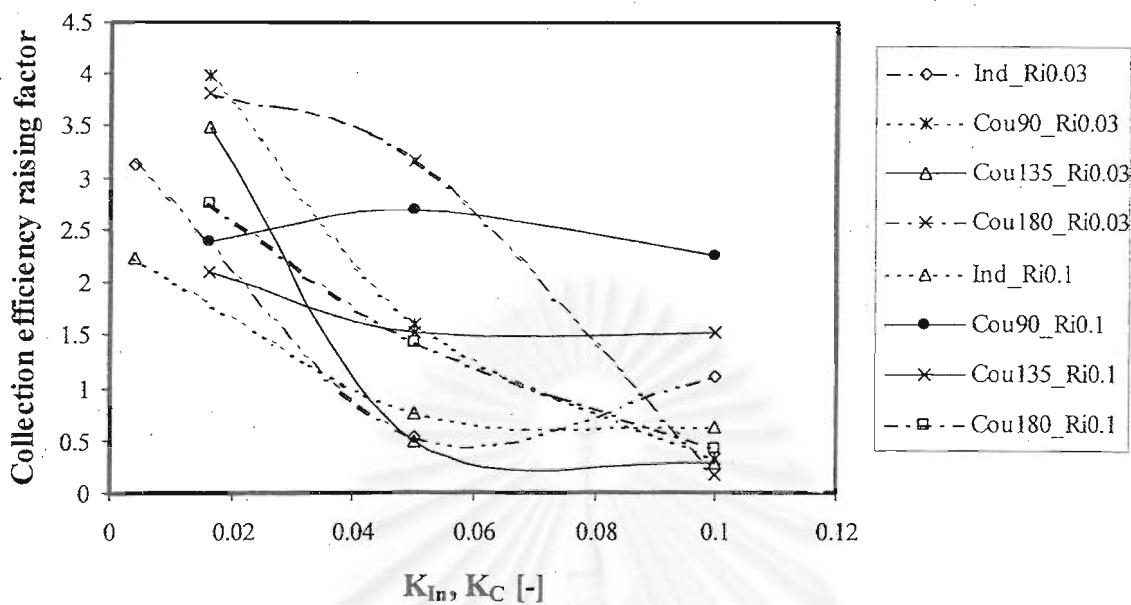
Figure 6.122 Relation between initial collection efficiency raising factor and
K_{In} or K_C and Gamma (Pe=200)
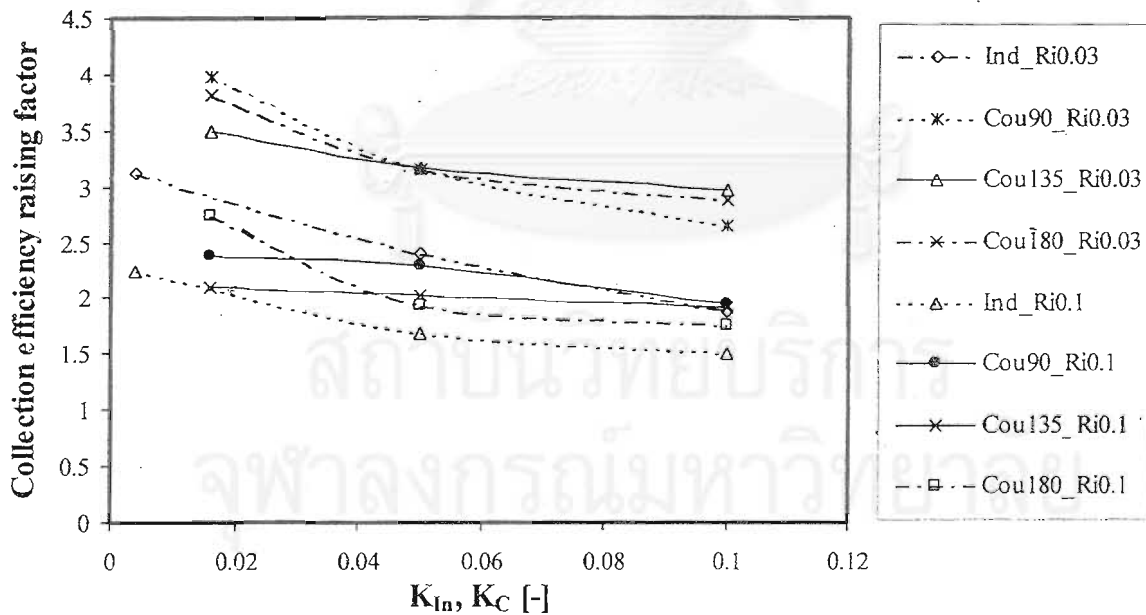
Figure 6.123 Relation between overall collection efficiency raising factor and
K_{In} or K_C and Gamma (Pe=200)

6.3.4   Comparison between present and previous results of induced force and
        coulombic force with diffusional effect

In this section, the results of previous and present works will be discussed and compared with experimental results performed by Prof. Kanaoka et al. The pictures of experimental results have been shown in section 5.6 (Figure 5.11-5.14). Prof. Kanaoka et al. studied the effect of electrical parameters, namely, induced force parameter and coulombic force parameter, on the deposition of aerosol on an electret fiber. They studied on the basis of using inertial impaction mechanism. They thought that the inertial effect was negligible. In addition, they found that at low electrical parameters, the results are not realistic and seem like the results derived from non-electret fiber as shown in Figure 5.1. As a result, they had to use the higher values of electrical parameters, i.e., 0.1 and 1. On the other hand, when they used higher values, they had to move slightly the captured particle to the rear side to make them more realistic. Furthermore, in the case of coulombic force, the effect of coulombic force parameter has to be decreased with an increase of dust load. But their model used the constant value. However, the advantage of their model is saving the computational time and memory. The previous results are shown in Figure 124-129.

For this present work, this model is based on the free flow. This means that particles can move freely in the flow field. Furthermore, it is not necessary to shift the captured particles to the rear side. And K_C is gradually decreases as dust load increases. In addition, the most advantageous aspect of this model is that it can be used in the experimental conditions, namely, $K_{In}=0.004$ or $K_C=0.016$, Pe=50000 and the results is more realistic than the previous results. And Figure 6.130-6.133 are the results of present model by means of the same conditions used in experiment to compared with the previous model.

Figure 6.134 shows the configuration of dendrite at constant $K_C=0.016$ compared with Figure 6.131 with gradually decreased K_C with dust load. It is found that the configuration is quite different especially for the rear side and the opposite polarity area. These areas have fewer captured particles. Due to the fact that the case of varied K_C has weaken K_C effect as dust load increases.

Front View   Top View   Side View

$K_{In}=0.1$, R=0.05, $\alpha=0.06$

$r_E=2d_P$
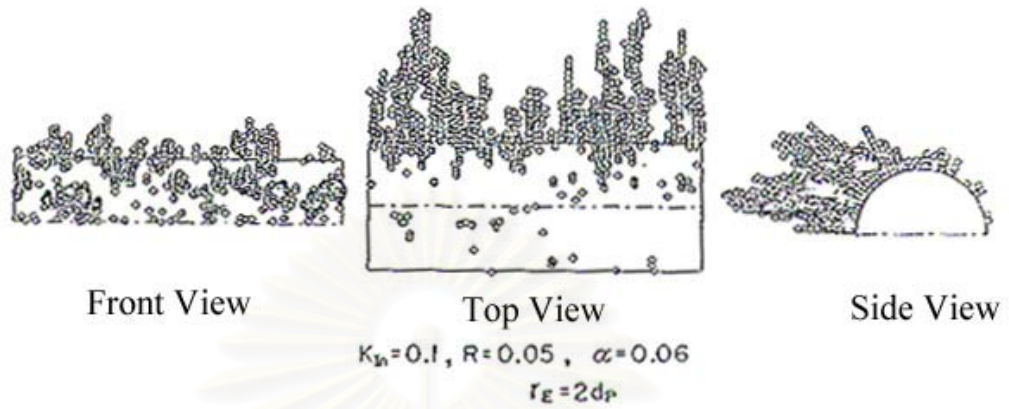
Figure 6.124 Typical configuration of dendrites of previous work for the case
of K_{In}=0.1 and Ri=0.05

Front View   Top View   Side View

$K_{In}=1$, R=0.05, $\alpha=0.06$

$r_E=2d_P$
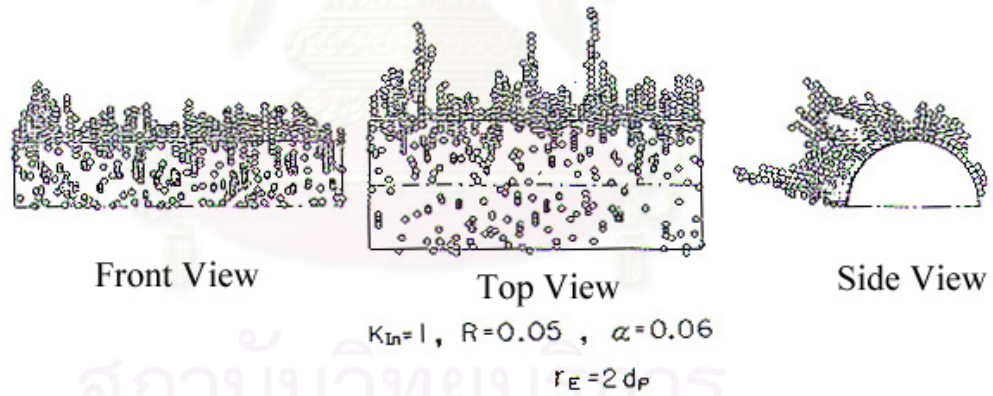
Figure 6.125 Typical configuration of dendrites of previous work for the case
of K_{In}=1 and Ri=0.05
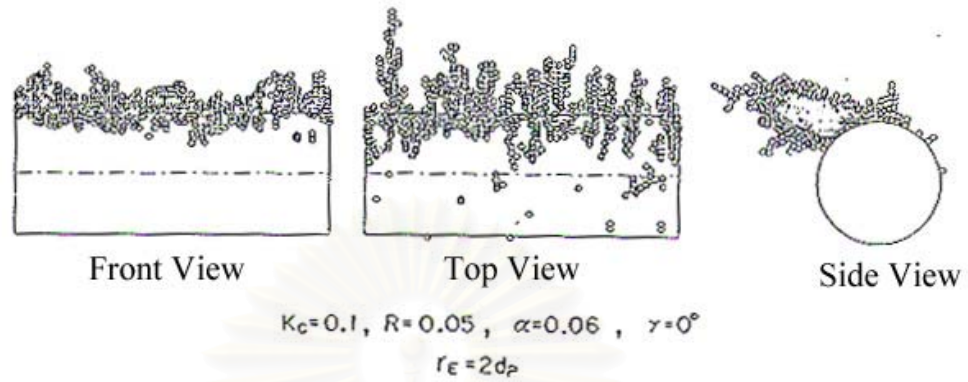
Figure 6.126 Typical configuration of dendrites of previous work for the case
of K_C=0.1, Gamma =0 and Ri=0.05
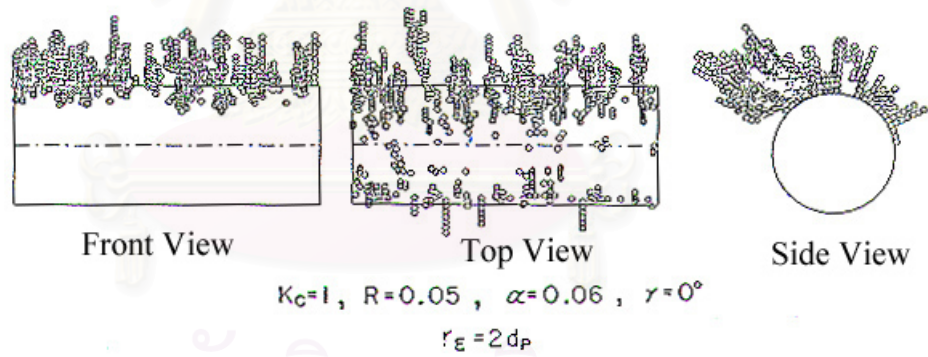
Figure 6.127 Typical configuration of dendrites of previous work for the case
of K_C=1, Gamma =0 and Ri=0.05

Front View   Top View   Side View

$K_c = 1$, $R = 0.05$, $\alpha = 0.06$, $\gamma = -45°$

$r_E = 2 d_P$
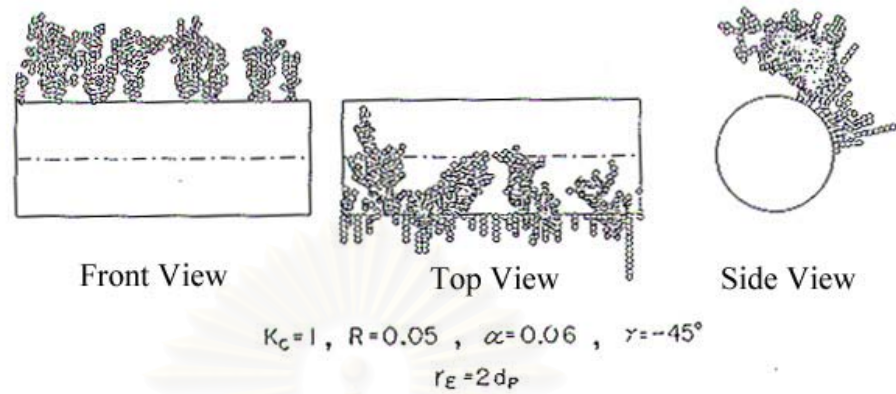
Figure 6.128 Typical configuration of dendrites of previous work for the case

of $K_C = 0.1$, Gamma = -45 and Ri = 0.05

Front View   Top View   Side View

$K_c = 1$, $R = 0.05$, $\alpha = 0.06$, $\gamma = 90°$

$r_E = 2 d_P$
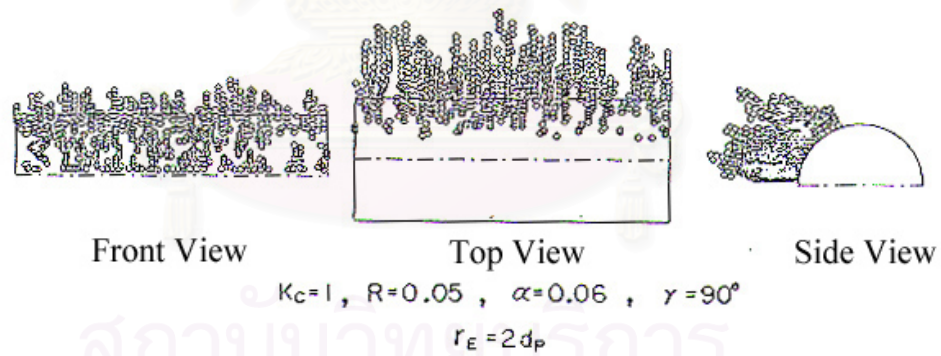
Figure 6.129 Typical configuration of dendrites of previous work for the case

of $K_C = 0.1$, Gamma = 90 and Ri = 0.05

Front View   Side View

Top View
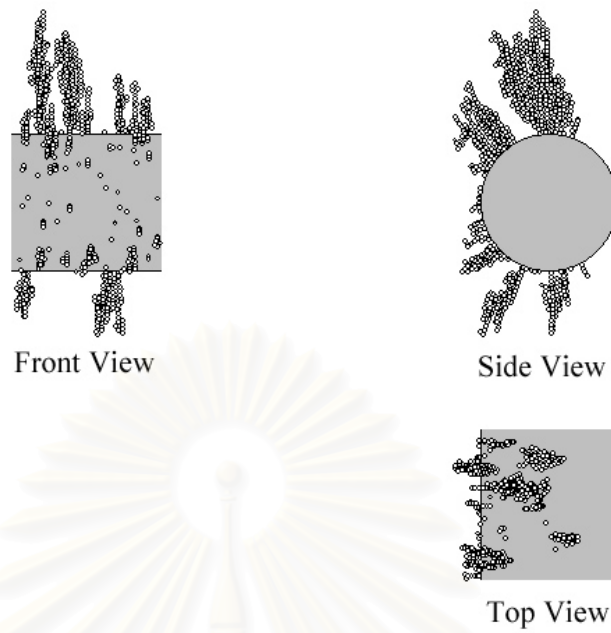
Figure 6.130 Typical configuration of dendrites of present work for the case
of K_{In}= 0.004, Ri=0.03 and Pe=50000

Front View   Side View

Top view
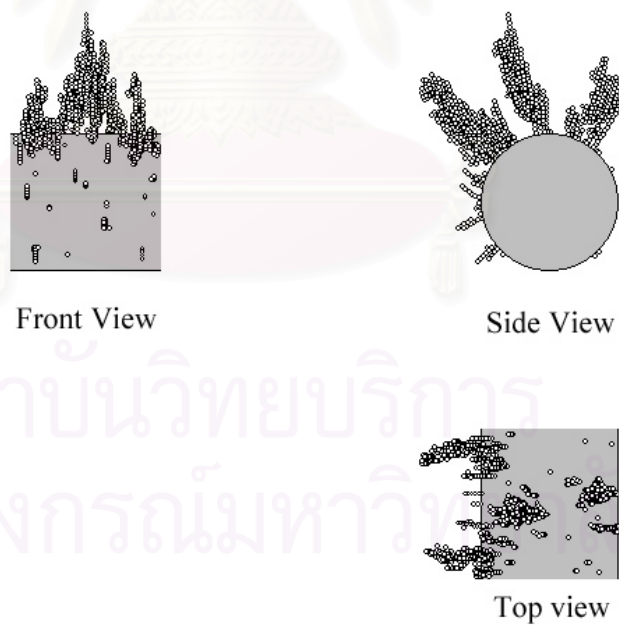
Figure 6.131 Typical configuration of dendrites of present work for the case
of K_C= 0.016, Gamma =90, Ri=0.03 and Pe=50000

Front View   Side View   Top View
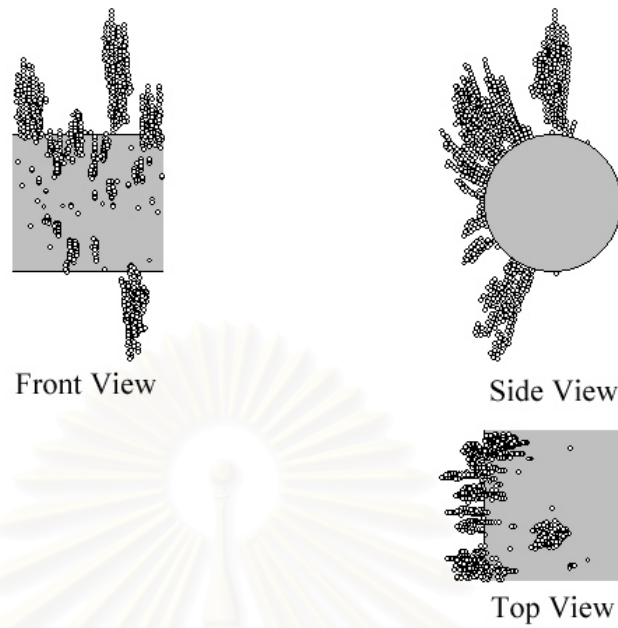
Figure 6.132 Typical configuration of dendrites of present work for the case
of K_C= 0.016, Gamma =135, Ri=0.03 and Pe=50000

Front View   Side View   Top View
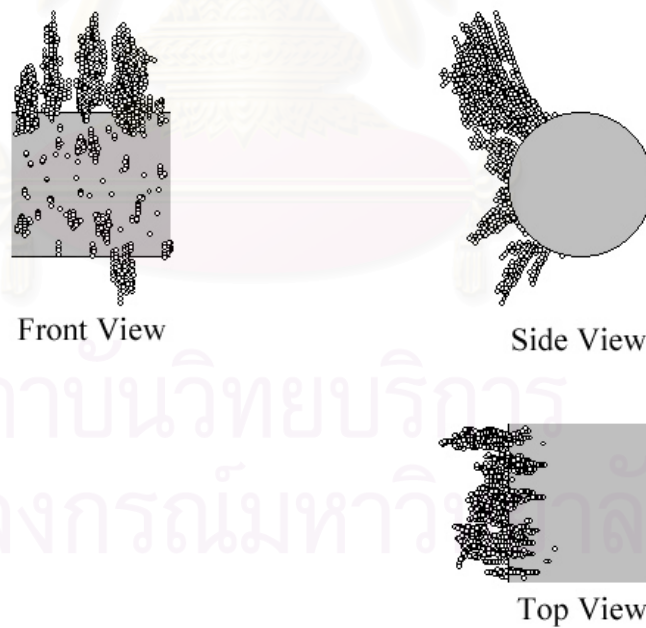
Figure 6.133 Typical configuration of dendrites of present work for the case
of K_C= 0.016, Gamma =180, Ri=0.03 and Pe=50000
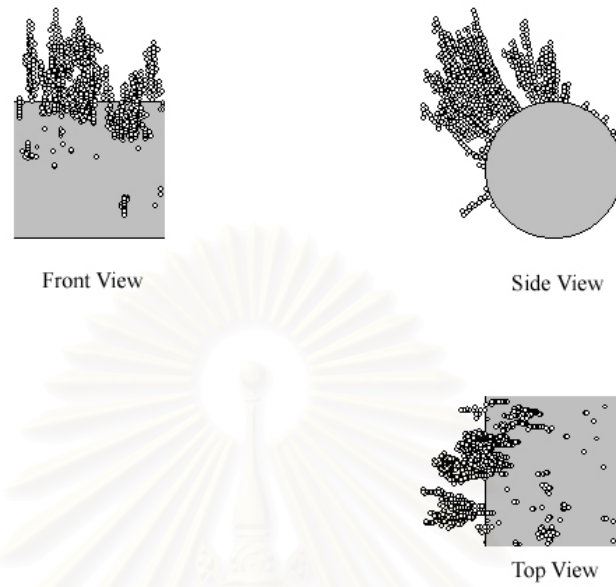
Figure 6.134 Typical configuration of dendrites of present work and for the
case of constant K_C= 0.016, Gamma =90, Ri=0.03 and Pe=50000

6.4 Comparison Between Ordinary and Electret Fiber

In this part, morphology and collection efficiency raising factor of ordinary and electret fiber are discussed.

Figure 6.135 shows discrepancy of dendrites on both non-electret and electret fiber at given conditions. It is obvious that the morphology of dendrite for both fibers is apparently different. The former is short and fat but the latter is taller and slimmer. However, the collection efficiency of electret fiber is higher than that of non-electret fiber. For the collection efficiency raising factor's point of view, the difference is shown in Table 6.9 for the case of Ri=0.05 and Pe=200, 1000 and 5000, respectively. It is found that λ derived from electret fiber is more than that of non-electret fiber about 2-5 times. This means that the electret fiber can collect much more particles. In contrast, it can produce higher pressure drop at the same time.
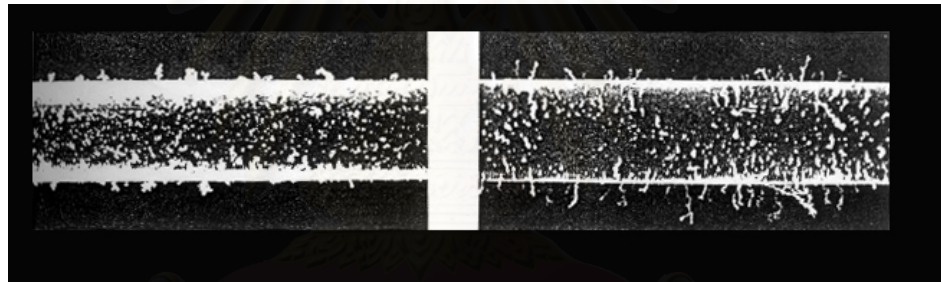
(a) Non-electret fiber   (b) Electret fiber

Figure 6.135 Particles agglomerate on the non-electret and electret fiber for
the case of Ri=0.013, Pe =10^5 and K_{In} = 0.002

Pe	Non-electret fiber		Electret fiber (Kin=0.004)	
	Ri 0.05	0.1	0.05	0.1
200	0.52	0.62	2.78	2.24
1000	2.39	2.00	7.32	4.29
5000	6.23	3.36	11.06	6.18

Table 6.9 Collection efficiency raising factor for non-electret and electret fiber

From Table 6.9, the ratios of collection efficiency raising factor for the case of electret fiber and non-electret fiber are 5, 3 and 2 for Pe =200, 1000 and 5000, respectively. However, it is interesting that the ratios are not equal. Because the morphology at Pe =200 for the case of non-electret fiber is relatively different from that of electret fiber. That is, for the case of non-electret fiber, it is short and fat and surrounded almost entire fiber surface, but the morphology of electret fiber is tall and slim and looks like straight line. These cause the ratio of the collection efficiency raising factor is so high. On the contrary, for the case of Pe =1000 and 5000, the ratio are 3 and 2 respectively. Because of the fact that the morphology of non-electret fiber are taller than that of Pe= 200, namely, the dendrites are taller and more slender. And the morphologies of electret fiber for Pe= 1000 and 5000 are tall and slender. The configuration of dendrites for both case of non-electret and electret fiber are shown in Figure 6.136 and 6.137, respectively.

a. Pe = 200　　Front View　　　　Side View

b. Pe = 1000　　Front View　　　　Side View

c. Pe = 5000　　Front View　　　　Side View
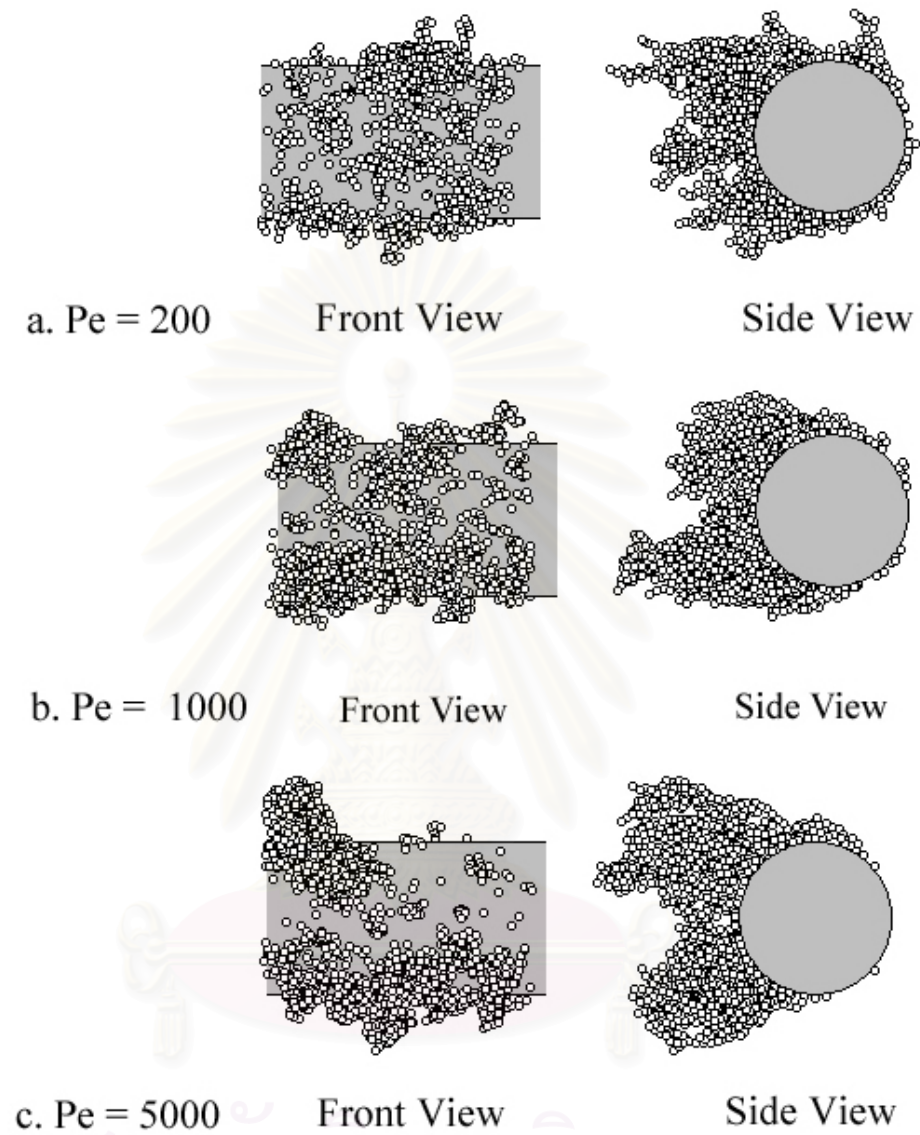
Figure 6.136 Typical configuration of dendrite for the case of non-electret
fiber at Ri = 0.03, Kin=0.004 and Pe= a.) 200, b.) 100 and
c.) 5000, respectively

a. Pe = 200   Front View   Side View

b. Pe = 1000   Front View   Side View

c. Pe = 5000   Front View   Side View
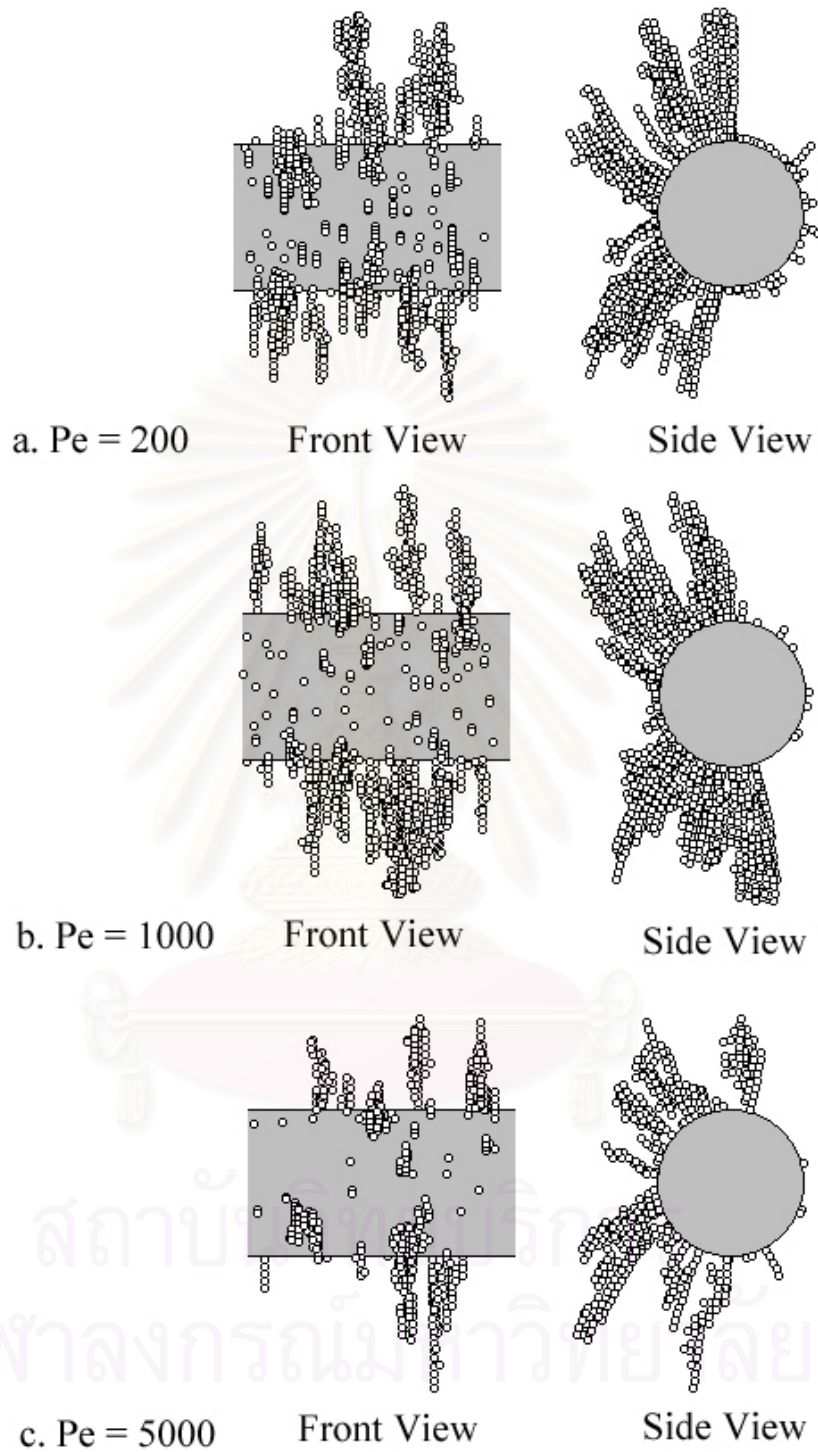
Figure 6.137 Typical configuration of dendrite for the case of electret fiber
at Ri = 0.03, Kin=0.004 and Pe= a.) 200,   b.) 100 and
c.) 5000, respectively

CHAPTER 7
CONCLUSIONS AND RECOMMENDATION

In this study, a three-dimensional stochastic model is utilized to simulate collection and agglomeration processes of particles on a cylindrical electret fiber. Major results are summarized as follows:

1. Compared with the experimental results, the morphology of the agglomerates on the electret fiber predicted by the present stochastic model is more realistic than that of a previous stochastic model because of the incorporation of convective diffusional effect to the induced and coulombic forces in the present model.

2. Time dependency of dendrite size distribution as well as age dependency of average dendrite size, which are useful for the investigation of the kinetics of aerosol deposition, the growth of dendritic population and the future development of an equivalent simplified deterministic model, have been obtained in the present investigation.

3. For the case of induced force effect, the initial collection efficiency obtained using the model agreed well with the clean-fiber value calculated from a semi-empirical correlation (Emi et al., 1987). However, for the case of coulombic force effect, discrepancy between the two values is quite significant especially in the case of high interceptional effect.

4. As expected, the initial collection efficiency generally increases as the electrical parameters of the fiber increase or the filtration velocity decreases (in term of Pe number).

5. From the simulation results, it is found that the electrostatic effect dominates particle collection in the early stage of the filtration especially in the case of small particle size. Consequently, the initial collection efficiency of particles will always be higher than the case of an ordinary (non-electret) fiber. It has been found that this electrostatically enhanced collection efficiency remains high in the early stage in the case of induced force effect but may even decreases slightly in the early stage in the case of coulombic force

effect. After a significant buildup of the dust load with the passage of time, the collection efficiency of particles generally increases almost linearly with dust load due to dominant effect of dust load on the fiber. In this case, the normalized collection efficiency, η/η_0, can be given by

$$\eta/\eta_0 = a + \lambda m$$

where η = collection efficiency

        η_0 = initial collection efficiency

        a   = initial collection efficiency derived from fitting curve

        λ = collection efficiency raising factor

      6. In the case of dominant electrical force effect, the normalized collection efficiency, η/η_0, can be represented by two linear correlations: the initial stage and the subsequent stage, respectively. The former is represented by $\eta/\eta_0 = a_I + \lambda_I m$ and the latter by $\eta/\eta_0 = a + \lambda m$, respectively. As mentioned above, the collection efficiency raising factor of the initial stage, λ_I, is smaller than that of the subsequent or overall dust-loaded period, λ.

      7. The collection efficiency raising factor, λ is known to be a function of the following dimensionless groups: interception parameter, R_I, Peclet number, Pe, induced force parameter, K_{In} and/or coulombic force parameter, K_C. In addition, the twist angle or polarization direction, γ, must also be considered in the case of coulombic force effect. According to the simulation results, the value of λ will be increased when Pe is increased. And this λ value will also be increased as R_I decreases. In the case of induced force effect, λ is smaller than that in the case of coulombic force. As in the case of induced force, λ in the case of coulombic force will be increased as K_C decreases. Furthermore, the effect of γ on λ is slightly different for

both high K_C and low K_C. However, the combined effect of K_C and K_{In} on λ has not been investigated here.

Recommendation

   Due to the shortage of reliable detailed experimental results, the present stochastic model has been validated only against certain conditions of the interception parameter, R_I, Peclet number, Pe, and electrical parameters, K_C/ K_{In}. The author recommends that future study should validate the model against a wider range of these conditions and against the other parameters mentioned below. In addition, the effects of these additional parameters on the agglomerative deposition of aerosol on the electret fiber should be investigated in details:

1. Polydisperse aerosol
2. Packing density of the filter, α
3. Effect of absence or presence of interception parameter
4. Number of electrostatic charge on each individual particle
5. Consideration for combined effect of coulombic and induced forces.

REFERENCES

Areephant A., <u>Master Degree Thesis</u>, Chulalongkorn University, (1996)

Barot, D. T., Tien, C. and Wang, C. S., <u>AIChE Journal</u>, 26, 289, (1980)

Baumgartner, H. and Loeffler, F., <u>J. Aerosol Sci</u>., Vol. 17, No. 3, (1986)

Baumgartner, H. and Loeffler, F., <u>J. Aerosol Sci</u>., Vol. 18, No. 6, (1987)

Baumgartner, H., Loeffler, F. and Umhauer H., <u>IEEE Trans. Elec. Insul</u>., Vol. EI-21, No. 3, (1986)

Bhutra, S.,and Payatakes, A.C., <u>J. Aerosol Sci.</u>, Vol. 10, (1979)

Billing, C.E., <u>Ph.D. Dissertation</u>, Calif. Int. Tech., Pasadena (1966)

Brown, R.C., <u>Air Filtration</u>, Pergamon Press, Oxford, U.K., (1993)

Davies, C.N., <u>Air Filtration</u>, Academic Press, (1973)

Emi, H., Okuyama, K.,and Yoshioka, N., <u>J. Chem. Eng. Japan</u>, Vol. 6, (1973)

Emi H., Kanaoka C., Otani Y. and Iiyama T., <u>International Conference on Electrostatics</u>, (1984)

Emi H., Kanaoka C., Otani Y. and Ishiguro T, <u>Particulate Science and Technology</u>, Vol. 5, (1987)

Fuchs, N.A., <u>Mechanics of Aerosols</u>, Pergamon Press, Oxford, (1964)

Gordon M.B.,and Bruce, M.P., <u>Ind. Eng. Chem. Process Des. Dev.</u>, Vol. 18, (1979)

Hinds, W.C., <u>Aerosol Technology</u>, 2[st]edition, John Wiley & Sons, Inc., (1999)

Hiragi S., <u>Doctoral Dissertation (in Japanese)</u>, Kanazawa University, (1995)

Kanaoka, C., Emi, H.,and Myojo, T., <u>J. Aerosol Sci.</u>, Vol. 11, (1980)

Kanaoka, C., Emi, H.,and Tanthapanichakoon, W., Paper presented at International Symposium on Powder Technology 81, Kyoto, Japan, (1981)

Kanaoka, C., Emi, H.,and Tanthapanichakoon, W., <u>AIChE Journal</u>, Vol. 29, No. 6, (1983)

Kanaoka C. and Tanthapanichakoon W., <u>Air Pollution (in Thai),</u> 1[st]edition, Technological Promotion Association (Thai-Japan), (1985)

Kanaoka, C., Emi, H., and Hiragi, S., <u>Proc. of 2nd Int. Aerosol Conf.</u>, Berlin, (1986)

Kanaoka, C., Emi, H., and Hiragi, S., and Myojo, T., <u>Soc. Powder Tech. Japan</u>, 24, 74, (1987)

Kanaoka, C.,and Hiragi, S., J. Aerosol Sci., Vol. 21, (1990)

Kanaoka, C. and Hiragi, S., Proc. 12 th Int. Symp. on Contamination Control, (1994)

Kanaoka C., Advances in Aerosol Filtration edited by Spurny K. R., 323-334, Lewis Publishers, (1998)

Kanaoka, C., Hiragi, S. and Tanthapanichakoon W., Powder Technology (accepted), Elsevier, (2001)

Kirsch, A.A. and Stechkina, J.B., Fundamental of Aerosol Science, edited by Shaw, D.T., Wiley, New York, (1978)

Kuwabara, S., J. Phy. Soc. Japan, Vol. 14, (1959)

Linoya K., Gotoh K. and Higashitani K., : Powder Technology Handbook, 1stedition, Marcel Dekker, Inc., (1991)

Myojo, T., Kanaoka, C. and Emi, H., J. Aerosol Sci., Vol. 15, (1984)

Payatakes, A.C.,and Tien, C., J. Aerosol Sci., Vol 7, (1976a)

Payatakes, A.C.,and Tien, C., Filtration and Separation, Vol. 14, (1976b)

Payatakes, A.C.,and Tien, C., Powder Tech., Vol. 14, (1976c)

Payatakes, A.C.,and Tien, C., AIChE Journal, Vol. 23, No. 2, (1977)

Payatakes, A.C.,and Gradon, L., AIChE Journal, Vol. 26, No. 3, (1980a)

Payatakes, A.C.,and Gradon, L., Chem. Eng. Sci., Vol. 35, (1980b)

Raduskvich, L.V., Colloid. J. U.S.S.R., Vol. 26, (1964)

Reist P. C., Aerosol Science and Technology, 2ndedition, McGraw-Hill, Inc., (1993)

Stechkina, I.B.,and Fuchs, N.A., Ann. Occup. Hyg., Vol. 9, (1966)

Stechkina, I.B., Kirst, A.A.,and Fuchs, N.A., Ann. Occup. Hyg., Vol. 12, (1969)

Tanthapanichakoon, W., Ph.D. Dissertation, University of Texas at Austin, Texas, (1978)

Tanthapanichakoon W., Final Report, Rachadapiseksompoch Fund, Chulalongkorn University, (1982)

Tanthapanichakoon, W. and Kanaoka, C., Proceedings 6th World Filtration Congress Japan, (1993)

Tien, C., Wang, C.S.,and Barot, D.T., Science, Vol. 196, (1977)

Wang C. S., Beizaie M. and Tien C., AIChE Journal. Vol. 23, No. 6, (1977)

Wongsri, M., Tanthapanichakoon, W., Kanaoka, C.,and Emi, H., <u>Advanced Powder Technol. Japan</u>, Vol. 2, No. 1, (1991)

Yoshioka, N., Emi, H.,and Sone, H., <u>Kagaku Kogaku (Chem. Eng. Japan)</u>, Vol. 33, (1969)

APPENDICES

APPENDICE A

Table A The diffusion coefficient D_{BM}, Cunningham slip correction factor C_m, and mobility β of particles in the air at 20^oC

Radius of particle (μm)	D_{BM} (cm^2/sec)	C_m	β
0.001	1.3×10^{-2}	110.2	3.19×10^{11}
0.005	5.3×10^{-4}	22.5	1.31×10^{10}
0.01	1.4×10^{-4}	11.56	3.35×10^{9}
0.02	3.6×10^{-5}	6.10	8.84×10^{8}
0.025	2.4×10^{-5}	5.03	5.83×10^{8}
0.05	6.8×10^{-6}	2.89	1.68×10^{8}
0.1	2.2×10^{-6}	1.88	5.45×10^{7}
0.15	1.24×10^{-6}	1.57	3.08×10^{7}
0.2	8.4×10^{-7}	1.42	2.06×10^{7}
0.225	7.2×10^{-7}	1.375	1.77×10^{7}
0.25	6.3×10^{-7}	1.334	1.55×10^{7}
0.5	2.76×10^{-7}	1.166	6.75×10^{6}
1.0	1.3×10^{-7}	1.083	3.13×10^{6}
2.0	6.16×10^{-8}	1.042	1.51×10^{6}
5.0	2.4×10^{-8}	1.017	5.88×10^{5}

APPENDICE B
CLEAN FIBER COLLECTION EFFICIENCY

Table B 1 The clean fiber collection efficiency of electrical deposition and
convective diffusion mechanism from simulation and Emi's correlation (1987) for the case
of K_{In}= 0.004 and K_C= 0.016 (%)

Mechanism	Efficiency	Pe 200	1000	5000	50000
Induction	RI 0.03	10.82	4.04	2.52	1.22
	Emi's correlation	11.45	5.29	3.19	2.33
	RI 0.05	11.77	4.83	2.67	1.46
	Emi's correlation	11.65	5.49	3.39	2.53
	RI 0.1	12.21	5.95	3.24	2.53
	Emi's correlation	12.93	6.78	4.67	3.81
Coulomb 90	RI 0.03	7.22	3.78	1.80	1.28
	Emi's correlation	10.39	4.22	2.11	1.26
	RI 0.05	9.46	4.43	2.06	1.67
	Emi's correlation	10.59	4.42	2.31	1.46
	RI 0.1	10.51	5.31	2.86	2.48
	Emi's correlation	11.87	5.70	3.59	2.74
Coulomb 135	RI 0.03	8.53	4.75	2.20	1.62
	Emi's correlation	10.39	4.22	2.11	1.26
	RI 0.05	9.93	5.29	2.48	2.09
	Emi's correlation	10.59	4.42	2.31	1.46
	RI 0.1	12.51	6.64	3.33	2.56
	Emi's correlation	11.87	5.70	3.59	2.74
Coulomb 180	RI 0.03	9.80	5.47	2.89	1.96
	Emi's correlation	10.39	4.22	2.11	1.26
	RI 0.05	11.91	6.01	2.95	2.31
	Emi's correlation	10.59	4.42	2.31	1.46
	RI 0.1	13.80	6.55	3.62	3.16
	Emi's correlation	11.87	5.70	3.59	2.74

Table B 2 The clean fiber collection efficiency of electrical deposition and
convective diffusion mechanism from simulation and Emi's correlation (1987) for the case
of K_{In}= 0.05 and K_C= 0.05 (%)

Mechanism	Efficiency	Pe 200	1000	5000	50000
Induction	RI 0.03	11.35	8.71	6.91	5.95
	Emi's correlation	14.91	8.75	6.65	5.79
	RI 0.05	12.57	8.58	6.74	5.80
	Emi's correlation	15.03	8.95	6.85	5.99
	RI 0.1	13.3	9.00	6.21	5.83
	Emi's correlation	16.39	10.23	8.13	7.27
Coulomb 90	RI 0.03	10.16	5.43	4.03	3.89
	Emi's correlation	11.59	5.43	3.33	2.47
	RI 0.05	10.90	5.86	5.69	4.32
	Emi's correlation	11.79	5.63	3.53	2.67
	RI 0.1	11.13	5.45	5.43	4.7
	Emi's correlation	13.07	6.91	4.81	3.95
Coulomb 135	RI 0.03	11.04	6.78	5.48	5.03
	Emi's correlation	11.59	5.43	3.33	2.47
	RI 0.05	10.44	6.05	5.50	4.65
	Emi's correlation	11.79	5.63	3.53	2.67
	RI 0.1	12.70	8.13	6.27	5.64
	Emi's correlation	13.07	6.91	4.81	3.95
Coulomb 180	RI 0.03	11.48	6.23	5.98	5.46
	Emi's correlation	11.59	5.43	3.33	2.47
	RI 0.05	12.52	7.41	6.48	4.96
	Emi's correlation	11.79	5.63	3.53	2.67
	RI 0.1	14.73	8.65	6.67	6.38
	Emi's correlation	13.07	6.91	4.81	3.95

Table B 3 The clean fiber collection efficiency of electrical deposition and convective diffusion mechanism from simulation and Emi's correlation (1987) for the case of K_{In}= 0.1 and K_C= 0.1 (%)

Mechanism	Efficiency	Pe 200	1000	5000	50000
Induction	RI 0.03	12.41	12.35	9.05	8.81
	Emi's correlation	16.64	10.49	8.38	7.52
	RI 0.05	15.83	9.69	9.14	8.63
	Emi's correlation	16.84	10.69	8.58	7.72
	RI 0.1	19.67	10.32	10.94	9.86
	Emi's correlation	18.12	11.97	9.86	9.01
Coulomb 90	RI 0.03	11.01	10.11	8.85	7.41
	Emi's correlation	13.03	6.88	4.77	3.91
	RI 0.05	11.71	10.21	8.38	7.87
	Emi's correlation	13.23	7.08	4.97	4.11
	RI 0.1	12.41	10.33	8.24	7.41
	Emi's correlation	14.51	8.36	6.25	5.39
Coulomb 135	RI 0.03	13.52	10.89	8.96	7.81
	Emi's correlation	13.03	6.88	4.77	3.91
	RI 0.05	12.13	11.51	8.85	8.77
	Emi's correlation	13.23	7.08	4.97	4.11
	RI 0.1	13.55	11.61	9.29	9.22
	Emi's correlation	14.51	8.36	6.25	5.39
Coulomb 180	RI 0.03	14.15	11.79	8.91	7.95
	Emi's correlation	13.03	6.88	4.77	3.91
	RI 0.05	15.90	12.41	10.12	9.87
	Emi's correlation	13.23	7.08	4.97	4.11
	RI 0.1	16.85	13.68	11.58	11.41
	Emi's correlation	14.51	8.36	6.25	5.39

APPENDICE C
COLLECTION EFFICIENCY RAISING FACTOR

Table C 1 The collection efficiency raising factor of electrical deposition and convective diffusion mechanism for overall stage based on Emi's correlation (1987) for the case of K_{In}= 0.004 and K_C= 0.016

Mechanism	Lamda	Pe	200	1000	5000	50000
Induction	RI 0.03		3.12	8.49	14.47	20.96
	RI 0.05		2.78	7.32	11.06	13.68
	RI 0.1		2.24	4.29	6.18	8.47
Coulomb 90	RI 0.03		3.98	10.00	20.67	39.34
	RI 0.05		3.33	8.14	15.96	25.37
	RI 0.1		2.38	5.51	9.36	12.92
Coulomb 135	RI 0.03		3.49	9.92	20.26	33.97
	RI 0.05		3.35	8.75	17.48	19.03
	RI 0.1		2.09	5.50	8.00	10.51
Coulomb 180	RI 0.03		3.81	9.33	22.05	34.13
	RI 0.05		3.27	8.41	15.29	24.62
	RI 0.1		2.74	6.32	9.46	11.60

Table C 2 The collection efficiency raising factor of electrical deposition and convective diffusion mechanism for both initial stage and overall or later stage based on Emi's correlation (1987) for the case of $K_{In} = 0.05$ and $K_C = 0.05$

Mechanism	Lamda	Pe	200	1000	5000	50000
Induction	RI 0.03		2.41	4.29	5.91	6.45
	Initial		0.53	2.43	2.71	1.86
	RI 0.05		2.10	3.83	5.43	5.70
	Initial		0.76	1.63	3.52	2.4
	RI 0.1		1.51	2.98	3.74	4.19
	Initial		1.40	2.52	3.08	2.58
Coulomb 90	RI 0.03		3.15	7.49	11.95	16.88
	Initial		1.61	5.39	14.21	16.31
	RI 0.05		2.88	6.27	11.08	12.02
	Initial		1.31	5.09	6.78	11.23
	RI 0.1		2.3	4.36	6.17	7.42
	Initial		2.69	3.22	5.89	6.67
Coulomb 135	RI 0.03		3.17	7.43	10.65	14.34
	Initial		0.50	3.12	7.79	11.23
	RI 0.05		3.17	6.47	10.89	11.41
	Initial		1.45	3.07	6.70	10.98
	RI 0.1		2.02	4.18	5.73	7.47
	Initial		1.53	3.57	2.83	5.63
Coulomb 180	RI 0.03		3.16	7.60	12.42	14.82
	RI 0.05		2.97	5.78	9.11	12.82
	RI 0.1		1.93	4.31	5.40	6.85
	Initial		1.43	2.24	4.05	3.50

Table C 3 The collection efficiency raising factor of electrical deposition and convective diffusion mechanism for both initial stage and overall or later stage based on Emi's correlation (1987) for the case of $K_{In} = 0.1$ and $K_C = 0.1$

Mechanism	Lamda	Pe	200	1000	5000	50000
Induction	RI 0.03		1.89	3.24	3.54	4.39
	Initial		1.11	0.39	1.71	0.73
	RI 0.05		1.70	3.04	3.58	4.09
	Initial		0.03	1.10	0.06	1.60
	RI 0.1		1.69	2.39	2.54	2.71
	Initial		0.62	1.62	2.18	2.29
Coulomb 90	RI 0.03		2.66	5.68	9.10	11.05
	Initial		0.33	3.58	3.15	5.51
	RI 0.05		2.47	5.11	6.89	7.13
	Initial		1.26	4.69	2.83	4.04
	RI 0.1		1.95	3.55	4.38	5.09
	Initial		2.25	2.55	3.39	5.35
Coulomb 135	RI 0.03		2.98	5.67	8.32	10.21
	Initial		0.28	1.41	2.47	5.64
	RI 0.05		2.55	4.63	6.34	7.70
	Initial		0.59	1.16	2.02	3.46
	RI 0.1		1.91	2.61	4.07	4.15
	Initial		1.53	1.93	2.67	5.24
Coulomb 180	RI 0.03		2.88	5.13	8.01	8.70
	Initial		0.17	2.38	1.49	2.15
	RI 0.05		2.28	4.68	5.67	7.49
	Initial		0.21	0.78	1.36	1.70
	RI 0.1		1.76	2.51	3.72	3.50
	Initial		0.41	1.75	2.30	2.70

VITA

Mr. Kreangkrai Maneeintr, third son of Col. Pinij and Mrs. Raweewan Maneeintr, was born on August 31, 1973 in Bangkok, Thailand. He attended Suankularb College in Bangkok and graduated in 1992. In April 1997, he received his Bachelor Degree of Engineering in Chemical Engineering from Faculty of Engineering, Chulalongkorn University, Bangkok, Thailand. After he worked for a while, he enrolled his Master Degree Program at Chulalongkorn University in 1998. He was granted the degree in April, 2001.